

MODELING ANTI-CANCER DRUG RESISTANCE USING TUMOR SPHEROIDS

A Dissertation

Submitted to

The Graduate Faculty of The University of Akron

In Partial Fulfillment

of the Requirements for the Degree

Doctor of Philosophy

Pradip Shahi Thakuri

December, 2019

MODELING ANTI-CANCER DRUG RESISTANCE USING TUMOR SPHEROIDS

Pradip Shahi Thakuri

Dissertation

Approved:

Advisor
Dr. Hossein Tavana

Committee Member
Dr. Marnie Saunders

Committee Member
Dr. Ge (Christie) Zhang

Committee Member
Dr. Sailaja Paruchuri

Committee Member
Dr. Nic D. Leipzig

Accepted:

Interim Department Chair
Dr. Rebecca Kuntz Willits

Interim Dean of the College
Dr. Craig Menzemer

Dean of the Graduate School
Dr. Chand Midha

Date

ABSTRACT

National Cancer Institute has estimated 1.8 million new cases of cancer and 0.6 million deaths from the disease in the United States in 2019. Cancer is heterogeneous disease with genetically different sub-populations of cells within the tumors (spatial heterogeneity), and sub-populations of cells that evolve with time adding to the cellular variations (temporal heterogeneity). Availability of advanced molecular analysis techniques in the past two decades has increased our understanding of molecular drivers of cancer. Understanding the drivers of cancer have shifted cancer therapy away from generally toxic and minimally effective cytotoxic chemotherapy towards targeted therapies. Despite the significant promise of targeted therapies for cancer treatment, they have failed to reduce the overall survival rate of cancer patients. A major impediment is resistance of cancer cells to targeted drugs through diverse mechanisms. Mechanistic understanding of drug resistance to targeted therapies and development of effective strategies can overcome drug resistance. Technological limitations to model and study drug resistance remain an obstacle.

Two-dimensional (2D) cultures of cells and animal models have been standard methods in cancer research to study drug resistance. However, the former method is too simplistic and lacks physiological relevance, whereas the latter method is too costly, slow, and complex. To address the need for preclinical drug resistance models, we developed and utilized three-dimensional (3D) aggregates of cancer cells known as tumor spheroids that display biological properties of solid tumors. We used a cell printing microtechnology

using an aqueous two-phase system (ATPS) for facile printing of tumor spheroids. Cancer cells confined within the denser dextran (DEX) solution were dispensed into the polyethylene glycol (PEG) solution to generate a compact spheroid. Adapting this approach to automated liquid handler and 384-well plates allowed high throughput forming of spheroids for drug screening. Long-term cultures of spheroids allowed modeling adaptation of cancer cells to targeted therapies.

As a disease model, we focused on colorectal cancer with mutations in KRAS and BRAF kinases. Our high throughput drug screening and multi-parametric analysis of short-term drug treatments showed that targeting mitogen-activated protein kinase (MAPK) pathway effectively inhibits growth of colorectal cancer spheroids. We then followed how patients receive chemotherapy by treating spheroids with drugs and allowing them to recover during long-term cultures and demonstrated adaptive resistance of spheroids to specific kinase inhibitors of MAPK signaling pathway. The MAPK pathway inhibition caused activation of PI3K/AKT signaling pathway in both KRAS and BRAF mutant colorectal cancer cells. Additionally, we identified activation of STAT kinases and upstream epidermal growth factor receptor proteins (EGFRs) in KRAS mutant colorectal cancer cells. This compensatory signaling allowed cancer cells to proliferate and survive MAPK pathway inhibition. We combined inhibitors of MAPK (MAPKi) and PI3K (PI3Ki) and identified low-dose synergistic combinations that inhibited growth of the spheroids over long-term cyclic treatments. Alternatively, we used combinations of MAPKi and EGFRi to overcome feedback signaling through EGFR and suppress growth of the spheroids. The combination strategies presented here are promising approaches that need to be tested *in vivo*.

Although combination treatments are essential to block feedback signaling and drug resistance in cancer cells, several clinical studies have shown that parallel administration of drugs may result in toxicity to cancer patients. To demonstrate the feasibility of using our technology to test alternative treatment regimens, we evaluated the potential of sequentially combining MEKi and PI3Ki. This approach suppressed growth of tumor spheroids and the effect was comparable to the parallel combination treatment. Future studies are needed to test toxicity of these combination treatment regimens to normal tissues.

Overall, this work demonstrated the advantages of our 3D tumor model to identify and target molecular drivers of resistance to targeted therapies. Future advancement of this technology by incorporating various components of the tumor microenvironment and using primary patient-derived cells will increase the translational relevance of the finding.

ACKNOWLEDGEMENT

I would like to express my deepest appreciation to my advisor, Dr. Hossein Tavana, for his unparalleled support and unwavering guidance throughout my graduate career. Thank you for giving me focus over these years, always with patience and insight. Your invaluable advices helped me develop as a meticulous researcher and a critical thinker.

I am also grateful to my advisory committee members Dr. Marnie Saunders, Dr. Ge (Christie) Zhang, Dr. Nic Leipzig, and Dr. Sailaja Paruchuri, for their constructive criticisms and practical suggestions to improve the quality of my research. I appreciate your support and willingness to help me. I would like to extend my sincere thanks to my co-author Dr. Gary D. Luker for helpful conversations in designing experiments and preparing manuscripts. Your expertise was instrumental in giving direction to my research.

Special thanks to my fellow lab members for creating a friendly, supportive and productive academic environment. I cannot begin to express my thanks to my wife, Ramila Joshi, who has been a relentless supporter and motivator of every work I pursue. I am also extremely grateful to my son Rushav for providing a happy distraction to rest my mind outside of my research.

Finally, I would like to express my love and gratitude to my parents, Nirmala and Kanchha Thakuri, for their endless encouragement and support in all my endeavors.

TABLE OF CONTENTS

LIST OF FIGURES	xiv
LIST OF TABLES.....	xxxi
I. INTRODUCTION	1
1.1 Significance	1
1.2 Drug Resistance	3
1.2.1 Target Mutation.....	5
1.2.2 Bypass Mechanism.....	5
1.2.3 Pathway Re-activation by Alteration in Upstream and Downstream Signaling	6
1.2.4 Tumor Microenvironment	7
1.3 Models of Drug Resistance.....	8
1.3.1 2D Cell Model.....	9
1.3.2 Mouse Model	10
1.3.3 3D In-vitro Model	11
1.4 Spheroid Model.....	12
1.5 Aqueous Two-Phase Systems (ATPS) Technology.....	13
1.6 Colorectal Cancer.....	14
1.7 Aims and Scope	16

II. MULTIPARAMETRIC ANALYSIS OF ONCOLOGY DRUG SCREENING	
WITH AQUEOUS TWO-PHASE TUMOR SPHEROIDS	21
2.1 Materials and Methods	24
2.1.1 Cell Culture	24
2.1.2 Spheroid Formation Using ATPS	24
2.1.3 Growth Kinetics of Spheroids	25
2.1.4 Immunohistochemical Analysis of Spheroids	26
2.1.5 Anticancer Drug Screening Against Tumor Spheroids	26
2.1.6 Western Blotting	28
2.1.7 Statistical Analysis for Selecting Effective Compounds	28
2.1.8 Combination Treatment of Spheroids	29
2.1.9 Correlation of Size and Metabolic Activity of Cells in Spheroids	30
2.2 Results and Discussion	30
2.2.1 Formation, Consistency, and Metabolic Activity of ATPS Tumor Spheroids	
.....	31
2.2.2 Growth and Matrix Deposition of ATPS Tumor Spheroids	32
2.2.3 Quantitative Analysis of Drug Responses of Tumor Spheroids	34
2.2.4 Ranking the Performance of Anticancer Compounds	36
2.2.5 Morphological Changes of Spheroids in Response to Treatments	40
2.2.6 Molecular Targeting of Pathway Inhibitors	41
2.2.7 Screening Experiments to Select Effective Compounds	42
2.2.8 Analysis of Combination Treatments Using Size of Spheroids	43

2.2.9 Predicting Treatment Outcomes Using Size of Spheroids	47
2.3 Summary	48

III. CYCLICAL TREATMENT OF COLORECTAL TUMOR SPHEROIDS

INDUCES RESISTANCE TO MEK INHIBITORS	62
3.1 Materials and Methods	64
3.1.1 Cell Culture	64
3.1.2 Spheroid Formation	65
3.1.3 Preparing Drug Solutions	66
3.1.4 Cyclical Treatment of Spheroids with Inhibitors and Recovery from Treatment	66
3.1.5 Dose Dependent Cyclical Treatment of Spheroids with MEKi and Recovery from Treatments	68
3.1.6 Analysis of Growth of Spheroids to Quantify Drug Resistance	68
3.1.7 Western Blotting	70
3.1.8 Short-term Combination Treatment of Spheroids	71
3.1.9 Long-term Cyclic Combination Drug Treatment/Recovery of Spheroids ...	72
3.2 Results and Discussion	72
3.2.1 Microprinting of Tumor Spheroids	73
3.2.2 Screening of Molecular Inhibitors Against Colorectal Tumor Spheroids	73
3.2.3 Long-Term Cyclic Treatment of Spheroids with MEKi	74
3.2.4 Molecular Analysis of Adaptive Drug Resistance in Colorectal Tumor Spheroids	77

3.2.4.1 Effect of MEKi treatments on MAPK Pathway Activity	78
3.2.4.2 Effect of MEKi Treatments on PI3K Pathway Activity	79
3.2.4.3 Effect of MEKi Treatments on B-RAF and STAT3 Signaling	80
3.2.5 Combination Therapy Effect on Treatment-Induced Drug Resistance	81
3.2.6 Molecular Effects of Combination Treatments.....	82
3.2.7 Growth Inhibition of Tumor Spheroids by Long-Term Cyclic Combination Treatments.....	83
3.3 Summary.....	85

IV. SYNERGISTIC INHIBITION OF KINASE PATHWAYS OVERCOMES

DRUG RESISTANCE OF COLORECTAL CANCER SPHEROIDS TO CYCLIC TARGETED THERAPIES	100
4.1 Materials and Methods	102
4.1.1 Cell Culture and Spheroid Formation	103
4.1.2 Drug Treatments.....	103
4.1.3 Combination Treatments of Spheroids.....	104
4.1.4 Western Blot Experiments	105
4.1.5 q-PCR Experiments.....	106
4.1.6 Confocal Microscopy	106
4.2 Results and Discussion.....	107
4.2.1 Microprinting of Tumor Spheroids and Their Growth Analysis	107
4.2.2 Dose-Response to Molecular Inhibitors	108

4.2.3 Resistance of Colorectal Tumor Spheroids to Cyclic Treatments of MAPKi	109
4.2.4 Mechanism of Drug Resistance	111
4.2.5 Combination Treatments to Suppress Resistance	112
4.2.6 Long-Term Cyclic Combination Treatments.....	115
4.3 Summary.....	117

V. COMBINED INHIBITION OF MAPK PATHWAY AND EGFR TO OVERCOME ADAPTIVE DRUG RESISTANCE OF COLORECTAL CANCER SPHEROIDS	127
5.1 Materials and Methods	129
5.1.1 Cell Culture and Spheroid Formation	129
5.1.2 Drug Tests.....	129
5.1.3 Cyclical Treatments.....	130
5.1.4 Western Blot Experiments	131
5.1.5 Phospho-RTK array.....	131
5.1.6 Combination Treatments of Spheroids	132
5.1.7 Long-term Cyclic Drug Combination Treatments	132
5.1.8 3D Invasion Assay	132
5.2 Results and Discussions	133
5.2.1 Screening of MAPK Pathway Inhibitors	133
5.2.2 Long-term Cyclical Treatment of Spheroids with MAPKi	134

5.2.3 Molecular Analysis of Adaptive Drug Resistance of Colorectal Tumor Spheroids	135
5.2.4 Combination Treatments of Colorectal Tumor Spheroids with MAPKi and EGFRi	139
5.2.5 Long-term Cyclic Combination Treatments of Colorectal Tumor Spheroids with MAPKi and EGFRi	141
5.2.6 Drug Combination Prevents Matrix Invasion of Colorectal Tumor Spheroid	142
5.3 Summary	144

VI. COMBINATION TREATMENT STRATEGIES TO OVERCOME DRUG

RESISTANCE IN TUMOR SPHEROIDS	154
6.1 Materials and Methods	156
6.1.1 Cell culture	157
6.1.2 Treatment Regimens	157
6.1.3 Testing Treatment Toxicity in HUVEC Spheroids	158
6.1.4 Short-term Combination Treatment Regimens	159
6.1.5 Long-term Combination Treatment Regimen	160
6.1.6 Western Blotting	160
6.2 Results and Discussions	160
6.2.1 Toxicity of Combination Drug Regimens	160
6.2.2 Efficacy of Treatment Regimens	162
6.3 Summary	165

VII. CONCLUSIONS	170
VIII. FUTURE WORK.....	173
BIBLIOGRAPHY.....	177
APPENDIX	200

LIST OF FIGURES

- Figure 1-1. Schematic of pre-existing and treatment induced resistance to targeted therapies in cancer treatment. Sensitive population (green), pre-existing resistant population (red) and treatment induced resistance (purple and yellow). (Adapted from Colombino M et.al, *J Carcinog Mutagen* 2014)..... 19
- Figure 1-2. Mutational status of colorectal cancer. (Adapted from <https://oncodesc.com/colorectal-cancer/>)..... 19
- Figure 1-3. Potential mechanism for activation of signaling pathways in cancer that leads to drug resistance. 20
- Figure 2-1. (a) Phase diagram of ATPS made with polyethylene glycol (PEG) and dextran (DEX) shows the composition of the initial solution (solid square) and resulting segregated phases (open squares). The inset image shows side view of the ATPS formed in a glass cuvette with the location of the interface indicated. (b) The top view of a spheroid of HT-29 colorectal cancer cells formed with the ATPS microtechnology. 52
- Figure 2-2. Histograms of diameter of spheroids of (a) HT-29 colorectal cancer cells, (b) U-87 MG brain cancer cells, and (c) MDA-MB-157 breast cancer cells show the consistency of size of spheroids (n=300). Fitted curves show that diameter of spheroids follows a Gaussian distribution. (d-f) Metabolic activity of spheroids,

measured as the fluorescence signal produced by cells metabolizing PrestoBlue, shows a linear correlation with the size of spheroids. Horizontal and vertical bars represent standard error of volume of spheroids and standard error of raw fluorescence intensity data (n=7 for each data point). (g-i) Volume growth kinetics of HT-29, U-87 MG, and MDA-MB-157 spheroids is shown over time. Images represent spheroids from different days of culture. The number of samples for each time point is 50 spheroids and error bars represent standard error of mean. Scale bar: 300 μm53

Figure 2-3. (a) Confocal images of a spheroid of HT-29 cells 4 days after formation taken every 10 μm from the top (Z=21) to the center (Z=1) of the spheroid, (b) 3D reconstructed image of half of the spheroid, and (c) maximum intensity stack image of the Z sections. Cells were stained with Hoechst.54

Figure 2-4. Histological staining of spheroids of HT-29 (top row), U-87 MG (middle row), and MDA-MB-157 (bottom row) cells for (a) Ki-67 cell proliferation marker, (b) type I collagen, (c) laminin, and (d) fibronectin. Blue represents nuclei staining with Hoechst and pink represents protein staining. Scale bar: 200 μm54

Figure 2-5. A representative dose-response curve is shown for experiment with selumetinib against HT-29 spheroids. Half-maximum inhibitory concentration (IC_{50}), maximum inhibition (E_{max}), and area under the curve (AUC) are used for multi-parametric analysis of cellular responses to drug compounds.55

Figure 2-6. Twenty-five anticancer compounds are listed in the top row. Values of Emax and log (IC50) for drug-treated spheroids of (a) HT-29, (b) U-87 MG, and (c) MDA-MB-157 are shown. Color bar indicates the range of Emax (0-1). In addition, Emax values for tested compounds are shown. * denotes the lack of an IC₅₀ value in the dose-response graph of the particular drug-cell pair.55

Figure 2-7. Ranking of effectiveness of compounds based on the AUC metric for spheroids of (a) HT-29, (b) U-87 MG, and (c) MDA-MB-157 cells.56

Figure 2-8. Growth inhibition of spheroids of HT-29 and U-87 MG cells after treatment with specific MEK and PI3K inhibitors. Panels (a-c) show dose-dependent blocking of HT-29 spheroids growth due to treatment with three different MEK inhibitors, consistent with measured viability data with each compound. (d) Comparison of growth inhibition of HT-29 spheroids at different concentrations of MEK inhibitors. Panels (e-g) display dose-dependent growth retardation of U-87 MG spheroids treated with three different PI3K inhibitors. (h) Comparison of growth inhibition of U-87 MG spheroids due to treatment with different PI3K inhibitors. Scale bar: 300 μm.....57

Figure 2-9. Morphological changes of spheroids of HT-29, U-87 MG, and MDA-MB-157 cells after treatment with (a) doxorubicin and (b) paclitaxel at different concentrations of drugs. Disintegration of HT-29 spheroids is observed with both chemotherapeutics. Growth of U-87 MG spheroids is blocked at sub-micromolar concentrations, whereas higher drug concentrations disintegrate the spheroids. HT-

29 and MDA-MB-157 spheroids show disintegration at all effective drug concentrations. MDA-MB-157 spheroids show complete resistance to paclitaxel and minimal morphological changes. Scale bar: 300 μm 58

Figure 2-10. (a) Trametinib inhibition of ERK1/2 phosphorylation in HT-29 spheroids and (b) pictilisib inhibition of AKT phosphorylation in U-87 MG spheroids are shown at two different time points.....58

Figure 2-11. Viability of HT-29 spheroids treated with 10 μM of 25 anticancer compounds shown below the graph. (b) Strictly standardized mean difference (SSMD) values corresponding to treatment with the drug compounds. Color coding corresponds to different effectiveness levels of compounds as shown in Table 2-4.59

Figure 2-12. Single-agent and combination drug treatments of HT-29 spheroids with (a) trametinib and dactolisib, (d) PD0325901 and dactolisib, and (g) selumetinib and dactolisib. (b, e, h) Computed area under the dose-response curve (AUC) values corresponding to panels a, d, and g. (c, f, i) Combination index (CI) values shown on a logarithmic scale as a function of the fraction of affected cells in spheroids for combination treatment experiments of panels a, d, and g. $\text{Log (CI)} > 0$ indicates antagonism, $\text{Log (CI)} = 0$ shows additive effect, and $\text{Log (CI)} < 0$ represents synergism.....60

Figure 2-13. (a) Dose dependent reduction in viability of HT-29 spheroids with different molecular inhibitors. Target of drug compounds and their IC₅₀ values against HT-29 spheroids.61

Figure 2-14. The size of spheroids reliably predicts outcomes of treatment with molecular inhibitors. (a-d) Correlation between the average values of fluorescence signal from Prestoblue assay and volume of spheroids from morphological images (n=14). R² represent goodness-of-the-fit parameter. Different data points in each graph represent different drug concentrations. Only those concentrations that did not disintegrate the spheroids were considered.61

Figure 3-1. Tumor spheroid formation using ATPS microprinting, and screening of inhibitors of MAPK and PI3K signaling pathways against HT-29 spheroids. (a) A robotic liquid handler dispensed 0.3 μL of the aqueous DEX phase solution containing HT-29 cancer cells into a microwell containing the aqueous PEG phase. (b,c) Cancer cells remained within the nanodrop and formed a compact spheroid. (d) Addition of culture medium or a drug to the microwell diluted out the ATPS into a single medium phase containing the spheroid. (e) Dose responses of HT-29 spheroids to RAF, MEK, and ERK inhibitors. (f) Normalized AUC values from drug tests with HT-29 spheroids. (g) Dose responses of HT-29 spheroids to PI3K inhibitors. (h) Normalized AUC values from their drug tests with HT-29 spheroids. Scale bar is 200 μm.90

Figure 3-2. Cyclic drug treatment and recovery of colorectal tumor spheroids. (a) The schematic shows the experimental protocol for three cycles of treatment of HT-29 spheroids with MEKi (5 nM trametinib, 100 nM PD0325901, and 100 nM selumetinib) separated by two recovery phases. A fixed concentration of each inhibitor was used for the three treatment rounds. (b-d) Average growth rates of HT-29 spheroids during the three rounds of treatments with trametinib, PD0325901, and selumetinib, respectively. k_c was calculated as the difference in volume of drug-treated spheroids at the end and beginning of each treatment round. k_0 was calculated as the difference in volume of non-treated spheroids at the end and beginning of each round. (e-g) Quantifying resistance to MEKi treatment using normalized growth rate (k_c/k_0) metric. $n=14$ and * $p<0.05$ 91

Figure 3-3. Cyclical treatment and recovery of spheroids. (a-c) Growth rates of HT-29 spheroids treated with MEKi for each cycles of treatment were calculated by subtracting the volume of spheroids ‘Before Treatment’ (inset images g-i, upper panels) and volume of spheroids After Treatment’ (inset images g-i, middle panels) 6 day treatment periods (See Figure 3-2b-d). (d-f) Growth rates of HT-29 spheroids non-treated with MEKi for each cycles of treatment were calculated by subtracting the volume of spheroids ‘Before Treatment’ (inset images g-i, upper panels) and volume of Untreated spheroids After Treatment’ (inset images g-i, lower panels) 6 day treatment periods. Each data point represents average of 14 replicates. Scale bar is 200 μm 92

Figure 3-4. Normalized growth rates of HT-29 spheroids treated with MEKi dose-dependently. Solid symbols in (a-c) represent T1 treatment of HT-29 spheroids with five different concentrations (multiple of IC₅₀) of the MEKi. Open symbols in (a-c) represent T2 treatment of HT-29 spheroids with five different concentrations (multiple of IC₅₀) of the MEKi. Spheroids that were used for T2 had been treated with 5 nM trametinib, 100 nM PD0325901, or 100 nM selumetinib during T1 and recovered from the treatment during R1 phase. (**p*<0.05). The * symbol above data points represents a statistically significant difference between the two treatment rounds. Error bars represent standard error of the mean.93

Figure 3-5. Cyclical treatment of HCT116 spheroid with 5 nM trametinib. n=16. * represents *p*<0.05 that is considered statistically significant difference between normalized growth rate between treatments.....93

Figure 3-6. Oncogenic levels of ERK1/2 and AKT in HT-29 spheroids treated with MEKi. Representative Western blots for p-ERK1/2, t-ERK1/2, p-AKT, and t-AKT at end of (a) treatment T1 phase, and at the end of (b) R1 phase. (d-e) and (g-h) are quantified results of p-ERK/t-ERK, and p-AKT/t-AKT, respectively. (c) ERK1/2 and AKT levels in MEKi-treated HT-29 spheroids at the end of of treatment T2 phase. Each MEKi treatment during T2 has different controls. Lane 1: Control trametinib (spheroids that received 5 nM trametinib during T1); Lane 2: 5nM trametinib treatment; Lane 3: Control PD0325901 (spheroids that received 100 nM PD0325901 during T1); Lane 4: 100 nM PD0325901 treatment; Lane 5: Control

selumetinib (spheroids that received 100 nM selumetinib during T1); and Lane 6: 100 nM selumetinib treatment. (f) Quantified p-ERK/t-ERK showed that trametinib and PD0325901 significantly downregulated the phosphorylation of ERK, but selumetinib treatment did not change ERK activity. (i) Quantified p-AKT/t-AKT showed that treatment of HT-29 spheroids with trametinib, PD0325901, and selumetinib significantly elevated AKT activity. Each experiment was repeated twice. Results are shown as mean \pm standard error. * $p < 0.05$ 94

Figure 3-7. Upregulation of AKT activity in HT-29 spheroids after MEKi treatments for 48 h..... 95

Figure 3-8. (a) Representative Western blots for *p*-ERK, *t*-ERK, *p*-AKT, and *t*-AKT. (b) Quantification of *p*-ERK/*t*-ERK levels showed downregulation of ERK activity. (c) Quantification of *p*-AKT/*t*-AKT levels showed upregulated AKT activity in the cells. 95

Figure 3-9. (a-b) Representative Western blots for *p*-BRAF, BRAF, *p*-STAT3, and STAT3 at end of T1 and R1 phases. (c-d) Quantification of *p*-BRAF/BRAF at the end of T1 and at the end of R1 phases show no significant changes in the level of *p*-BRAF induced due to the MEKi treatments. (e-f) Quantification of *p*-STAT3/STAT3 at the end of T1 and at the end of R1 phases show no significant changes in the level of *p*-TAT3 due to the MEKi treatments. Each experiment was repeated twice. Results are shown as mean \pm standard error. 96

Figure 3-10. Combination treatments of colorectal tumor spheroids with MEKi and dactolisib. Combination and single-agent drug treatments of HT-29 spheroids with (a) trametinib and dactolisib, (b) PD0325901 and dactolisib, and (c) selumetinib and dactolisib for a 6-day treatment. Open square symbols connected by dotted blue lines represent dose dependent response of HT-29 spheroids to single-agent dactolisib treatments, open circle symbols connected by dotted red lines represent dose dependent response of HT-29 spheroids to single-agent MEKi treatments, and solid triangle symbols connected by green lines represent dose dependent response of HT-29 spheroid to combination treatment of MEKi with dactolisib. Inset images show spheroids after dose-dependent combination drug treatments. The image in the top left of panels (a-c) show a control, non-treated spheroid. Scale bar is 300 μm . Synergy plots for the combination experiments show combination index (CI) versus Fraction affected (F_a) at combination drug concentrations for (d) trametinib and dactolisib, (e) PD0325901 and dactolisib, and (f) selumetinib and dactolisib. $CI < 1$ indicates synergism, whereas $CI > 1$ indicates antagonism.97

Figure 3-11. Combinations of MEKi and dactolisib downregulate ERK1/2 and AKT signaling in HT-29 spheroids. Representative Western blots and quantified results for *p*-ERK1/2, *t*-ERK1/2, *p*-AKT, and *t*-AKT from spheroids treated with (a-c) trametinib and dactolisib, (d-f) PD0325901 and dactolisib, and (g-i) selumetinib and dactolisib, for 48 hrs. Each experiment was repeated twice. Results are shown as mean \pm standard error. * $p < 0.05$ denotes comparing each treatment with its respective vehicle control.98

Figure 3-12. Long-term cyclic combination treatments. Volumes of spheroids are shown during treatment and recovery cycles (Figure 3-2a): Vehicle control (open inverted triangles), MEKi treatment (open circles), dactolisib treatments (open squares), and combination treatments (solid triangles). All treatments were done using lowest synergistic concentrations of the MEKi and dactolisib. $n=7$ and $p<0.001$. Means of growth rates in each panel (a-c) at the end of 30 days that do not share a letter are significantly different. Scale bar is 300 μm 99

Figure 4-1. Formation and growth of tumor spheroids. (a) A 0.3 μl drop of the aqueous DEX phase containing HCT116 cancer cells immersed in the aqueous PEG phase settles to the well bottom. Cancer cells remain within the DEX drop and form a spheroid. (b) Confocal image of spheroids shows fully viable cells and a 3D z-stack reconstruction of a portion of a spheroid. (c) Size of HCT116 spheroids increases during incubation indicating cell proliferation. Inset images from left to right represents spheroids on days 2, 4, 6, and 8. Error bars represent standard error of the mean ($n=14$). Scale bar is 200 μm in panels (a-c)..... 120

Figure 4-2. Responses of spheroids to MAPK and PI3K inhibitors. Dose-responses of HCT116 spheroids to inhibitors of (a) MAPK pathway and (b) PI3K pathway. (c) The list of molecular inhibitors used, their targets, and LD_{50} values against HCT116 spheroids. The symbol ‘—’ indicates an LD_{50} value could not be obtained. 121

Figure 4-3. Correlation between average values of fluorescence signal from Prestobleue assay and volume of spheroids from morphological images of spheroids treated

with MAPKi (n=14). R2 represent goodness-of-the-fit parameter. Different data points in each graph represent different drug concentrations. Only those concentrations that did not disintegrate the spheroids were used for the analysis.
..... 121

Figure 4-4. Cyclic drug treatment and recovery of tumor spheroids. (a) HCT116 spheroids were cyclically treated with inhibitors of MEK (0.01 μ M trametinib), ERK (0.15 μ M SCH772984), and RAF (1 μ M AZ628). (b-d) Kinetics of growth of spheroids during cyclical treatment and recovery. Each data point in the line graph is an average of 32 replicates. (e-g) Growth rate (k_c) of HCT116 spheroids during four treatment rounds with (e) trametinib, (f) SCH772984, and (g) AZ628. n=14 and * denotes statistically significant differences in the growth rates between treatment rounds. Error bars in panels (b-g) represent the standard error of a mean value. 122

Figure 4-5. Fold change in expression of proliferation genes in tumor spheroids during cyclic treatment and recovery with MEKi. The bar graphs show the fold change values of 10 prominent proliferation genes after treatments with (a) 10 nM trametinib, (b) 150 nM SCH772984, and (c) 1 μ M AZ628. The fold change values after R1, T3, and R3 are relative to T1. * denotes $p < 0.05$ when compared with T1.
..... 123

Figure 4-6. Activity levels of ERK1/2 and AKT proteins in tumor spheroids treated with inhibitors of MAPK pathway. (a) Western blots for phosphorylated and total levels of ERK1/2 and AKT at the end of T1. (b) Quantified results of p-ERK/t-ERK in

vehicle control and treated spheroids. (c) Quantified levels of p-AKT/t-AKT in vehicle control and treated spheroids. Results are shown as mean \pm standard error. Each Western blot experiment was repeated twice. * denotes $p < 0.05$ when comparing each treatment and the vehicle control. 124

Figure 4-7. Combination treatments of spheroids with inhibitors of MAPK and PI3K pathways. Heatmap plots representing fraction of cells affected (Fa) by single-agent and combination treatments of (a) trametinib/dactolisib, (d) SCH772984/dactolisib, and (g) AZ628/dactolisib. Heatmaps representing combination indices (CI) following combination treatments of spheroids with (b) trametinib/dactolisib, (e) SCH772984/dactolisib, and (h) AZ628/dactolisib. The combination concentrations resulting in greater cell death (larger Fa values) and higher synergy (smaller CI values) are boxed in the heatmaps of panels (a–f). This pair of concentrations from each pair of inhibitors was selected for Western blots of active and total ERK1/2 and AKT shown in panels (c, f and i). Bar graphs represent quantified *p*-ERK/*t*-ERK and *p*-AKT/*t*-AKT levels for single-agent and combination treatments. Each Western blot experiment was repeated twice. Results are shown as mean \pm standard error. * $p < 0.05$ denotes comparing single-agent MAPKi treatments with the vehicle control and also combination treatments with the corresponding single-agent MAPKi treatments. 125

Figure 4-8. Long-term single-agent and combination treatment/recovery of spheroids. (a) Size of spheroids under cyclic single-agent and combination treatments with

trametinib and dactolisib.. Inset images show spheroids from single-agent and combination treatments at the end of 32 days of culture. Scale bar is 250 μm . (b) Representative Western blots of active and total ERK1/2 and AKT for single-agent and combination treatments at the end of T1 and T3. Quantified levels of (c) p-ERK/t-ERK and (d) p-AKT/t-AKT. Western blot experiment was repeated twice. Each data point in the graph is an average of 32 replicates. Error bars represent standard error of the mean. 126

Figure 5-1. Inhibition of MAPK pathway in colorectal tumor spheroids (MAPKi). Dose-response curves of (a) HCT116 and (b) DLD1 spheroids to MAPKi. Ranking of MAPKi according to AUC analysis for spheroids of (c) HCT116 and (d) DLD1 cells. (e) LD₅₀ values of MAPKi against HCT116 and DLD1 spheroids. The symbol ‘-’ indicates lack of an LD₅₀ value. 145

Figure 5-2. Modeling drug resistance with cyclic treatment/recovery of spheroids. Growth kinetics of (a) HCT116 and (c) DLD1 spheroids treated with LD₅₀ concentrations of MAPKi (trametinib, SCH772984, and AZ628) for four treatment cycles T1, T2, T3, and T4 with recovery intervals R1, R2, and R3. Growth rates (k_c) of (b) HCT116 and (d) DLD1 spheroids during four cycles of treatments with MAPKi. * denotes statistically significant differences k_c values. n=32. Error bars in are standard error of a mean. 146

Figure 5-3. Phospho-level of AKT and STAT in MAPKi-treated spheroids. Representative blots for phosphorylated and total levels of AKT and quantified values of p-AKT/t-

AKT in (a) HCT116 and (b) DLD1 spheroids at the end of T1 phase. Western blots for phosphorylated level of (c) STAT1 and quantified value of p-STAT1/ β -actin in HCT116 spheroids and (d) STAT6 and quantified value of p-STAT6/ β -actin in DLD1 spheroids at the end of T1 phase. n=2. * denotes statistical significance measured at $p < 0.05$ between control and treatment..... 147

Figure 5-4. Phosphorylated levels of RTKs in MAPKi-treated spheroids. Phospho-RTKs in (a) vehicle control HCT116 spheroids or treated with 10 nM trametinib, 150 nM SCH772984, and 1×10^3 nM AZ628, and (b) vehicle control DLD1 spheroids or treated with 35 nM trametinib, 700 nM SCH772984, and 10×10^3 nM AZ628. Quantified levels of phospho-RTKs upregulated following treatments with MAPKi. The bar graphs show pixel density of each protein from treatments normalized with the respective vehicle control. Error bars are standard errors of mean values (n=2)..... 148

Figure 5-5. Inhibition of MEK1/2 and EGFR in colorectal tumor spheroids. Combination treatment of (a) HCT116 and (b) DLD1 spheroids with trametinib and neratinib and the respective single-agent treatments. AUC values from combination and single-agent treatments of (c) HCT116 and (d) DLD1 spheroids. Synergy plots show the combination index (CI) versus (1-viability) (Fa) by each concentration pair in (e) HCT116 and (f) DLD1 spheroids. 149

Figure 5-6. Molecular effects of simultaneous inhibition of MEK1/2 and EGFR in colorectal tumor spheroids. Combinations of trametinib and neratinib downregulate

p-ERK1/2 and p-AKT in (a) HCT116 and (b) DLD1 spheroids but are ineffective against (c) p-STAT1 in HCT116 cells and (d) p-STAT6 in DLD1 cells. 150

Figure 5-7. Cyclical treatment of single-agent and combination of spheroids. Volumes of (a) HCT116 and (b) DLD1 spheroids under cyclic treatments with trametinib, neratinib, and their combinations. n=32. Error bars are standard errors of the mean values. * on the single-agent treatments represents statistically significant difference with the combination drug treatments ($p < 0.05$). 150

Figure 5-8. Matrix invasion of colorectal tumor spheroids. Spheroids were treated with trametinib alone, neratinib alone, or their combination for 4 days before embedding them in the collagen matrix. Representative images of collagen invasion of vehicle control and pre-treated (a) HCT116 spheroids (b) and DLD1 spheroids after 5 days. Scale bar is 300 μm . Quantified invasion area/spheroid area for vehicle control and pre-treated spheroids of (c) HCT116 and (d) DLD1 cells. Error bars are standard errors of the mean values. n=4. 'ns' indicates no significant difference and $p < 0.001$ represents statistical difference at a 99.9% confidence interval. 151

Figure 5-9. Responses of colorectal tumor spheroids to EGFR inhibitors. (a) Dose-responses of (a) HCT116 spheroids and (b) DLD1 spheroids to molecular inhibitors of EGFR. (c) The EGFR inhibitors, their molecular targets, and LD_{50} values of these compounds against HCT116 and DLD1 tumor spheroids. The symbol '–' indicates dose dependent treatment did not reach the LD_{50} value. 152

Figure 5-10. Invasion of spheroids into collagen matrix. Spheroids were pre-treated with trametinib only, neratinib only, or their combination for 4 days before embedding them in a collagen matrix. Representative images of collagen invasion of vehicle control and pre-treated (a) HCT116 spheroids and (b) DLD1 spheroids after 3 days. Scale bar is 300 μm . Quantified invasion area/spheroid area for vehicle control and pre-treated (c) HCT116 and (d) DLD1 spheroids. Error bars are standard error of the mean. $n=4$. There was no collagen invasion of vehicle control and neratinib-treated HCT116 spheroids after 3 days. ‘ns’ indicates no significant difference. ‘ $p<0.05$ ’ and ‘ $p<0.001$ ’ represent statistical difference at 95% and 99.9% confidence intervals. 153

Figure 6-1. The schematic of parallel (top) and sequential (bottom) treatment regimens. 166

Figure 6-2. Cytotoxicity test with parallel and sequential combinations of MEK and PI3K inhibitors against HUVEC spheroids. (a) Viability of spheroids after T1 of parallel and sequential treatments. Inset images below shows live/dead staining of HUVEC spheroids following sequential (b, top) and parallel (b, below) treatment regimens. Scale bar is 250 μm 166

Figure 6-3. Parallel and sequential combinations in colorectal tumor spheroids. Viability of spheroids after T1 of parallel and sequential treatments in (a) DLD1 and (b) HCT116 tumor spheroids. Area under the curve (AUC) compares the two regimens. 167

Figure 6-4. Long-term parallel and sequential combinations of MEK and PI3K inhibitors against colorectal tumor spheroids of MEK and PI3K inhibitors. (a-f) Volume of spheroids is shown during parallel and sequential combination treatments of DLD1 and HCT116 spheroids. n=14 and * represent statistical significance at $p < 0.001$.
..... 168

Figure 6-5. Parallel and sequential combinations of trametinib and dactolisib against colorectal tumor spheroids. 4.37 nM/200 nM and 1.25 nM/200 nM drug pairs were used against DLD1 and HCT116 spheroids. Representative western blot of p-ERK1/2, t-ERK1/2, p-AKT, and t-AKT from spheroids of (a) DLD1 and (d) HCT116 cells after T1 and T2 of parallel and sequential treatments. Quantified p-AKT/t-AKT in (b) DLD1 and (e) HCT116 spheroids. Quantified p-ERK1/2/t-ERK1/2 in (c) DLD1 and (f) HCT116 spheroids. n=2. Error bars are standard errors of means. 169

LIST OF TABLES

Table 1-1. Major spheroid forming techniques.....	18
Table 2-1. List of anticancer compounds and their main targets	50
Table 2-2. Actionable mutations in target cell lines.....	50
Table 2-3. Pearson’s correlation coefficient shows relationship between dose-dependent decrease in viability of U-87 mg and HT-29 spheroids and their growth inhibition by different inhibitors.....	51
Table 2-4. Classification of strength of compounds according to their resulting SSMD values.....	51
Table 3-1. List of MAPK inhibitors and their targets.....	87
Table 3-2. List of PI3K inhibitors and their targets	87
Table 3-3. IC ₅₀ values of molecular inhibitors against HT-29 spheroids measured after 6 days of treatment.....	87
Table 3-4. The ranges of combination index, and description of each range of CI values as described by Chou and Talalay.....	88
Table 3-5. Growth rates of HT-29 spheroid for control, single agent, and combination treatment.....	88

Table 3-6. Growth rates of HT-29 spheroid for control, single agent, and combination treatment.....89

Table 4-1. List and sequence of primers for 10 genes that were analyzed in spheroids treated with mapk inhibitors. 118

Table 4-2. Combination treatments with (a) trametinib and dactolisib, (b) SCH772984 and dactolisib, and (c) AZ628 and dactolisib. The quantities in the vertical and horizontal directions represent the coefficients of LD₅₀ for each compound used in combination treatments. The fraction of LD₅₀ of drug pairs used in combination is shown inside the bracket in each table (a-c). The concentration pairs that resulted in disintegration of spheroids are highlighted in red..... 119

CHAPTER I

INTRODUCTION

Portions of this chapter are reused from:

P. Shahi Thakuri, C. Liu, G. D. Luker, and H. Tavana, “Biomaterials-Based Approaches to Tumor Spheroid and Organoid Modeling,” *Adv.Healthcare.Mater*, vol. 7, no. 6, pp. 1700980, March. 2018. © 2017 by WILEY-VCH Verlag GmbH & Co. KGaA, Weinheim. <https://onlinelibrary.wiley.com/doi/full/10.1002/adhm.201700980>

“Synergistic Inhibition of Kinase Pathways Overcomes Drug Resistance of Colorectal Cancer Spheroids To Cyclic Targeted Therapies.,” *ACS Pharmacol. Transl. Sci.*, vol. 2, no. 4, pp. 275–284, July. 2019. Copyright @ 2018 by ACS Pharmacology and Translational Science. Reprinted by permission of ACS publications. <https://pubs.acs.org/doi/abs/10.1021/acsptsci.9b00042>

1.1 Significance

The National Cancer Institute estimated 1,762,450 new cases and 606,880 deaths from cancer in the United States in 2019. [1] In addition to significantly affecting the quality of life of patients, cancer poses a major economic burden both to patients’ families and the healthcare system. The overall mortality due to cancer has however declined since 1990. The most recent Surveillance, Epidemiology, and End Results Program (SEER) cancer statistics review released in 2018 showed that mortality from cancer decreased by 1.8% in men from 2006 to 2015, and by 1.4% in women from 2006 to 2015. This is due to the decline in the mortality caused by common types of cancer such as lung, colorectal, breast, and prostate. This improvement is attributed to the development of novel screening tools and treatment modalities for cancer. Despite improvements in cancer treatments and

overall reduced mortality, 23.6 million new cancer diagnosis are estimated by 2030 worldwide (estimated new cases of cancer in 2018 was 17 million). [2]

Historically, cancer treatment has relied on surgery, radiation, and cytotoxic chemotherapy. Surgery and radiotherapy have been used for the treatment of solid cancers since 1960s. Chemotherapy involves using chemical compounds that target actively proliferating cancer cells by interfering with cell cycle and preventing DNA repair mechanisms, thereby causing cell death. Unfortunately, chemotherapeutics also block cell cycle of normal cells, resulting in non-specific activity and excessive toxicity to normal cells and tissues. [3] The failure of chemotherapy is in part due to the lack of specificity to cancer cells. Another complexity of treating cancer is the lack of early diagnosis. Often at the point of diagnosis of many cancers, malignant cells have already metastasized, making the disease incurable. The development of cancer biomarker screening tools has improved diagnosis of cancer. [4], [5] Timely surgical removal of precancerous lesions also increase the likelihood of treatment success.

Significant developments in genomic and proteomic analysis of tumors have broadened our understanding of the disease. It is now well recognized that tumors are often highly heterogeneous in their composition of cancer cells and vary significantly from one patient to another despite having the same type or even subtype of cancer. [6] These tools have led to the identification of molecular drivers of cancer to shift treatments from cytotoxic chemotherapy toward personalized medicine where type of disease guides treatments with targeted drug compounds. [7] The use of targeted therapies over the last two decades has revolutionized cancer treatment. Development of targeted therapies have decreased cancer death rate among the most common forms of cancer but mortality rate

from other, less common types of cancer has not changed or has even increased. [8] Despite significant investment in developing targeted drugs, these drugs fail by 85-95% due to toxicity to normal tissue, compromised immune system, relapse of tumor, and drug resistance. [9]

Drug resistance has emerged as a major cause of failure of targeted therapies because cancer cells have the ability to adapt to the treatments by developing therapy escape mechanisms. [10] Drug combinations have improved the outcome of treatments by overcoming adaptive drug resistance, but this approach often falls short to reduce failure rates of targeted therapies due to significant toxicity to cancer patients. [11] Early diagnosis, understanding mechanisms of drug resistance in a patient-specific manner, and using rational drug combinations guided by molecular mechanisms of the disease are of paramount importance to reduce the failure rates of targeted therapies.

1.2 Drug Resistance

Cancer is heterogeneous disease with genetically different sub-populations of cells within the tumors (spatial heterogeneity), and sub-populations of cells that evolve with time adding to the cellular variations (temporal heterogeneity). [12], [13] The complex spatial and temporal tumor heterogeneities can be examined by multi-region sequencing, single-cell sequencing and analysis of biopsy samples. [14]–[16] Sampling of heterogeneous tumors allows identifying “actionable mutations” of clonally dominant populations. [17] Therapeutic targeting of “actionable mutations” of dominant populations in the bulk of tumors is a major strategy to treat tumors but it may not be sufficient to completely eradicate the tumors because of small sub-populations of cells resistance to the

targeted therapy used. The sub-population of cancer cells that do not respond to the targeted drugs proliferates, leading to tumor growth again, [18] primarily due to the selective pressure of targeted drugs that results in the sub-clonal selection and development of drug resistance. This phenomenon is common with targeted inhibition of oncogenic pathways in cancer. Although the approach of targeted therapy produces initial success, it often leads to the growth of resistant cancer cells and adaptation of cancer cells to the drugs through various mechanisms. [19], [20]

Resistance to targeted drugs can be categorized as intrinsic and acquired resistance. [10], [21] The resistance may be pre-existent or induced by drug treatments (acquired). The schematic in Figure 1-1 shows targeting of a dominant green population. A pre-existing resistant sub-population shown in red survives the treatment to later grow and develop tumors. The pre-existent drug resistance is also referred to as *de novo* resistance or quick adaptive response. On the other hand, the sensitive sub-population under selective pressure may develop into entirely different clones, shown in purple and yellow, and resist the therapy. These sub-populations acquire drug resistant phenotypes/genotypes, rendering treatments ineffective. Secondary or acquired resistance generally occurs in cancer patients after prolonged exposure to anti-cancer drugs. A large body of evidence suggests that acquired resistance to targeted agents could be through both the selection of cell clones with oncogenic mutations and development of new mutations. The drug-induced selective pressure may lead to further genetic modifications such as gene amplification, deletion, or point mutations to allow cancer cells to utilize alternative survival pathways, thus inducing acquired resistance. [22] Major causes of resistance to targeted therapies are briefly outlined in the subsections below.

1.2.1 Target Mutation

The mutation of functional targets or alteration in drug binding sites prevents drug from binding to its therapeutic target. [23] These mutations are known to exist at relatively low frequencies before drug treatment and undergo positive selection during exposure to targeted therapies. [24], [25] Therefore, the originally active oncogenic kinase continuously activates the downstream signaling pathways despite the presence of inhibitors. For example, EGFR T790M mutation was observed in more than 50% of patients with lung cancer that resulted in acquired resistance to gefitinib or erlotinib. [26], [27] Similarly, V211D mutation in MEK1 caused resistance to the MEK inhibitor, binimetinib, in *BRAF*^{K601E} colorectal cancer by both increasing the catalytic activity of MEK1 and reducing its affinity for the drug. [28]

1.2.2 Bypass Mechanism

The second category involves activation of alternative signaling routes independent of the drug target, also known as bypass mechanism, to resist inhibition of drug target. This occurs by two mechanisms: 1) mutation in serine or threonine kinase of parallel signaling pathway, 2) activation of receptor tyrosine kinases (RTKs) (by itself or through feedback regulation). Resistance to the inhibitors of RTKs, and MAPK and PI3K pathways is commonly initiated by activation of bypass pathway.

For example, whole genome sequencing of melanoma tumors showed 22% mutation in PI3K/PTEN/AKT pathway with acquired resistance to BRAF inhibition. [29] Similarly, resistance to inhibition of an oncogenic RTK occurs by activation of other RTKs to sustain downstream kinase signaling. For example, despite inhibition of oncogenic EGFR, non-small cell lung cancers (NSCLC) rely on MET to reactivate downstream

kinase signaling such as PI3K/AKT and MEK/ERK. A clonal analysis revealed presence of pre-existing resistant population (1%) harboring MET amplification in pre-treatment samples, which indicated the possibility of cells existing at low frequency before the treatment. [30] The bypass mechanism may happen due to ligand-induced activation or amplification of RTKs. Colorectal cancer patients undergoing treatment with anti-EGFR monoclonal antibody resisted the treatment by upregulating expression of *MET* receptor. [31] Furthermore, activation of TGF- β that modulated epithelial-mesenchymal transition (EMT) of cancer cells and immune response conferred resistance to tyrosine kinase inhibition in multiple cancer types. [32]

1.2.3 Pathway Re-activation by Alteration in Upstream and Downstream Signaling

-Negative feedback loop

RTKs are the transmembrane proteins that relay signaling from the extracellular to the intracellular space by activating several downstream signaling pathways that regulate cellular processes such as cell migration, survival, proliferation and differentiation. For example, the ligand induced activation of EGFR activates downstream RAS/RAF/MEK/ERK pathway. The ERK kinase induces negative feedback loops to suppress the EGFR signaling. This means that when RAS/RAF/MEK/ERK pathway is inhibited, RTK signaling is elevated, hence diminishing the effect of inhibitors. [33]

The relieve of negative feedback loops is a means of drug resistance, specially against the inhibitors of MAPK and PI3K pathways. For example, inhibition of PI3K pathway in breast and ovarian cancer resulted in release of the negative feedback mechanism, causing enhanced signaling due to more than one ErbB RTK family proteins. [34], [35] Moreover, ErbB and/or IGFIR signaling were activated in several cancer types

post MEK inhibition. [36], [37] The inhibition of MEK relieved MAPK-dependent feedback on the pathway and induction of RTK signaling. [38] Furthermore, BRAF-mutant colorectal cancer showed resistance to BRAF inhibitor, vemurafenib. The suppression of ERK activity by inhibition of BRAF led to increased signaling output from RTKs that restored the ERK signaling. [39], [40]

-Downstream signaling activation

Colorectal cancer patients initially respond to anti-EGFR therapy. However, the suppression of EGFR resulted in alteration in downstream kinase proteins and activation of downstream signaling pathways despite inhibition of EGFR. For example, colorectal cancer resisted cetuximab or panitumumab (EGFR monoclonal antibodies) treatment as a result of downstream pathway activation by somatic mutation in *KRAS*. [41], [42] In addition, colorectal cancer patients that initially responded well to anti-EGFR therapy showed amplification or focal mutation in *KRAS* resisted anti-EGFR therapy resistance . [43]–[45]

1.2.4 Tumor Microenvironment

In addition to genetic composition (tumoral heterogeneity), the tumor microenvironment significantly contribute in shaping tumor evolution. [46] The tumor microenvironment consists of blood vessels/capillaries, inflammatory cells, fibroblasts, immune cells, soluble and surface-bound signaling molecules, and the extracellular matrix proteins. Interactions of tumor cells with different cells and the extracellular matrix in the tumor microenvironment promote growth of tumors and contribute to the resistance to targeted therapies. [47] Studies using genetic manipulation techniques targeting a single gene in cancer cells do not recapitulate the complex interactions of the tumor and its stroma

(microenvironment). For example, data from animal studies show that resistance to vascular endothelial growth factor receptor (VEGFR) inhibitor is evicted when VEGFR-resistant tumor tissue is re-implanted into untreated mice. This suggests that resistance to some extent is related to the alteration in tumor microenvironment, enabling re-establishment of angiogenesis. [48] This establishes the importance of incorporating components of the tumor microenvironment and dissecting the role of the tumor microenvironment in mediating drug resistance.

Various studies have developed models of interactions among connective tissue cells (also known as stromal cells) and tumor cells *in vitro* and demonstrated that these interactions promote tumor invasiveness and drug resistance of several cancer types. A study demonstrated diminished effect of targeted drugs on cancer cells when co-cultured with stromal cells. [49]. The stromal cells secreted hepatocyte growth factor that bound to MET receptors resulting in reactivation of the MAPK and PI3K/AKT pathways in cancer. [49] In addition, the extracellular matrix plays a vital role in drug resistance of cancers. Targeting ECM is a potential strategy to overcome cancer progression and overcome drug resistance. [50]

1.3 Models of Drug Resistance

Identifying early onset of drug resistance is important to design new and effective therapies. Preclinical models are often used to identify molecular basis of resistance to molecular agents and to design and test novel therapeutic strategies for clinical translation. In general, acquired resistance can be modeled by the following methods: 1) Genetic manipulation of model genotypes of acquired resistance: Genetic changes can be

accomplished by introducing oncogenes using transfection/transduction methods. Transient transfection is used to study short-term resistance, whereas permanent transfection is performed to study long-term drug resistance; 2) *In vitro* and *in vivo* selection of tumor models: An *in vitro* or *in vivo* selection method is created by continuously exposing cells in 2D culture or mouse to cancer drugs to generate resistant clones. This selection method is a lengthy process and can take approximately 3-6 months. [51] The commonly used preclinical models of drug resistance are discussed below.

1.3.1 2D Cell Model

Cancer cell lines in 2D cultures have been widely used to investigate biological properties of tumors. Major advantages of 2D cell models are as follows. First, cancer cell lines can be maintained for long periods of time via serial passaging. [52] Second, they are relatively easy to manipulate to investigate the role of a particular gene in cancer development by reducing its expression or overexpressing it via gene transfection/transduction. [52], [53] Third, there are a wide variety of cancer cell lines that represent cancers of many different types and are easily accessible commercially and readily available for cancer research and drug discovery purposes. [54] Although the 2D model is convenient to use, several limitations of 2D cultures of cancer cell limit their use in cancer research. [55] First, 2D cultures lack spatial heterogeneity present in solid tumors. The ability of cancer cell lines to proliferate long-term *in vitro* is likely due to various genetic alterations, most of which may not be present in primary cells. In native tumors, cancer cells interact and stromal cells (immune cells, fibroblasts) to regulate tumor progression. However, 2D cancer cell cultures do not represent architecture of tumors and interactions in the microenvironment including cell-cell and cell-ECM interactions. [56]

These disadvantages of 2D cultures of cancer cells underline the need for alternative tumor models to study drug resistance.

1.3.2 Mouse Model

Most commonly-used animal models are genetically engineered mouse tumor models (GEMs) or patient-derived tumor xenografts (PDX). GEMs are created either by knocking down tumor suppressor genes or inducing tumor oncogenes, or by combining both methods to determine the effects of various genetic interactions during tumorigenesis. [57] GEMs are immunocompetent and can be used to investigate resistance to immunotherapy drugs. [57] On the other hand, PDX models are generated by implanting surgically resected tumors from cancer patients into immunodeficient mice. PDX can be generated either in the anatomical position of patient tumor (orthotopically), or in a different location that is not related to the patient tumor (heterotopically). [58] PDX are frequently used to study both intrinsic and acquired drug resistance. LLC (Lewis Lung Carcinoma) tumor was engrafted in mouse to mimic clinical setting of Lewis lung carcinoma lymphoma to study resistance to an anti-VEGF monoclonal antibody. [59]

Although animal models mimic physiology of native solid tumors, they have several disadvantages. The GEMT model does not faithfully recapitulate the human cancer in terms of the genetics and histology of human cancers, and microenvironmental factors, including stromal cell components and an immune system, limiting its utility. Additionally, the generation of GEMT models are both costly and time consuming. It generally takes up to eight months to develop GEMT. With the shift in cancer treatments towards personalized therapies, many patients can not wait for very long time due to seriousness of their disease. Also the success of engraftment depends on tumor types. [60] For example the engraftment

rate of breast and renal cell carcinoma in nude mice strain was less than 15%. [61], [62] The development of PDTX models requires the use of immunodeficient mice that are costly to generate. In addition, the shortage of tissue biopsies is another concern to generate PDTX. [60] To overcome these shortcomings of animal models and 2D cell cultures, there is a need for novel preclinical models of drug resistance.

1.3.3 3D In-vitro Model

The need for better *in vitro* cancer models has fueled intense research both in academia and in industry. This has led to three-dimensional (3D) models for basic cancer research and drug discovery applications. [63] These models, which are generated using different technologies, offer various degrees of complexity including self-assembled and freestanding spherical aggregates of cancer cells as cellular spheroids, tumor spheres, organotypic spheroids, matrix-mediated assembled cellular aggregates, multilayered cultures of cancer cells or tumor slices, organoids, and microfluidics-assisted and microfabricated-mediated cultures of cancer cells. [64]–[70] In addition, spheroids generated using different technologies have several advantages and disadvantages. The pros and cons of some spheroid forming techniques are listed in Table 1-1.

Importantly, inclusion of various stromal cells (such as carcinoma-associated fibroblasts, immune cells, and vascular cells), addition of matrices of generic or defined compositions, modulation of mechanical and biochemical properties of the stroma, and generation of physiologic levels of fluid flow have all been demonstrated in a broad range of studies. These 3D *in vitro* models for drug resistance have been used to mimic tumor microenvironments and are promising to study resistance to therapeutic compounds. However, with the increasing complexity of the system, it is difficult to address the role of

individual components that mediate drug resistance. In this work, we will demonstrate the use of spheroid model to model resistance to targeted therapeutics.

1.4 Spheroid Model

Cancer cell spheroids, also known as multicellular spheroids or tumor spheroids, are the simplest *in vitro* model of solid tumors. Spheroids are generated due to the inherent property of epithelial cancer cells to form intercellular adhesions and self-assemble into a compact aggregate on a non-adherent surface or within a 3D matrix. Spheroids of different sizes ranging from a few tens of microns to a millimeter in scale can conveniently be made. The 3D morphology of spheroids mimics avascular tumors in terms of close cell-cell and cell-ECM adhesions, exposure of cells within a spheroid to non-uniform concentrations of soluble factors, low oxygen tension in the core of a spheroid resulting in hypoxic, slow cycling, and dormant cells, and an acidic extracellular environment. These properties are implicated in a wide range of biological processes in cancer as highlighted with the following examples: loss of cell-cell contacts through downregulation of cadherin junctions and catenins allows detachment of cancer cells from a tumor mass, enabling transition of the cells to a migratory, mesenchymal-like state to facilitate metastasis; [71], [72] cancer cell-ECM signaling mediated by adhesion complexes promotes cell proliferation and survival; [73] dynamic cell-ECM adhesion and detachment through integrins leads to traction forces connecting the matrix to actomyosin filaments to facilitate cancer cell migration; [74], [75] a hypoxic tumor environment promotes cancer stem cells with the ability to repopulate a tumor mass and resist drug treatments; [76], [77] and low pH in the acidic extracellular environment reduces the uptake of weakly basic drugs, such

as doxorubicin, conferring resistance to chemotherapy. [78] Additionally, spheroids offer the flexibility of incorporating different stromal components to accommodate studies on how physical interactions between cancer cells and tumor stroma and intercellular signaling regulate tumor growth, angiogenesis, invasion, and drug resistance. Therefore, despite being a relatively simple model, spheroids are inherently suited for a broad range of tumor biological studies to understand mechanisms of drug resistance.

1.5 Aqueous Two-Phase Systems (ATPS) Technology

Aqueous solutions of various polymers, including polyethylene glycol (PEG) and dextran (DEX), above certain concentrations phase separate and give two immiscible, highly aqueous phases. [79] PEG–DEX ATPS provide a mild environment for various cells, including cancer cells. ATPS have been widely used for cell and biomolecule micropatterning applications. [80] The PEG–DEX ATPS was used to develop a scaffold-free approach to conveniently generate spheroid cultures of cancer cells. The denser aqueous DEX phase solution containing cancer cells was dispensed as a submicroliter drop into a nonadherent microwell containing the immersion aqueous PEG phase. [81], [82] An ATPS was formulated with specific concentrations and molecular weights of PEG and DEX to result in an ultralow interfacial tension of 0.012 mJ m^{-2} between the two aqueous phases and effectively partition cancer cells to the DEX phase drop. [83] Confinement of cancer cells within the nanodrop promoted their self-assembly and aggregation into a single spheroid within 24 h of incubation. This technique is versatile to form co-cultures of stromal cells with cancer cells to study interactions of tumor-stromal signaling. The co-culture model of cancer-associated fibroblast (CAFs) and triple negative breast cancer

(TNBC) cells established that tumorigenic potential of TNBC cells is modulated by CAFs through activating MAPK and PI3K signaling pathways. [84] A more physiological organotypic model of TNBCs was established by encapsulating cancer spheroids in collagen that has dispersed stromal cells. [85] The stromal cells increased the tumor invasiveness by activating signaling molecules such as ERK and AKT.

Throughout this PhD project, we used colorectal cancer as the disease model to study drug resistance. However, the drug resistance studies can be extended with spheroids of other cancer cells as demonstrated by the versatility of ATPS to form spheroids from several cells lines. [86]

1.6 Colorectal Cancer

Colorectal cancer is the third common cause of deaths due to cancer in the United States. [87] According to a genome scale analysis of human colorectal tumors by the Cancer Genome Atlas Network in 2012 and an international consortium in 2015, [88], [89] around 50% of colorectal cancers contain frequent mutations in RAS and RAF and 25% have mutation in PI3K/AKT pathway (Figure 1-2). These mutations lead to hyper-activation of highly conserved RAF/MEK/ERK and PI3K/AKT signaling pathways, leading to uncontrolled proliferation, growth, and survival of colorectal cancer cells. Targeted drugs are developed to target mutations in RAF and PI3K. However, there are currently no available targeted drugs for RAS. In normal cells, RAS is central to activation of many receptor tyrosine signaling-mediated intracellular kinase signaling pathways. For example, binding of epidermal growth factor (EGF) to EGFR leads to the autophosphorylation of EGFR on several tyrosine sites. The binding of Grb2/Sos complex

to these phosphorylated tyrosine sites catalyzes RAS GTP/GDP exchange leading to the activation of RAS, ultimately stimulating a cascade of protein kinases of MAPK and PI3K signaling pathway. [90] Given the lack of targeted therapies against RAS, strategies to target signaling downstream of RAS such as RAF, MEK, and ERK or PI3K, AKT, and mTOR are developed. However, these strategies have been largely unsuccessful. For example, although MEK and RAF inhibitors (MEKi and RAFi) suppress growth of colorectal tumors *in vivo*, [91], [92] cancer cells often develop resistance to these inhibitors (Figure 1-3) through several potential mechanisms: (i) Activation of signaling pathways such as PI3K/AKT/mTOR or JAK/STAT mediates resistance to MEKi; [93] (ii) Feedback activation of RTKs such as EGFR, epidermal growth factor receptor 2 (HER2), and epidermal growth factor receptor 2 (HER3) causes resistance to RAFi and MEKi; [94]–[96] (iii) Continuous exposure to a MEKi may lead to mutation of MEK; [97] (iv) Continuous exposure to RAFi may lead to amplification of B-RAF or other components of the MAPK pathway. [98], [99] To overcome resistance to a single targeted agent, combining MAPK and PI3K inhibitors showed promising results against tumors during preclinical trials, but this strategy was largely unsuccessful due to toxicity to the patients. [100] The failure in part reflects the lack of preclinical models to study and predict drug resistance and toxicity. Physiologically relevant tumor models will help understand mechanisms of drug resistance and serve as a valuable tool to develop treatment strategies to overcome resistance with minimal or no toxicity. In this work, we focused on colorectal cancer cell lines harboring KRAS and BRAF mutations because these mutations are present in nearly 50% of the total mutation in colorectal cancer. (Figure 1-2) We explored

therapeutic targeting of kinase pathway downstream of RAS, i.e., RAF/MEK/ERK kinases in these cell lines to model drug resistance and develop strategies to overcome it.

1.7 Aims and Scope

In this doctoral dissertation, we established the broad utility of our ATPS 3D tumor spheroid model to study resistance to targeted therapies. Our 3D tumor model offers a unique approach to study adaptive resistance to targeted drugs and identify effective treatment strategies. We will (i) perform high throughput cancer drug screening and molecular analysis of drug responses of tumor spheroids, ii) model adaptive drug resistance of cancer cells using cancer spheroids, and iii) identify effective treatment regimens to overcome drug resistance. The feasibility of using tumor spheroids to evaluate treatment responses will be demonstrated through different phases of this work. Validation of high throughput screening, long-term growth, and molecular analysis to correlate the cellular responses and molecular targets of drugs in spheroids will be presented in Chapter II. We will demonstrate high throughput generation of consistently-sized tumor spheroids in 384 micro-well plates using multiple cells lines, perform long-term growth and biological characterization of spheroids, conduct high throughput screening of anti-cancer drugs against spheroids of multiple cell lines, and employ multi-parametric and statistical approaches to quantify cellular responses to the drug compounds used both in single-agent and combination treatments. It is necessary to culture spheroids for long periods of time to study adaptive resistance to cancer drugs. In chapter III, we will establish a long-term cyclic treatment model to predict development of drug resistance by culturing spheroids for ~30 days. Despite initial efficacy of drug compounds, we will demonstrate adaptive resistance

to cyclic treatments. Molecular analysis during various stages of treatment and recovery will identify molecular drivers of drug resistance, enabling design of rational combination drug treatment strategies against colorectal cancer cell in 3D cultures. We will demonstrate that a rationally-designed combination approach is essential to suppress long-term growth of tumor spheroids.

Combination of drugs often result in toxicity. One approach to reduce toxicity is to identify low-dose combination concentrations. In chapter IV, we will demonstrate a matrix-based drug combination approach using inhibitors of MAPK and PI3K pathways to find low combination concentrations of these drug inhibitors. We will show that this approach effectively inhibits growth of tumor spheroids by blocking MAPK and PI3K signaling during long-term cyclical treatment. An alternative strategy to overcome resistance to MAPKi will be established in Chapter V. We will demonstrate upregulation of EGFR following MAPK inhibition and that combined inhibition of MEK and EGFR synergistically suppress growth and invasiveness of colorectal tumor spheroids. Toxicity of drug combination is a major challenge in cancer treatment. In Chapter VI, we will demonstrate testing and identifying multiple drug combination strategies to potentially decrease toxicity in normal cells. Major conclusions of this dissertation and directions for future work will be presented in Chapters VII and VIII, respectively.

Table 1-1. Major spheroid forming techniques

Spheroid generating technique	Pros	Cons
Rotary vessel/Spinner flask	Simple, multiple spheroids formation, and suitable long-term culture	Non-uniform spheroids, incompatible for high throughput screening
Hanging drop array	Uniform and single spheroid formation per drop, compatible with robotic liquid handler, and suitable for co-culture	Tedious, require special plates, and incompatible with plate readers
Liquid overlay microplate	Simple, easy-to-use, high throughput, suitable for use with robotic handlers and plate readers	Non-uniform and multiple spheroid formation
Aqueous two-phase system (ATPS)	Uniform single spheroid formation per well, high throughput, compatible with robotics, suitable for heterotypic cultures, and compatible with plate readers	Require optimization of liquid handling dispensing at sub-microliter volume
Microfabricated microwell array	Uniform and single spheroid formation per well, and high throughput	Special requirement for fabrication, lack compatibility with plate readers, and robotics

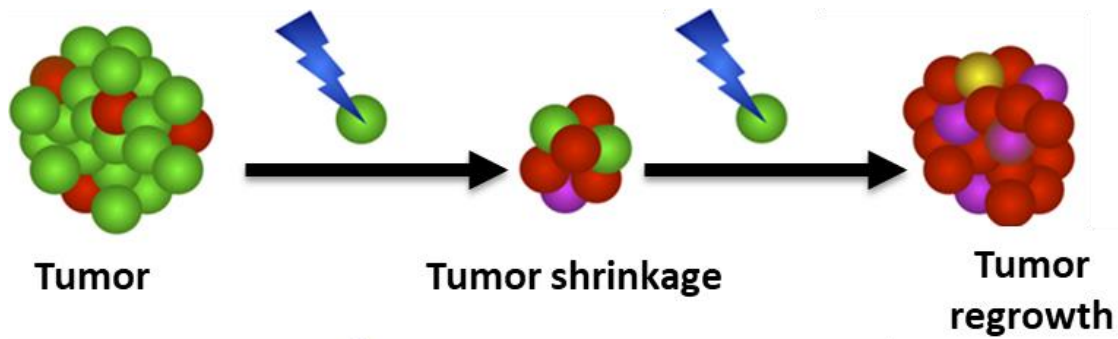


Figure 1-1. Schematic of pre-existing and treatment induced resistance to targeted therapies in cancer treatment. Sensitive population (green), pre-existing resistant population (red) and treatment induced resistance (purple and yellow). (Adapted from Colombino M et.al, *J Carcinog Mutagen* 2014)

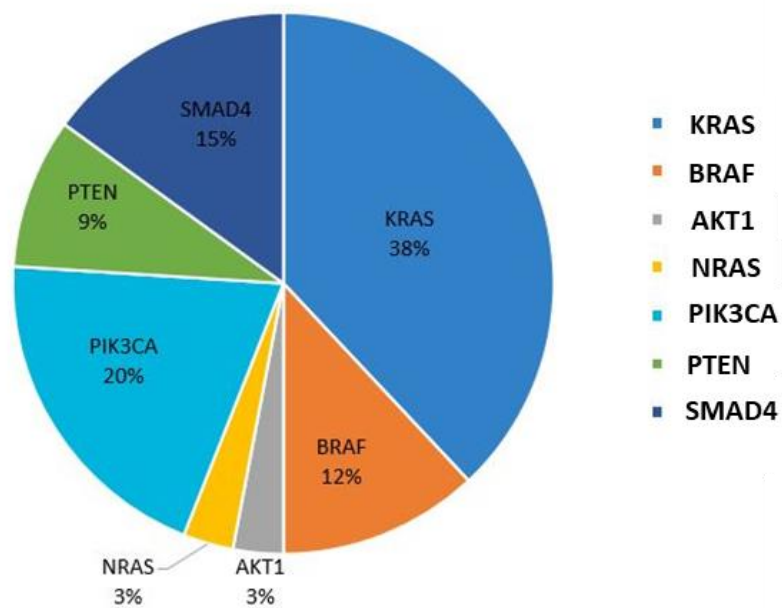


Figure 1-2. Mutational status of colorectal cancer. (Adapted from <https://oncodesc.com/colorectal-cancer/>)

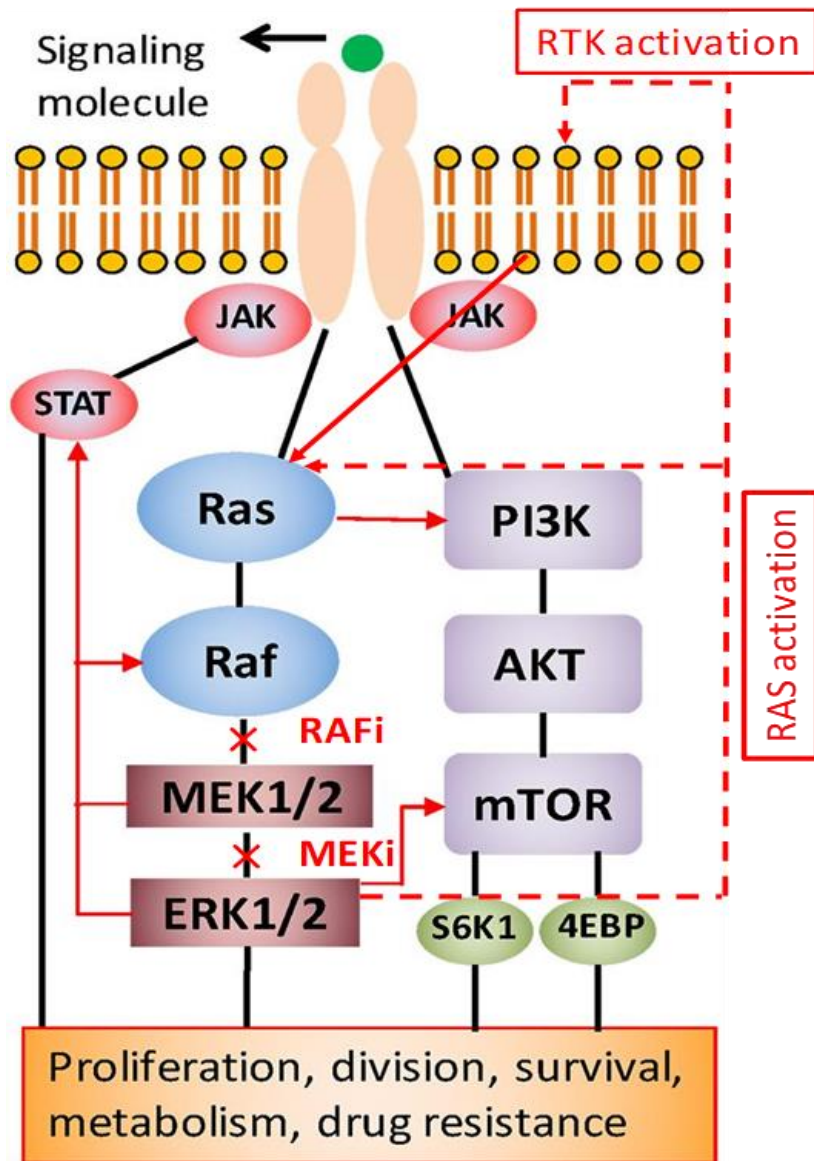


Figure 1-3. Potential mechanism for activation of signaling pathways in cancer that leads to drug resistance.

CHAPTER II

MULTIPARAMETRIC ANALYSIS OF ONCOLOGY DRUG SCREENING WITH AQUEOUS TWO-PHASE TUMOR SPHEROIDS

Portions of this chapter are reused from:

1. P. Shahi Thakuri, S. L. Ham, G. D. Luker, and H. Tavana, "Multiparametric analysis of oncology drug screening with aqueous two-phase tumor spheroids," *Mol. Pharm.*, vol. 13, no. 11, pp. 3724–3735, Nov. 2016. Copyright © 2016 by Molecular Pharmaceutics. Reprinted by permission of ACS publications. <https://pubs.acs.org/doi/abs/10.1021/acs.molpharmaceut.6b00527>
2. P. Shahi Thakuri and H. Tavana, "Single and combination drug screening with aqueous biphasic tumor spheroids," *SLAS Discov.*, vol. 22, no. 5, pp. 507–515, Jun. 2017. Copyright © 2017 by SLAS Discovery. Reprinted by permission of SAGE publications. <https://journals.sagepub.com/doi/10.1177/2472555217698817>
3. P. S. Thakuri, M. Gupta, M. Plaster, and H. Tavana, "Quantitative Size-Based Analysis of Tumor Spheroids and Responses to Therapeutics," *Assay Drug Dev. Technol.*, vol. 17, no. 3, pp. 140–149, Apr. 2019. Copyright © 2019 by Assay and Drug Development Technologies. Reprinted by permission of Manny Ann Libert, Inc Publications. <https://www.liebertpub.com/doi/abs/10.1089/adt.2018.895>

Cell cultures introduced as a tool for compound screening in the 1950s are essential for the process of oncology drug discovery. [101] In preclinical studies, monolayer (2D) cultures of cancer cells are routinely used to assess efficacy of hundreds of candidate drug compounds. However, due to major differences between 2D cultures and three dimensional (3D) tumor microenvironments of cancer cells *in vivo*, 2D cultures often fail to predict drug activities *in vivo*. [102] This significantly increases attrition rates and costs of anticancer drug development. [103] Despite considerable investments, the rate of introduction of novel drugs has remained relatively constant over the past few decades and only two to

three agents in new drug classes make it to the market annually. [104]–[106] To improve drug discovery outcomes, it is critical to employ cellular models that mimic structural, biological, and functional properties of tumors. [107] Spheroids are 3D compact clusters of cancer cells that model avascular parts of solid tumors in terms of close cell-cell contacts, matrix deposition by cells and cell-matrix interactions, diffusion limitations of oxygen, nutrients, metabolites, waste products, cell migration, [108] and gene expression profiles of parent tumors. [109]–[115] Despite their clear benefits, spheroids are not routinely used in compound screening applications for anticancer drug discovery. Most spheroid culture techniques face difficulties with mass production of consistently-sized spheroids in standard labware, compatibility with robotic instruments for automation of standard drug testing protocols, ease of culture, maintenance, treatment, and analysis of cellular responses. These difficulties hamper the use of spheroids in mainstream drug development and discovery. [56] To overcome this barrier, we recently developed a tumor spheroid microtechnology based on the use of a polymeric aqueous two-phase system (ATPS) with polyethylene glycol (PEG) and dextran (DEX) as phase-forming polymers. [83], [116], [117] Using an optimized robotic liquid handling protocol, a submicroliter drop of the denser aqueous DEX phase containing cancer cells is dispensed into the immersion aqueous PEG phase in each well of standard microwell plates. Due to an ultralow interfacial tension between the aqueous PEG and DEX phases, [118] cells remain confined within the drop phase and spontaneously self-assemble into a single, fully viable spheroid. [83] Spheroids within each plate are individually addressable with drug compounds, enabling testing of multiple drugs over a wide concentration range. Unlike several other methods, the use of standard labware and robotics with the ATPS technology significantly

simplifies formation, maintenance, drug treatment, and *in situ* optical and biochemical analysis of spheroids. To establish the feasibility of incorporating the robotic ATPS tumor spheroid microtechnology into drug screening applications, we conducted a comprehensive high-throughput screening of 25 different anticancer compounds against tumor spheroids of colorectal cancer, glioblastoma multiforme, and triple negative breast cancer (TNBC) cells. We conducted drug testing, renewal, addition of biochemical analysis reagents, and analysis of cellular responses sequentially in the same 384-well plate in which spheroids formed initially. To show the broad utility of this technology, we selected the collection of compounds to contain both cytotoxic chemotherapeutics and molecular inhibitors. In addition to demonstrating the capabilities of robotic drug testing with this microtechnology, we evaluated drug responses of cancer cells in spheroids using two different approaches. First, we analyzed dose-dependent responses of drug-treated tumor spheroids using a multiparametric approach based on drug efficacy (E_{\max}), potency (IC_{50}), and the area under the dose-response curve (AUC). This approach helped rank all compounds tested against spheroids of each of the three cancer cells and identify the most effective compounds against each cell type. Second, we used morphological changes such as growth inhibition and disintegration of spheroids after drug exposure as an independent measure of effectiveness of certain compounds. Finally, we performed a target validation study using protein expression analysis to confirm that phenotypic screening results from testing of specific molecular inhibitors were indeed due to on-target effects of drug compounds. Through this comprehensive set of tests and analyses, we substantiated that the robotic polymeric ATPS approach to 3D culture of cancer cells is uniquely suited for

high-throughput compound screening and molecular analysis to significantly expedite the discovery of effective anticancer drugs.

2.1 Materials and Methods

Below, the ATPS spheroid technology is discussed detailing formation and maintenance of tumor spheroids, drug testing of spheroids, multi-parametric analysis of drug response of treated spheroids, and molecular analysis of drug treatments.

2.1.1 Cell Culture

Three different lines of cancer cells were used. MBA-MB-157 breast cancer cells (ATCC), HT-29 colorectal cancer cells (ATCC), and U-87 MG brain cancer cells (ATCC) were maintained in Dulbecco's Modified Eagle Medium (DMEM), McCoy's 5A, and Eagle's Minimum Essential Medium (EMEM), respectively, each supplemented with 10% fetal bovine serum (FBS, Sigma), 1% antibiotic (Life Technologies), and 1% glutamine (Life Technologies). Cells were cultured in a humidified incubator at 37 °C and 5% CO₂. Cells were dissociated using 0.25% trypsin (Life Technologies) from an 80% to 90% confluent monolayer in tissue culture flasks. Trypsin was neutralized using the complete growth medium of each cell type. The cell suspension was centrifuged down at 1000 rpm for 5 min. After removing the supernatant, cells were suspended in 1 mL of culture medium and counted using a hemocytometer prior to spheroid formation.

2.1.2 Spheroid Formation Using ATPS

Polyethylene glycol (PEG, Sigma), Mw 35 kDa, and dextran (DEX, Pharmacosmos), Mw 500 kDa, were dissolved in the culture medium of each cell type to

obtain final stock solution concentrations of 5% (w/v) PEG and 12.8% (w/v) DEX (Figure 2-1a). A standard 384-well round-bottom ULA plate (Corning), labeled as destination plate, was loaded with 30 μL of the aqueous PEG phase medium. A density of 1×10^5 cells/mL was prepared by suspending cells in the culture medium of each cell type. The suspension was thoroughly mixed with an equal volume of the 12.8% (w/v) aqueous DEX phase medium. This reduced DEX concentration to 6.4% (w/v) and adjusted the density of cells to 0.5×10^5 cells/ml. A single column of a flat-bottom 384-well plate (Corning), labeled as source plate, was filled with this cell suspension. Using a robotic liquid handler (Bravo SRT, Agilent), 0.3 μL of cell suspension was aspirated and dispensed into each well of the destination plate containing the aqueous PEG phase. This process was done column-by-column to minimize the required number of cells in the source plate. Prior to each aspiration step, the cell suspension in the source plate was robotically mixed to ensure a uniform mixture. Cells remained confined within the DEX phase drop and formed a single spheroid in each well (Figure 2-1b). Consistency of spheroid formation was assessed by measuring the diameter of spheroids for each cancer cell line.

2.1.3 Growth Kinetics of Spheroids

A total of 50 spheroids were imaged daily to assess growth kinetics of spheroids based on their volumes and metabolic activity. Culture medium was renewed every 3 days for a period of 9 days. Phase contrast images of spheroids were captured using an inverted fluorescence microscope (Axio Observer, Zeiss) equipped with a high-resolution camera (AxioCam MRm, Zeiss). Diameter of each spheroid was measured using ImageJ, and volume of each spheroid was calculated assuming a spherical shape. Additionally, on each day, metabolic activity of cells in spheroids was determined by adding a Presto Blue

reagent (Life Technologies) to wells at 10% of total volume in each well, incubating the plates for 4 h, and measuring fluorescence intensity using a plate reader (Synergy H1M, Biotek Instruments). [81]

2.1.4 Immunohistochemical Analysis of Spheroids

Spheroids were harvested on day 4 of culture, fixed with 3.7% paraformaldehyde, embedded in a freezing medium, and sectioned to 10 μm -thick slices using a cryostat (Leica CM 1850). The largest sections were selected and immunostained for a cell proliferation marker protein Ki-67 (Cell Signaling Technology), and extracellular matrix proteins type I collagen (Abcam), laminin (Sigma), and fibronectin (Sigma). Nuclei were stained with Hoechst (Life Technologies). Fluorescence images were captured using an inverted fluorescence microscope.

2.1.5 Anticancer Drug Screening Against Tumor Spheroids

The following 25 different anticancer compounds were used: doxorubicin, paclitaxel, 5-fluouracil, ponatinib, oxaliplatin, cisplatin, staurosporine, 17-AAG, crizotinib, ribociclib, KX2-391, VER155008, panobinostat, trametinib, selumetinib, PD0325901, GSK1059615, PI-103, dactolisib, pictilisib, YM155, SP600125, LY2784544, tirapazamine, and hyaluronan- resveratrol (H-R). The first 23 compounds were obtained from Selleckchem and dissolved in DMSO (ATCC) according to the manufacturer's protocols. Stock solutions of these compounds were prepared such that the highest drug concentration used for testing contained less than 0.5% DMSO. [119] At this DMSO concentration, spheroids of cancer cells were viable similar to control spheroids in complete growth media. Tirapazamine was purchased from Sigma, and H-R was kindly

provided by Dr. Y. H. Yun. Stock solutions of the compounds were prepared in sterile distilled water. Main molecular targets of the compounds are listed in Table 2-1. With each compound, six different concentrations of 2 nM, 20 nM, 200 nM, 2 μ M, 20 μ M, and 100 μ M were prepared by serially diluting a respective stock solution in culture media of the cells. These solutions were prepared twice the final concentrations for testing against tumor spheroids. Next, 30 μ L from each of these concentrations for a given drug solution was added to each well of the destination plate that contained a spheroid in the DEX phase drop immersed in 30 μ L of the aqueous PEG phase. This addition step diluted concentrations of PEG and DEX, converting the ATPS to a single medium phase containing trace amounts of polymers, and reduced drug concentrations to 1 nM, 10 nM, 100 nM, 1 μ M, 10 μ M, and 50 μ M. After 72 h, 30 μ L of each drug at these concentrations was added to the corresponding wells. We have shown that presence of trace concentrations of PEG and DEX do not interfere with drug diffusion through culture media. [81] To minimize evaporation of media and avoid variations in drug concentrations and media osmolality during the testing period, the outermost wells of the destination plate were filled with sterile water. After 6 days of drug treatment, spheroids were imaged for morphological characterization. Next, PrestoBlue was added to wells, and after 4 h of incubation, the fluorescence signal was measured with a plate reader. A total of 14 replicates was used for both control (untreated) and drug-treated spheroids. Viability of spheroids treated with each concentration of a drug was normalized to that of untreated, control spheroids and expressed as percent viability. GraphPad Prism 5 was used to fit a 4-parameter sigmoidal dose-dependent response curve to the raw viability data and measure IC_{50} , E_{max} , and AUC.

2.1.6 Western Blotting

Spheroids were harvested from 384-well plates and transferred into a 50 mL conical tube. After centrifugation and removing of the supernatant, spheroids were washed with PBS, lysed in 500 μ L of complete RIPA buffer (50mM Tris-HCl, 150 mM NaCl, 1% NP-40, 0.5% sodium deoxycholate, and 0.1% SDS, pH 7.4 ± 0.2) with protease inhibitor (complete mini, Roche Diagnostics) and phosphatase inhibitor (Life Technologies). To ensure complete lysis, spheroids were sonicated (Vibra-Cell, Sonics) for 5 s twice at a 50% amplitude level. Total protein concentration was determined using a BCA quantification assay kit (LifeTechnologies). Twenty microliters of protein was loaded onto a 4–15% gel (Biorad) for electrophoresis, and the gel was transferred onto a nitrocellulose membrane by electroblotting. Membranes were blocked with 5% BSA (Sigma) for 1 h. Primary antibodies used were phospho-p44/42 MAPK (Erk1/2), p44/42 MAPK (Erk1/2), phospho-AKT (Ser473), and AKT (pan) (C67E7), all purchased from Cell Signaling Technology. Solutions of primary antibodies were prepared at concentrations recommended by the manufacturer. Membranes were incubated overnight at 4 °C with primary antibody solutions. After repeated washing, membranes were incubated with a horseradish peroxidase (HRP)-conjugated secondary antibody for 1 h, followed by another round of repeated washing. Detection was carried out with an ECL chemiluminescence detection kit (GE Healthcare) using FluorChem E imaging system (ProteinSimple).

2.1.7 Statistical Analysis for Selecting Effective Compounds

We used strictly standardized mean difference (SSMD), [120] a statistical metric to select compounds from our preliminary screening of 25 drugs against HT-29 spheroids. SSMD is the ratio of the difference in the mean values from two sets of data to the square

root of the sum of squares of the corresponding standard deviations, i.e., $SSMD = \frac{\mu_1 - \mu_2}{\sqrt{\sigma_1^2 + \sigma_2^2}}$.

Here, μ_1 and σ_1 are the mean and the standard deviation of viability of spheroids that received no treatment, and μ_2 and σ_2 represent mean and standard deviation of viability of spheroids that were treated with a drug compound, respectively. SSMD is a measure of the strength of drug effect on viability of spheroids when compared to the control, untreated spheroids (Table 2-2). Raw fluorescence readouts from the samples were used for SSMD calculations.

2.1.8 Combination Treatment of Spheroids

Three MEK inhibitors, trametinib, selumetinib, and PD0325901, were used in combination with dactolisib (AKT inhibitor) in separate experiments with HT-29 spheroids. The IC_{50} value for each drug against HT-29 spheroids was obtained from its respective dose-response curve. Solutions of each drug were prepared at seven different concentrations of multiples (0.125, 0.25, 0.5, 1, 2, 4, 8) of its IC_{50} by serially diluting the stock solution in the culture medium. Drugs were combined according to a method of fixed concentration ratios. [121] Each combination of concentrations of a pair of drugs used 14 replicates. The calculated AUC from each experiment was used to quantify the effectiveness of combination and single drug treatments. Furthermore, the logarithmic value of a combination index (i.e., $\log(CI)$) was used to determine synergism between drug combinations.

2.1.9 Correlation of Size and Metabolic Activity of Cells in Spheroids

To correlate the size and metabolic activity of cells in the spheroids, the kinase inhibitors trametinib (MEK inhibitor), sorafenib (RAF inhibitor), dactolisib (AKT inhibitor), and ponatinib (multi-kinase inhibitor) were selected against HT-29 spheroids. All four compounds were purchased from Selleckchem. All compounds were dissolved in DMSO except for dactolisib, which was dissolved in dimethylformamide. The stock solutions of trametinib, dactolisib, ponatinib, and sorafenib were 10, 10, 50, and 50 mM, respectively. Stock solutions were stored at -80 °C. For dose-response experiments, 1×10^{-3} μM , 1×10^{-2} μM , 1×10^{-1} μM , 1×10^0 μM , 1×10^1 μM , and 5×10^1 μM concentrations of inhibitors were used. At the highest concentration of drugs used in our experiments, DMSO concentration did not exceed 0.5%. These inhibitors were tested dose-dependently against HT-29 spheroids according to our protocol previously described in the section 2.1.5. Pearson's correlation analysis between the volume of spheroids and the corresponding fluorescence signal from the PrestoBlue assay was performed using Microsoft Excel.

2.2 Results and Discussion

Below, the results of validating high throughput drug screening of the ATPS spheroid technology are presented. This includes high throughput generation of tumor spheroids from various cell lines, the feasibility of maintaining and growing the spheroids, and the utility of incorporating this technology in high throughput screening applications in preclinical cancer drug discovery studies.

2.2.1 Formation, Consistency, and Metabolic Activity of ATPS Tumor Spheroids

One of the key challenges of current 3D cell culture technologies is to conveniently mass-produce uniformly sized spheroids that are individually addressable with chemical compounds. Inconsistency of shape and nonuniformity of size of spheroids cause differences in their biological activities due to variations in the distribution of actively proliferating and dormant and necrotic cells within spheroids. [56], [122] This introduces a major difficulty in drug screening applications that often use metabolic activity-based assays such as Alamarblue and MTT for end point cell viability quantification. Significant variations in baseline metabolic activities of cells in different spheroids due to their size/shape differences complicate the interpretation of drug effects on cellular viability. [56] Therefore, producing uniformly shaped and sized spheroids that show a similar baseline metabolic activity is essential for toxicity tests using such assays. Existing spheroid culture techniques such as spinner flask and rotary vessel generate a large number of nonuniform spheroids. [123] Although the hanging drop array approach results in consistent spheroids, culturing, handling, and drug treating of spheroids are cumbersome and require specialized plates that are incompatible with standard plate readers, necessitating transfer of spheroids to standard plates for downstream analysis of drug responses of cells. [124], [125]

Using the robotic ATPS microtechnology, we demonstrated the capability to mass-produce consistently-sized spheroids of three different cancer cells in ultralow attachment 384-well plates. This approach generates a single spheroid in each well within 24 h for MDA-MB-157 breast cancer cells and HT-29 colorectal cancer cells and 48 h for U-87 MG brain cancer cells. Figure 2-2a-c shows the histogram of diameter of HT-29, U-87

MG, and MDA-MB-157 spheroids measured 72 h after printing with a density of 1.5×10^4 cells. Spheroids of these three cells show a diameter of $420 \pm 24 \mu\text{m}$, $390 \pm 39 \mu\text{m}$, and $294 \pm 6 \mu\text{m}$, respectively. Diameter of spheroids of all three cells within a plate follows a Gaussian distribution. The minimal variations in the diameter of spheroids indicate the reliability of this protocol for use in screening application. Next, we showed that size of spheroids directly correlates with their baseline metabolic activity levels. With all three cancer cells, we observed a strong linear correlation between volume of growing spheroids and the fluorescence signal resulting from metabolizing of PrestoBlue (Figure 2-2d–f). This emphasizes the importance of producing uniformly-sized spheroids for studies that use metabolic assays to measure changes in cell viability and distinguishing effects of different treatments. We note that during long-term cultures of spheroids, development of protrusions or budding from the periphery of some spheroids may infrequently happen, causing irregularities in shape and introducing variations in their metabolic activity from that of round spheroids. Therefore, morphological examination of spheroids may provide additional information that cannot be readily captured with biochemical assays. Finally, we performed confocal microscopy to reconstruct the 3D architecture of spheroids made with the ATPS technology (Figure 2-3).

2.2.2 Growth and Matrix Deposition of ATPS Tumor Spheroids

We imaged spheroids daily to determine changes in their size (Figure 2-4g–i). With a density of 1.5×10^4 cells, HT-29 cells produced the largest spheroids of $0.038 \pm 0.0017 \text{ mm}^3$ at the beginning of the experiment. With the same cell density, U-87MG and MDA-MB-157 spheroids were $0.031 \pm 0.0023 \text{ mm}^3$ and $0.013 \pm 0.0003 \text{ mm}^3$ on average, respectively. Analysis of growth curves by curve fitting showed that during the first week

of culture, spheroids had a rapid growth that slowed subsequently. The rapid growth phase was approximately exponential for all three systems. Within the culture period, HT-29 spheroids showed the largest growth and increased in size to $0.16 \pm 0.0022 \text{ mm}^3$ corresponding to a 321% increase in volume. This was followed by U-87 MG and MDA-MB-157 spheroids with 0.124 ± 0.0025 and $0.016 \pm 0.0003 \text{ mm}^3$, corresponding to 300% and 23% volume increase, respectively. Therefore, spheroids of different cancer cells generated with the ATPS technology showed normal growth kinetics over time. Slower growth of MDA-MB-157 spheroids could potentially be due to longer cell cycle and compactness of these cells in 3D culture that limits availability of nutrients and oxygen to the cells beyond the peripheral zone of spheroids.

Next, we confirmed proliferative status of cells through histological staining of spheroids for the cell proliferation marker Ki-67. Spheroids of all three cell lines showed positive staining of the Ki-67 protein (Figure 2-4a), validating the morphological measurements above. HT-29 colorectal cancer spheroids contained substantially larger number of Ki-67⁺ cells than spheroids of brain and breast cancer cells. This is consistent with the morphological measurements above that showed greater proliferation of HT-29 spheroids. Ki-67⁺ cells were distributed more toward the periphery of spheroids (in particular for HT-29 spheroids), indicating that these cells consume most of nutrients and oxygen available in the culture medium. Additionally, we immunostained cryosections of spheroids of all three cells for major extracellular matrix (ECM) proteins, i.e., type I collagen, laminin, and fibronectin (Figure 2-4b–d). Positive staining indicates that cells in the spheroids deposit the matrix proteins during culture and that collagen I and laminin are more abundant than fibronectin. Considering that cell-matrix signaling is a major regulator

of various functions of cancer cells including cell proliferation, [126]–[128] spheroids provide a model to study targeting of ECM in a tumor microenvironment. [50], [113]

2.2.3 Quantitative Analysis of Drug Responses of Tumor Spheroids

Analysis of cellular responses to therapeutics in high-throughput screening applications requires an easy-to-use assay to quickly and reliably resolve viability of drug-treated cells. We used a PrestoBlue assay to determine the level of metabolic activity of cells as an indirect measure of cell viability. This assay only involves a single step of reagent addition to wells and subsequently measuring the fluorescence or absorbance signal that correlates with the number of viable cells. We have previously optimized the PrestoBlue assay for use with spheroid cultures to facilitate measuring viability of drug-treated cells. [81], [82] We screened a collection of 25 anticancer compounds against tumor spheroids of HT-29, U-87 MG, and MDA-MB-157 cells. These compounds included standard chemotherapy drugs used clinically and specific molecular inhibitors to target mutations in these cells (Table 2-1). Pathophysiology of these cancers involves dysregulated activities of multiple kinase pathways; as such, we included several kinase inhibitors in our collection to evaluate the effect of targeting of kinase pathways on cancer cells residing in spheroids.

Conducting these tests dose-dependently using six drug concentrations and 14 replicates for each concentration generated 75 dose–response graphs similar to that shown in Figure 2-5 for HT-29 spheroids treated with selumetinib. From each dose–response graph, we computed IC_{50} and E_{max} values that are classical measures of potency and efficacy of a drug (Figure 2-5), respectively. Generally, a low IC_{50} value is desirable as it indicates that the drug is effective at low concentrations. For anticancer compounds, E_{max}

(normalized by 100%) varies between 1 and 0, corresponding to no drug effect and death of all the cells, respectively.

Figure 2-6 shows results for spheroids of all three cancer cell lines. The top row of the figure lists the drugs. Figure 2-6a–c shows the values of E_{max} and $\log(IC_{50})$ for HT-29, U-87 MG, and MDA-MB-157 spheroids, respectively. Close examination of Figure 2-6a shows that there are several drugs that generate very small E_{max} values of smaller than 0.1, i.e., larger than 90% cell death. These include staurosporine, ponatinib, 17-AAG, YM155, and panobinostat. Nevertheless, the corresponding IC_{50} values vary significantly between 0.06 μM for staurosporine to 4.42 μM for ponatinib. Out of five standard chemotherapeutics, cisplatin resulted in the smallest E_{max} of 0.26 and an IC_{50} value of 63 μM , whereas paclitaxel compromised the viability of 54% of cells and showed the smallest IC_{50} of 0.032 μM . Among all 25 compounds, the MEK1/2 inhibitor trametinib produced the smallest IC_{50} of 0.0015 μM and an E_{max} of 0.21. The other two MEK inhibitors, PD0325901 and selumetinib, also gave very low IC_{50} values of 0.089 and 0.081 μM with moderate E_{max} values of 0.32 and 0.36, respectively. Responsiveness of HT-29 spheroids to MEK inhibitors is consistent with presence of B-Raf mutations (Table 2-2) in these cells and demonstrates that ATPS tumor spheroids can reliably predict treatment responses to targeted therapeutic agents. [129], [130]

With U-87 MG spheroids, five compounds generated E_{max} values of smaller than 0.2: pictilisib, staurosporine, YM155, panobinostat, and crizotinib. The corresponding IC_{50} values ranged from 0.120 μM for YM155 to 6.280 μM for pictilisib. Considering the activation of the PI3K pathway in U-87 MG cells (Table 2-2), [131]–[133] except for pictilisib, the remaining pathway-specific inhibitors only showed moderate effects on cell

viability. Among the chemotherapy drugs, doxorubicin was the most potent with an IC_{50} of 0.236 μ M and produced a maximum cell death of 71%. The MDA-MB-157 TNBC spheroids were least responsive to the tested compounds. Only cisplatin and YM155 dropped cell viability below 10%. The IC_{50} values of these two compounds were 19.847 and 3.761 μ M, respectively. Although tirapazamine resulted in E_{max} of 0.18, an IC_{50} could not be obtained due to a nonsigmoidal dose–response curve that showed a high cell viability except for the largest drug concentration. Interestingly and despite mutations in the TP53 gene (Table 2-2) that drive oncogenic activation of PI-3K and MAPK pathways in MDA-MB-157 cells, [134]–[136] these spheroids were highly resistant to specific inhibitors of these pathways and maintained high cell viability of 79–100%. In addition, MDA-MB-157 spheroids were completely resistant to paclitaxel, 5-fluorouracil, and oxaliplatin despite responding well to the drugs when cultured as a monolayer. [81] Close cell–cell contacts and expression of drug transporters have been suggested to cause resistance in 3D culture of these cells. [81], [137]–[139]

2.2.4 Ranking the Performance of Anticancer Compounds

Potency and efficacy are useful measures to evaluate the response of cancer cell spheroids to a chemical compound. Nevertheless, comparing the performance of different agents against spheroids of the same cancer cells based on these two metrics is difficult. For example, a particular compound may result in a large cell death at high concentrations, whereas a second compound may be moderately toxic to cancer cells at very low concentrations. This issue is clear from screening results in Figure 2-6. To overcome this problem, we computed the area under the dose-response curve (AUC) resulting from each treatment. AUC combines drug potency and efficacy into a single parameter and thus offers

a quantitative metric to compare performance of different drugs used against spheroids of each cancer cell line. [140] AUC for selumetinib-treated HT-29 spheroids is shown in Figure 2-5 using the hatched area. All AUC values were normalized to a 0–1 range for ease of comparison. AUC values approaching zero indicate both high potency and efficacy. We used this approach to generate a ranking system in Figure 2-7 for compounds tested against each of the three cancer cell lines.

With HT-29 spheroids (Figure 2-7a), the MEK1/2 inhibitor trametinib received an AUC score of 0.31 and ranked first. This result is consistent with the presence of a gain-of-function B-Raf mutation and high activity of the Raf/MEK/ERK signaling pathway in HT-29 cells (Table 2-2). [141]–[143] The other two MEK inhibitors PD0325901 and selumetinib were also effective and resulted in AUC scores of 0.6 and 0.63, respectively; however, compared to trametinib, they were 20-fold less potent. Greater effect of trametinib is likely due to specificity of targeting both MEK1 and MEK2 compared to PD0325901 and selumetinib. [144] High potency of trametinib against HT-29 spheroids agrees well with a previous study that showed significant suppression of tumor growth in HT-29 xenografts in nude mice. [145] The protein kinase C (PKC) inhibitor staurosporine ranked second with an AUC value of 0.46. Consistent with previous studies, [146] our result suggests that PKC activity is highly upregulated in HT-29 cells and that staurosporine effectively reduces the activity of this signaling molecule in HT-29 spheroids. Other kinase inhibitors in this collection had moderate to minimal effects on HT-29 cells. Specific inhibitors of PI3K pathway including dactolisib, pictilisib, GSK1059615, and PI-103 produced AUC values of 0.82–1. Moderate effect of dactolisib is likely due to inhibition of phosphorylation of AKT in HT-29 cells, [147] consistent with

the PIK3CA mutation that leads to the activation of downstream protein AKT in these cells (Table 2-2). Large AUC values of >0.95 with the other three PI3K pathway inhibitors suggest low sensitivity of HT-29 cell spheroids to PI3K-targeting drugs. Survivin suppressant YM-155, heat shock protein 90 inhibitor 17-AAG, and histone deacetylase (HDAC) inhibitor panobinostat were also very effective against HT-29 spheroids and ranked third, fourth, and seventh. We note that these three compounds resulted in greater cell death than trametinib, but their higher IC_{50} resulted in larger AUC values and lower ranking than trametinib. This emphasizes the importance of simultaneous consideration of potency and efficacy parameters in screening applications to provide a quantitative comparison of performance of a panel of compounds.

Among the five standard chemotherapy drugs used, paclitaxel and doxorubicin were more effective against HT-29 cells (Figure 2-7a). The highest ranked compound against U-87 MG spheroids was YM-155 with AUC value of 0.42, followed by the HDAC inhibitor panobinostat that produced an AUC value of 0.61 (Figure 2-7b). U-87 MG spheroids were sensitive to three chemotherapy compounds doxorubicin, paclitaxel, and 5-fluorouracil that generated AUC values of 0.63–0.82 but showed complete resistance to both platinum-based drugs. Moderate effects of staurosporine and KX2-391 were potentially due to CDK2 and CDC2 inhibition-mediated cell cycle arrest and blocking of SRC kinase-induced oncogenic EGFR signaling in glioblastoma, respectively. [148], [149] Despite PTEN mutation and activation of PI3K/AKT signaling pathway in U-87 MG cells (Table 2-2), the PI3K inhibitors only showed minimal toxicity. With an AUC of 0.83, pictilisib ranked highest among the four PI3K inhibitors used. Among the MEK inhibitors, trametinib was slightly effective against U-87 MG, suggesting that the MAPK/ERK

pathway may be active in these cells. [150] Large AUC values with other compounds indicate minimal or lack of toxicity to U-87 MG spheroids.

MDA-MB-157 spheroids were not responsive to the majority of tested compounds; only three compounds showed moderate effects against these cells. Doxorubicin, YM155, and ponatinib ranked highest with AUC values of 0.62, 0.73, and 0.75, respectively. It has been shown that P53 mutation in breast cancer cells significantly increases expression of survivin that leads to cell survival and resistance to therapy. [151] Sensitivity of MDA-MB-157 spheroids to YM155, a survivin suppressant, suggests that the P53 mutation may be indirectly targeted using YM155. H-R produced minimal toxicity possibly due to expression of hyaluronan receptor CD44 on MDA-MB-157 cells that improves the uptake of resveratrol. [152] Remaining compounds were ineffective and generated AUC values of greater than 0.91. Both structural and biological properties of MDA-MB-157 spheroids may contribute to their drug resistance. Unlike HT-29 and U-87 MG cells, these breast cancer cells form densely packed spheroids. These cells are also known to express drug efflux pumps to avoid drug-induced toxicity. [137] In addition, loss of tumor suppressor protein p16 in these cells is associated with stem cell characteristics that drive therapeutic resistance. [153]

Overall, the use of AUC parameter enabled quantitative comparison of performance of different drugs against spheroids of cancer cells. This approach allowed identifying compounds such as YM155 and doxorubicin that were effective against spheroids of all three cancer cell lines, suggesting them as useful agents against different cancers. Additionally, it identified compounds such as tirapazamine that resulted in large AUC values for all three cancer cell spheroids, suggesting that this hypoxia-activated

compound is not effective against spheroids that mimic early stage tumors and may lack hypoxia.

2.2.5 Morphological Changes of Spheroids in Response to Treatments

We captured daily images of spheroids to monitor their morphological changes due to treatments with effective compounds. Our observations revealed two types of effects: growth retardation or disintegration. MEK inhibitors trametinib, selumetinib, and PD0325901 blocked growth of B-Raf mutant HT-29 spheroids in nanomolar-range concentrations (Figure 2-8a–c). The FDA approved drug, trametinib, effectively inhibited growth of spheroids starting at a 10 nM concentration (Figure 2-8d). The other two MEK inhibitors showed a similar effect at and above 100 nM (Figure 2-8d). The PI3K pathway-targeting compounds dactolisib, GSK1059615, and PI-103 inhibited growth of PTEN mutant U-87 MG spheroids at low micromolar concentrations (Figure 2-8e–h). We observed a strong positive correlation between growth inhibition of spheroids based on morphological characterization and cell viability measurements using metabolic activity data (Table 2-4). This is consistent with the linear relationship between volume of untreated spheroids and their viability data (Figure 2-2g and h). Therefore, morphological measurements may be used as an additional metric to evaluate effectiveness of compounds against tumor spheroids and select concentrations that block growth of spheroids. We note that 17-AAG, ponatinib, staurosporine, and 5-fluorouracil also displayed growth inhibition effects against HT-29 and U-87 MG spheroids. Using high concentrations of these four compounds and MEK and PI-3K inhibitors led to disintegration of spheroids. Due to minimal morphological changes of MDAMB-157 spheroids, they were excluded from this analysis.

Morphological changes of spheroids treated with standard chemotherapy drugs was cell-type dependent. The response of U-87 MG spheroids to chemotherapeutics was similar to molecular inhibitors in terms of growth inhibition at lower drug concentrations and disintegration when larger concentrations were used, whereas HT-29 and MDA-MB-157 spheroids were disintegrated at all effective concentrations (Figure 2-9). Spheroids of MDA-MB-157 cells showed complete resistance to chemotherapy drugs paclitaxel, 5-fluorouracil, and oxaliplatin. This response could not be captured with monolayer culture of cells. When treated with paclitaxel, the monolayer of these cells gave an IC_{50} value of 8 nM. [81] Resistance to standard chemotherapeutics including taxanes is a major hurdle in treating triple negative breast cancers. [137], [154], [155] Our data underline the importance of implementing relevant tumor models in drug research and discovery to elicit realistic responses from cells.

2.2.6 Molecular Targeting of Pathway Inhibitors

We conducted a target validation study to confirm that growth inhibition of tumor spheroids by MEK and PI3K inhibitors are indeed due to on-target effects. This was an important step to establish that ATPS spheroids could reliably be used to determine mechanisms of action of different drugs. Our analysis of compound screening with HT-29 spheroids ranked trametinib as the most effective MEK inhibitor that significantly blocked growth of spheroids. HT-29 cells have constitutive B-Raf mutation and deregulated activity of the Raf/MEK/ERK pathway (Table 2-2). [129], [130] To evaluate whether trametinib-mediated growth inhibition of HT-29 spheroids was due to blocking of ERK1/2 activity, we determined total and phosphorylated levels of ERK1/2. Our result showed that HT-29 cells have constitutive ERK phosphorylation that was completely inhibited after 24 and 48

h of treatment with trametinib (Figure 2-10a), indicating a major role for ERK1/2 in growth of HT-29 spheroids. Among PI3K inhibitors used, pictilisib was the most effective compound against growth of U-87 MG spheroids. PTEN is a major suppressor of the PI3K/AKT pathway, [156] and its mutation in U-87 MG cells results in PI3K/AKT pathway activation and enhanced cell proliferation and survival (Table 2-2). [132] Our protein expression analysis confirmed constitutive AKT phosphorylation in U-87 MG spheroids and complete inhibition of phosphorylation after 24 and 48 h of treatment with pictilisib (Figure 2-10b). This validates that growth retardation of U-87 MG spheroids by pictilisib is due, at least in part, to blocking of PI3K/AKT pathway in U-87 MG spheroids. Thus, our protein expression data indicates that tumor spheroids generated with the ATPS microtechnology provide a relevant 3D model to reliably identify intracellular targets of compounds. Additionally, the ability to find drugs that are cytostatic at low concentrations may offer new opportunities for treating patients along with a cytotoxic drug.

2.2.7 Screening Experiments to Select Effective Compounds

In section 2.2.3, and 2.2.4, we performed dose dependent drug screening of 25 compounds. However, some of the compounds resulted in a AUC value of close to one, indicating their lack of efficacy. It would be useful to identify these ineffective compounds early and avoid using them in dose-response tests. To accomplish this, we used a statistical approach to identify hit compounds prior to dose-response drug treatment experiments.

We performed a preliminary screening of 25 anticancer drug compounds at a single concentration of 10 μ M to identify effective compounds against HT-29 spheroids. The measured viability of HT-29 cells from each treatment is shown in Figure 2-11a. To statistically evaluate the effectiveness of the compounds, we calculated a strictly

standardized mean difference (SSMD) value from each drug treatment (Figure 2-11b). Then we ranked all SSMD values according to Table 2-4. Staurosporine, 17-AAG, trametinib, panobinostat, and YM155 resulted in SSMD values of greater than 5 (green symbols), indicating extremely strong effects of these compounds on HT-29 spheroids. Ponatinib, selumetinib, and PD0325901 produced SSMD values between 3 and 5 and ranked as compounds with very strong effects (blue symbols). With an SSMD of 2.95, doxorubicin ranked as a strong compound (yellow symbol). This was followed by paclitaxel, oxalipaltin, dactolisib, KX2-391, and SP600125, which showed fairly strong to moderate effects with SSMD values in the range of 1.77 to 1.53 (orange symbols). The remaining 11 compounds that gave SSMD values of smaller than 1 (red symbols) were discarded from further consideration. Thus, this preliminary screening helped identify 14 drug compounds effective against HT-29 cells in spheroid cultures. We note that selection of the single concentration for this screening is arbitrary, and lower drug concentrations may also be used if it is desired to conduct fewer dose-response experiments.

2.2.8 Analysis of Combination Treatments Using Size of Spheroids

The screening study showed that the MEK inhibitors, especially trametinib, are highly effective against HT-29 spheroids due to targeting of the RAS/RAF/MEK/ERK pathway. Despite promising antitumor activities of inhibitors of this pathway, emerging evidence from animal studies and clinical trials suggests that colorectal tumors often develop resistance to these inhibitors through activation and compensatory signaling of other kinase pathways, including the PI3K pathway. [157] This is consistent with the prevalent *PIK3CA* mutation in most colorectal cancer cells. [158] Therefore, simultaneous targeting of both pathways offers a potential strategy to overcome resistance of colorectal

cancer cells to single-agent therapy with MEK inhibitors. To establish the feasibility of performing combination therapy using ATPS tumor spheroids, we selected the three MEK inhibitors (trametinib, PD0325901, selumetinib) and used them in combination with a dual PI3K/mTOR inhibitor, dactolisib. Our rationale for selecting this compound was that among the four inhibitors of the PI3K pathway used in our preliminary screening, only dactolisib passed the SSMD >1 criterion. In addition, our dose-response experiment with dactolisib generated an AUC value of 0.82, indicating moderate effects of the compound on HT-29 cells.

We determined IC₅₀ values from screening experiments with each compound (shown in Figure 2-6a) and generated seven combination concentrations of each MEK inhibitor, trametinib and dactolisib at multiples (0.125, 0.25, 0.5, 1, 2, 4, 8) of the ratio of the IC₅₀ values of each pair. In parallel to each combination therapy experiment, spheroids of HT-29 cells were treated with the corresponding MEK inhibitor and dactolisib only (single-agent treatment) at the same concentrations of each compound used for the combination experiment. Figure 2-12 shows the dose response of HT-29 spheroids to the combination of trametinib and dactolisib and compares it to the treatments with each individual inhibitor. Combination of the MEK1/2 and PI3K/mTOR inhibitors enhanced the response by ~20% compared with the treatments with either compound alone (Figure 2-12a), consistent with the smaller AUC value (Figure 2-12b). HT-29 spheroids showed greater sensitivity to the combination of PD0325901 and dactolisib (Figure 2-12d). The maximum reduction in cell viability by single agent PD0325901 and dactolisib treatment was up to 35%. Significantly the largest pair of concentrations (i.e., 0.56 μM PD0325901 and 23.2 μM dactolisib) compromised the viability of cells by over 70% compared with

single-agent treatment. Using the combination treatment, the AUC decreased to 0.26, that is, over 30% reduction compared with the treatments with each inhibitor alone (Figure 2-12e). Combining selumetinib and dactolisib enhanced the cellular response by ~15% compared with individual drug treatment and reduced the AUC to 0.45 (Figure 2-12g and h).

To elucidate whether reduction in cell viability in the combination experiments was synergistically regulated by pairs of compounds, we computed a combination index (CI) for each experiment. $CI < 1$ indicates synergism, $CI = 1$ shows an additive effect, and $CI > 1$ represents antagonism between the pair of compounds. [159] Pairs of drugs with $CI < 0.1$ are considered very strongly synergistic. Figure 2-12c shows that reduced cell viability by trametinib and dactolisib is synergistic at all combinations of concentrations used. PD0325901 and dactolisib (Figure 2-12f) were synergistic at all concentrations except for the lowest combined concentrations resulting from 0.125 multiple of the IC_{50} of each compound. Importantly, these two compounds produced very strong synergism at four and eight multiples of IC_{50} of each compound, that is, $\text{Log}(CI) < -1$. Finally, except for the first two pairs of concentrations, selumetinib and dactolisib also synergistically enhanced the response of HT-29 spheroids to the treatment.

Cancer cells often contain mutations in several signaling pathways, which may also vary among the population of cancer cells due to their inherent heterogeneity. Despite significant toxic effects of certain drugs (e.g., trametinib at low nanomolar concentrations generates significant toxicity to HT-29 cells; see Figure 2-6a), repeated use of a single drug often fails to fully suppress cancer cells due to the ability of cells to activate compensatory survival signaling pathways and develop resistance to the drug used, among other potential

mechanisms of resistance. [160], [161] In HT-29 cells that are *BRAF* and *PI3KCA* mutant, targeting a signaling protein in the mitogen-activated protein kinase (MAPK) pathway triggers cells to activate compensatory signaling through the PI3K pathway and enable them to survive otherwise lethal treatments. [162] This is evident from trametinib resistance of colorectal cancers. [96] Therefore, co-targeting of multiple pathways with “crosstalk” ability provides a rational therapeutic strategy to tackle the challenge of drug resistance. Our experiments showed that targeting of these survival pathways through combining specific MEK and PI3K inhibitors synergistically compromised the viability of HT-29 cells compared with treatment with a single inhibitor, indicating the role of both pathways in cell survival and the importance of simultaneous blocking of their signaling.

Identifying synergism or antagonism between two drugs using physiologically relevant spheroid cultures is a useful strategy for selecting drug combinations that will likely produce synergistic effects *in vivo*. Interpreting such data in terms of potential responses of cancer patients is difficult due to differences in drug pharmacokinetics and other factors among patients that influence drug sensitivity. Nevertheless, information from *in vitro* experiments can serve early trials of combination therapies in animal models to evaluate synergistic drug responses *in vivo*. Overall, this study demonstrated the utility of our facile ATPS tumor spheroid technology for drug screening, identification of effective compounds against specific cancer cells, and design and analysis of rational drug combination studies with 3D cancer cell cultures. In conjunction with molecular studies, this approach will enable a mechanistic understanding of effects of specific drug combinations on cancer cells and offer valuable insights prior to expensive and tedious animal model studies.

2.2.9 Predicting Treatment Outcomes Using Size of Spheroids

Our screening used a Prestoblué biochemical assay to quantify effects of anti-cancer drug compounds at the end point of experiments. However, the use of biochemical assays requires a large number of spheroids, especially during long-term experiments with multiple time points for analysis of drug responses of cells. In long-term experiments, each compound is used at multiple doses, each with a sufficient number of replicates to enable reliable statistical analysis. An experiment with each pair of compounds often requires several hundred spheroids multiplied by the number of analysis time points. [163], [164] Screening different pairs of inhibitors will need an exceedingly large number of spheroids. This will significantly increase the quantity of samples and labor associated with production and maintenance of cultures in long-term experiments. To overcome this challenge, we developed a simple method to analyze the size of spheroids to predict drug responses of cells. Unlike with the biochemical assays, we use the spheroids over time.

To demonstrate this approach, we treated HT-29 spheroids dose-dependently with specific kinase inhibitors. Biochemical analysis using PrestoBlue showed that molecular inhibitors reduced growth of spheroids to different extents and with different efficacies (Figure 2-13a and b). Trametinib was the most effective inhibitor against HT-29 spheroids at low nanomolar concentrations of <10 nM. Above this concentration, spheroids were either fluffy or disintegrated. Similarly, sorafenib was effective above 100 nM drug concentrations, whereas ponatinib and dactolisib showed efficacy at micromolar concentrations. To determine a correlation between these metabolic activity-based results and size of spheroids, we selected spheroids from drug concentrations that were effective, but did not disintegrate the spheroids. We found that the volume of spheroids treated with

these inhibitors linearly correlated with the fluorescence signal from the PrestoBlue assay. The goodness-of-fit parameter (R^2) demonstrated a linear correlation (Figure 2-14c-f). We found that Pearson's correlation coefficients between dose-dependent reduction in volume of spheroids and fluorescence intensity from the biochemical analysis were 0.975, 0.978, 0.966, and 0.986 for treatments with trametinib, sorafenib, ponatinib, and dactolisib, respectively. This analysis substantiated the validity of the size-based analysis of drug-treated spheroids to predict treatment outcomes.

This method can become significantly beneficial when performing high-throughput, long-term combination treatments with molecular inhibitors to identify effective pairs. In the following chapters, we will use this approach to predict development of drug resistance in cancer cells.

2.3 Summary

The polymeric aqueous two-phase system (ATPS) microtechnology enables robotic mass-production of uniformly sized tumor spheroids in standard 384-microwell plates. Resulting spheroids reproduce key features of tumors such as growth and matrix deposition. We demonstrated that an inherent power of this microtechnology is enabling convenient high-throughput screening of drug compounds. Dose-dependent screening of a collection of 25 chemical compounds with different targets and mechanisms of action against brain, colorectal, and breast cancer spheroids combined with a multi-parametric analysis approach identified compounds that effectively blocked growth of spheroids of cancer cells. Furthermore, we used a statistical tool, SSMD, to identify hit compounds for the specific cancer type. Additionally, we showed that morphology of spheroids contains

useful information, which is not necessarily captured with metabolic activity-based cell viability assays, and provides a secondary tool to evaluate differential effects of various drugs on tumor spheroids. This approach also enabled identifying drugs with cytostatic effects for potential use in combination with cytotoxic compounds. The size-based analysis predicted outcomes of treatments, offering a straightforward approach to quantify responses of cells to cytostatic therapeutics. As a proof-of-concept, we used the size-based analysis in this chapter to show development of resistance in colorectal cancer cells to specific kinase inhibitors. We will use this approach in Chapters 3, 4, 5, and 6.

Incorporating this user-friendly 3D cancer cell culture microtechnology into the drug discovery pipeline in pharmaceutical industries and core research centers will help bridge a major gap between currently-used monolayer cell cultures with known limitations and expensive animal models for screening anticancer drugs, reduce the number of animal tests by eliminating ineffective compounds from further consideration, and dramatically reduce costs and increase efficiency.

Table 2-1. List of anticancer compounds and their main targets

Compound	Target
Paclitaxel	Microtubules
Oxaliplatin	DNA crosslinker
5-Fluorouracil	Thymidylate synthase
Cisplatin	DNA crosslinker
Doxorubicin	Topoisomerase II
Dactolisib	mTOR/PI3K
PI-103	PI3K
Pictilisib	PI3K
GSK1059615	PI3K
PD0325901	MEK1
Selumetinib	MEK1
Trametinib	MEK1/2
SP600125	JNK
Staurosporine	PKC
Ponatinib	TK
VER155008	HSP70
17-AAG	HSP90
YM155	Survivin
Ribociclib	CDK
Panobinostat	HDAC
LY2784544	JAK2
KX2-391	SRC
Crizotinib	C-MET/ALK
H-R	ROS
Tirapazamine	Hypoxia

Table 2-2. Actionable mutations in target cell lines

Cell line	Mutation
HT-29	B-RAF (p.V600E), PI3KCA (p.P449T), TP53 (p.R273H)
U-87 MG	PTEN, TCRA
MDA-MB-157	TP53, NF1

Table 2-3. Pearson's correlation coefficient shows relationship between dose-dependent decrease in viability of U-87 mg and HT-29 spheroids and their growth inhibition by different inhibitors.

Drugs	HT-29	U-87 MG
Trametinib	0.980	–
Selumetinib	0.988	–
PD0325901	0.971	–
Pictilisib	–	0.851
Dactolisib	–	0.961
GSK1059615	–	0.803
Ponatinib	0.965	0.954
5-Flurouracil	0.983	0.919
17-AAG	0.825	0.964
Staurosporine	0.989	0.868

Table 2-4. Classification of strength of compounds according to their resulting SSMD values

Effect subtype	Thresholds for SSMD
Extremely strong	SSMD>5
Very strong	5>SSMD>3
Strong	3>SSMD>2
Fairly strong	2>SSMD>1.645
Moderate	1.645>SSMD>1.28
Fairly moderate	1.28>SSMD>1
Fairly weak	1>SSMD>0.75
Weak	0.75>SSMD>0.5
Very weak	0.5>SSMD>0.25
Extremely weak	0.25>SSMD>0

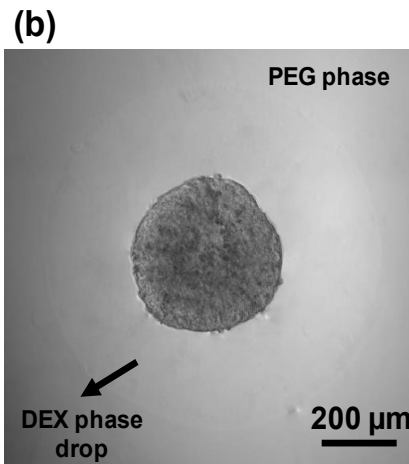
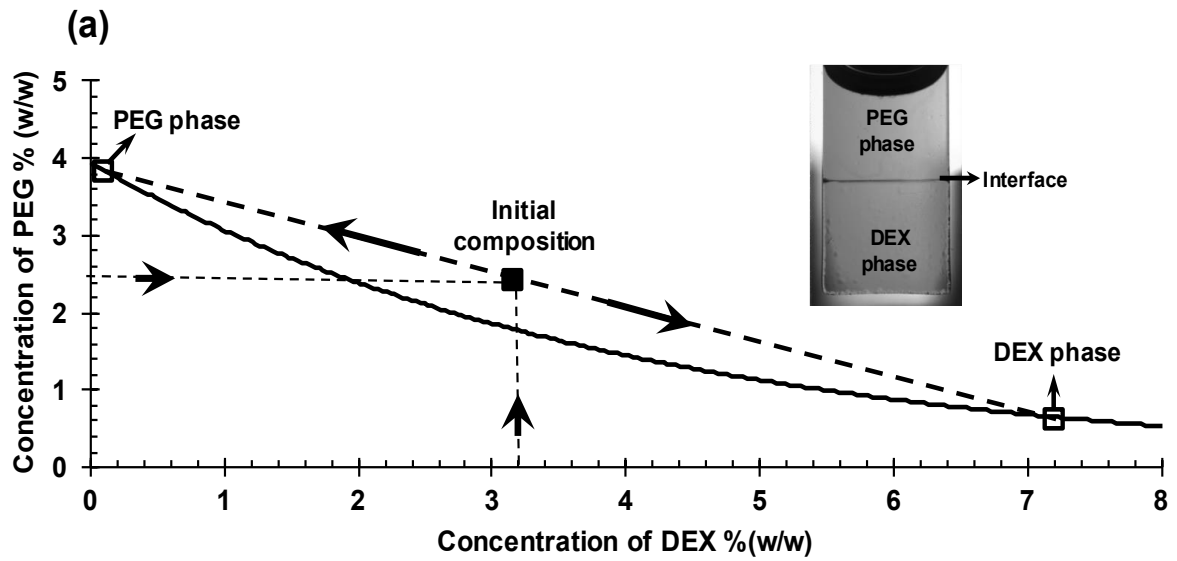


Figure 2-1. (a) Phase diagram of ATPS made with polyethylene glycol (PEG) and dextran (DEX) shows the composition of the initial solution (solid square) and resulting segregated phases (open squares). The inset image shows side view of the ATPS formed in a glass cuvette with the location of the interface indicated. (b) The top view of a spheroid of HT-29 colorectal cancer cells formed with the ATPS microtechnology.

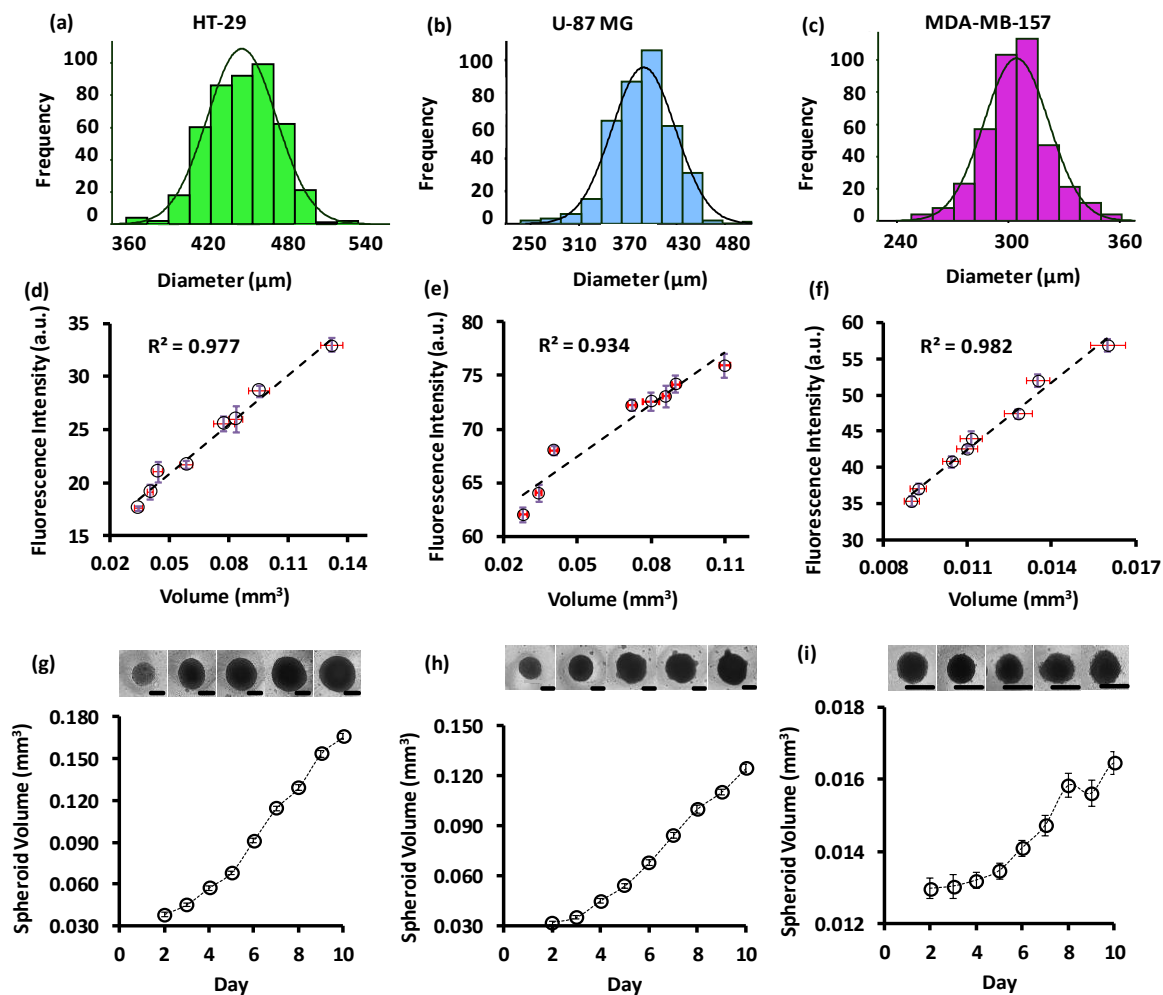


Figure 2-2. Histograms of diameter of spheroids of (a) HT-29 colorectal cancer cells, (b) U-87 MG brain cancer cells, and (c) MDA-MB-157 breast cancer cells show the consistency of size of spheroids ($n=300$). Fitted curves show that diameter of spheroids follows a Gaussian distribution. (d-f) Metabolic activity of spheroids, measured as the fluorescence signal produced by cells metabolizing PrestoBlue, shows a linear correlation with the size of spheroids. Horizontal and vertical bars represent standard error of volume of spheroids and standard error of raw fluorescence intensity data ($n=7$ for each data point). (g-i) Volume growth kinetics of HT-29, U-87 MG, and MDA-MB-157 spheroids is shown over time. Images represent spheroids from different days of culture. The number of samples for each time point is 50 spheroids and error bars represent standard error of mean. Scale bar: 300 μm .

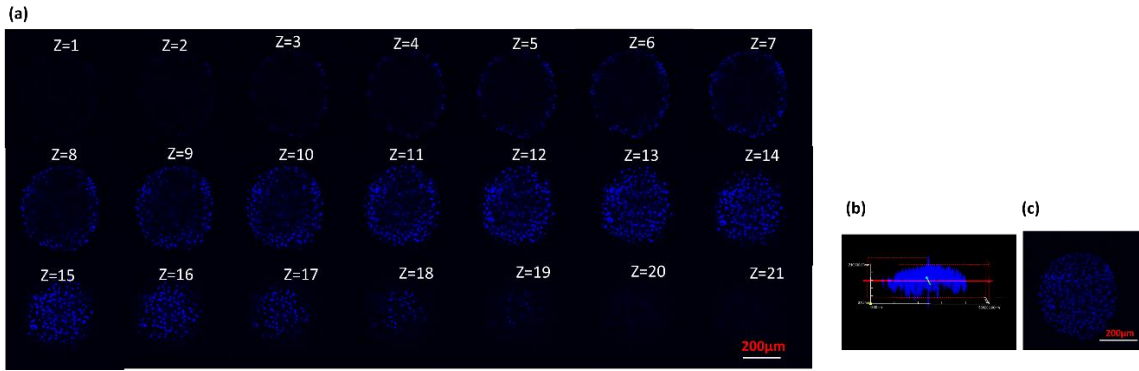


Figure 2-3. (a) Confocal images of a spheroid of HT-29 cells 4 days after formation taken every 10 μm from the top ($Z=21$) to the center ($Z=1$) of the spheroid, (b) 3D reconstructed image of half of the spheroid, and (c) maximum intensity stack image of the Z sections. Cells were stained with Hoechst.

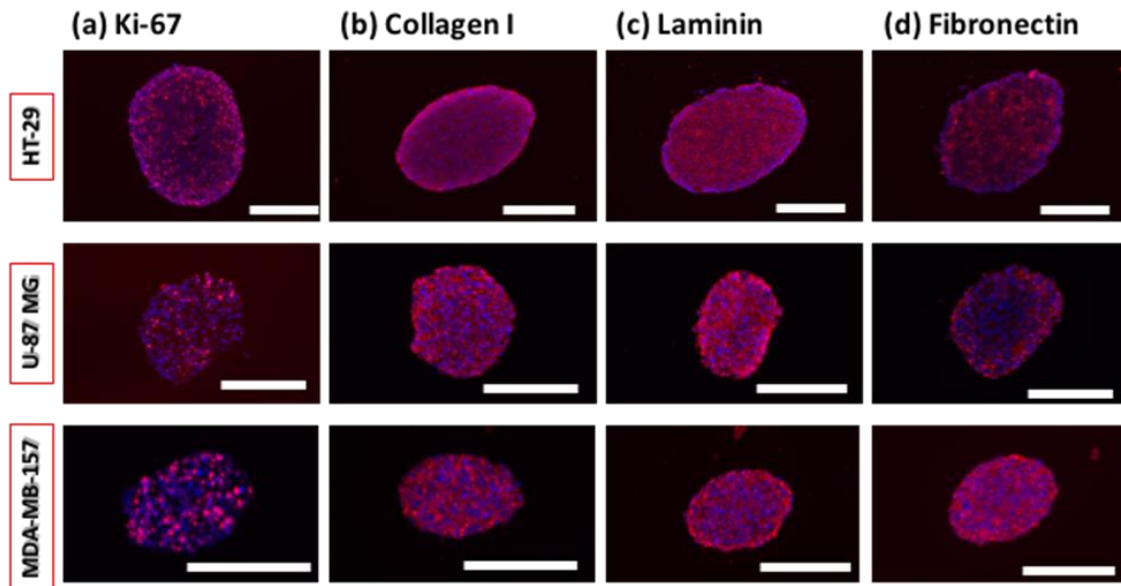


Figure 2-4. Histological staining of spheroids of HT-29 (top row), U-87 MG (middle row), and MDA-MB-157 (bottom row) cells for (a) Ki-67 cell proliferation marker, (b) type I collagen, (c) laminin, and (d) fibronectin. Blue represents nuclei staining with Hoechst and pink represents protein staining. Scale bar: 200 μm

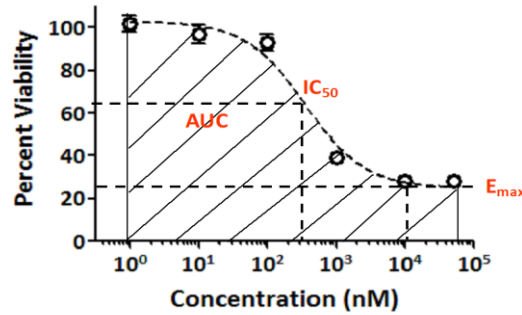


Figure 2-5. A representative dose-response curve is shown for experiment with selumetinib against HT-29 spheroids. Half-maximum inhibitory concentration (IC_{50}), maximum inhibition (E_{max}), and area under the curve (AUC) are used for multi-parametric analysis of cellular responses to drug compounds.

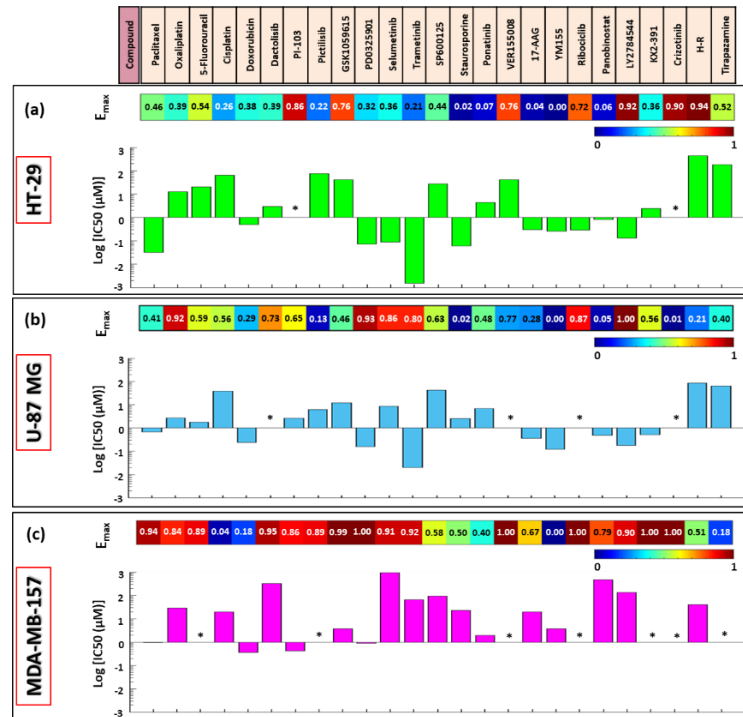


Figure 2-6. Twenty-five anticancer compounds are listed in the top row. Values of E_{max} and $\log(IC_{50})$ for drug-treated spheroids of (a) HT-29, (b) U-87 MG, and (c) MDA-MB-157 are shown. Color bar indicates the range of E_{max} (0-1). In addition, E_{max} values for tested compounds are shown. * denotes the lack of an IC_{50} value in the dose-response graph of the particular drug-cell pair.

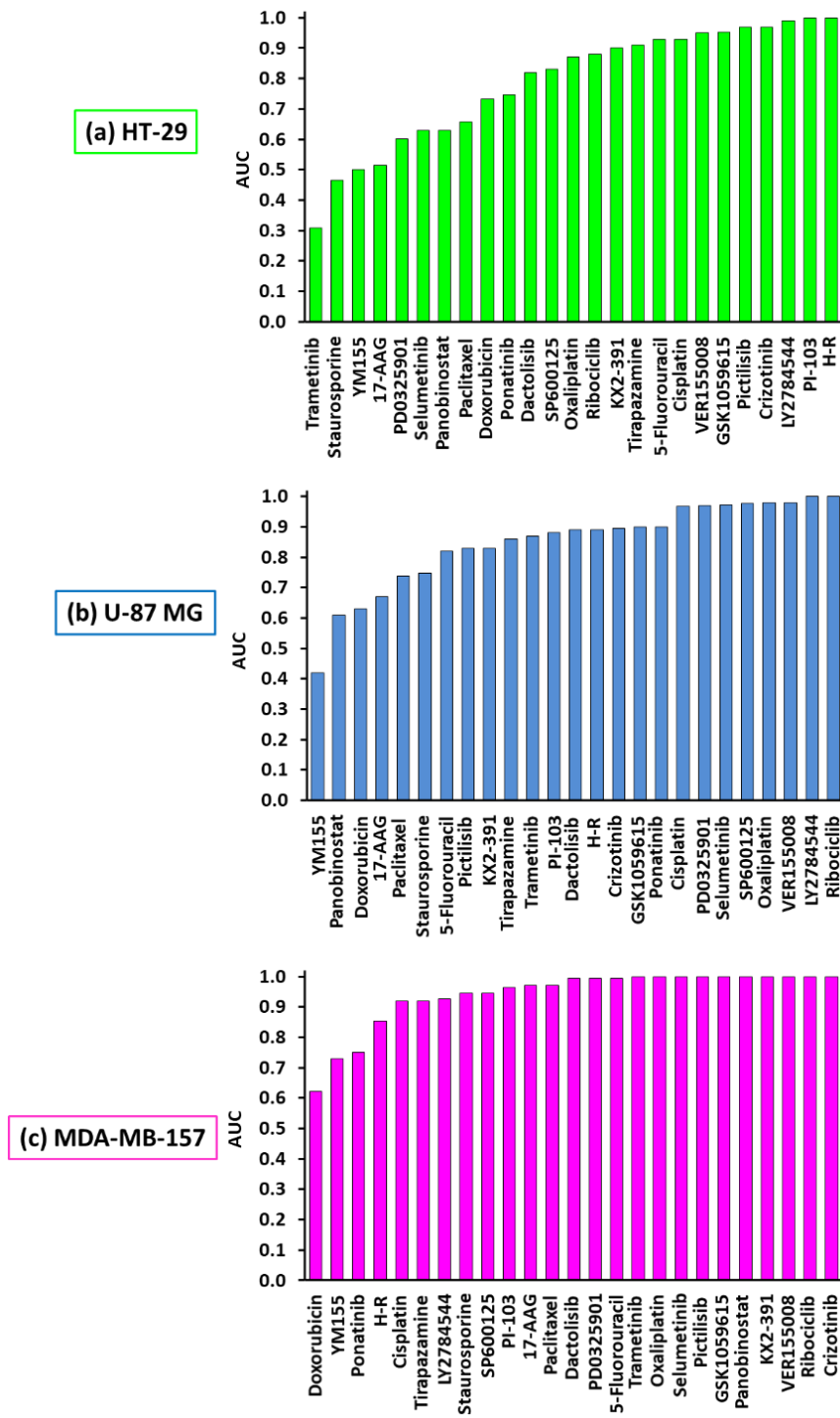


Figure 2-7. Ranking of effectiveness of compounds based on the AUC metric for spheroids of (a) HT-29, (b) U-87 MG, and (c) MDA-MB-157 cells.

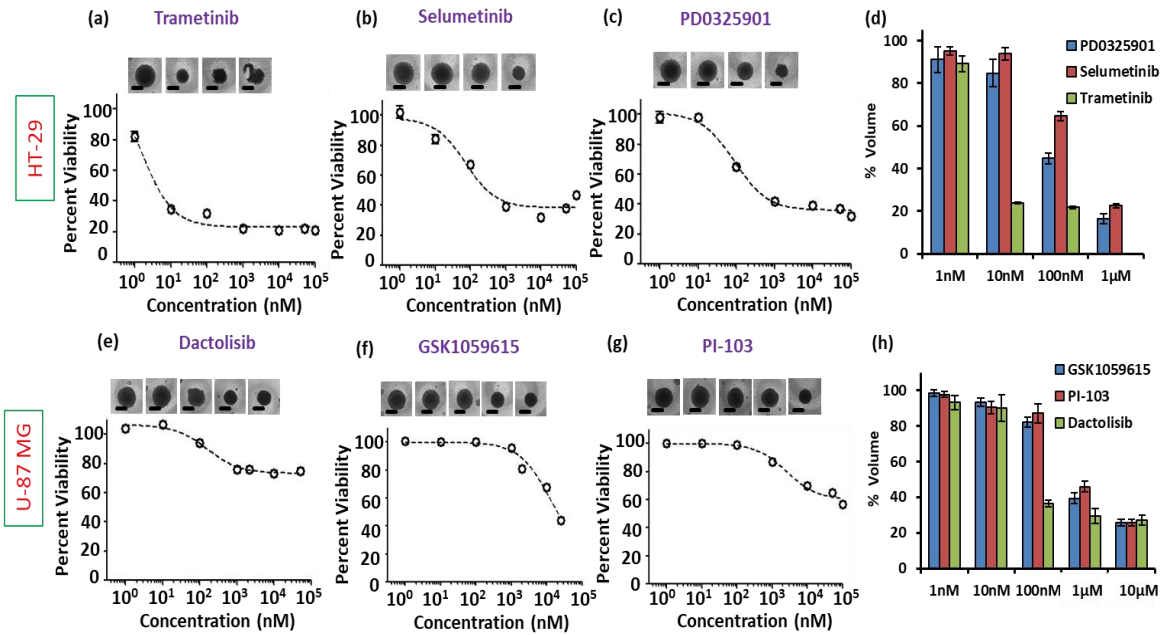


Figure 2-8. Growth inhibition of spheroids of HT-29 and U-87 MG cells after treatment with specific MEK and PI3K inhibitors. Panels (a-c) show dose-dependent blocking of HT-29 spheroids growth due to treatment with three different MEK inhibitors, consistent with measured viability data with each compound. (d) Comparison of growth inhibition of HT-29 spheroids at different concentrations of MEK inhibitors. Panels (e-g) display dose-dependent growth retardation of U-87 MG spheroids treated with three different PI3K inhibitors. (h) Comparison of growth inhibition of U-87 MG spheroids due to treatment with different PI3K inhibitors. Scale bar: 300 μm

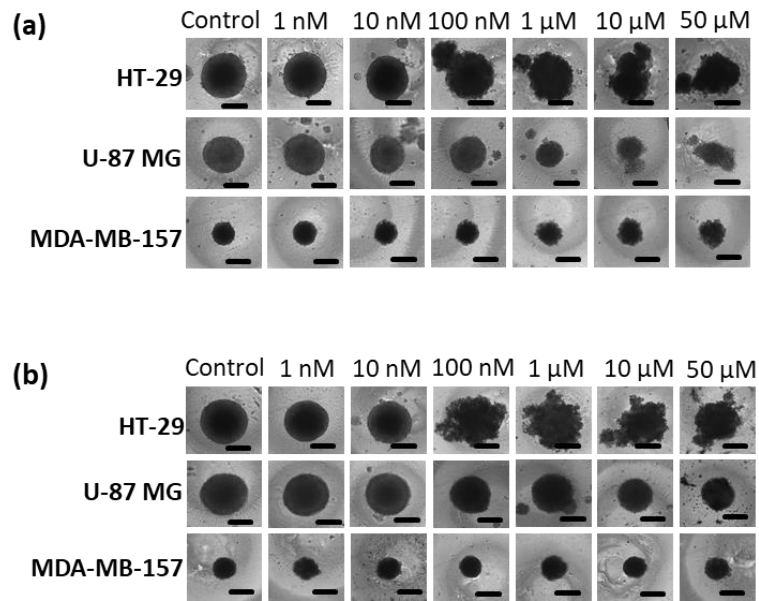


Figure 2-9. Morphological changes of spheroids of HT-29, U-87 MG, and MDA-MB-157 cells after treatment with (a) doxorubicin and (b) paclitaxel at different concentrations of drugs. Disintegration of HT-29 spheroids is observed with both chemotherapeutics. Growth of U-87 MG spheroids is blocked at sub-micromolar concentrations, whereas higher drug concentrations disintegrate the spheroids. HT-29 and MDA-MB-157 spheroids show disintegration at all effective drug concentrations. MDA-MB-157 spheroids show complete resistance to paclitaxel and minimal morphological changes. Scale bar: 300 μ m

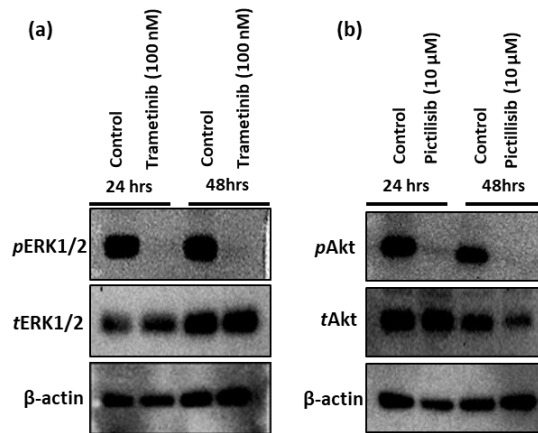


Figure 2-10. (a) Trametinib inhibition of ERK1/2 phosphorylation in HT-29 spheroids and (b) pictilisib inhibition of AKT phosphorylation in U-87 MG spheroids are shown at two different time points.

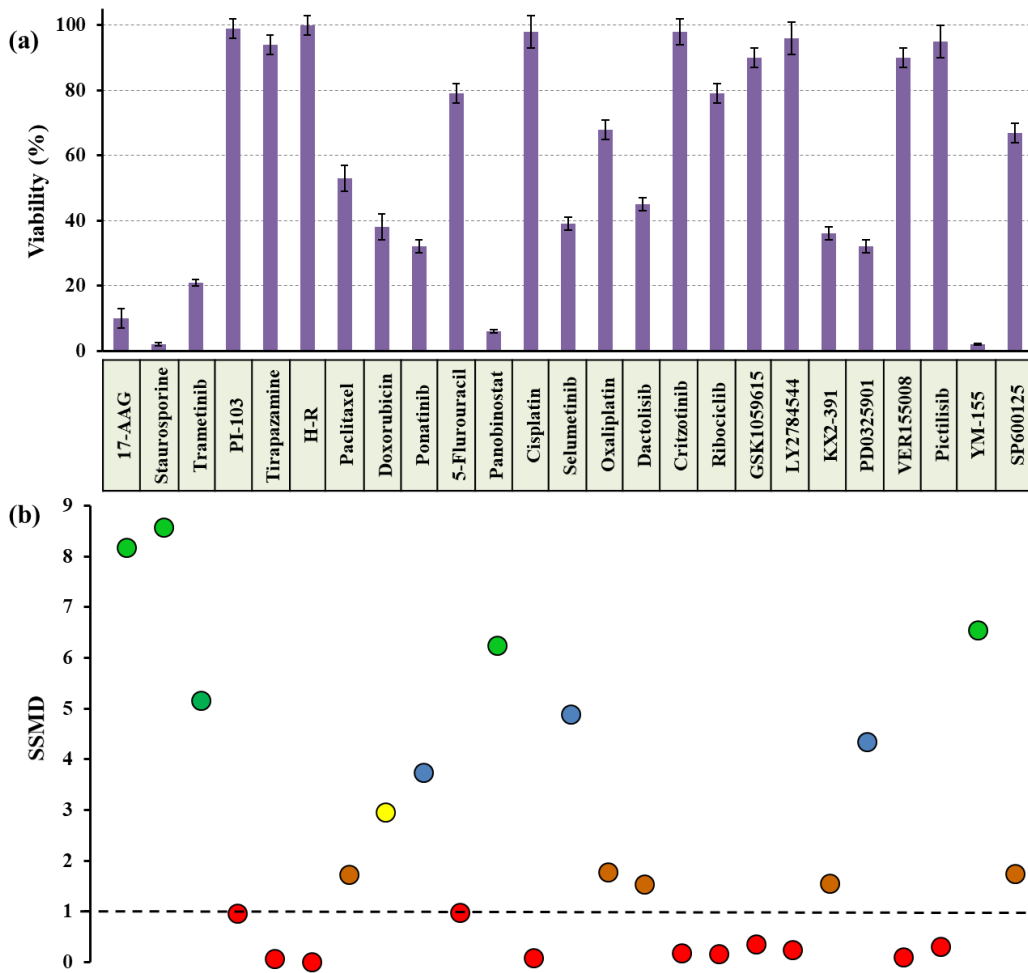


Figure 2-11. Viability of HT-29 spheroids treated with 10 μ M of 25 anticancer compounds shown below the graph. (b) Strictly standardized mean difference (SSMD) values corresponding to treatment with the drug compounds. Color coding corresponds to different effectiveness levels of compounds as shown in Table 2-4.

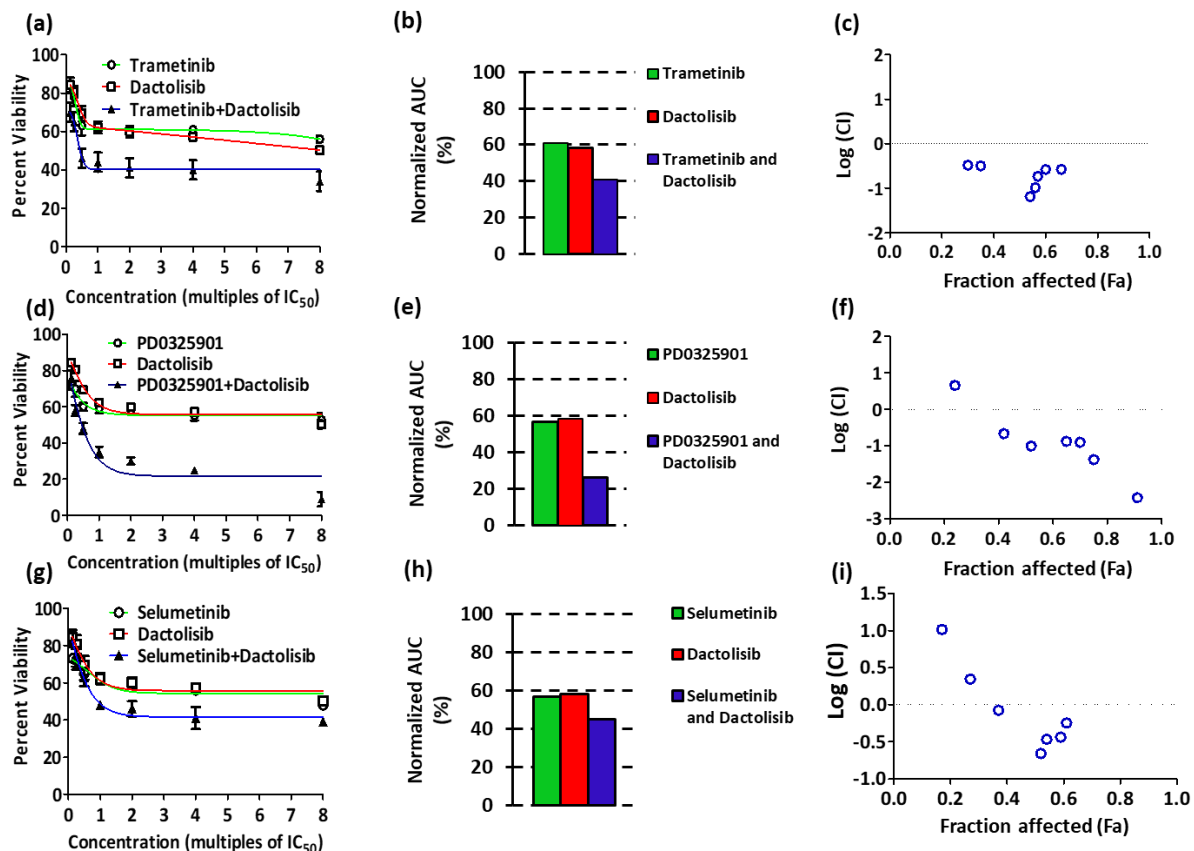


Figure 2-12. Single-agent and combination drug treatments of HT-29 spheroids with (a) trametinib and dactolisib, (d) PD0325901 and dactolisib, and (g) selumetinib and dactolisib. (b, e, h) Computed area under the dose-response curve (AUC) values corresponding to panels a, d, and g. (c, f, i) Combination index (CI) values shown on a logarithmic scale as a function of the fraction of affected cells in spheroids for combination treatment experiments of panels a, d, and g. $\text{Log}(\text{CI}) > 0$ indicates antagonism, $\text{Log}(\text{CI}) = 0$ shows additive effect, and $\text{Log}(\text{CI}) < 0$ represents synergism.

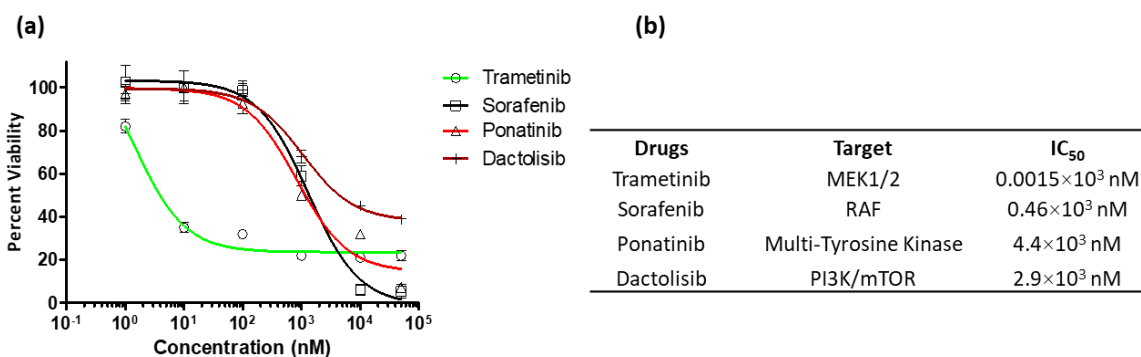


Figure 2-13. (a) Dose dependent reduction in viability of HT-29 spheroids with different molecular inhibitors. Target of drug compounds and their IC₅₀ values against HT-29 spheroids.

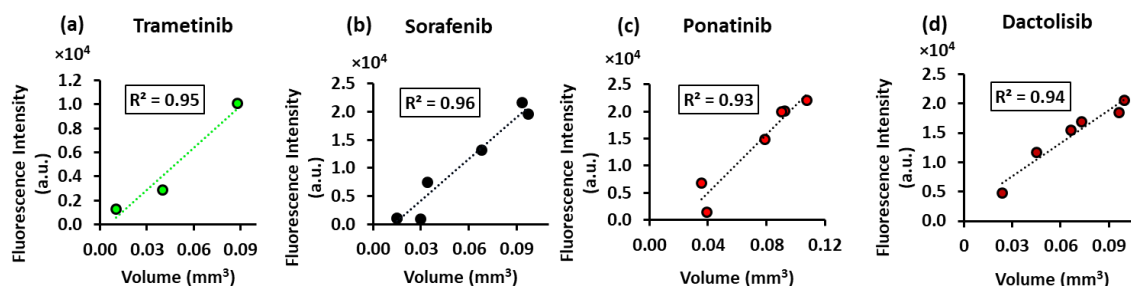


Figure 2-14. The size of spheroids reliably predicts outcomes of treatment with molecular inhibitors. (a-d) Correlation between the average values of fluorescence signal from Prestoblu assay and volume of spheroids from morphological images ($n=14$). R^2 represent goodness-of-the-fit parameter. Different data points in each graph represent different drug concentrations. Only those concentrations that did not disintegrate the spheroids were considered.

CHAPTER III

CYCLICAL TREATMENT OF COLORECTAL TUMOR SPHEROIDS INDUCES RESISTANCE TO MEK INHIBITORS

Portions of this chapter are reused from P. Shahi Thakuri, G. D. Luker, and H. Tavana, “Cyclical treatment of colorectal tumor spheroids induces resistance to MEK inhibitors.,” *Transl. Oncol.*, vol. 12, no. 3, pp. 404–416, Dec. 2019. Copyright @ 2018 by Translational Oncology. Reprinted by permission of Elsevier publications through Open Access Policy. <https://www.ncbi.nlm.nih.gov/pubmed/30550927>

Preclinical studies are essential to cancer drug discovery. Historically, these studies have been carried out primarily using two-dimensional (2D) cell cultures and then validated in animal models. However, 2D cultures lack key morphological and biological properties of human tumors. The use of 2D cultures is thought to be a major contributing factor to the high attrition rate of drug candidates in animal studies and failures in clinical trials. [103] To address this problem, 3D cultures of cancer cells as tumor spheroids have recently been used in cancer research. Spheroids resemble both the morphology and biologic characteristics of solid tumors. [56], [165], [166] Despite the increasing use of spheroids to identify effective drugs, their potential to study cancer drug resistance remains underexplored. Major barriers include difficulties with long-term culture and periodic drug treatment of spheroids, intense labor associated with handling the cultures, and quantitative analysis of drug responses of cancer cells in spheroid cultures. [56] We addressed these challenges and demonstrated the utility of tumor spheroids to model resistance to molecular inhibitors and explore the underlying molecular mechanisms.

Colorectal cancer is the third leading cause of cancer death in the United States. [87] Approximately, 30–40% of colorectal cancers have KRAS mutations, 10–15% contain B-RAF mutations, and 10–20% have an activating PIK3CA mutation. [167]–[169] These mutations cause aberrant activities of oncogenic pathways RAS/RAF/MEK/ERK (MAPK) and PI3K/AKT/mTOR. As such, these pathways present attractive therapeutic targets. Several studies showed that specific molecular inhibitors of MEK (MEKi) and RAF (RAFi) suppressed growth of colorectal tumors *in vivo*. [91], [92] Nevertheless, colorectal cancer cells often show resistance to these inhibitors by activating other signaling pathways such as PI3K/AKT/mTOR or JAK/STAT to mediate resistance to MEKi. [93] Feedback activation of receptor tyrosine kinases (RTKs) such as epidermal growth factor receptor (EGFR) causes resistance to RAFi. [94] Alternatively, continuous exposure to a MEKi may lead to mutation of MEK, [170] while resistance to continuous exposure to RAFi may occur through amplification of B-RAF or other components of the MAPK pathway. [99], [171] Therefore, understanding mechanisms of drug resistance and developing strategies to overcome them is crucial to improve colorectal cancer treatments. To model drug resistance of colorectal cancer, we used our ATPS technology to generate tumor spheroids of colorectal cancer cells harboring B-RAF and PIK3CA mutations. Using a pulsed-dosing regimen to mimic intermittent cycles of chemotherapy administered to patients, we cyclically treated tumor spheroids with three MEKi. [172] The pulsed-dosing strategy has shown advantages over continuous drug administration by producing prolonged anti-tumor activity *in vivo*. [173], [174] The pulsed dosing strategy using the B-RAF inhibitor, vemurafenib, delayed acquired resistance in a melanoma mouse model. [175] This dosing regimen approach has also been adopted in clinical trials of targeted therapies against

colorectal cancer. [176] Our results showed that repeated exposure of colorectal tumor spheroids to a MEKi significantly upregulates AKT activity without affecting other possible mediators of resistance, such as STAT3 and B-RAF, in HT-29 cells. To overcome this adaptive resistance of cells to MEKi, we demonstrated that combination treatments of MEK and PI3K inhibitors synergistically inhibited growth of tumor spheroids during long-term cycles of treatment and recovery and downregulated signaling through these pathways. Importantly, this proof-of-concept study using cyclical treatment of tumor spheroids reproduced adaptive drug resistance of cancer cells due to feedback signaling of kinase pathways known from animal studies. Our study presents a unique approach to identify mechanisms of drug resistance and evaluate rationale therapeutic interventions to overcome resistance in 3D tumor models of cell lines with different genetic backgrounds and with patient-derived cells.

3.1 Materials and Methods

The methods for long-term culture of spheroids to model adaptive drug resistance to MEKi, molecular analysis of drug resistance, and design of rational combination approach to overcome drug resistance over long-term cyclic treatment in colorectal tumor spheroids are described below.

3.1.1 Cell Culture

Mc Coy's 5A medium (Sigma) was used to culture HT-29 (ATCC) and HCT116 (ATCC) colorectal cancer cells. The medium was supplemented with 10% fetal bovine serum (FBS) (Sigma), 1% Streptomycin/Penicillin (Thermo Fisher Scientific), and 1% glutamine (Thermo Fisher Scientific). Cells were cultured in a humidified incubator at 37

°C and 5% CO₂. Cells were dissociated from 80–90% confluent monolayer cultures in tissue culture flasks using 0.25% trypsin (Thermo Fisher Scientific). Trypsin was neutralized using the complete growth medium. The cell suspension was centrifuged down at 1000 rpm for 5 min. After removing the supernatant, cells were suspended in 1 ml of the culture medium and counted using a hemocytometer prior to spheroid formation.

3.1.2 Spheroid Formation

A polymeric aqueous two-phase system was used to form colorectal tumor spheroids. Bio-ultra polyethylene glycol (PEG) with a molecular weight of 35 kDa (Sigma) and dextran (DEX) with a molecular weight of 500 kDa (Pharmacosmos) were dissolved in the complete growth medium to obtain solutions with concentrations of 5.0% (w/v) PEG and 12.8% (w/v) DEX. A round-bottom ultralow attachment 384-well plate (Corning) was used as the “destination plate”. Each well of this plate was loaded with 30 µL of the aqueous PEG phase medium. A suspension of 1×10^8 cells/mL was prepared and 100 µL of the suspension was thoroughly mixed with 100 µL of the 12.8% (w/v) aqueous DEX phase medium. This reduced the concentration of the DEX polymer to 6.4% (w/v) and adjusted the density of cells to 5×10^7 cells/mL. Each well from one column of a flat-bottom 384-well plate (Corning), which was used as the “source plate,” was loaded with 25 µL of the resulting cell suspension in the DEX phase medium. A robotic liquid handler, Bravo SRT (Agilent Technologies), was used to aspirate 0.3 µL of the suspension containing 1.5×10^4 cells from each well and dispense it into each well of the destination plate containing the aqueous PEG phase. This aspiration and dispensing process was done column by column. Uniformity of the high-density cell suspension in the source plate was maintained by robotically mixing the content of the wells prior to each aspiration step. The destination

plate was incubated for 48 hours to allow cells in each well to aggregate into a compact spheroid.

3.1.3 Preparing Drug Solutions

Trametinib, PD0325901, selumetinib, sorafenib, AZ628, GDC0994, ulixertinib, dactolisib, PI-103, GSK1059615, and pictilisib were purchased from Selleckchem (Houston, TX). Stock solutions of these molecular inhibitors were prepared according to the manufacturer's instructions. Except for dactolisib that was dissolved in dimethylformamide, other compounds were dissolved in dimethyl sulfoxide (DMSO). Stock solutions of the inhibitors were stored in -80°C . The inhibitors were tested against tumor spheroids according to the protocol we described previously. [86], [177]

3.1.4 Cyclical Treatment of Spheroids with Inhibitors and Recovery from Treatment

Sub-lethal concentrations of trametinib (5 nM), PD0325901 (100 nM), and selumetinib (100 nM) were selected based on dose dependent drug tests against HT-29 spheroids. We selected these concentrations to produce growth inhibition in HT-29 tumor spheroids. Spheroids were subjected to three rounds of drug treatment separated by two rounds of recovery phases. The three rounds of treatment were designated as T1, T2, and T3. The recovery periods were designated as R1 and R2. Each phase lasted 6 days. Each treatment phase included drug addition to spheroids at the beginning and drug renewal 72 hours later, whereas each recovery phase included culture medium addition to spheroids at the beginning and culture medium renewal 72 hours later. Concentration of each drug was maintained constant during the treatment phases. Concentrations of 10 nM trametinib, 200 nM PD0325901, and 200 nM selumetinib were prepared by serially diluting their

respective stock solutions in the culture medium. These solutions were prepared twice the final concentrations for testing against colorectal tumor spheroids. Next, 30 μ L from each of these drug solutions was added to each well of the destination plate that contained a spheroid in the DEX phase drop immersed in 30 μ L of the aqueous PEG phase. This addition diluted concentrations of PEG and DEX, converting the two-phase system to a single medium phase containing trace amounts of the polymers. It also reduced drug concentrations to 5 nM trametinib, 100 nM PD0325901, and 100 nM selumetinib. After 72 hours, 30 μ L of each drug solution at its working concentration was added to the corresponding wells. At the end of T1, the culture medium containing the inhibitors was robotically aspirated out of the microwells and repeatedly diluted with cell culture medium leaving trace amount of drug. Next, to start the recovery phase, 30 μ L of fresh medium was added to the wells containing the spheroids. Another 30 μ L of fresh medium was added 72 hours later. At the end of R1, half of the medium was carefully aspirated from each well. The T2 treatment was initiated by adding a drug solution containing 2 \times concentration of each inhibitor in 30 μ L of the medium, and renewal was done by adding 30 μ L of each drug solution at 1 \times concentration after 72 hours. In parallel, 30 μ L of fresh medium was added to spheroids from R1, and 30 μ L fresh medium was renewed after 72 hours. These spheroids that were grown in the medium were used as the non-treated group for the T2 treatment. At the end of T2, drug solutions were removed from the wells and the R2 phase was initiated. This was followed by another round of treatment (T3) that was initiated by adding a drug solution containing 2 \times the concentration of each inhibitor in 30 μ L of the medium, and renewed by adding 30 μ L of each inhibitor at 1 \times the concentration after 72 hours. In parallel, 30 μ L of fresh medium was added to spheroids from Recovery 2, and 30

μL of fresh medium was renewed after 72 hours. These spheroids that were grown in the medium were used as the non-treated group for the T3 treatment.

3.1.5 Dose Dependent Cyclical Treatment of Spheroids with MEKi and Recovery from Treatments

To compare dose responses of spheroids to the MEKi, spheroids were assigned into two groups. Spheroids of the first group were treated with each inhibitor, i.e., 5 nM trametinib, 100 nM PD0325901, and 100 nM selumetinib, followed by a recovery phase. The experimental protocol for T1 and R1 phases was described above. Then, the recovered spheroids were treated with different concentrations of the inhibitors during treatment T2, i.e., $0.25 \times \text{IC}_{50}$, $0.5 \times \text{IC}_{50}$, $1 \times \text{IC}_{50}$, $2 \times \text{IC}_{50}$, and $4 \times \text{IC}_{50}$ of the MEKi. IC_{50} values of the three MEKi are listed in Table 3-3. To initiate the treatment T2, the volume of the medium in microwells was measured, and the solution of each MEKi at twice the desired concentrations was added to wells. The treatments were renewed by adding each inhibitor solution at a $1 \times$ concentration in 30 μL of the medium after 72 hours. On the other hand, spheroids in the second group were treated only once with each of the MEKi at $0.25 \times \text{IC}_{50}$, $0.5 \times \text{IC}_{50}$, $1 \times \text{IC}_{50}$, $2 \times \text{IC}_{50}$, and $4 \times \text{IC}_{50}$ concentrations during T1. The effects of dose-dependent treatments on spheroids from the two groups were quantitatively compared as described below.

3.1.6 Analysis of Growth of Spheroids to Quantify Drug Resistance

Prior to the start of experiments and at the end of each cycle of treatment and recovery, phase images of spheroids were captured using an inverted microscope (Axio Observer, Zeiss) equipped with a high-resolution camera (AxioCam MRM, Zeiss). The

images were analyzed using ImageJ software (NIH) to measure the diameter of spheroids. The volume of spheroids was determined from the diameter data assuming a spherical shape for spheroids. The inhibitor concentration, c , and the treatment and recovery time, $t = 6$ days, were the same during each round. A growth rate parameter (k_c) was calculated for spheroids that were treated with a MEKi by finding the difference in the volume of spheroids at the end and beginning of each round of treatment. Similarly, the growth rate (k_0) was calculated for spheroids that were not treated with MEKi but cultured in the medium by finding the difference in the volume of spheroids at the end and beginning of each round. A normalized growth rate parameter was found by dividing the growth rate of treated spheroids by the growth rate of untreated spheroids, i.e., k_c/k_0 , to quantify resistance. Experiments for each condition used $n = 14$ spheroids. Statistical analysis was performed using student's t-test in Microsoft Excel and considering a significance level of $p < 0.05$ between the treatment groups.

Similarly, we calculated the growth rate of spheroids for the two groups of spheroids treated with different concentrations of each MEKi described above. The growth rates of spheroids at five different treatment concentrations, i.e., $k_n \cdot IC_{50}$, where $n = 0.25, 0.5, 1, 2, \text{ and } 4$, were calculated by subtracting the volumes of spheroids measured at the beginning and end of treatments. Similarly, the growth rate of untreated spheroids (k_0) was calculated by subtracting the volume of untreated spheroids measured at the beginning and end of each round. A normalized growth rate parameter was computed by dividing the growth rate of treated spheroids by the growth rate of untreated spheroids, i.e., k_c/k_0 , to quantify resistance. Furthermore, a parametric approach using area under the dose response curve (AUC) was employed to quantify the resistance to the MEKi. [86] Experiments for

each condition used $n = 7$ spheroids. Statistical analysis was performed using student's t-test in Microsoft Excel and considering a significance level of $p < 0.05$ between the two treatment groups.

3.1.7 Western Blotting

For all Western blot experiments, spheroids were harvested from 384-well plates after treatment and transferred into 50 ml conical tubes. After centrifugation and removing of the supernatant, spheroids were washed with PBS, and lysed in 500 μ L of complete RIPA buffer (50 mM Tris-HCl, 150 mM NaCl, 1% NP-40, 0.5% sodium deoxycholate, and 0.1% SDS, pH 7.4 ± 0.2) with protease inhibitor (complete mini, Roche Diagnostics) and phosphatase inhibitor (Thermo Fisher Scientific). To ensure complete lysis, spheroids were sonicated (Vibra-Cell, Sonics) twice for 5 s at a 20% amplitude level. Total protein concentration was determined using a BCA quantification assay kit (Thermo Fisher Scientific). Then, 10–20 μ g of the protein solution was loaded onto a 4–15% gel (Bio-Rad) for electrophoresis and the gel was transferred onto a nitrocellulose membrane by electroblotting. Membranes were blocked with 5% BSA (Sigma) for 1 h. Primary antibodies for phospho-p44/42 MAPK (Erk1/2), p44/42 MAPK (Erk1/2), phospho-AKT (Ser473), AKT (pan) (C67E7), phospho-BRAF (Ser445), BRAF (D9T6S), phospho-STAT3 (Tyr705), and STAT3 (79D7) were purchased from Cell Signaling Technology. Solutions of primary antibodies were prepared at concentrations recommended by the manufacturer. Membranes were incubated overnight at 4 °C with primary antibody solutions. After repeated washing, membranes were incubated with a horseradish peroxidase (HRP)-conjugated secondary antibody for 1 h, followed by repeated washing.

Detection was carried out using an ECL chemiluminescence detection kit (GE Health Care) and FluorChem E imaging system (ProteinSimple).

3.1.8 Short-term Combination Treatment of Spheroids

Trametinib, PD0325901, and selumetinib were used in combination with dactolisib in separate experiments. The IC_{50} value for each inhibitor against HT-29 spheroids was obtained from its respective dose–response curve (Table 3-3). Each of the three MEKi and dactolisib were combined at fixed concentration ratios of multiples (0.25, 0.5, 1, 2, 4) of the respective IC_{50} values. Solutions with these concentrations were made by serially diluting the stock solutions in the culture medium. Each combination of concentrations for a pair of drugs used $n = 14$ replicates. In parallel to each combination treatment, spheroids of HT-29 cells were treated with the MEKi or dactolisib used as single agents. Next, PrestoBlue was added to wells and after incubating the spheroids for 4 hours, the fluorescence signal was measured with a plate reader (Synergy H1M, BioTek Instruments). Both control (untreated) and drug-treated groups had $n = 14$ replicates. Viability of spheroids treated with each concentration of an inhibitor was normalized to that of non-treated spheroids and expressed as percent viability. The viability data is a relative measure of live cells in treatment compared to the vehicle control spheroids. GraphPad Prism 5 was used to fit a four-parameter sigmoidal dose–response curve to the viability data and to determine AUC. A combination index (CI) was used to determine synergism between combinations of the inhibitors.

3.1.9 Long-term Cyclic Combination Drug Treatment/Recovery of Spheroids

Specific pairs of concentrations of each of the three MEKi and dactolisib that generated synergistic responses in HT-29 spheroids during T1 treatment were selected for long-term experiments. These concentrations were $0.25 \times IC_{50}$ for trametinib/dactolisib, $0.25 \times IC_{50}$ for PD0325901/dactolisib, and $0.5 \times IC_{50}$ for selumetinib/dactolisib pairs. In parallel to each combination treatment, HT-29 spheroids were treated with the single-agent MEKi or dactolisib. The effectiveness of long-term treatment with each drug combination was assessed by comparing the growth inhibitory effects of the combination pair and each inhibitor used alone. The growth rates of spheroids under no treatment (vehicle control), single-agent treatments, and combination treatments were calculated by subtracting the volume of spheroids at the end of the 30-day treatment period and the volume of spheroids at the beginning. To calculate growth inhibitory effects at the end of day 30, the difference in growth rates of control spheroids (k_0) versus treated spheroids (k_c) were divided by k_0 , i.e., Growth inhibition = $(k_0 - k_c)/k_0$. One-way ANOVA was used to analyze the difference among the single-agent treatments, combination treatments, and vehicle control followed by a post-hoc Tukey test. The analysis was performed using Minitab ($n = 7$).

3.2 Results and Discussion

Below, results of modeling drug resistance using 3D tumor model under long-term cyclical treatment are presented. A mechanistic approach to identify the molecular basis of drug resistance and rationally designed combination approach used to overcome drug resistance in colorectal cancer spheroids are shown and discussed.

3.2.1 Microprinting of Tumor Spheroids

The aqueous two-phase system (ATPS) microprinting approach effectively confined cancer cells in a DEX phase nanodrop to facilitate self-assembly into a compact spheroid within 48 hours in each well of 384-well plates (Figure 3-1a-c). [178] Immersion of the nanodrop within the aqueous PEG phase ensured diffusive influx of nutrients into the drop phase to nourish the cells and efflux of waste products of cells into the immersion phase. [81] Unlike several other cell printing/patterning techniques, this microprinting approach does not exert any mechanical, thermal, or chemical stresses on cells, producing spheroids containing fully viable cells. [81] Renewing the culture medium or adding a drug solution reduced concentrations of PEG and DEX polymers below a threshold required to maintain two separate phases (Figure 3-1d). [179] Thus, this approach was solely used to conveniently micropattern spheroids and was not needed after spheroids formed. Medium exchanges every 72 hours ensured availability of fresh nutrients and removal of waste products of cells to support cellular metabolic activities. We have previously shown that our robotic spheroid technology generates consistently-sized spheroids that reproduce biologic properties of solid tumors. [86], [164]

3.2.2 Screening of Molecular Inhibitors Against Colorectal Tumor Spheroids

B-RAF and PIK3CA mutations in HT-29 cancer cells constitutively activate signaling through MAPK and PI3K pathways. [141] Targeting these oncogenic pathways has shown efficacy against colorectal cancer both *in vitro* and *in vivo*. [129], [180], [181] To identify effective inhibitors against these pathways in our model of drug resistance, we selected a panel of inhibitors of MAPK and PI3K pathways and screened them dose-dependently against the colorectal tumor spheroids. The list of the inhibitors and their

molecular targets are given in Tables 3-1 and 3-2. Our selection of molecular inhibitors of MAPK and PI3K pathways was based on selectivity of the compounds against their targets and their use in pre-clinical studies either alone or in combination therapies against colorectal cancers. We compared effectiveness of the inhibitors based on AUC analysis previously described. [86] The AUC value ranges from 0 to 1. An AUC value of 0 means 100% cell death, whereas an AUC value of 1 indicates 100% viability. This analysis segregates compounds with low AUC values that are more effective from the less effective compounds with higher AUC values. Among the inhibitors of MAPK (Figure 3-1e-f) and PI3K (Figure 3-1g-h) pathways, trametinib, PD0325901, and selumetinib received AUC scores of 0.33, 0.59, and 0.63, respectively, and ranked as the most effective compounds. This screening revealed that suppressing the MEK1/2 kinase in HT-29 spheroids most effectively inhibited growth of spheroids. The sensitivity of the colorectal cancer cells to these MEKi is consistent with studies that showed dependence of cancer cells on MEK1/2 for survival and proliferation, [182] and thus, development of various MEKi to target these kinases. [183] Thus, we selected these three MEKi to model acquired drug resistance of colorectal tumor spheroids.

3.2.3 Long-Term Cyclic Treatment of Spheroids with MEKi

To demonstrate treatment-induced (adaptive) resistance of colorectal cancer cells to MEKi, we determined effectiveness of the three MEKi against HT-29 spheroids for three six-day cycles of treatment separated by six-day recovery intervals (Figure 3-2a). We calculated the growth rate parameter, k_c , for drug-treated spheroids (Figure 3-3a-c) and k_0 for control spheroids (Figure 3-3d-f). Representative images of spheroids before drug

treatments, and images of drug-treated and non-treated spheroids from different rounds are shown in Figure 3-3g-i. The values for k_c and k_0 from different rounds are tabulated in Figure 3-2b-d. This resulted in average k_c/k_0 values of -0.1941 , -0.2275 , and -0.0632 for the three rounds of treatment with 5 nM trametinib. The negative k_c/k_0 values during the three treatment rounds indicate that trametinib produced a cytotoxic effect. Our analysis showed that the values of k_c/k_0 during T2 and T3 were significantly different ($p < 0.05$) (Figure 3-2e). The average k_c/k_0 values with 100 nM PD0325901 treatment significantly increased from 0.0272 to 0.2930 and to 0.5294 for the three consecutive rounds of treatment ($p < 0.05$), respectively (Figure 3-2f). The k_c/k_0 value of T1 treatment indicates that PD0325901 was cytostatic but this effect did not persist in subsequent treatment rounds. The average k_c/k_0 values with 100 nM selumetinib treatment also showed a significant increase from 0.1777 to 0.3231, and to 0.4745 for the three treatment rounds ($p < 0.05$) (Figure 3-2g). The k_c/k_0 values indicate that selumetinib did not generate a cytostatic effect on HT-29 cells. Overall, increasing k_c/k_0 values from T1 to T3 treatments with all three MEKi indicate that effects of the compounds diminished during the cyclical treatments.

To ensure that treatment-induced resistance of HT-29 spheroids to the MEKi was not limited to a single drug concentration, we performed dose-dependent tests with each MEKi and compared the normalized growth rate of spheroids treated with five different drug concentrations during T1 and T2. We used the IC_{50} value of each MEKi against HT-29 spheroids (Table 3-3) and selected the working concentrations as multiples of the IC_{50} values. Results showed that normalized growth rates of HT-29 spheroids significantly decreased during the second treatment round at all the concentrations (Figure 3-4a-c)

($p < 0.05$), except for treatments with trametinib at higher concentrations of $2 \times IC_{50}$ and $4 \times IC_{50}$. In addition, we quantitatively compared growth rates during T1 and T2 under each MEKi treatment by computing the respective AUC. The results showed an increase of 1.53 folds, 3.18 folds, and 2.59 folds in AUC for treatments with trametinib, PD0325901, and selumetinib, respectively. This validated that HT-29 spheroids developed resistance to the MEKi over a wide range of concentrations. Additionally, to validate the utility of our tumor spheroids to model treatment-induced resistance, we performed cyclical treatment and recovery of spheroids of a different colorectal cancer cell line, HCT116, with MEKi. Treatment with 5 nM trametinib significantly increased the normalized growth rate (k_c/k_0) from -0.3795 to 0.0408 and to 0.3292 during three consecutive rounds of treatment ($p < 0.05$), respectively (Figure 3-5).

We modeled treatment-induced resistance to MEKi by cyclically treating colorectal tumor spheroids with potent molecular inhibitors of MEK1/2 and recovering them from the treatments. Although complex mathematical approaches have been developed to model growth, transition, and dissemination dynamics in drug-sensitive and drug-resistant cancer cells, [184], [185] for simplicity, we used growth rate of spheroids as a metric to quantify evolving resistance of cancer cells to the MEKi in our experimental model. We and others have demonstrated that growth of spheroids from morphological measurements closely correlates with that from biochemical analyses using MTT and Prestoblue. [86], [186], [187] Therefore, we used size measurements of spheroids as a straightforward approach to determine effects of drug treatments and evolution of drug resistance in spheroids. Normalized growth rate (k_c/k_0) of spheroids takes into account changes in the size of spheroids during cycles of treatments with molecular inhibitors. We identified drug

resistance of spheroids if their growth rate during a treatment cycle was significantly larger than its preceding treatment phase, i.e., $(k_c/k_0)_{i+1} > (k_c/k_0)_i$. Our quantitative study using the growth rate metric established that repeated use of MEKi induces resistance in colorectal tumor spheroids independent of drug concentration (Figures 3-2, 3-3, and 3-4). Our result is consistent with *in vivo* studies that showed cyclic treatments of tumor xenografts with MEKi did not reduce tumor size. [188], [189]

The treatment-induced resistant cell population has highly likely a different genetic makeup than the sensitive population of cells. These resistant population may consist of stem cell-like cells that thrive the treatment. Alternatively, resistant cells can activate multiple signaling pathways to thrive and continuously grow. We will analyze the resistant population using molecular analysis to investigate activation of signaling pathways that promote proliferation of cancer cells despite repeated treatments with MEKi.

3.2.4 Molecular Analysis of Adaptive Drug Resistance in Colorectal Tumor Spheroids

Despite inhibition of MEKi, colorectal cancer cells often show resistance to these inhibitors by activating other signaling pathways such as PI3K/AKT/mTOR or JAK/STAT to mediate resistance to MEKi. [93] Alternatively, continuous exposure to a MEKi may lead to mutation of MEK, [170] while resistance to continuous exposure to RAFi may occur through amplification of B-RAF or other components of the MAPK pathway. [99], [171] Therefore, understanding mechanisms of drug resistance and developing strategies to overcome them is crucial to improve colorectal cancer treatments. Below, we present and discuss our results on the effects of MEKi treatments on MAPK, PI3K, and STAT signaling pathways.

3.2.4.1 Effect of MEKi treatments on MAPK Pathway Activity

To elucidate molecular mechanisms of treatment-induced resistance of HT-29 spheroids to the MEKi, we first probed activity of ERK proteins because HT-29 cells have gain-of-function mutations in the MAPK pathway. [168] We found that unlike selumetinib, trametinib and PD0325901 significantly reduced ERK phosphorylation in HT-29 spheroids during treatment T1 by 16% and 25%, respectively (Figure 3-6a and d). We also investigated ERK phosphorylation in spheroids that were recovered from MEKi treatments for 6 days and found that the protein activity returned to levels comparable to those in control spheroids grown in drug-free medium for 12 days (Figure 3-6b and e). Furthermore, we determined ERK activity after the second round of treatment (T2) and found that ERK phosphorylation was significantly reduced with 5 nM trametinib and 100 nM PD0325901 treatments, but not with 100 nM selumetinib treatment (Figure 3-6c and f). Thus, cells still showed transient responses to the former two inhibitors.

Our molecular analysis showed that trametinib and PD0325901 only moderately downregulated ERK phosphorylation during the first round of treatment, despite specificity of these MEKi toward their target. We suspect that the moderate effects of these MEKi was due to their low concentrations used in our experiments (Figure 3-6a and d). Our previous study using a higher trametinib concentration (100 nM) showed complete inhibition of ERK activity in HT-29 spheroids. [86] Despite moderate effects of these compounds, ERK phosphorylation fully recovered during the recovery phase (Figure 3-6b and e), indicating that the MEKi produced a transient response in the cancer cells. Gain of ERK activity during the recovery phase allowed the colorectal tumor spheroids to show sensitivity to the MEKi during the second round of treatments with trametinib and

PD0325901 (Figure 3-6c and f). The inability of selumetinib to downregulate ERK signaling during subsequent treatment rounds was likely a reason for the increase in growth rate and resistance of colorectal tumor spheroids to this compound.

3.2.4.2 Effect of MEKi Treatments on PI3K Pathway Activity

Activation of PI3K pathway is a major mechanism of feedback signaling in many cancers including colorectal cancers. [190]–[192] We investigated whether treating HT-29 spheroids with a MEKi during T1 augments activity of the PI3K pathway in HT-29 spheroids by probing phosphorylation of AKT. Unlike in control spheroids, treatments with all three MEKi significantly increased AKT phosphorylation in cells by 19.7, 11.4, and 12.1 folds for trametinib, PD0325901, and selumetinib, respectively (Figure 3-6a and g). Shorter exposure of HT-29 spheroids to the MEKi for 48 hours also resulted in markedly higher *p*AKT than that in respective control spheroids (Figure 3-7). To determine whether recovery of spheroids from MEKi treatments reduces AKT activity, we quantified the *p*AKT/*t*AKT ratio at the end of R1 phase. Results showed that AKT activity reduced during R1 but still remained significantly higher by 2.3, 1.6, and 1.7 folds in spheroids recovered from trametinib, PD0325901, and selumetinib, respectively, than in control spheroids maintained in culture medium for 12 days (Figure 3-6b and h).

To elucidate if treatment-induced feedback signaling persisted in tumor spheroids, we determined AKT activity after treatment T2. Phosphorylation of AKT in spheroids after T2 was significantly higher than that in spheroids that were treated during T1, recovered (R1), but did not receive any treatment during T2 (Figure 3-6c and i). This increase was 1.2, 3.6, and 1.8 folds for treatments with trametinib, PD0325901, and selumetinib,

respectively. These results suggest that MEKi treatments quickly increase AKT signaling that is sustained even when the drug is removed and when spheroids are exposed to drugs again.

As a validation step and to explore whether upregulated AKT activity due to the MEKi treatments was not limited to B-RAF mutant colorectal cancer cells, we treated spheroids of HCT116 colorectal cancer cells, which harbor KRAS mutation, with trametinib. Although trametinib treatment downregulated ERK activity in HCT116 spheroids, it induced AKT signaling (Figure 3-8a-c). This indicates that MEKi treatment induces feedback signaling through the PI3K/AKT pathway irrespective of B-RAF or KRAS mutations in the cell lines we studied. Our results are consistent with other reports that showed phosphorylation of AKT in various RAF-mutant and RAS-mutant lung and colorectal cancer cells under RAFi or MEKi treatments, [162], [193] and in a genetically engineered Apc-mutant and KRAS-mutant colorectal cancer mouse model under MEK162 treatment. [194]

The cell lines used in this study harbor B-RAF and PIK3CA mutations. Future studies will require use of cell lines that lack mutations in B-RAF, RAS, or PIK3CA to validate that MEKi treatment induces feedback signaling through PI3K/AKT pathway.

3.2.4.3 Effect of MEKi Treatments on B-RAF and STAT3 Signaling

It was reported that targeting MEK in colorectal cancer resulted in amplification of B-RAF, an upstream kinase of MEK, that in turn increased abundance of phosphorylated MEK and impaired the ability of selumetinib to inhibit ERK signaling. [99], [195] Because we did not observe a major suppression of ERK after treatment with a MEKi, we asked

whether MEKi treatments cause B-RAF amplification. Our result did not show significant changes in B-RAF activity after treatment T1 of HT-29 spheroids with the MEKi and after the R1 phase (Upper panel blots in (Figure 3-9a-b and 3-9c-d). Furthermore, it was shown that c-MET/STAT3 signaling mediates adaptive resistance of B-RAF mutant colorectal cancer to MEKi. [93] Therefore, we examined if treating HT-29 spheroids with the MEKi leads to the activation of this pathway. Our result showed that there was no upregulation of STAT3 kinase in the MEKi-treated HT-29 spheroids after T1 and R1 phases (Lower panel blots in (Figure 3-9a-b and 3-9e-f).

3.2.5 Combination Therapy Effect on Treatment-Induced Drug Resistance

We combined each of the three MEKi with dactolisib, a potent PI3K/mTOR inhibitor, to study whether this approach could block treatment-induced resistance to MEKi in the colorectal tumor spheroids. Dactolisib was selected for the combination experiment because it was more effective than other PI3K inhibitors tested against HT-29 spheroids (Figure 3-1g-h). We used a constant ratio approach to treat the spheroids and evaluated responses of spheroids to the treatments at the end of the six-day period, i.e., T1, using AUC and synergism analysis. [196] The computed AUC values showed that the combination of trametinib and dactolisib was 28% and 30% more effective than the respective single-agent treatments (Figure 3-10a). We also found that the combination of PD0325901 and dactolisib enhanced the response by 36% and 41% than treatments with PD0325901 or dactolisib alone, respectively (Figure 3-10b). The combination of selumetinib and dactolisib also increased effectiveness by 15% and 18% compared to that when we used each respective inhibitor alone (Figure 3-10c). Additionally, the combination of each MEKi with dactolisib prevented growth of the spheroids and markedly

reduced their size (Figure 3-10a-c). Both trametinib/dactolisib and PD0325901/dactolisib pairs were synergistic ($CI < 1$) at all combinations of concentrations tested (Figure 3-10d and e). Except for the $0.25 \times IC_{50}$ concentrations pair, the selumetinib/dactolisib pair was also synergistic at all other concentrations used (Figure 3-10f). Furthermore, we determined the strength of synergism for each combination of drugs using the range of CI values shown in Table 3-4. We successfully blocked this feedback signaling by combining a MEKi and dactolisib and showed that all the combinations synergistically inhibited growth of HT-29 spheroids.

3.2.6 Molecular Effects of Combination Treatments

We studied the effect of combination therapies with the MEKi and dactolisib to inhibit feedback signaling in colorectal tumor spheroids. We treated HT-29 spheroids with three different multiples of IC_{50} of each of the MEKi and dactolisib for 48 hours, and determined protein level activities of ERK1/2 and AKT in HT-29 spheroids. The inhibitors at these concentrations showed synergism in dose-dependent experiments (Figure 3-10). Table 3-3 shows the IC_{50} value of each inhibitor against HT-29 spheroids.

The trametinib/dactolisib pair reduced ERK activity marginally, but significantly, only at the combined IC_{50} concentrations (Figure 3-11a-b). The inhibitors significantly reduced AKT phosphorylation dose-dependently at all three concentration pairs. The largest inhibition of AKT activity was 47% at the IC_{50} concentrations (Figure 3-11a and c). The synergy between trametinib and dactolisib combination (Figure 3-10a and d) is likely due to the downregulation of *p*-AKT, at least for the two lower combination pairs, i.e., $0.25 \times IC_{50}$ and $0.5 \times IC_{50}$.

The PD0325901/dactolisib pair significantly downregulated ERK phosphorylation at the combined concentrations and in a dose-dependent manner. The largest inhibition was 98% at the combined IC_{50} concentrations (Figure 3-11e). Although this combination did not suppress AKT activity at the $0.25 \times IC_{50}$ and $0.5 \times IC_{50}$ concentrations, it reduced AKT phosphorylation by 24% at the combined IC_{50} concentrations (Figure 3-11d and f). This result suggests that the synergy between these two inhibitors (Figure 3-11b and e) is largely due to the downregulated ERK activity.

Selumetinib and dactolisib also significantly and dose-dependently reduced ERK phosphorylation by 58%–89% of the vehicle control (Figure 3-11g and h). At these concentrations, AKT activity was also significantly inhibited by 52%–27% (Figure 3-11g-i), albeit it showed an increase with increased drug concentrations. It appears that simultaneous downregulation of AKT and ERK activities facilitated the synergy between selumetinib and dactolisib (Figure 3-10c and f).

Combination of MEKi and dactolisib downregulated phosphorylation of both ERK and AKT when we used sufficiently high concentrations of the compounds. This molecular finding supports our phenotypic data of successfully blocking feedback signaling by combining a MEKi and dactolisib. Our findings are also in agreement with previous reports that MEKi and PI3K/mTOR inhibitor combinations generated anti-proliferative effects in colorectal cancer cells by reducing ERK, AKT, and S6 activities. [162], [188], [197], [198]

3.2.7 Growth Inhibition of Tumor Spheroids by Long-Term Cyclic Combination

Treatments

Our single-agent treatments of colorectal spheroids with MEKi activated AKT signaling. Importantly the protein activity was sustained during the long-term single-agent

MEKi treatments, providing a rationale for combination therapy of the spheroids. Thus, we asked whether specific drug combinations would be effective against growth of tumor spheroids during long-term treatment/recovery cycles (Figure 3-2a). We used the lowest synergistic concentration pairs of each of the MEKi and dactolisib, i.e., $0.25 \times IC_{50}$ for trametinib/dactolisib, $0.25 \times IC_{50}$ for PD0325901/dactolisib, and $0.5 \times IC_{50}$ for selumetinib/dactolisib to demonstrate long-term efficacy of the combination treatments. We also performed single-agent treatments with the same concentration of each inhibitor used in the respective combination treatments. In addition, we considered spheroids maintained in cell culture medium for 30 days as the vehicle control. Both the single-agent and combination treatments followed the scheme of Figure 3-2a. Comparing growth kinetics of spheroids for the vehicle control, single-agent treatments, and combination treatment in each panel of Figure 3-12a-c showed that the respective combination treatment significantly delayed growth of the spheroids over the 30-day period.

To quantitatively compare efficacy of various treatments, we first calculated growth rate of spheroids as the difference in the volume of spheroids over time. Tables 3-5, 3-6 and 3-7 show the average values of growth rates for all the treatments and the vehicle control. Next, we calculated the growth inhibition of spheroids by each treatment as the difference in the growth rates of treated and vehicle control spheroids divided by the growth rate of the vehicle control spheroids. The selumetinib/dactolisib pair was the most effective and inhibited the growth of HT-29 spheroids by 88%. This was followed by the PD0325901/dactolisib pair that showed a growth inhibition of 80%, and the trametinib/dactolisib pair with a 63% inhibitory effect. Figure 3-12a-c also includes the quantified growth inhibition of all single-agent and combination treatments.

Our results are consistent with studies that showed intermittent/cyclic dosing of MEKi with PI3K inhibitors significantly suppresses growth of tumors in animal models. For example, the MEKi GDC-0943 exhibited synergy with the PI3K inhibitor GDC-0941 by inhibiting tumor growth and inducing apoptosis in DLD-1 colorectal tumor xenografts. [188] Similarly, the MEKi PD0325901 exhibited synergy with the PI3K inhibitor GDC-0941 in non-small cell lung cancer xenografts, [199] and HCT116 and HT-29 colorectal xenografts. [200] Importantly, we demonstrated that long-term cyclic treatments of colorectal tumor spheroids with combinations of MEKi and dactolisib effectively prevented growth of the spheroids by as high as 88% compared to the untreated vehicle controls. We achieved this improved activity at significantly lower doses of MEKi and dactolisib, an effect that was significantly greater than that with either single-agent treatment at the same drug concentration. Although some clinical trials combining MAPK and PI3K inhibitors has been unsuccessful because of toxicity, [100] using a lower concentration of each compound or temporal changes in dosing such as in cyclic treatments may help reduce toxicity. Our 3D resistance model enables high throughput testing of different drug combinations over a wide concentration range to select effective pairs of drugs at optimal doses and also allows testing different treatment regimens to identify those with reduced toxicity than dual combination treatments.

3.3 Summary

This study presented a novel model of cyclic drug treatment and recovery of tumor spheroids to demonstrate that single-agent treatments with targeted kinase inhibitors leads to adaptive drug resistance of cancer cells. The utility of our spheroid technology to model

treatment-induced resistance of colorectal cancer cells coupled with a comprehensive molecular analysis identified molecular makers of resistance and helped rationally design combination treatments that effectively blocked growth of tumor spheroids. Our 3D resistance model will advance mechanistic understanding of drug resistance in different cancers and testing of therapeutics and different regimens to overcome resistance with reduced toxicity. Furthermore, the use of this model with patient derived cells of different genetic signatures may offer a major precision medicine tool to improve treatment outcomes.

Table 3-1. List of MAPK inhibitors and their targets

Inhibitor	Target
Trametinib	MEK1/2
PD0325901	MEK1/2
Selumetinib	MEK1/2
Sorafenib	RAF-1, B-RAF, VEGFR-2
AZ628	B-RAF, BRAFV600E, c-RAF1
GDC0994	ERK1/2
Ulixertinib	ERK1/2

Table 3-2. List of PI3K inhibitors and their targets

Inhibitor	Target
Dactolisib	PI3K/mTOR
PI-103	PI3K
GSK1059615	PI3K/mTOR
Pictilisib	PI3K

Table 3-3. IC₅₀ values of molecular inhibitors against HT-29 spheroids measured after 6 days of treatment

Inhibitor	IC₅₀ (μM)
Trametinib	0.00154
Selumetinib	0.09
PD0325901	0.07
Dactolisib	2.9

Table 3-4. The ranges of combination index, and description of each range of CI values as described by Chou and Talalay

Range of Combination Index	Description
<0.1	very strong synergism
0.1-0.3	strong synergism
0.3-0.7	synergism
0.7-0.85	moderate synergism
0.85-0.90	slight synergism
0.90-1.10	nearly additive
1.10-1.20	slight antagonism
1.20-1.45	moderate antagonism
1.45-3.3	Antagonism
3.3-10	strong antagonism
>10	very strong antagonism

Table 3-5. Growth rates of HT-29 spheroid for control, single agent, and combination treatment

	Control	1/4 × IC₅₀ trametinib	1/4 × IC₅₀ Dactolisib	Trametinib/dactolisib combination 1/4 × IC₅₀
Initial volume (mm³)	0.0281	0.0281	0.0281	0.0281
Final volume (mm³)	0.3842	0.3231	0.2201	0.1605
Growth rate (mm³/day)	0.0118	0.0098	0.0064	0.0044

Table 3-6. Growth rates of HT-29 spheroid for control, single agent, and combination treatment

	Control	$1/4 \times IC_{50}$ PD0325901	$1/4 \times IC_{50}$ dactolisib	PD0325901/dactolisib combination $1/4 \times IC_{50}$
Initial volume (mm ³)	0.0281	0.0281	0.0281	0.0281
Final volume (mm ³)	0.3842	0.2448	0.2201	0.1019
Growth rate (mm ³ /day)	0.0118	0.0072	0.0064	0.0024

Table 3-7. Growth rates of HT-29 spheroid for control, single agent, and combination treatment

	Control	$1/2 \times IC_{50}$ selumetinib	$1/2 \times IC_{50}$ dactolisib	Selumetinib/dactolisib combination $1/4 \times IC_{50}$
Initial volume (mm ³)	0.0281	0.0281	0.0281	0.0281
Final volume (mm ³)	0.3842	0.2672	0.2093	0.0691
Growth rate (mm ³ /day)	0.0118	0.0079	0.0060	0.0014

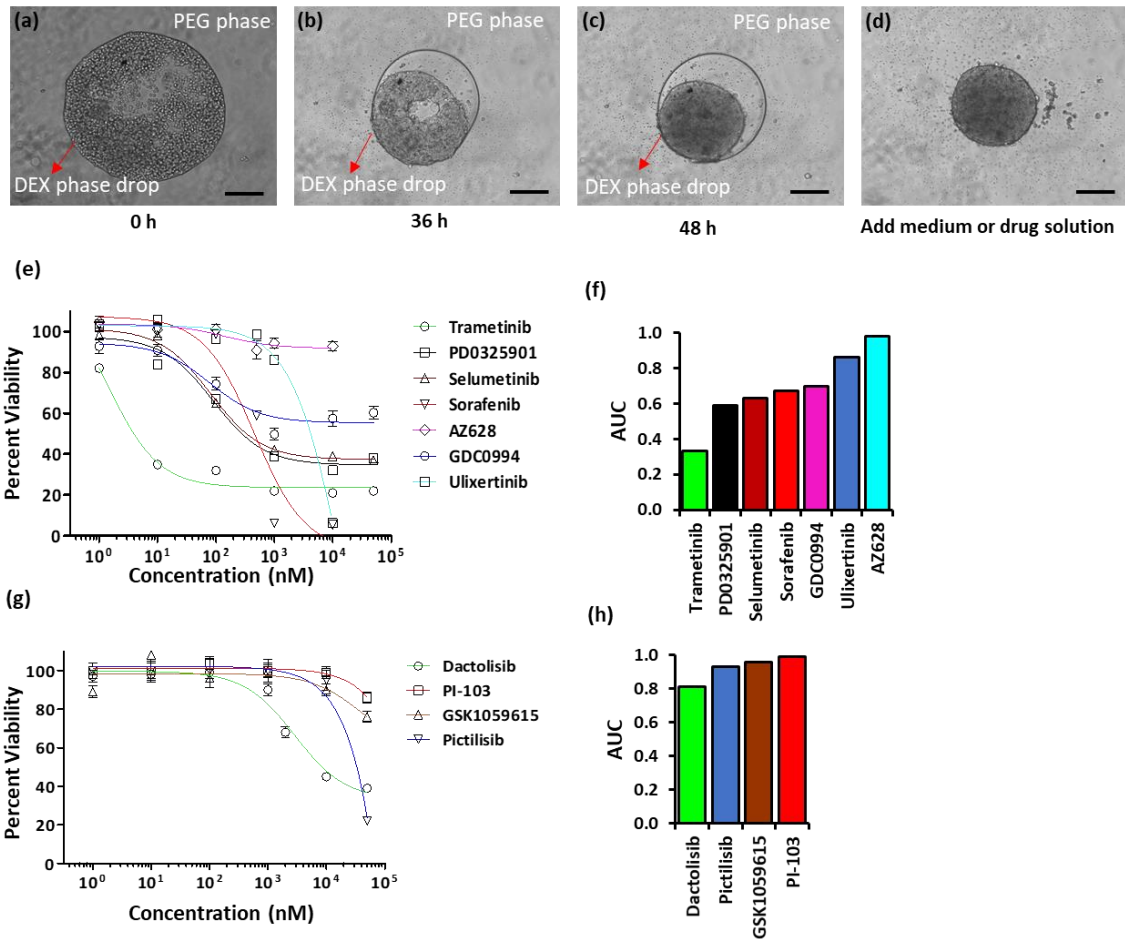


Figure 3-1. Tumor spheroid formation using ATPS microprinting, and screening of inhibitors of MAPK and PI3K signaling pathways against HT-29 spheroids. (a) A robotic liquid handler dispensed 0.3 μ L of the aqueous DEX phase solution containing HT-29 cancer cells into a microwell containing the aqueous PEG phase. (b,c) Cancer cells remained within the nanodrop and formed a compact spheroid. (d) Addition of culture medium or a drug to the microwell diluted out the ATPS into a single medium phase containing the spheroid. (e) Dose responses of HT-29 spheroids to RAF, MEK, and ERK inhibitors. (f) Normalized AUC values from drug tests with HT-29 spheroids. (g) Dose responses of HT-29 spheroids to PI3K inhibitors. (h) Normalized AUC values from their drug tests with HT-29 spheroids. Scale bar is 200 μ m.

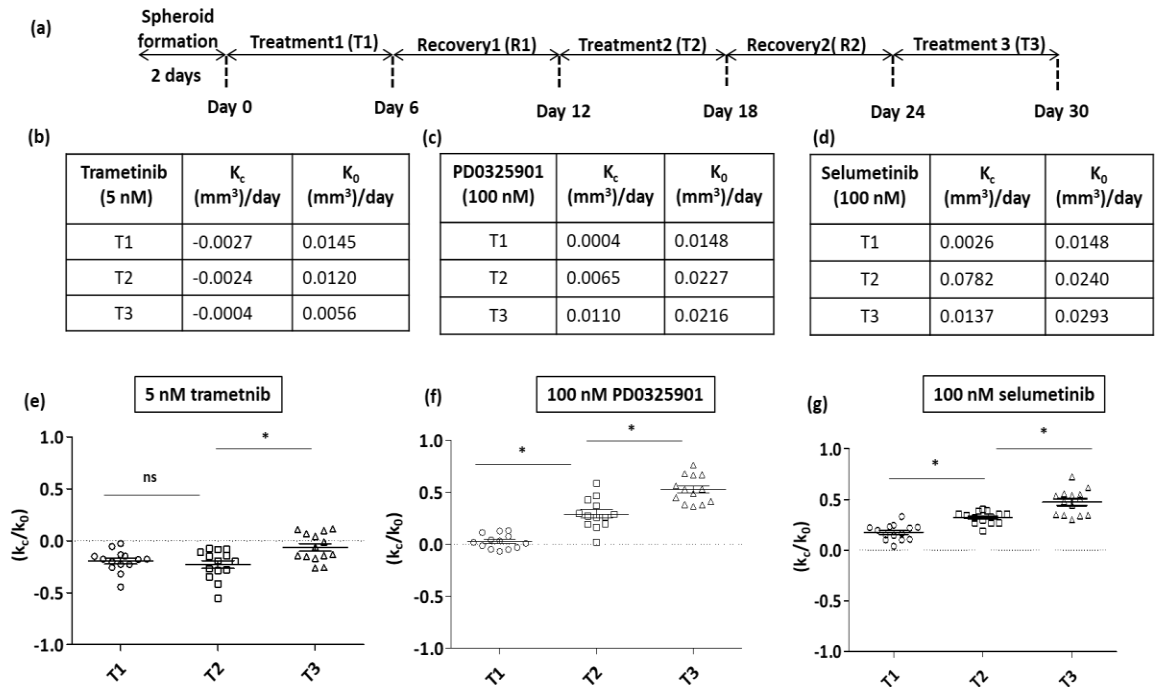


Figure 3-2. Cyclic drug treatment and recovery of colorectal tumor spheroids. (a) The schematic shows the experimental protocol for three cycles of treatment of HT-29 spheroids with MEKi (5 nM trametinib, 100 nM PD0325901, and 100 nM selumetinib) separated by two recovery phases. A fixed concentration of each inhibitor was used for the three treatment rounds. (b-d) Average growth rates of HT-29 spheroids during the three rounds of treatments with trametinib, PD0325901, and selumetinib, respectively. k_c was calculated as the difference in volume of drug-treated spheroids at the end and beginning of each treatment round. k_0 was calculated as the difference in volume of non-treated spheroids at the end and beginning of each round. (e-g) Quantifying resistance to MEKi treatment using normalized growth rate (k_c/k_0) metric. $n=14$ and * $p<0.05$.

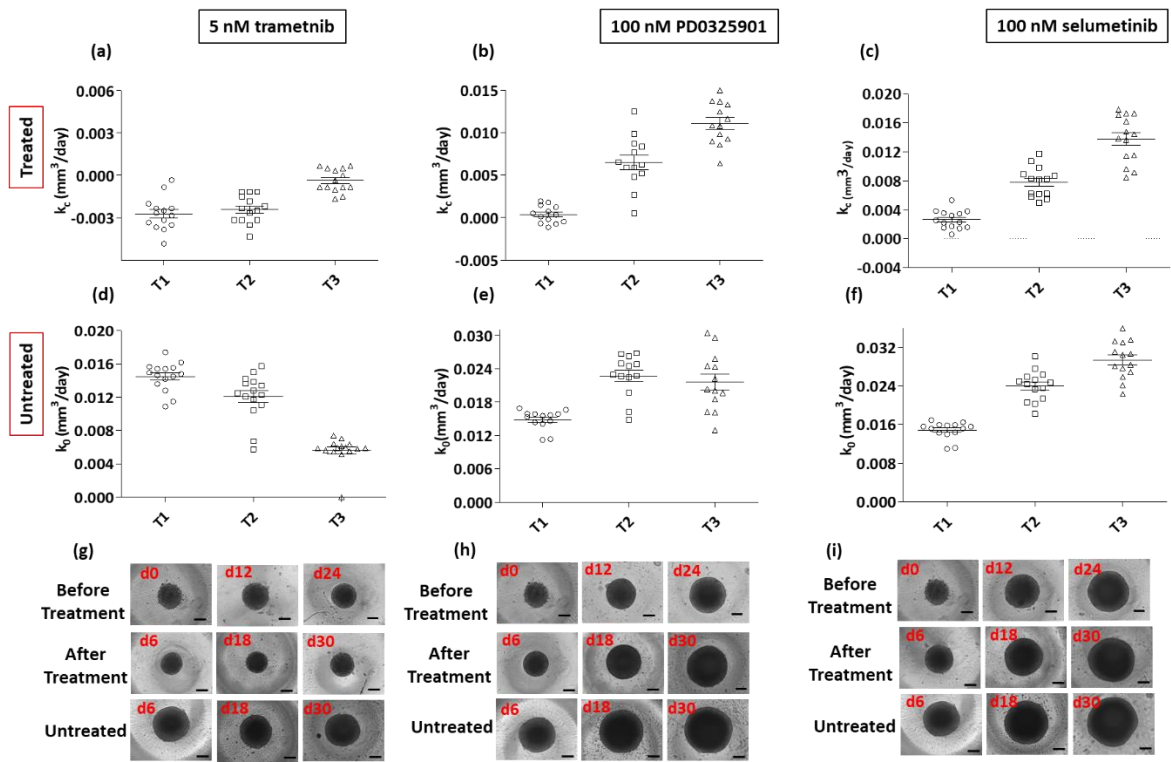


Figure 3-3. Cyclical treatment and recovery of spheroids. (a-c) Growth rates of HT-29 spheroids treated with MEKi for each cycles of treatment were calculated by subtracting the volume of spheroids ‘Before Treatment’ (inset images g-i, upper panels) and volume of spheroids After Treatment’ (inset images g-i, middle panels) 6 day treatment periods (See Figure 3-2b-d). (d-f) Growth rates of HT-29 spheroids non-treated with MEKi for each cycles of treatment were calculated by subtracting the volume of spheroids ‘Before Treatment’ (inset images g-i, upper panels) and volume of Untreated spheroids After Treatment’ (inset images g-i, lower panels) 6 day treatment periods. Each data point represents average of 14 replicates. Scale bar is 200 μm .

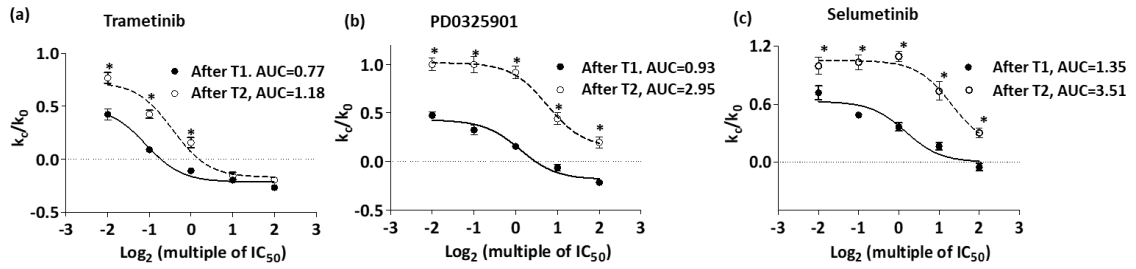


Figure 3-4. Normalized growth rates of HT-29 spheroids treated with MEKi dose-dependently. Solid symbols in (a-c) represent T1 treatment of HT-29 spheroids with five different concentrations (multiple of IC_{50}) of the MEKi. Open symbols in (a-c) represent T2 treatment of HT-29 spheroids with five different concentrations (multiple of IC_{50}) of the MEKi. Spheroids that were used for T2 had been treated with 5 nM trametinib, 100 nM PD0325901, or 100 nM selumetinib during T1 and recovered from the treatment during R1 phase. (* $p < 0.05$). The * symbol above data points represents a statistically significant difference between the two treatment rounds. Error bars represent standard error of the mean.

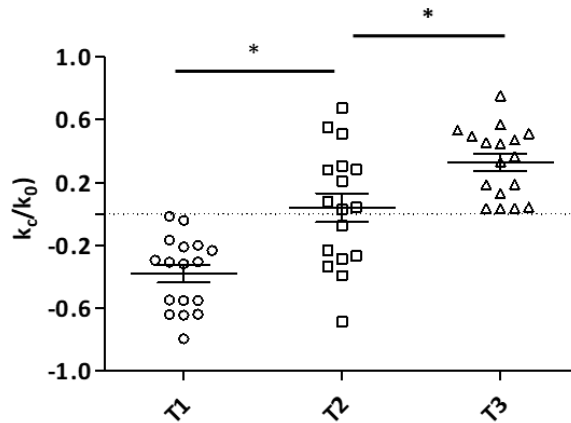


Figure 3-5. Cyclical treatment of HCT116 spheroid with 5 nM trametinib. $n=16$. * represents $p < 0.05$ that is considered statistically significant difference between normalized growth rate between treatments.

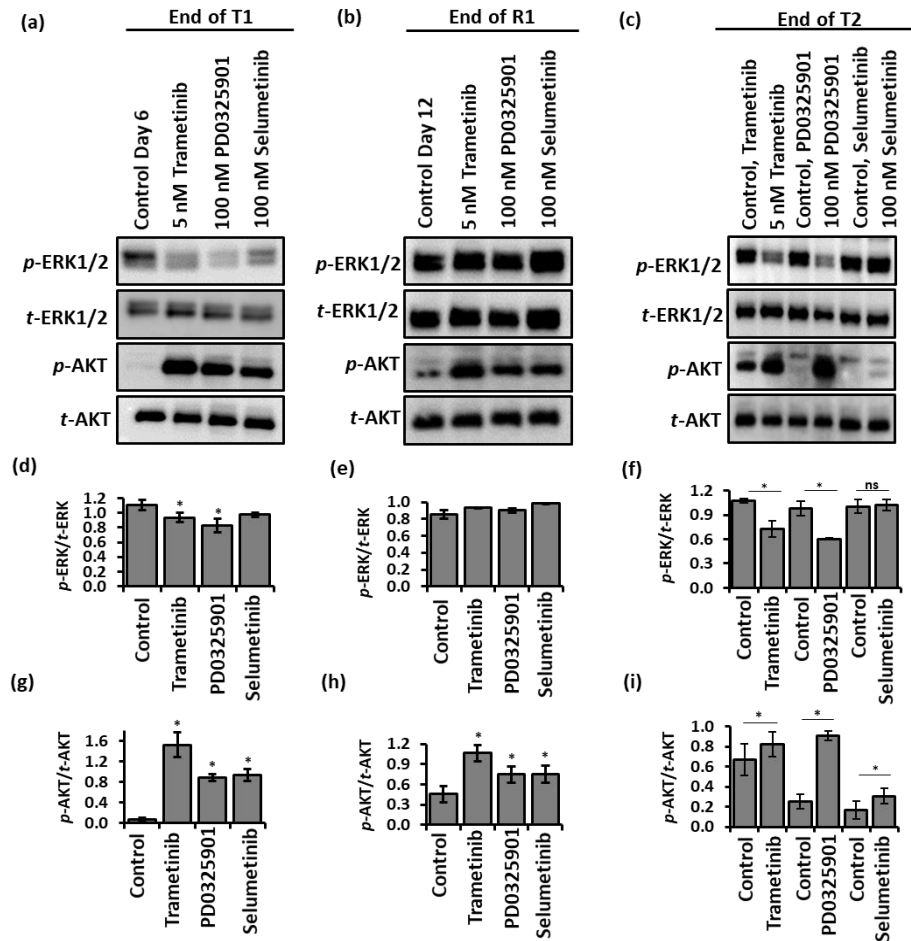


Figure 3-6. Oncogenic levels of ERK1/2 and AKT in HT-29 spheroids treated with MEKi. Representative Western blots for p-ERK1/2, t-ERK1/2, p-AKT, and t-AKT at end of (a) treatment T1 phase, and at the end of (b) R1 phase. (d-e) and (g-h) are quantified results of p-ERK/t-ERK, and p-AKT/t-AKT, respectively. (c) ERK1/2 and AKT levels in MEKi-treated HT-29 spheroids at the end of of treatment T2 phase. Each MEKi treatment during T2 has different controls. Lane 1: Control trametinib (spheroids that received 5 nM trametinib during T1); Lane 2: 5nM trametinib treatment; Lane 3: Control PD0325901 (spheroids that received 100 nM PD0325901 during T1); Lane 4: 100 nM PD0325901 treatment; Lane 5: Control selumetinib (spheroids that received 100 nM selumetinib during T1); and Lane 6: 100 nM selumetinib treatment. (f) Quantified p-ERK/t-ERK showed that trametinib and PD0325901 significantly downregulated the phosphorylation of ERK, but selumetinib treatment did not change ERK activity. (i) Quantified p-AKT/t-AKT showed that treatment of HT-29 spheroids with trametinib, PD0325901, and selumetinib significantly elevated AKT activity. Each experiment was repeated twice. Results are shown as mean \pm standard error. * $p < 0.05$

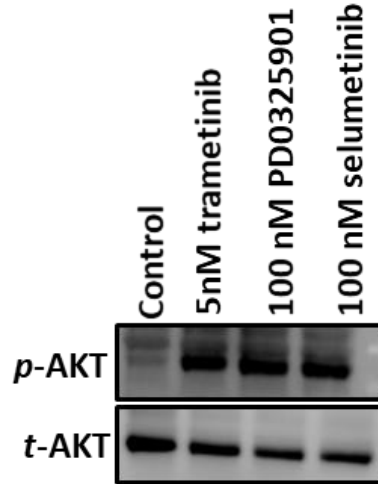


Figure 3-7. Upregulation of AKT activity in HT-29 spheroids after MEKi treatments for 48 h.

End of T1

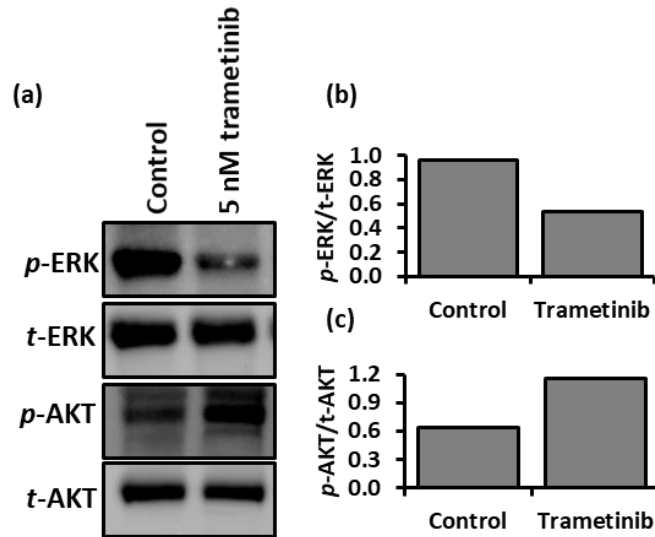


Figure 3-8. (a) Representative Western blots for *p*-ERK, *t*-ERK, *p*-AKT, and *t*-AKT. (b) Quantification of *p*-ERK/*t*-ERK levels showed downregulation of ERK activity. (c) Quantification of *p*-AKT/*t*-AKT levels showed upregulated AKT activity in the cells.

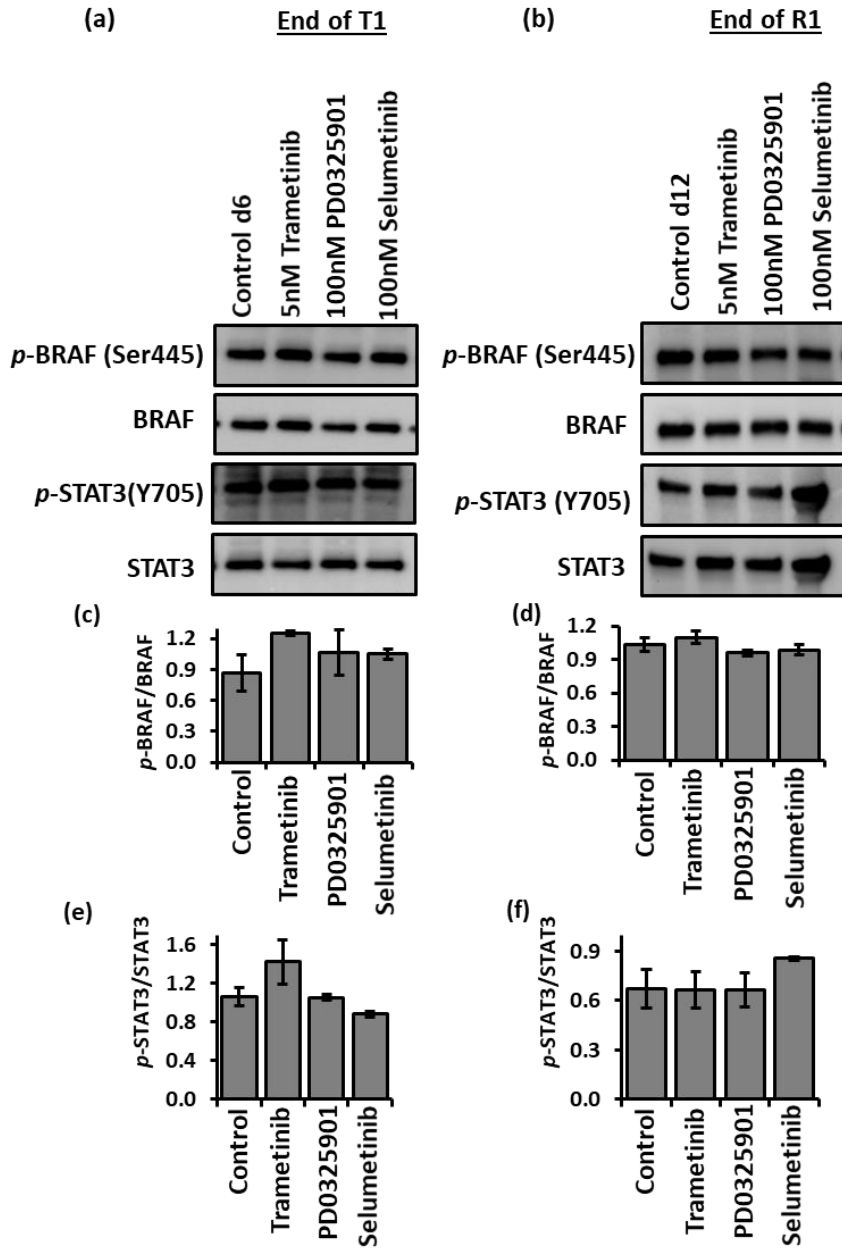


Figure 3-9. (a-b) Representative Western blots for *p*-BRAF, BRAF, *p*-STAT3, and STAT3 at end of T1 and R1 phases. (c-d) Quantification of *p*-BRAF/BRAF at the end of T1 and at the end of R1 phases show no significant changes in the level of *p*-BRAF induced due to the MEKi treatments. (e-f) Quantification of *p*-STAT3/STAT3 at the end of T1 and at the end of R1 phases show no significant changes in the level of *p*-TAT3 due to the MEKi treatments. Each experiment was repeated twice. Results are shown as mean ± standard error.

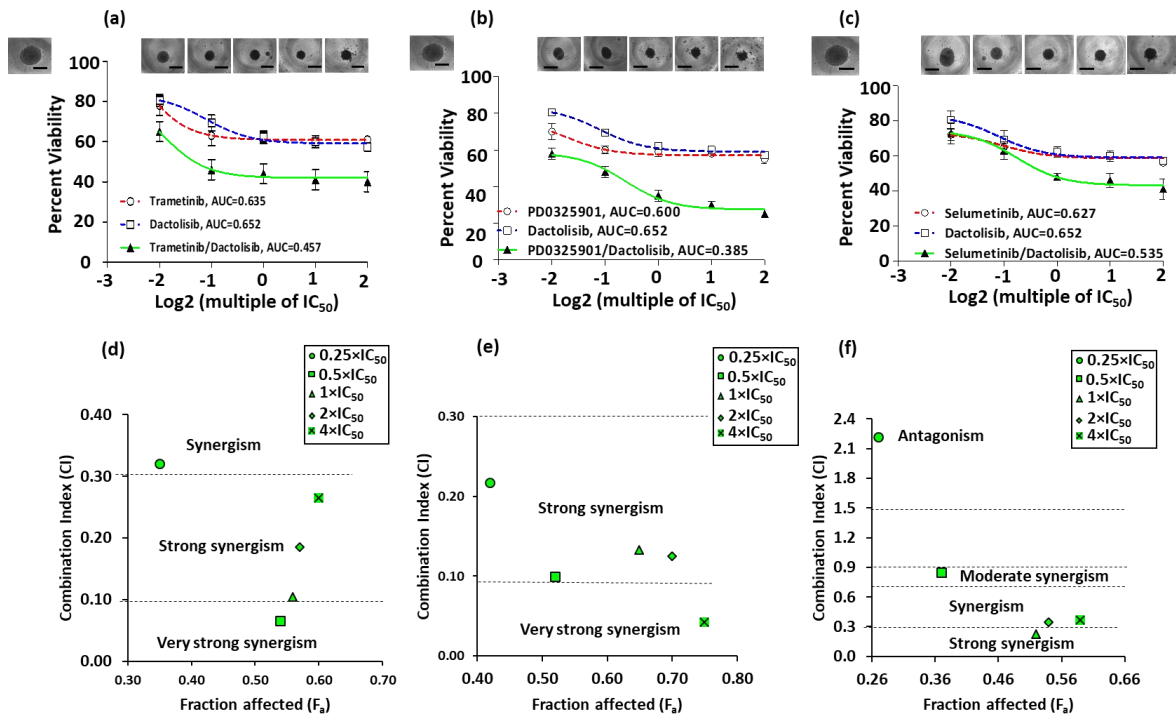


Figure 3-10. Combination treatments of colorectal tumor spheroids with MEKi and dactolisib. Combination and single-agent drug treatments of HT-29 spheroids with (a) trametinib and dactolisib, (b) PD0325901 and dactolisib, and (c) selumetinib and dactolisib for a 6-day treatment. Open square symbols connected by dotted blue lines represent dose dependent response of HT-29 spheroids to single-agent dactolisib treatments, open circle symbols connected by dotted red lines represent dose dependent response of HT-29 spheroids to single-agent MEKi treatments, and solid triangle symbols connected by green lines represent dose dependent response of HT-29 spheroid to combination treatment of MEKi with dactolisib. Inset images show spheroids after dose-dependent combination drug treatments. The image in the top left of panels (a-c) show a control, non-treated spheroid. Scale bar is 300 μ m. Synergy plots for the combination experiments show combination index (CI) versus Fraction affected (F_a) at combination drug concentrations for (d) trametinib and dactolisib, (e) PD0325901 and dactolisib, and (f) selumetinib and dactolisib. CI<1 indicates synergism, whereas CI>1 indicates antagonism.

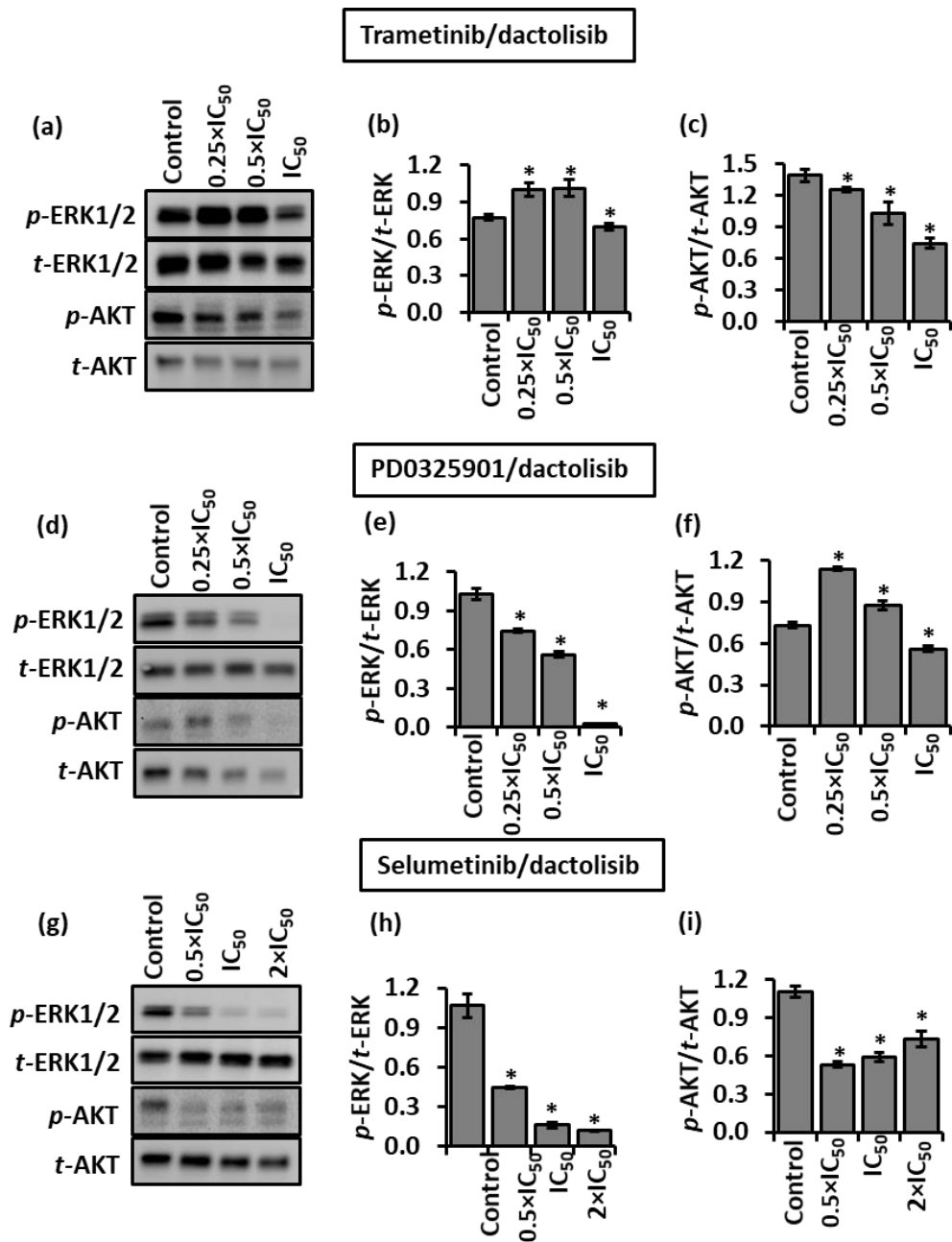


Figure 3-11. Combinations of MEKi and dactolisib downregulate ERK1/2 and AKT signaling in HT-29 spheroids. Representative Western blots and quantified results for *p*-ERK1/2, *t*-ERK1/2, *p*-AKT, and *t*-AKT from spheroids treated with (a-c) trametinib and dactolisib, (d-f) PD0325901 and dactolisib, and (g-i) selumetinib and dactolisib, for 48 hrs. Each experiment was repeated twice. Results are shown as mean \pm standard error. * $p < 0.05$ denotes comparing each treatment with its respective vehicle control.

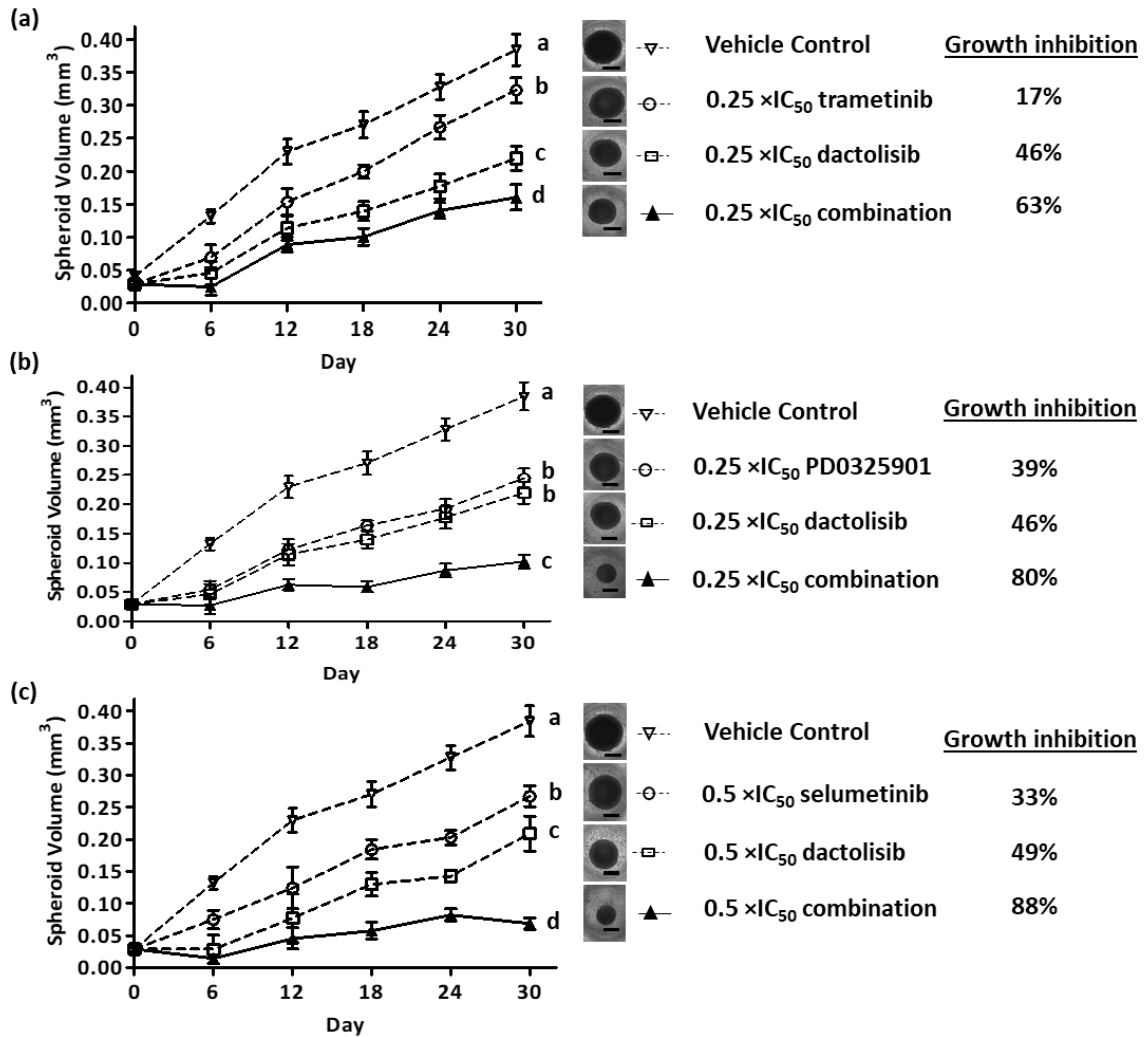


Figure 3-12. Long-term cyclic combination treatments. Volumes of spheroids are shown during treatment and recovery cycles (Figure 3-2a): Vehicle control (open inverted triangles), MEKi treatment (open circles), dactolisib treatments (open squares), and combination treatments (solid triangles). All treatments were done using lowest synergistic concentrations of the MEKi and dactolisib. $n=7$ and $p<0.001$. Means of growth rates in each panel (a-c) at the end of 30 days that do not share a letter are significantly different. Scale bar is 300 μ m.

CHAPTER IV

SYNERGISTIC INHIBITION OF KINASE PATHWAYS OVERCOMES DRUG
RESISTANCE OF COLORECTAL CANCER SPHEROIDS TO CYCLIC TARGETED
THERAPIES

Portions of this chapter are reused from P. Shahi Thakuri, G. D. Luker, and H. Tavana, “Synergistic Inhibition of Kinase Pathways Overcomes Drug Resistance of Colorectal Cancer Spheroids To Cyclic Targeted Therapies.,” *ACS Pharmacol. Transl. Sci.*, vol. 2, no. 4, pp. 275–284, July. 2019. Copyright © 2018 by ACS Pharmacology and Translational Science. Reprinted by permission of ACS publications. <https://pubs.acs.org/doi/abs/10.1021/acsptsci.9b00042>

Advancements in identifying molecular drivers of cancer have shifted treatments toward precision medicine, where molecular subtype of tumors guide treatments with targeted drugs. [7] Although this approach is often initially successful, the selective pressure that a targeted drug exerts can lead to resistance of cancer cells through various mechanisms. [19], [20] Additionally, due to the heterogeneity of cancer cells, a subpopulation of tumor cells not responsive to the targeted drug thrives to promote tumor growth. [18] Mitogen-activated protein kinase (MAPK) is an oncogenic signal transduction pathway in colorectal cancer. Because this pathway is often highly deregulated, it presents an attractive therapeutic target to suppress tumor growth using inhibitors of RAF, MEK, or ERK (RAF_i, MEK_i, or ERK_i). These inhibitors have been shown to suppress growth of colorectal tumors *in vivo*. [91], [92] Nevertheless, cancer cells often develop resistance to these inhibitors through several mechanisms: (i) Activation of alternative signaling pathways such as PI3K/AKT/mTOR or JAK/STAT mediates resistance to MEK_i; [93] (ii) feedback activation of receptor tyrosine kinases (RTKs) such as epidermal growth factor

receptors (EGFR, HER2, and HER3) causes resistance to RAFi and MEKi; [94], [95], [201] (iii) continuous exposure to MEKi may lead to mutation of MEK; [170] and (iv) continuous exposure to RAFi may lead to amplification of B-RAF or other components of the MAPK pathway. [98], [99] To overcome drug resistance of cancer cells, combination treatments using inhibitors of RAF and MEK have been approved to treat BRAF mutant melanoma and, more recently, BRAF mutant colorectal cancer.

Over 50% of colorectal cancers have mutations in MAPK or PI3K/AKT/mTOR pathways. [202] Genetic abnormalities often activate both of these pathways, resulting in a reduced response to MAPK pathway inhibition through cross-talk with the PI3K pathway. Therefore, combining inhibitors of these two pathways is a rational therapeutic approach. This approach showed promising anti-tumor effects in pre-clinical trials, but it was largely unsuccessful due to excessive toxicity to patients. [203]–[206] The failure in part reflects insufficiency of preclinical models to predict drug resistance and toxicity. Dose reduction is a feasible approach to manage toxicities particularly with drugs that produce anti-tumor effects at low concentrations. However, it is difficult to test large arrays of drug combinations in standard models widely used in cancer research such as animal models. Availability of simpler preclinical models would allow identifying specific concentrations of drug combinations that generate desirable biologic effects and then advancing them to animal model tests. Physiologically relevant, three-dimensional (3D) cultures of cancer cells are promising preclinical models to address this need because they mimic the architecture and key biologic properties of tumors, facilitate understanding mechanisms of drug resistance, and help identify effective drug combinations. [56], [165], [166] Because chemo-resistance often develops over time, a major barrier to model this

event has been technological limitations for long-term, 3D culture of cancer cells. We recently established this capability and showed that treatment of tumor spheroids in a regimen that mimics clinical chemotherapy leads to drug resistance. [163]

Here, we establish the utility of this approach to identify mechanisms of drug resistance and determine low-dose effective combination treatments to maintain drug sensitivity of cancer cells. We periodically treated KRAS-mutant colorectal cancer spheroids with several MAPKi and showed that effectiveness of the inhibitors to suppress proliferation of cells and growth of spheroids significantly reduced during successive treatment cycles. Molecular analysis showed that suppression of MAPK pathway was only short-lived and that repeated exposure of spheroids to MAPKi significantly activated the PI3K/AKT/mTOR pathway and led to proliferation of cancer cells. High-throughput screening of combinations of several MAPK and PI3K inhibitors helped identify low-dose synergistic concentrations to effectively reduce activities of both pathways and suppress tumor spheroids growth in long-term cyclic treatments. Our design-driven approach offers a useful tool for mechanistic understanding of drug responses of cancer cells and identifying low-dose, highly synergistic drug combinations to block drug resistance.

4.1 Materials and Methods

The methods for long-term culture of spheroids to model adaptive drug resistance to MAPKi and design of a rational combination approach to identify low synergistic drug combination concentration to overcome drug resistance during cyclic treatments in colorectal tumor spheroids are described below.

4.1.1 Cell Culture and Spheroid Formation

HCT116 cells (ATCC) were cultured in McCoy's 5A medium (Sigma) supplemented with 10% fetal bovine serum (Sigma), 1% streptomycin/penicillin (Thermo Fisher Scientific), and 1% glutamine (Thermo Fisher Scientific). Cells were cultured in a humidified incubator at 37 °C and 5% CO₂ and subcultured when they were 80–90% confluent. A 0.25% trypsin solution (Thermo Fisher Scientific) was used to dissociate cells from culture flasks. The complete growth medium was used to neutralize trypsin. The resulting cell suspension was centrifuged down at 1000 rpm for 5 min at 4 °C. After removing the supernatant, cells were suspended in 1 mL of the culture medium and counted using a hemocytometer prior to spheroid formation. Spheroids with a density of 1.5×10^4 cells were formed in round-bottom ultralow attachment 384-well plate (Corning) using our aqueous two-phase system (ATPS) technology, as described before. [80], [164] HCT116 spheroids were imaged using an inverted fluorescence microscope (AxioObserver, Zeiss) daily for 10 days to evaluate their growth.

4.1.2 Drug Treatments

Trametinib, SCH772984, AZ628, dactolisib, apitololisib, VS5584, PI-103, and GSK1059615 were purchased from Selleckchem. All compounds were dissolved in dimethyl sulfoxide (DMSO) except for dactolisib that was dissolved in dimethylformamide. Stock solutions were stored in –80 °C. All compounds were tested dose dependently against HCT116 spheroids. Except for SCH772984, all other compounds were prepared at concentrations of 2×10^{-3} μM, 2×10^{-2} μM, 1×10^{-1} μM, 2×10^{-1} μM, 1×10^0 μM, 2×10^0 μM, and 2×10^1 μM. SCH772984 solutions were prepared at 2×10^{-4} μM, 2×10^{-3} μM, 2×10^{-2} μM, 1×10^{-1} μM, 2×10^{-1} μM, 1×10^0 μM, and 2×10^0 μM

concentrations. The volume of the medium in the spheroid culture plate was measured and an equal volume from the above drug solution was pipetted into the well of the plate. This diluted the drug concentrations in half. The DMSO content in the drug solutions did not exceed 0.1% to ensure no effect on viability of cells in spheroids. [86] Vehicle control untreated spheroids were grown in drug-free cell culture medium. After 4 days of drug treatment, 10% (v/v) Prestoblue was added to wells, and the metabolic activity of cells in spheroids was measured using a microplate reader (Synergy H1M, BioTek Instruments). [86], [177] The fluorescence signal from drug-treated spheroids was normalized with that from the vehicle control spheroids and used to construct dose–response curves (GraphPad Prism). A 50% lethal dose (LD₅₀) value was obtained from the dose–response curve of each compound. In addition to the Prestoblue biochemical assay, phase images of spheroids were captured at the end of each treatment cycle. Diameter of each spheroid was measured in ImageJ (NIH) and converted to volume assuming a spherical shape. Correlation analysis was performed between volume of spheroids and the corresponding fluorescence signal from the Prestoblue assay.

4.1.3 Combination Treatments of Spheroids

Trametinib, SCH772984, and AZ628 were used in combination with dactolisib, each inhibitor at six different concentrations. These concentrations were multiples (0.125, 0.25, 0.5, 1, 2, and 4) of LD₅₀ of each compound. For combination experiments, solutions of 4× concentrations of multiples of LD₅₀ of each compound were prepared (i.e., 0.5, 1, 2, 4, 8, and 16 times). From these solutions, 20 μL of each MAPKi solution and 20μL of dactolisib solution were added to each well containing a spheroid in 40 μL of cell culture medium to dilute each compound four folds. As each concentration of MAPKi was

combined with six different concentrations of dactolisib, this resulted in a 6×6 matrix of concentration pairs for each combination treatment. In addition, single-agent treatments with MAPKi and dactolisib were performed to compare with the combination treatments. Solutions of $2\times$ concentration (i.e., 0.25, 0.5, 1, 2, 4, and 8 times) were prepared, and 40 μL of each solution was added to each microwell containing a spheroid in 40 μL of cell culture medium. Vehicle control spheroids were cultured in cell culture medium. Treatments were done for 4 days, and viability of cells was quantified using a Prestobblue assay. The fraction of cells affected by each treatment was calculated as $(1 - \text{viability})$. A synergy analysis was performed using the Chou and Talalay method. [159] The analysis generated 36 combination indices (CI) for the 36 combination concentrations from a pair of inhibitors. In addition, images of spheroids were captured to quantify the size of spheroids as a measure of effect of drug treatments.

4.1.4 Western Blot Experiments

Western blot analysis with spheroids was performed according to our established protocol. [84], [86] Solutions of primary antibodies for phosphop44/42 MAPK (Erk1/2), p44/42 MAPK (Erk1/2), phospho-AKT (Ser473), and AKT (pan) (C67E7) were prepared at concentrations recommended by the manufacturer, Cell Signaling Technology. Membranes were incubated overnight at 4 °C with primary antibody solutions. After repeated washing, membranes were incubated with a horseradish peroxidase (HRP)-conjugated secondary antibody for 1 h, followed by repeated washing. Detection was carried out using an ECL chemiluminescence detection kit (GE Healthcare) and FluorChem E imaging system (ProteinSimple).

4.1.5 q-PCR Experiments

Gene expression analysis was done after T1, R1, T3, and R3. All fold changes values were expressed relative to that after T1. Spheroids were lysed using a Total RNA Kit (TRK) lysis buffer (Omega Biotek), and the lysate was homogenized by passing it through homogenizer mini columns (Omega Biotek). Total RNA was obtained using an RNA isolation kit (Omega Biotek). After removing DNA using RNase-free DNase (Omega Biotek), purity and concentration of isolated RNA were assessed using optical density (OD) 260/280 spectrophotometry (Synergy H1M, Biotek Instruments). cDNA was synthesized from 1 µg of total RNA using random hexamer primers (Roche). Real-time q-PCR was performed in a LightCycler 480 instrument II using a SYBR Green Master Mix (Roche). After combining 50 ng of cDNA with the primer and the SYBR Green Master Mix to a final volume of 15 µL, the reactions were incubated at 95 °C for 5 min followed by 45 cycles of amplification, that is, at 95 °C for 10 s, at 60 °C for 10 s, and at 72 °C for 10 s. The primer sequences for the genes are listed in Table 4-1. Expression levels of mRNA for different proliferation gene markers were calculated relative to β-actin and hypoxanthine phosphoribosyltransferase (HPRT) using the $\Delta\Delta C_t$ method. The fold change in mRNA expression was determined according to the $2^{-\Delta\Delta C_t}$ method. [207], [208] Statistical analysis was performed using a Student's t-test in Microsoft Excel software.

4.1.6 Confocal Microscopy

Prior to forming spheroids, HCT116 cells were stained with 2 µM of Calcein AM dye (Thermo Fisher Scientific) when cells were in a monolayer culture. Confocal microscopy of spheroids was performed using a Nikon A1 confocal system with 10× objective. The FITC filter was used to capture image stacks with a z-spacing of 20 µm. NIS

Elements software was used for image acquisition, and ImageJ (NIH) was used for analysis and 3D reconstruction.

4.2 Results and Discussion

Below results of modeling drug resistance to long-term cyclical treatment of colorectal tumor spheroids with MAPKi, i.e., inhibitors of MAPK pathway, (RAFi, MEKi, ERKi) are presented. The molecular analysis and design of matrix-based combination approach to overcome drug resistance over long-term studies are also discussed.

4.2.1 Microprinting of Tumor Spheroids and Their Growth Analysis

The aqueous DEX phase nanodrop containing cancer cells stably remained immiscible from the PEG phase solution. [83] This facilitated aggregation of cancer cells into a spheroid within 48 h (Figure 4-1a). The ATPS environment allowed a free diffusional influx of nutrients into the drop phase to nourish the cells and efflux of waste products of cells into the immersion phase. The ATPS microprinting approach provided a mild environment for cells to form spheroids of fully viable cells. [81], [178] Medium exchange every 48 h provided fresh nutrients and removed waste products of cells. This also significantly reduced concentrations of the polymers and resulted in a single medium phase. Thus, ATPS was solely used to quickly and conveniently generate spheroids. We have shown that at the same cell density, the ATPS approach generates spheroids that are ~30% more compact than those from the ULA plate method. [209] Additionally, we have adapted the ATPS technology to robotic liquid handling to form large quantities of consistently sized spheroids in 384-microwell plates. [210] With a density of 1.5×10^4 HCT116 cells per DEX drop, a variation of <5.5% from an average diameter of 468 μm

resulted. HCT116 spheroids had a distinct boundary and a round and compact morphology, indicated by both phase and confocal imaging (Figure 4-1a and b). Our morphological image analysis showed an increase in the average diameter of spheroids from 468 μm on day 1 to 650 μm on day 9, that is, $\sim 38\%$ increase in the diameter of spheroids. Approximating the spheroids as spherical clusters, this corresponds to a 2.16- fold volume increase, indicating proliferation of cancer cells within the spheroids (Figure 4-1c).

4.2.2 Dose-Response to Molecular Inhibitors

KRAS and PIK3CA mutations in HCT116 cells activate oncogenic MAPK and PI3K/AKT/mTOR pathways. [141] Therefore, we aimed to determine the effect of blocking signaling through these pathways in HCT116 spheroids using a set of molecular inhibitors including trametinib, SCH772984, and AZ628 against the MAPK pathway and dactolisib, apitolisib, VS5584, PI-103, and GSK1059615 against the PI3K/AKT/mTOR pathway. The MAPKi dose-dependently reduced cell viability in spheroids (Figure 4-2a). Trametinib was the most effective inhibitor with an LD_{50} of 10 nM. Above 100 nM, trametinib treatment led to fluffiness or disintegration of spheroids. SCH772984 was effective above 100 nM concentrations and resulted in an LD_{50} of 150 nM, whereas AZ628 treatment significantly reduced cell viability at low micromolar concentrations and gave an LD_{50} of 1 μM . Additionally, the PI3K/AKT/mTOR inhibitors reduced viability of HCT116 cells dose-dependently but at significantly larger, mainly micromolar concentrations than the MAPKi did (Figure 4-2b and c). The volume of spheroids treated with the MAPKi showed a linear correlation with the cellular metabolic activity from a Prestoblue assay. The goodness-of-fit parameter (R^2) values were 0.997, 0.973, and 0.887 for treatments with trametinib, SCH772984, and AZ628, respectively (Figure 4-3). The

corresponding Pearson's correlation coefficients between dose-dependent reduction in the volume of spheroids and metabolic activity from the biochemical analysis were 0.99, 0.98, and 0.94. The volume of spheroids treated with these PI3K pathway inhibitors also linearly correlated with the fluorescence signal obtained using Prestoblue assay, confirming the validity of using morphology-based size analysis of colorectal tumor spheroids treated with kinase molecular inhibitors. [209]

4.2.3 Resistance of Colorectal Tumor Spheroids to Cyclic Treatments of MAPKi

Our screening above showed that HCT116 spheroids were more sensitive to inhibition of the MAPK pathway than targeting of the PI3K/AKT/mTOR pathway, suggesting blocking of the MAPK pathway as a strategy to inhibit proliferation of cells in spheroids. We evaluated responses of HCT116 spheroids to long-term, cyclic treatment and recovery with the LD₅₀ concentrations of the three MAPKi (Figure 4-4a). We used this regimen to mimic the cyclic chemotherapy of patients. As expected, the compounds potently inhibited proliferation of cancer cells during the first treatment round (T1) (Figure 4-4b–d). The size of spheroids treated with trametinib, SCH772984, and AZ628 decreased by 1.80-, 1.42-, and 1.67-fold, respectively. However, after the first recovery round (R1), the inhibitors were significantly less effective during treatment T2. Despite repeated treatments, the HCT116 spheroids grew larger. At the end of the 32-day treatment and recovery, spheroids treated with trametinib, SCH772984, and AZ628 were 2.34-, 4.14-, and 4.04-fold larger than those at the end of treatment T1, respectively. Furthermore, we used a growth rate metric (k_c) to quantify the effects of treatments (Figure 4-4e-g). Although k_c for HCT116 spheroids significantly reduced during T1, it increased during the subsequent rounds of treatment. The k_c values of spheroids from T1 to T4 significantly

increased from -0.0061 to 0.0021 mm^3/day for trametinib treatment, from -0.0040 to 0.0052 mm^3/day for SCH772984 treatment, and from -0.0050 to 0.00271 mm^3/day for AZ628 treatment. The significant decrease in the efficacy of the MAPKi indicates that cancer cells in spheroids quickly adapt to the inhibition of different proteins (RAF, MEK, and ERK) in this pathway. Interestingly, our drug resistance model reliably emulated several *in vivo* studies that showed cyclic treatments of tumor xenografts with MEK1/2 inhibitors did not reduce the tumor size, necessitating other treatments. [188], [199]

Next, we aimed to study whether increasing growth of cancer cells during cyclic inhibition of MAPK pathway could be detected at a gene level. We selected 10 prominent genes involved in cell cycle and proliferation based on a literature review (Table 4-1). Our rationale for this selection was that these genes are activated by transcriptional factors downstream of MAPK and PI3K signaling pathways, which are drivers of the growth of HCT116 cells in tumor spheroids. We compared the expression of each gene after the first and third cycles of treatment and recovery, that is, T1, R1, T3, and R3. Expression of each gene after R1, T3, and R3 is shown in Figure 4-5 as a fold change relative to that after T1. Most of the genes showed a significant upregulation during the cycles of treatment and recovery irrespective of the inhibitor used. With all three inhibitors, the largest expression of proliferation genes almost always occurred during recovery phases, especially the R3 phase, with only few exceptions. In addition, during T3, expression levels of some of the genes slightly reduced compared to the R1 phase, indicating a transient response to the treatments. However, this reduction was not significant in most cases, which is also evident from the growth of spheroids during T3 (Figure 4-4b-g). Overall, relatively higher expression levels of proliferation genes in R3 than in R1 and in T3 than in T1 corroborate

our findings of increased resistance of cancer cells to MAPKi with successive cycles of drug exposure.

4.2.4 Mechanism of Drug Resistance

Next, we investigated the molecular basis of increasing resistance of cancer cells to cyclic single-agent treatments with the MAPKi. Studies have shown that inhibition of MEK1/2 can activate the PI3K/AKT/mTOR pathway due to extensive cross-talk between the two pathways. [190], [211] Thus, we performed a Western blot analysis for both ERK1/2 and AKT in HCT116 spheroids cyclically treated with the three MAPKi (Figure 4-6a). All three inhibitors significantly reduced pERK1/2 levels. Consistent with the phenotypic analysis result (Figure 4-4), trametinib most effectively downregulated ERK1/2 activity by ~85% during T1 (Figure 4-6b). This was followed by SCH772984 and AZ628 treatments that reduced pERK1/2 levels by 56% and 25%, respectively (Figure 4-6b). However, trametinib, SCH772984, and AZ628 treatments significantly increased pAKT levels by 37%, 52%, and 46% of the vehicle control spheroids, respectively (Figure 4-6a and c). This established that the targeting MAPK pathway at different levels (RAF, MEK, and ERK) results in feedback activation of PI3K/AKT/mTOR pathway. [212], [213] Additionally, we found that several proliferation genes downstream of AKT such as CCNA1, PCNA, and CCND1 were upregulated by the MAPKi treatments. For example, CDC25C that encodes cyclin-dependent kinase (CDK2) and CCNA2 that encodes cyclin A mediate formation of the PI3K/AKT-dependent CDK2/cyclin complex, which is responsible for cell proliferation. [212], [213] Furthermore, AKT-dependent phosphorylation of p21 prevents a complex formation with proliferating cell nuclear antigen (PCNA), which inhibits DNA replication. [214] Increase in PCNA during cyclic

trametinib and AZ628 treatments indicates AKT-mediated release of PCNA for DNA replication and growth of tumor spheroids. We also suspect that pathways other than PI3K/AKT/mTOR could drive growth of tumor spheroids. Our previous study showed that the increased growth of spheroids during successive treatment/recovery cycles and development of resistance to MEKi treatments is in part due to incomplete suppression of ERK activity. [163] We identified several cell cycle-regulating genes downstream of ERK such as CCND1, CDC25C, and MYC that were significantly upregulated during R1, T3, and R3, indicating that incomplete suppression of ERK by MEKi treatments also leads to cell proliferation and growth of spheroids.

4.2.5 Combination Treatments to Suppress Resistance

Next, we evaluated the potential of a combination treatment strategy to block resistance of HCT116 spheroids to MAPKi treatments. We combined trametinib, SCH772984, and AZ628 with a PI3K/mTOR inhibitor, dactolisib, which had the smallest LD₅₀ value among the PI3K/AKT/mTOR inhibitors used against HCT116 spheroids (Figure 4-2b and c). Each combination treatment included 36 pairs of concentrations of a pair of inhibitors. We computed the fraction of cells affected (Fa) by treatment as the relative measure of cell death (Fa=1-the normalized cell viability). Figure 4-7a, c, and g shows the results for combination treatments of trametinib/dactolisib, SCH772984/dactolisib, and AZ628/dactolisib pairs, respectively, as well as a single agent treatment with each inhibitor. The Fa values increased at higher concentration pairs, represented by a darker shade of red in the heatmaps. Combination treatments were also significantly more effective than respective single-agent treatments at similar concentrations. To determine if drug combinations were synergistic, we computed a CI for

each pair. Using COMPUSYN software, we performed a synergy analysis to generate a CI value for each concentration pair. $CI < 1$ indicates synergism and the synergy level increases as CI approaches zero. [159] All 36 concentration pairs resulted in $CI < 1$, indicating synergistic interactions between each of the MAPKi and dactolisib and the potential of blocking these two pathways to block cancer cell proliferation and survival. The CI values ranged from 0.11 to 0.94 for trametinib/dactolisib, 0.05 to 0.48 for SCH772984/dactolisib, and 0.09 to 0.85 for AZ628/dactolisib (Figure 4-7b, e, and h). In addition, we captured the morphology of spheroids in each experiment. The combination pairs, especially at higher concentrations, partially or completely disintegrated spheroids, suggesting toxicity to cancer cells. [86] From each combination treatment, the pairs of concentrations that disintegrated the spheroids are highlighted in red in Table 4-2.

To study inhibitory effects of combination treatments on MAPK and PI3K/AKT pathways, we performed Western blotting of spheroids following treatment T1. Treatments included 5 nM/200 nM trametinib/dactolisib, 75 nM/400 nM SCH772984/dactolisib, and 500 nM/800 nM AZ628/dactolisib. This selection reflects strong synergistic growth inhibitory effects ($CI = 0.1-0.3$) against HCT116 spheroids at sufficiently low, nanomolar concentrations that did not disintegrate the spheroids (Figure 4-7b, e, and h and Table 4-2). We also used a single-agent treatment with each inhibitor to compare with combination treatments. As expected, single-agent treatments with the MAPKi significantly downregulated p-ERK levels (top lanes in Figure 4-7c, f, and i), leading to growth inhibition of HCT116 spheroids. Nevertheless, AKT activity significantly increased (third lanes in Figure 4-7c, f, and i). Interestingly, the p-AKT level did not significantly reduce after single-agent dactolisib treatment. Dactolisib is a potent inhibitor of PI3K and mTOR.

It is likely that the growth inhibitory effect of dactolisib is through mTOR inhibition. [215] For example, it was shown that downregulated activities of substrates of mTORC1 such as pS6 and p4EBP1 inhibited growth of HCT116 cells. [162] Dactolisib also inhibits DNA-PK and class II PI3Ks, which may contribute to its growth inhibition of HCT116 cells. [216]

Unlike significant activation of AKT in response to inhibition of MAPK pathway, there was no significant increase in the level of p-ERK1/2 following dactolisib treatment of HCT116 spheroids. This implies an absence of feedback activation of MAPK pathway by PI3K/AKT pathway inhibition in these cells. Combined inhibitors of MAPK and PI3K pathways significantly reduced active levels of both ERK1/2 and AKT proteins. Trametinib/dactolisib, SCH772984/dactolisib, and AZ628/dactolisib pairs reduced p-ERK1/2 levels by 70%, 53%, and 67% of the vehicle control, respectively (4-7c, f and i). Each combination treatment also further reduced pERK1/2 levels than the single-agent treatment with the corresponding MAPKi. The largest reduction of 60% was with the AZ628/ dactolisib pair compared to AZ628 alone. This was followed by the SCH772984/dactolisib pair that reduced the pERK1/2 level 24% more than that when SCH772984 was used alone. The trametinib/dactolisib pair also reduced the pERK1/2 level 13% more than that with trametinib treatment only. We note that this small decrease in the pERK1/2 level by the trametinib/dactolisib pair is because trametinib treatment alone was very effective against ERK1/2 activity. Most importantly, combination treatments were highly effective against feedback signaling of kinase pathways. Compared to single-agent treatments with trametinib, SCH772984, and AZ628 that led to activation of PI3K/AKT/mTOR pathway, the compounds simultaneously administered with dactolisib

downregulated pAKT levels 3.17, 6.32, and 1.74 folds, respectively. In all three combination treatments, the pAKT levels were significantly lower than that of the vehicle control spheroids. These results, which are consistent with several animal model studies, [162], [188], [217] indicate the need for simultaneous blocking of compensatory signaling pathways that mediate resistance to single-agent therapies. Importantly, we identified growth inhibition of tumor spheroids using synergistic nanomolar concentrations of compounds for the subsequent long-term drug combination studies below.

4.2.6 Long-Term Cyclic Combination Treatments

We established that combinations of MAPKi and dactolisib act synergistically on HCT116 spheroids in short-term, 4-day experiments. To evaluate the effectiveness of this strategy during long-term cyclic treatments (Figure 4-4a), we used trametinib/dactolisib against HCT116 spheroids. We selected 5 nM trametinib and 200 nM dactolisib concentrations that resulted in $F_a = 0.73$ and a strong synergism with $CI = 0.14$ (Figure 4-6a and d). In parallel, we performed single-agent treatments at the same concentration of each inhibitor used in the combination treatment. Unlike trametinib or dactolisib treatments alone, their combination significantly and effectively suppressed the growth of spheroids over a 32-day period (Figure 4-8a). To quantitatively compare the combination and single agent treatments, we calculated the growth rate of spheroids. The average values of k_c for 5 nM trametinib, 200 nM dactolisib, and their combination were 0.0006, 0.0014, and $-0.00135 \text{ mm}^3/\text{day}$, respectively. The positive k_c values indicate that the efficacy of trametinib and dactolisib treatments diminished over time. On the other hand, the combination treatment resulted in a negative k_c value, indicating continuous growth suppression of tumor spheroids. Our molecular analysis corroborated this result. We

compared active AKT and ERK1/2 levels after T1 and T3 for single-agent and combination treatments. Although trametinib treatment alone reduced ERK1/2 activity during T1, which caused a significant shrinking of the spheroids, it was ineffective during T3, and the ERK1/2 activity significantly increased (Figure 4-8b and c). The reduced effectiveness of the single-agent trametinib treatment is also consistent with the upregulation of proliferation genes downstream of ERK such as MYC, CDC25, and CCND1 (Figure 4-5a). [218] In addition to the p-ERK increase during T3, trametinib-induced activation of p-AKT persisted (Figure 4-8b and d), resulting in growth of HCT116 spheroids (Figure 4-8a). Dactolisib treatment alone did not suppress p-AKT levels, and despite the treatment, the AKT activity increased from T1 to T3 (Figure 4-8b and d). The reduced effect of dactolisib used alone is also consistent with the upregulation of proliferation genes downstream of AKT such as CCNA2, PCNA, and CCND1. [219] Therefore, elevated activities of AKT and ERK1/2 account for growth of spheroids over the long-term, single-agent cyclic treatments. On the other hand, the trametinib/dactolisib combination maintained the p-ERK and p-AKT levels low (Figure 4-8c and d). Thus, inhibition of both pathways was critical to suppress the growth of cancer cells. Anti-tumor effects of combinations of MEK and PI3K inhibitors in animal model studies support our results, demonstrating the potential of our tumor spheroid model in cyclic treatments to identify synergistic drug pairs against cancer cell growth. [194], [200], [203], [217]

Drug concentrations used in our study is comparable to those used clinically to treat cancer patients. During clinical trials, 2 mg trametinib is used in combination with other drugs to treat advanced cancers. Assuming a volume of 5 liters of blood, the 2 mg of trametinib diluted in blood gives a concentration of 0.4 $\mu\text{g/ml}$ of trametinib in blood

plasma. Considering the molecular weight of trametinib as 615.39 g/mol, this is equivalent to 650 nM trametinib concentration. In addition, the amount of trametinib measured in the biopsy sample on day 15 of treatment was 9.51-18.2 ng/ml, [220] which is equivalent to 15 nM-28 nM concentration of trametinib. Therefore, the 10 nM concentration of trametinib used in our study is consistent with clinical doses of the drug.

4.3 Summary

We established that colorectal cancer cells in spheroids under cyclic, single-agent treatments with MAPK pathway inhibitors develop resistance by activation of the PI3K feedback signaling. Using a rational-design strategy guided by molecular analysis of drug resistance, we combined inhibitors of initially active (MAPK) and feedback-activated (PI3K) pathways to overcome drug resistance. Our systematic, high throughput drug treatments of spheroids identified low-dose, strongly synergistic combinations of concentrations from a pair of inhibitors to effectively suppress tumor spheroids growth and block cross-talk between kinase pathways during long-term treatments. Our design-driven approach to determine highly synergistic drug pairs and concentrations against resistance to single-agent treatments offers a valuable tool to prioritize compounds for subsequent animal studies in preclinical tests. This approach will significantly reduce the number of animal studies and accelerate the discovery of effective treatments for clinical use.

Table 4-1. List and sequence of primers for 10 genes that were analyzed in spheroids treated with mapk inhibitors.

Primer	Sequence	Length
CCNA2 F	5'-GCTGGCGGTAAGTC-3'	18
CCNA2 R	5'-CAAGGAGGAACGGTGACAT-3'	19
CCNB1 F	5'-TGTAGGTCCTTGGCTGGT-3'	18
CCNB1 R	5'-GCCATGTTGATCTTCGCCTTA-3'	21
CCND1 F	5'-GTGTCCTACTTCAAATGTGTGC-3'	22
CCND1 R	5'-AGCGGTCCAGGTAGTTCA-3'	18
CCNE1 F	5'-ACAAGACCCTGGCCTCA-3'	17
CCNE1 R	5'-TCACGTTTGCCTCCTCTTC-3'	20
MYC F	5'-TCCTCGGATTCTCTGCTCTC-3'	20
MYC R	5'-TCTTCCTCATCTTCTGTTCTC-3'	23
E2F1 F	5'-AAGTCCAAGAACCACATCCAG-3'	21
E2F1 R	5'-CTGCTGCTCGCTCTCCT-3'	17
RB1 F	5'-GACCTGCCTCTCGTCAG-3'	17
RB1 R	5'-ACCTCCCAATACTCCATCCA-3'	20
PCNA F	5'-GTCTGAGGGCTTCGACAC-3'	18
PCNA R	5'-CCAAGGTATCCGCGTTATCTTC-3'	22
CHEK1 F	5'-AGTACTGTAGTGGAGGAGAGC-3'	21
CHEK1 R	5'-CCAATACCATGCAGATAAACCAC-3'	23
CDC25C F	5'-CCAGATGTCCCTAGAACTCCA-3'	21
CDC25C R	5'-TCACTGTCCACCAAGTTTCC-3'	20

Table 4-2. Combination treatments with (a) trametinib and dactolisib, (b) SCH772984 and dactolisib, and (c) AZ628 and dactolisib. The quantities in the vertical and horizontal directions represent the coefficients of LD₅₀ for each compound used in combination treatments. The fraction of LD₅₀ of drug pairs used in combination is shown inside the bracket in each table (a-c). The concentration pairs that resulted in disintegration of spheroids are highlighted in red.

(a)

		Dactolisib (×LD ₅₀)					
		0.125	0.25	0.5	1	2	4
Trametinib (×LD ₅₀)	0.125	(0.125,0.125)	(0.125, 0.25)	(0.125, 0.5)	(0.125, 1)	(0.125,2)	(0.125,4)
	0.25	(0.25,0.125)	(0.25, 0.25)	(0.25, 0.5)	(0.25, 1)	(0.25,2)	(0.25,4)
	0.5	(0.5,0.125)	(0.5, 0.25)	(0.5, 0.5)	(0.5, 1)	(0.5,2)	(0.5,4)
	1	(1,0.125)	(1, 0.25)	(1, 0.5)	(1, 1)	(1,2)	(1,4)
	2	(2,0.125)	(2, 0.25)	(2, 0.5)	(2, 1)	(2,2)	(2,4)
	4	(4,0.125)	(4, 0.25)	(4, 0.5)	(4, 1)	(4,2)	(4,4)

(b)

		Dactolisib (×LD ₅₀)					
		0.125	0.25	0.5	1	2	4
SCH772984 (×LD ₅₀)	0.125	(0.125,0.125)	(0.125, 0.25)	(0.125, 0.5)	(0.125, 1)	(0.125,2)	(0.125,4)
	0.25	(0.25,0.125)	(0.25, 0.25)	(0.25, 0.5)	(0.25, 1)	(0.25,2)	(0.25,4)
	0.5	(0.5,0.125)	(0.5, 0.25)	(0.5, 0.5)	(0.5, 1)	(0.5,2)	(0.5,4)
	1	(1,0.125)	(1, 0.25)	(1, 0.5)	(1, 1)	(1,2)	(1,4)
	2	(2,0.125)	(2, 0.25)	(2, 0.5)	(2, 1)	(2,2)	(2,4)
	4	(4,0.125)	(4, 0.25)	(4, 0.5)	(4, 1)	(4,2)	(4,4)

(c)

		Dactolisib (×LD ₅₀)					
		0.125	0.25	0.5	1	2	4
AZ628 (×LD ₅₀)	0.125	(0.125, 0.125)	(0.125, 0.25)	(0.125, 0.5)	(0.125,1)	(0.125,2)	(0.125, 4)
	0.25	(0.25, 0.125)	(0.25, 0.25)	(0.25, 0.5)	(0.25,1)	(0.25,2)	(0.25, 4)
	0.5	(0.5, 0.125)	(0.5, 0.25)	(0.5, 0.5)	(0.5,1)	(0.5,2)	(0.5, 4)
	1	(1, 0.125)	(1, 0.25)	(1, 0.5)	(1,1)	(1,2)	(1, 4)
	2	(2, 0.125)	(2, 0.25)	(2, 0.5)	(2,1)	(2,2)	(2, 4)
	4	(4, 0.125)	(4, 0.25)	(4, 0.5)	(4,1)	(4,2)	(4, 4)

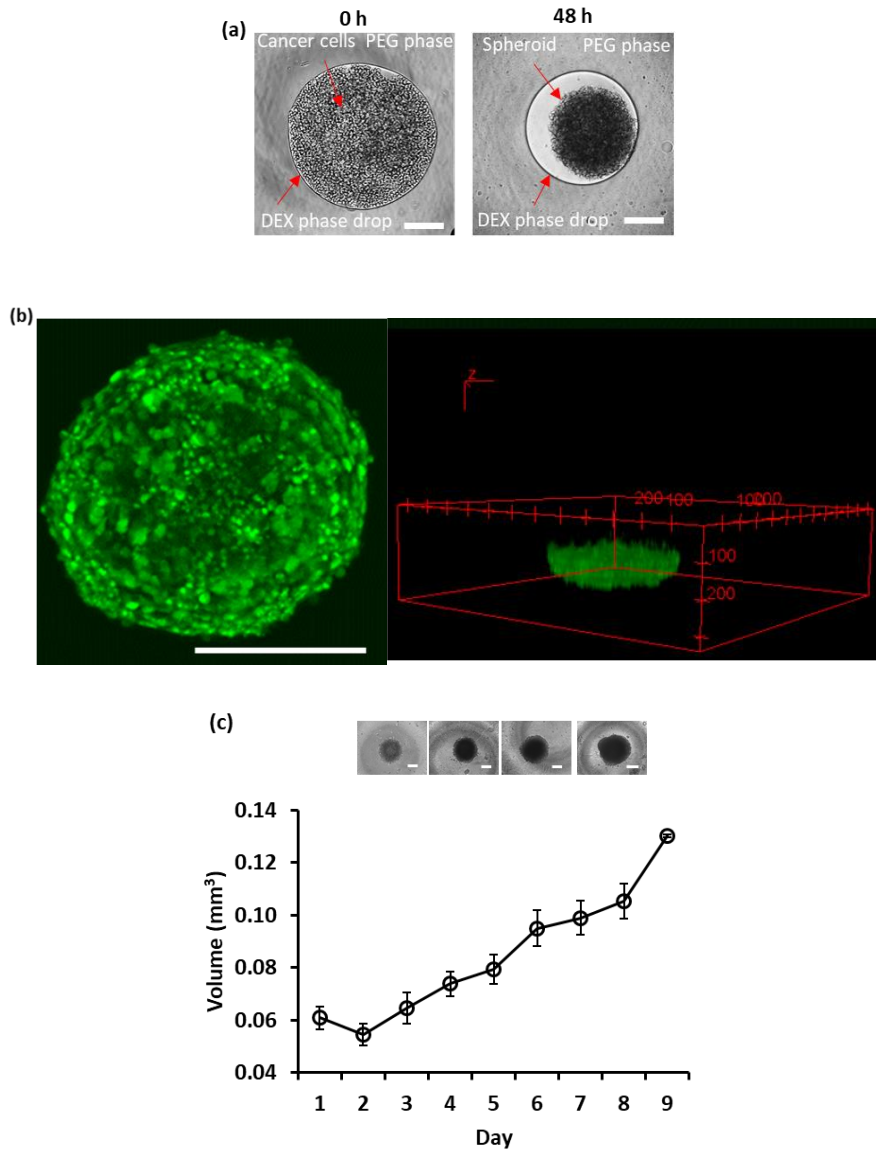


Figure 4-1. Formation and growth of tumor spheroids. (a) A 0.3 μl drop of the aqueous DEX phase containing HCT116 cancer cells immersed in the aqueous PEG phase settles to the well bottom. Cancer cells remain within the DEX drop and form a spheroid. (b) Confocal image of spheroids shows fully viable cells and a 3D z-stack reconstruction of a portion of a spheroid. (c) Size of HCT116 spheroids increases during incubation indicating cell proliferation. Inset images from left to right represents spheroids on days 2, 4, 6, and 8. Error bars represent standard error of the mean ($n=14$). Scale bar is 200 μm in panels (a-c).

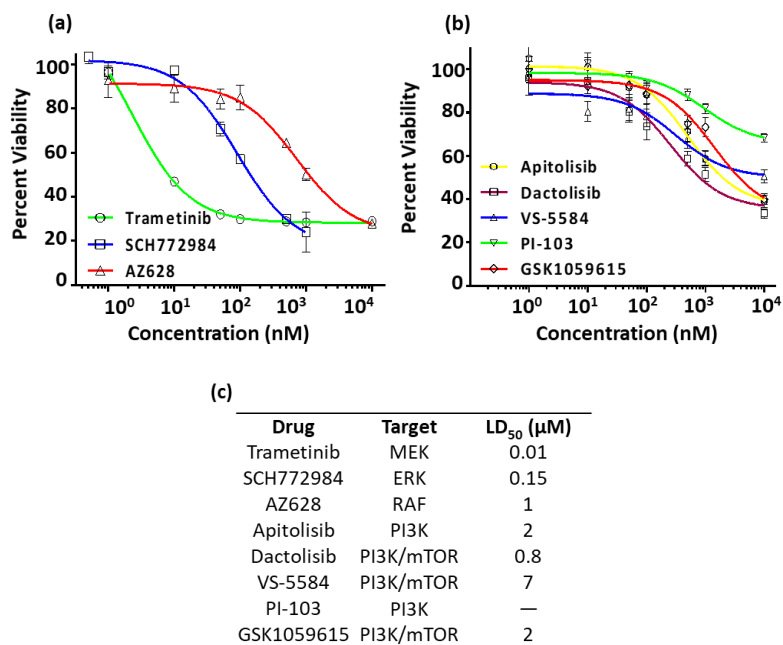


Figure 4-2. Responses of spheroids to MAPK and PI3K inhibitors. Dose-responses of HCT116 spheroids to inhibitors of (a) MAPK pathway and (b) PI3K pathway. (c) The list of molecular inhibitors used, their targets, and LD₅₀ values against HCT116 spheroids. The symbol ‘—’ indicates an LD₅₀ value could not be obtained.

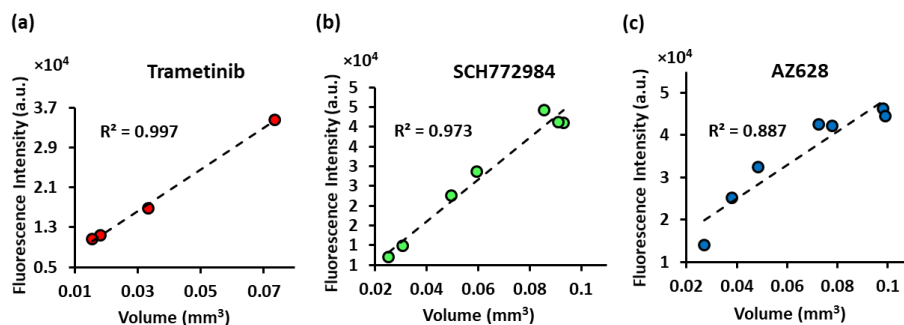


Figure 4-3. Correlation between average values of fluorescence signal from Prestoblue assay and volume of spheroids from morphological images of spheroids treated with MAPKi (n=14). R² represent goodness-of-the-fit parameter. Different data points in each graph represent different drug concentrations. Only those concentrations that did not disintegrate the spheroids were used for the analysis.

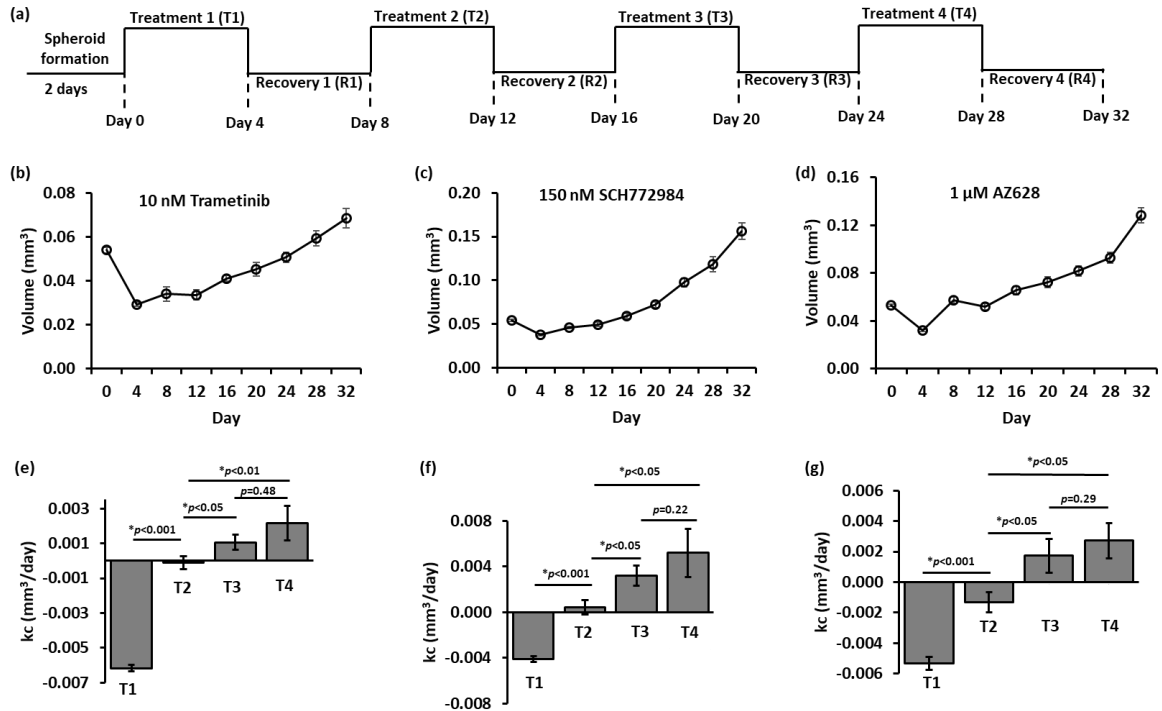


Figure 4-4. Cyclic drug treatment and recovery of tumor spheroids. (a) HCT116 spheroids were cyclically treated with inhibitors of MEK (0.01 μM trametinib), ERK (0.15 μM SCH772984), and RAF (1 μM AZ628). (b-d) Kinetics of growth of spheroids during cyclical treatment and recovery. Each data point in the line graph is an average of 32 replicates. (e-g) Growth rate (k_c) of HCT116 spheroids during four treatment rounds with (e) trametinib, (f) SCH772984, and (g) AZ628. $n=14$ and * denotes statistically significant differences in the growth rates between treatment rounds. Error bars in panels (b-g) represent the standard error of a mean value.

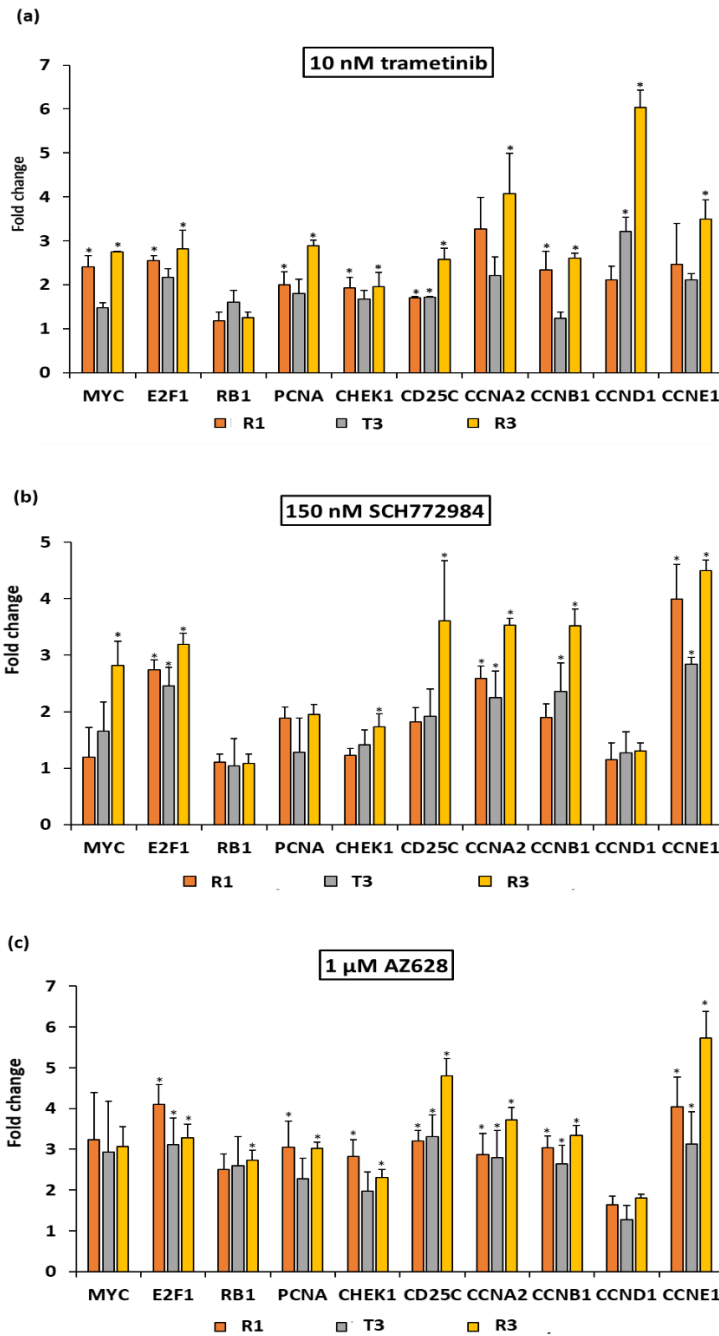


Figure 4-5. Fold change in expression of proliferation genes in tumor spheroids during cyclic treatment and recovery with MEKi. The bar graphs show the fold change values of 10 prominent proliferation genes after treatments with (a) 10 nM trametinib, (b) 150 nM SCH772984, and (c) 1 μ M AZ628. The fold change values after R1, T3, and R3 are relative to T1. * denotes $p < 0.05$ when compared with T1.

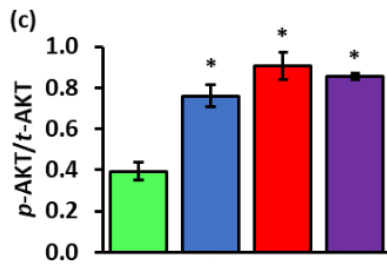
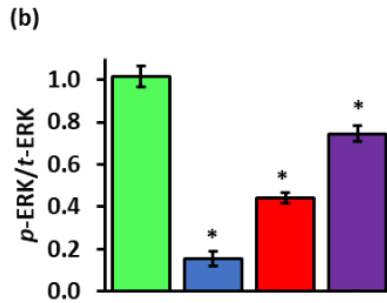
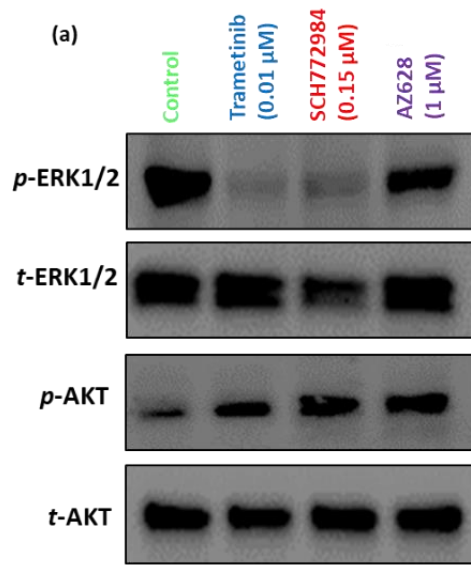


Figure 4-6. Activity levels of ERK1/2 and AKT proteins in tumor spheroids treated with inhibitors of MAPK pathway. (a) Western blots for phosphorylated and total levels of ERK1/2 and AKT at the end of T1. (b) Quantified results of p-ERK/t-ERK in vehicle control and treated spheroids. (c) Quantified levels of p-AKT/t-AKT in vehicle control and treated spheroids. Results are shown as mean \pm standard error. Each Western blot experiment was repeated twice. * denotes $p < 0.05$ when comparing each treatment and the vehicle control.

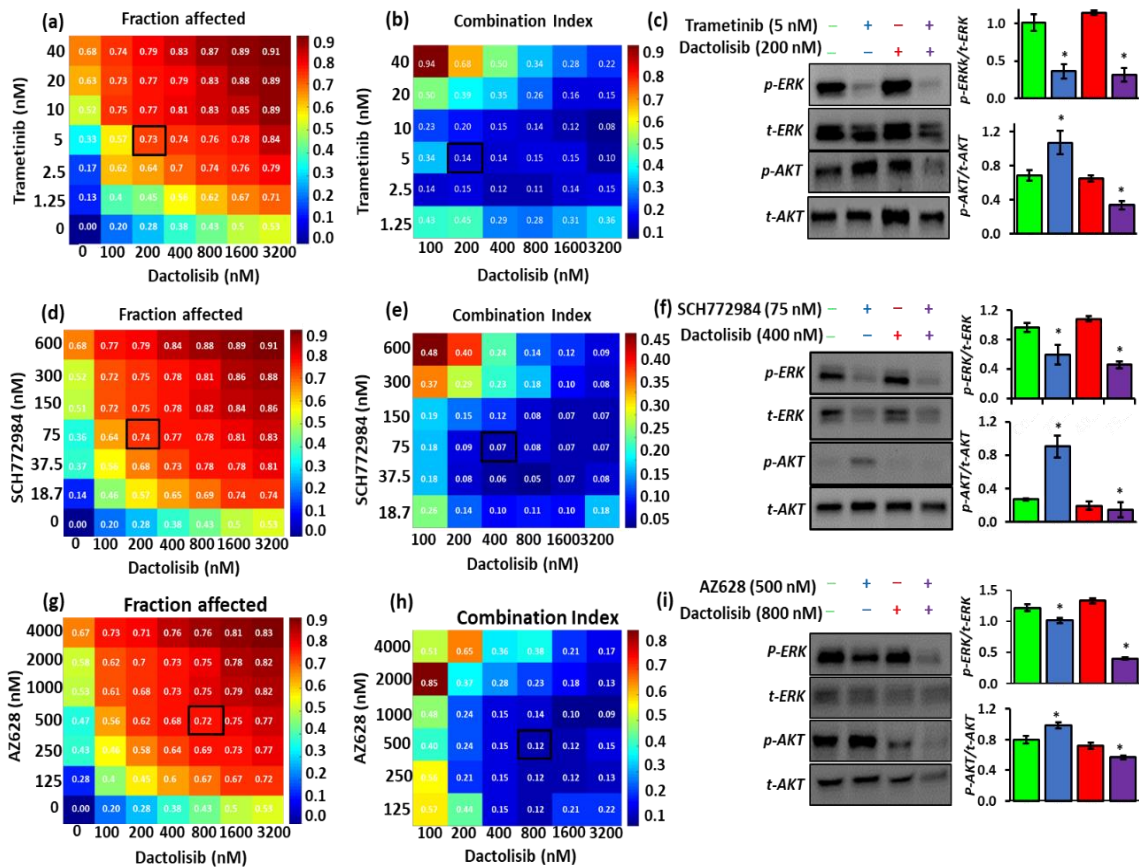


Figure 4-7. Combination treatments of spheroids with inhibitors of MAPK and PI3K pathways. Heatmap plots representing fraction of cells affected (Fa) by single-agent and combination treatments of (a) trametinib/dactolisib, (d) SCH772984/dactolisib, and (g) AZ628/dactolisib. Heatmaps representing combination indices (CI) following combination treatments of spheroids with (b) trametinib/dactolisib, (e) SCH772984/dactolisib, and (h) AZ628/dactolisib. The combination concentrations resulting in greater cell death (larger Fa values) and higher synergy (smaller CI values) are boxed in the heatmaps of panels (a–f). This pair of concentrations from each pair of inhibitors was selected for Western blots of active and total ERK1/2 and AKT shown in panels (c, f and i). Bar graphs represent quantified *p*-ERK/*t*-ERK and *p*-AKT/*t*-AKT levels for single-agent and combination treatments. Each Western blot experiment was repeated twice. Results are shown as mean \pm standard error. **p* < 0.05 denotes comparing single-agent MAPKi treatments with the vehicle control and also combination treatments with the corresponding single-agent MAPKi treatments.

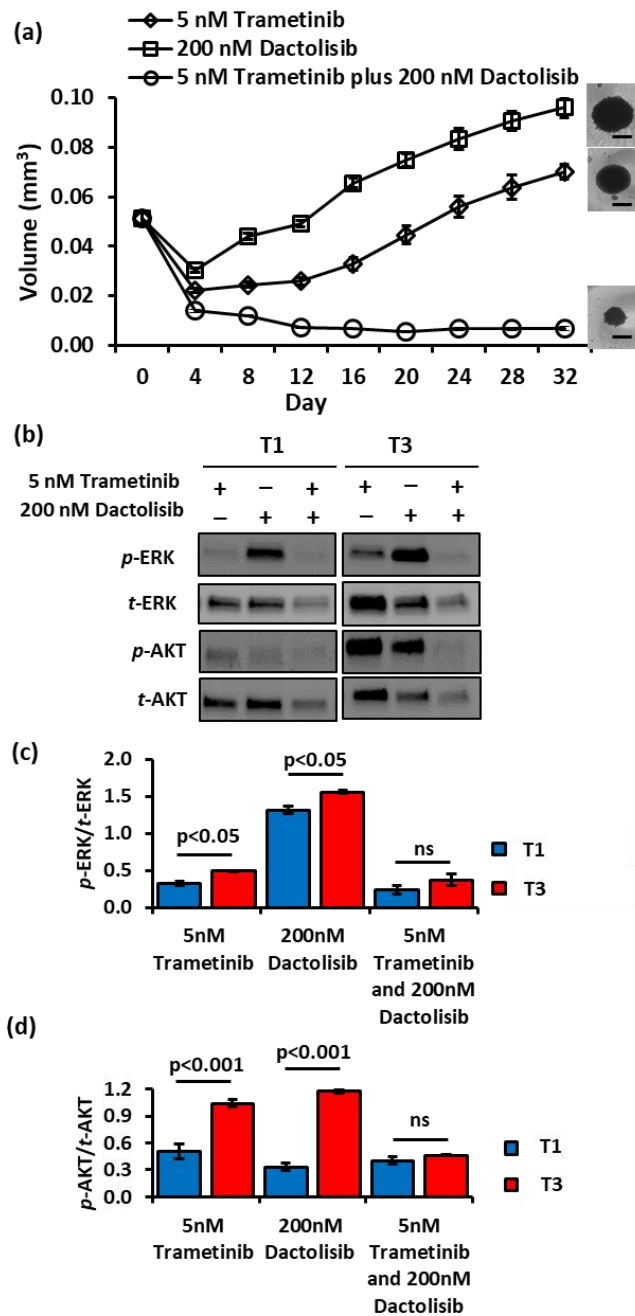


Figure 4-8. Long-term single-agent and combination treatment/recovery of spheroids. (a) Size of spheroids under cyclic single-agent and combination treatments with trametinib and dactolisib. Inset images show spheroids from single-agent and combination treatments at the end of 32 days of culture. Scale bar is 250 μm . (b) Representative Western blots of active and total ERK1/2 and AKT for single-agent and combination treatments at the end of T1 and T3. Quantified levels of (c) p-ERK/t-ERK and (d) p-AKT/t-AKT. Western blot experiment was repeated twice. Each data point in the graph is an average of 32 replicates. Error bars represent standard error of the mean.

CHAPTER V

COMBINED INHIBITION OF MAPK PATHWAY AND EGFR TO OVERCOME ADAPTIVE DRUG RESISTANCE OF COLORECTAL CANCER SPHEROIDS

Although promising therapeutics have been developed for colorectal cancers, KRAS-mutant disease that accounts for 35-45% of malignant colorectal cancers continues to have poor prognosis and limited therapy options. [221], [222] Pre-clinical studies have evaluated compounds that target effectors of RAS, mainly inhibitors of MAPK and PI3K signaling pathways. However, cancer cells adapt to these inhibitors by switching on to alternative oncogenic signaling networks. For example, colorectal cancer cells develop resistance to single-agent inhibition of MAPK pathway by activating PI3K/AKT or JAK/STAT pathways or by activating receptor tyrosine kinases (RTKs). [96], [223], [224] As KRAS is constitutively active and central to many intracellular signaling pathways are driven by RTKs, it can also bypass RTKs-driven signaling cascades and impair the clinical efficacy of RTK inhibitors. [44] This suggests the need for dual and multi-targeting strategies to block drug resistance of cancer cells. However, despite the rationale for drug combinations, dose-limiting toxicities remain a major concern. For example, blocking extensive cross-talk between MAPK and PI3K pathways by combining inhibitors of these pathways significantly inhibited tumor growth but also resulted in excessive toxicity in cancer patients. [203] Although dose reduction is a potential approach to overcome toxicity in patients, alternative combination treatment strategies are also being sought, such as co-targeting components of the MAPK pathway and upstream RTKs. For example,

simultaneous inhibition of type-1 insulin-like growth factor receptor (IGF1R) and MEK synergistically inhibited growth of colorectal tumors in xenografts. [225]

Pre-clinical models to recreate drug resistance of cancer cells are important tools to identify mechanism of resistance and design and test novel treatment strategies. Monolayer (2D) cultures of cancer cells are convenient to screen large arrays of drug combinations. However, 2D cultures are insufficient due to their lack of structural and biological complexities of solid tumors and incompatibility with long-term cultures to reproduce adaptation of cancer cells to drugs. [56], [165] Animal models are extensively used to study intrinsic and adaptive drug resistance, but high cost and difficulty of testing arrays of drug combinations and identifying molecular mechanisms of drug resistance in animals are major drawbacks. [51] Three-dimensional (3D) cancer models offer an attractive tool to bridge this gap between 2D cultures and animal models. [56], [165], [226] We have shown that spheroids of cancer cells reproduce biological features of avascular tumors and treatment outcomes. [164], [227] Recently, we used spheroids as a novel model to identify and overcome adaptive drug resistance by rationally designing drug combinations. [163] Here, we used this established model and demonstrated that targeting various kinases downstream of KRAS, such as RAF, MEK, and ERK, transiently suppressed the growth of KRAS-mutant colorectal cancer cells by downregulating p-ERK1/2 levels. However, colorectal cancer cells in spheroids quickly adapted to the treatments and activated AKT and STAT signaling to continue proliferating. We also identified upregulation of EGFR family members in response to MAPK pathway inhibition. Combinations of inhibitors of MAPK pathway and EGFR synergistically inhibited growth of colorectal cancer spheroids and suppressed MAPK and PI3K pathways. However, they were ineffective against STAT

signaling that can promote tumor growth and invasiveness of cancer cells, emphasizing the need of simultaneous targeting of multiple processes in tumor microenvironment. Our model allows understanding mechanism of drug resistance of cancer cells and carrying out several design-driven combinations to identify synergistic drugs that block drug resistance and potentially other malignant processes in tumors.

5.1 Materials and Methods

The methods to model adaptive drug resistance to MAPKi, analyze multiple signaling pathways to identify drug resistance, and design alternative drug combination modality to suppress growth and metastasis of KRAS mutant colorectal tumor spheroids are described below.

5.1.1 Cell Culture and Spheroid Formation

Two colorectal cancer cell lines, HCT116 and DLD1, were purchased from the ATCC. McCoy's 5A and RPMI-1640 media were used to culture HCT116 and DLD1 cells, respectively. Each medium was supplemented fetal bovine serum (10%) (FBS, Sigma), streptomycin/penicillin (1%) (Life Technologies), and glutamine (1%) (Life Technologies). Cell cultures were done using the methods described in previous chapters (II, III, and IV). Spheroids from each cell line were formed using 1.5×10^4 cells as previously described. [81], [116], [178]

5.1.2 Drug Tests

Trametinib, PD0325901, selumetinib, dabrafenib, sorafenib, AZ628, GDC0994, SCH772984, ulixertinib, neratinib, sapitinib, and lapatinib were purchased from

Selleckchem. These compounds were dissolved in dimethyl sulfoxide (DMSO) and stored in -80°C . All compounds were tested dose dependently against spheroids of HCT116 and DLD1 cells. Except for SCH772984, all the other compounds were prepared at concentrations of 2×10^{-3} μM , 2×10^{-2} μM , 1×10^{-1} μM , 2×10^{-1} μM , 1×10^0 μM , 2×10^0 μM , and 2×10^1 μM . SCH772984 solutions were prepared at 1×10^{-3} μM , 2×10^{-3} μM , 2×10^{-2} μM , 1×10^{-1} μM , 2×10^{-1} μM , 1×10^0 μM , and 2×10^0 μM concentrations. These solutions were prepared at $2 \times$ of the final concentrations. The volume of the solutions in the microwells was measured and an equal volume of the drug solution was added. This addition reduced the drug concentrations in half. Vehicle control spheroids were grown in cell culture medium. Viability and dose response curve analysis were performed according to the methods described in section 2.1.5.

5.1.3 Cyclical Treatments

Trametinib, SCH772984, and AZ628 were used at their LD_{50} concentrations to cyclically treat spheroids of HCT116 and DLD1 cells. That is, 10 nM trametinib, 150 nM SCH772984, and 1 μM of AZ628 with HCT116 spheroids, and 35 nM trametinib, 700 nM SCH772984, and 10 μM AZ628 with DLD1 spheroids. Each experiment included four cycles of treatment (T1, T2, T3, and T4), and three recovery periods (R1, R2, and R3). The treatment and recovery phase were kept constant for 4 days. During each treatment drug was added to the well containing spheroids at the beginning only. At the end of each treatment phase, drug solutions were thoroughly removed from the wells to allow the spheroids to recover from the treatment. The same concentration of each drug was used throughout the treatment periods. At the end of each treatment and recovery cycle, the size of the spheroids was measured. To quantify resistance of spheroids to each inhibitor, a

growth rate metric (k_c) was defined as the difference in the size of spheroids after and before each treatment.

5.1.4 Western Blot Experiments

Western blot was performed using the protocol described previously [86], [163]. Primary antibodies purchased from Cell Signaling Technology included phospho-p44/42 MAPK (Erk1/2), p44/42 MAPK (Erk1/2), phospho-AKT (Ser473), AKT (pan) (C67E7), phospho-STAT1 (Tyr701), phospho-SAT6 (Tyr641), and β -actin (13E5). These antibodies were diluted according to manufacturers' recommendation. Membranes blocking, washing and detection were performed as described in section 2.1.6.

5.1.5 Phospho-RTK array

A human phospho-RTK dot array (ARY001B; RandD Systems) was used to simultaneously screen level of 49 human receptor tyrosine kinases. An equal amount of cell lysate (300 μ g) from each cell line was used for these experiments. The array was visualized using FluorChem E Imaging system. All arrays of each experiment were exposed simultaneously. An adequate exposure time was selected to capture the differences in receptor protein kinase activity between vehicle control and treatment groups. A pixel density module in ImageJ was used to quantify phosphorylation levels of the proteins. The pixel density of the background signal was subtracted from the average of the measured signal of a pair of dots for each protein on the array. The phosphorylated level of each protein in a treated group was determined by normalizing it with the pixel density value in the respective vehicle control group.

5.1.6 Combination Treatments of Spheroids

Seven concentration pairs of trametinib and neratinib were used for drug combinations. For comparison with the combination treatments, single agent treatment of trametinib and neratinib were performed. drug treatments, and viability and synergy analysis were performed as described in section 4.1.3.

5.1.7 Long-term Cyclic Drug Combination Treatments

Of the trametinib/neratinib drug pairs, 35 nM/200 nM and 10 nM/500 nM concentrations were used against DLD1 and HCT116 spheroids, respectively. In parallel, spheroids were treated with trametinib or neratinib only. The long-term effectiveness of the treatments was computed by using growth rates of spheroids (k_c) under combination and single-agent treatment after 16 days of treatment. The growth rates of spheroids were calculated as the difference in the volume of spheroids at the end and at the beginning of 16-day treatment period.

5.1.8 3D Invasion Assay

Of the trametinib/neratinib drug pairs, 35 nM/200 nM and 10 nM/500 nM concentrations were used against DLD1 and HCT116 spheroids, respectively. In parallel experiments, spheroids were treated with trametinib or neratinib only. After 4 days, spheroids were suspended in a 4 mg/ml collagen solution. Incubation at 37°C for 30 min resulted in collagen gelation. Invasion of cells from spheroids into the collagen matrix was captured using confocal microscopy (Nikon A1 confocal system) using a 10x objective after 3 and 5 days. Z-stack images (20 μ m) were captured using FITC filter and images were captured using NIS Elements software. Z-projected images were reconstructed by

collapsing the stacks in ImageJ (NIH). Cell invasion was quantified by normalizing the invasion pixel area with the spheroid pixel area.

5.2 Results and Discussions

Below results of adaptive resistance to MAPKi, i.e., inhibitors of MAPK pathway, (RAFi, MEKi, ERKi) are presented. The result of molecular analysis of multiple signaling pathways and molecular screening of RTKs and design rational combination approach to overcome drug resistance over long-term studies are also discussed.

5.2.1 Screening of MAPK Pathway Inhibitors

HCT116 and DLD1 have have MAPK and PI3K signaling pathways due to mutations in KRAS and PIK3CA. [141] We previously demonstrated that single-agent inhibition of MAPK pathway more effectively blocked the growth of colorectal tumor spheroids than using a PI3K/AKT pathway inhibitor, [163], [228] suggesting dependency of cancer cells on MAPK signaling to proliferate. This prompted us to screen several molecular inhibitors that target various levels of the MAPK pathway, such as BRAF, MEK, and ERK. We screened 9 different MAPK inhibitors (MAPKi) against HCT116 and DLD1 spheroids. The inhibitors dose-dependently reduced viability of both cell lines in spheroid cultures but showed significant differences in effectiveness (Fig. 5-1a-b). Our AUC analysis of dose-response curves resulted in the lowest AUC values of 0.41 and 0.45 with trametinib treatments of HCT116 and DLD1 spheroids (Fig. 5-1c-d). Interestingly, the other two inhibitors of MEK, PD0325901 and selumetinib, resulted in the second and third lowest AUC values of 0.45 and 0.60 for HCT116 spheroids, and 0.51 and 0.75 for DLD1 spheroids. This indicates that the colorectal tumor spheroids were more sensitive to MEK

inhibition than its upstream or downstream kinases. Additionally, the ERKi were more effective than the BRAFi, as shown in Fig. 5-1c-d. Based on these results, we selected trametinib, SCH772984, and AZ628 as the most effective MEKi, ERKi, and BRAFi against both cell lines. The LD₅₀ values of the compounds are shown in Fig. 5-1e. Overall, our results showed that single-agent treatments with MAPKi more effectively inhibit growth of spheroids of these colorectal cancer cells than using PI3Ki. Thus, we used single-agent inhibition of MAPK pathway to study adaptive resistance of colorectal tumor spheroids.

Our study showed that single-agent inhibition of MAPK pathway is effective over single-agent inhibition of PI3K pathway in colorectal cancer cells harboring KRAS and PIK3CA mutations. [163], [228], [229] Although EGFR drives both MAPK and PI3K signaling pathways, inhibition of EGFR, HER2, or HER3 was either less effective or completely ineffective in colorectal cancers (Fig. 5-9). This indicates only a partial response of KRAS-mutant colorectal cancer cells to EGFRi, consistent with other studies. [230], [231] The effectiveness of MAPKi against the colorectal cancer cells indicates dependency of the cells on MAPK pathway for growth and proliferation.

5.2.2 Long-term Cyclical Treatment of Spheroids with MAPKi

We evaluated changes in effectiveness of MAPKi against HCT116 and DLD1 spheroids during long-term cyclic treatments with LD₅₀ concentration of each compound. Trametinib, SCH772984, and AZ628 potently inhibited growth of HCT116 cells during T1 and decreased the size of spheroids by 1.80, 1.42, and 1.67 fold, respectively (Fig. 5-2a). The spheroids at the end of T4 were 3.17, 2.91, and 1.90 fold larger than after T1 by trametinib, SCH772984, and AZ628 treatments. Furthermore, growth rate (k_c) of HCT116

spheroids were significantly higher after successive treatments (Figure 5-2b). To demonstrate that this adaptive resistance was not specific to a cell line, we repeated the cyclic treatments with DLD1 spheroids. The size of DLD1 spheroids decreased by 1.84, 1.41, and 1.71 fold with trametinib, SCH772984, and AZ628 treatments, respectively, after T1 (Fig. 5-2c). But repeated exposure of cells to the MAPKi led to drug resistance and growth of spheroids by 2.46, 2.80, and 2.71 fold, respectively. Also, the growth rates of DLD1 spheroids were significantly higher following successive treatments (Figure 5-2c). The reduced effectiveness of the inhibitors indicates that cancer cells develop adaptive responses to MAPK pathway inhibition. Despite significant inhibition of growth of spheroids by MAPKi during short-term treatments, our long-term cyclical treatment shows adaptive response of spheroids to the inhibitors. The inhibition of MAPK pathway only generated a transient anti-proliferative effect and cells quickly activated adaptive responses to treatments with RAFi, MEKi, and ERKi (Fig. 5-2). Importantly, the adaptive resistance observed in our model is consistent with *in vivo* tests showing reduced efficacy of MEK1/2 inhibitors during cyclic treatments of tumor xenografts. [188], [199]

5.2.3 Molecular Analysis of Adaptive Drug Resistance of Colorectal Tumor Spheroids

Next, we performed molecular analysis to identify driver of resistance in colorectal cancer cells following MAPKi treatments. Studies from various cancers show that MAPK pathway inhibition may lead to the activation of PI3K pathway, JAK/STAT pathway, or upstream RTKs that can in turn activate signaling of oncogenic kinase pathways. Thus, we performed a comprehensive molecular analysis of HCT116 and DLD1 spheroids cyclically treated with MAPKi.

- *PI3K/AKT kinases*

Cross-talk between MAPK/ERK and PI3K/AKT pathways is common in many cancers, including colorectal cancer. [190]–[192] We previously showed that MEK1/2 inhibition of BRAF-mutant HT-29 spheroids amplify PI3K/AKT signaling pathway. [163] Thus, we determined if this effect is still true if we target RAF, MEK, and ERK kinases of MAPK signaling pathway. Quantifying AKT kinase activity following MAPKi treatments of colorectal cancer spheroids showed significant phosphorylation of AKT only after four days of treatment with MEKi, ERKi, and RAFi (Fig. 5-3a-b). Trametinb, SCH772984, and AZ628 treatments respectively increased p-AKT levels in HCT116 cells by 37%, 52%, and 46% (Fig. 5-3a) and in DLD1 cells by 100%, 80%, and 90% (Fig. 5-3b). This established that suppressing MAPK pathway at various levels induces upregulation of AKT kinase of PI3K pathway in the tested colorectal cancer cells.

- *STAT kinases*

Activation of the JAK/STAT pathway in colorectal cancer has been suggested as a mechanism of resistance to MEKi. [224] This prompted us to study potential changes in the JAK/STAT signaling pathway following treatments with MAPKi. Our Western blot analysis did not show any significant changes in JAK proteins (data not shown). However, STAT proteins were activated in a cell line dependent manner. Trametinib, SCH772984, and AZ628 treatments increased p-STAT1 level in HCT116 cells by 112%, 91%, and 71% (Fig. 5-3c) and p-STAT6 level in DLD1 cells by 40%, 10%, and 36% (Fig. 5-3d). Except for p-STAT6 in SCH772984-treated DLD1 cells, the increased activities of the STAT kinases due to MAPKi treatments were statistically significant.

- *Receptor tyrosine kinases (RTKs)*

Feedback activation of AKT and STAT kinases indicates the role of these pathways in colorectal cancer cells to survive MAPK pathway inhibition. It has also been reported that suppressing the RAF/MEK/ERK cascade may activate upstream RTKs in colorectal cancers, [96], [191], [223], [232] which in turn can activate PI3K/AKT and JAK/STAT pathways. For example, suppression of EGFR/MAPK/ERK cascade in KRAS-mutant colorectal cancer cells resulted in RTK-dependent PI3K activation. [223] To determine which RTKs may be activated after targeting different kinases of the MAPK pathway in colorectal tumor spheroids, we used a phospho-RTK blot array to quantify activities of 49 different RTKs. The blot arrays for vehicle control and treated HCT116 and DLD1 spheroids are shown in Fig. 5-4a-b. We quantified phosphorylated levels of each protein from a treatment group with respect to the respective vehicle control group. This analysis showed significant upregulation of EGFR, HER2, and HER3 in colorectal tumor spheroids following treatments with the MAPKi. All three EGFR proteins were upregulated in HCT116 cells irrespective of inhibition of RAF, MEK, or ERK. Trametinib, SCH772984, and AZ628 treatments of HCT116 spheroids enhanced phosphorylation of EGFR by 3, 4.13, and 4.11 fold, HER2 by 1.70, 1.60 and 1.70 fold, and HER3 by 1.29, 1.05, 1.16 fold, respectively. In DLD1 spheroids treated with trametinib, SCH772984, and AZ628, phosphorylation of EGFR increased by 1.11, 1.23, and 1.14 fold, and phosphorylation of HER3 increased by 1.39, 1.35, and 1.19 fold, respectively. Activity of HER2 increased only after trametinib treatment of DLD1 spheroids by 1.27 fold. SCH772984 and AZ628 did not alter HER2 activity in these cells. It has been reported that significant upregulation of other RKTs such as c-MET following MEK inhibition leads to activation STAT3

signaling to promote tumor growth and MEKi resistance in colorectal cancer. [224] However, we did not observe c-MET activity following MAPK pathway inhibition.

We previously demonstrated that single-agent MEK1/2 inhibition downregulates p-ERK levels and significantly decreased cell viability in BRAF-mutant colorectal cancer spheroids, but results in feedback activation of AKT. [163], [228] In this study, we showed that inhibition of RAF, MEK, or ERK in KRAS-mutant colorectal cancer cells also leads to AKT activation (Fig. 5-3). These results suggest that amplification of PI3K signaling pathway is a common mechanism of drug resistance in colorectal cancer. In addition, we observed activation of STAT kinases following MAPK pathway inhibition (Fig. 5-3c-d). Unlike other studies that showed activation of STAT3 in colorectal cancer cells following MAPKi treatments, [224], [233] our results showed phosphorylation of STAT1 and STAT6 in a cell line dependent manner. Considering that JAK/STAT is a cytokine pathway, our result suggests that activation of these specific STAT proteins may not necessarily be a mechanism of escape from the MAPKi treatments. More complex tumor models that incorporate immune components will help explain whether activation of these STAT proteins potentially leads to an immunosuppressive phenotype in cancer cells.

The oncogenic PI3K/AKT and JAK/STAT pathways drive growth, survival, and metastasis of colorectal cancers. [234]–[239] Blocking activities of either of these pathways along with the MAPK pathway has been effective to suppress growth of colorectal tumors and overcome their drug resistance. [198], [233], [240], [241] Despite anti-tumor effects of this approach, it may also lead to excessive toxicity to cancer patients. For example combination of MAPK and PI3K inhibitors have led to excessive toxicities in several advanced cancers, including colorectal cancer. [203] Dose reduction is a potential

strategy to overcome this issue. [242] Nevertheless, feedback activation of multiple intracellular signaling pathways in addition to the constitutively active MAPK pathway limits the effectiveness of the dual combination treatments. Using more than two drugs simultaneously is also not feasible due to toxicity. A rational strategy to tackle this major issue is combining inhibitors of an RTK and MAPK pathway. Screening for phosphorylation of 49 RTKs showed only significant upregulation of EGFR, HER2, and HER3 in the colorectal cancer spheroids treated with MAPKi (Fig. 5-4). The EGFRs activates multiple intracellular kinase signaling pathways (i.e., MAPK, PI3K, and JAK/STAT pathways), [243], [244] and combined inhibition of MAPKi and EGFRi is essential to suppress activities of these downstream pathways.

5.2.4 Combination Treatments of Colorectal Tumor Spheroids with MAPKi and EGFRi

Suppression of MAPK pathway upregulated activities of AKT and STAT kinases and upstream EGFR, HER2, and HER3. These RTKs often initiate signaling through multiple pathways including PI3K/AKT and JAK/STAT. [245], [246] Although AKT was activated in both colorectal cancer cell lines following MAPK pathway inhibition, activation of STAT kinases was cell line-dependent. Therefore, we asked whether targeting upstream RTKs along with MAPK pathway would be effective against feedback activation of these signaling pathways to overcome adaptive resistance to MAPKi. We demonstrated that colorectal cancer cells were more responsive to the MEKi than RAFi or ERKi (Fig. 5-1). Additionally, resistance to the MEKi occurred slower than that to the RAFi or ERKi (Fig. 5-2). This suggested combining trametinib (MEKi) with an EGFRi to inhibit growth of colorectal cancer spheroids. First, we tested three EGFRi against HCT116 and DLD1 spheroids (Fig. 5-9). Neratinib and sapatinib, but not lapatinib, dose-dependently reduced

viability of DLD1 spheroids. With HCT116 spheroids, except for neratinib that showed a minimal effect, the other two EGFRi were ineffective. Based on these results, we selected neratinib as the EGFRi for combination treatments.

Following both single-agent and combination treatments of HCT116 and DLD1 spheroids (Fig. 5-5a-b), we computed the corresponding AUC values to quantitatively compare efficacy of the treatments. Combined use of trametinib and neratinib with HCT116 spheroids resulted in an AUC value of 0.50, which was significantly lower than those with the respective single-agent treatments (Fig. 5-5c). Similarly, with DLD1 spheroids, the combination treatment significantly reduced the AUC value to 0.44 from 0.52 with trametinib alone and 0.64 with neratinib alone (Fig. 5-5d). We computed a combination index (CI) for the combination treatments to determine synergism of the trametinib and neratinib. The value of CI less than one indicates synergism, and as CI approaches zero it indicates additive effect. [121], [177] Except for the lowest pair of concentrations with both cell lines, all other pairs resulted in CI value less than one, indicating synergistic effects of the two drugs to block signaling that promotes cancer cell proliferation (Fig. 5-5e-f).

Next, we studied molecular effects of simultaneous inhibition of MEK1/2 and EGFR on MAPK, PI3K/AKT, and STAT pathways. We used three pairs of concentrations with spheroids of each cell line based on the dose-response results (Fig. 5-5a-b). The combination treatments very effectively downregulated AKT and ERK activities at all three concentration pairs both in HCT116 and DLD1 spheroids (Fig. 5-6a-b). However, STAT kinases still remained active in HCT116 cells and even upregulated in DLD1 cells (Fig. 5-6c-d). This suggests either insufficient inhibition of EGFR by neratinib or feedback

activation of other RTKs to sustain the activity of STA1 and STAT6 kinases in HCT116 and DLD1 spheroids, respectively. In addition, the results suggest that concurrent inhibition of AKT and ERK accounts for the synergy of combining trametinib and neratinib.

5.2.5 Long-term Cyclic Combination Treatments of Colorectal Tumor Spheroids with MAPKi and EGFRi

We confirmed that trametinib and neratinib synergistically reduced viability of colorectal tumor spheroids during 4-day treatment. Next, we evaluated the efficacy of the drug combination during cyclical treatments and compared it to the respective single-agent treatments. We selected concentrations of the two compounds based on the dose-response (Fig. 5-5) and protein activity (Fig. 5-6) results. Combination of trametinib and neratinib significantly reduced the growth of HCT116 and DLD1 spheroids during a 16-day period compared to the respective single-agent treatments (Fig. 5-7a-b). In addition, we computed growth rate of spheroids (k_c) to quantitatively compare the effect of combination and single agent treatments. The k_c values for trametinib, neratinib, and their combination were -0.00068, -0.00019, and -0.00150 mm³/day against HCT116 spheroids and -0.00014, 0.00022, and -0.00215 mm³/day against DLD1 spheroids, respectively. The growth rate of spheroids after combination treatment was significantly lower than the growth rates of spheroids after single agent inhibition by neratinib or trametinib (Fig. 5-1a-b). The greater negative k_c values for the combination treatments than those for the respective single-agent treatments indicates a continuous growth suppression of tumor spheroids. We demonstrated that combinations of MEKi and EGFRi synergistically inhibited growth of colorectal tumor spheroids both during short-term continuous treatment and long-term

cyclic treatment and recovery (Fig. 5-5 and 5-6). Our results are consistent with the effectiveness of this strategy on growth inhibition of colorectal tumors *in vivo*. [95], [247], [248]

5.2.6 Drug Combination Prevents Matrix Invasion of Colorectal Tumor Spheroids

Although combined trametinib and neratinib suppressed growth of colorectal tumors spheroids by downregulating ERK and AKT kinases, they were not effective against STAT proteins in HCT116 and DLD1 spheroids (Fig. 5-6c-d). It has been shown that signaling of STAT kinases promotes invasion and metastasis of colorectal cancer. [239], [249], [250] Given the elevated activities of STAT kinases in the cancer cells under combination treatments, we hypothesized that these colorectal tumor spheroids could exhibit an invasive phenotype compared to single-agent treatment with neratinib or trametinib. To test this hypothesis, we first treated HCT116 and DLD1 spheroids with neratinib, trametinib, or their combination for 4 days and maintained a group of spheroids untreated. Then, we embedded the spheroids in a collagen hydrogel and examined matrix invasion of cancer cells from spheroids for 5 days. To account for the size differences of drug treated and control spheroids, we quantified the invasion area relative to the spheroid area.

HCT116 spheroids did not show invasive protrusions after 24 h. The vehicle control and neratinib-treated spheroids did not invade collagen even after 72 h (Fig. 5-10a and c), whereas trametinib and combination treatments promoted invasion of HCT116 spheroids by 140% and 110% (Fig. 5-10a and c). Matrix invasion under trametinib treatment was significantly higher than that with the combination treatment (Fig. 5-10a and c). After 120 h, vehicle control and neratinib-treated spheroids showed minimal collagen invasion of

16% and 8%, respectively (Fig. 5-8a and c). Trametinib-treated and combination drug-treated spheroids invaded collagen by 470% and 460%, which correspond to 29.37 and 28.75 fold increase in invasion compared to the invasion of vehicle control spheroids (Fig. 5-8a and c).

Vehicle control DLD1 spheroids invaded collagen matrix by 38.6% after 72 h. Neratinib and trametinib-treated spheroids showed collagen invasion of 5%, 59.5%, which respectively correspond to 7.70 folds less invasion and 1.54 folds more invasion than that of the vehicle control spheroids. DLD1 spheroids under the combination treatment only showed 2.2% invasion, i.e., 17.52 fold reduced invasion compared to the vehicle control spheroids (Fig. 5-10b and d). After 120 h, vehicle control DLD1 spheroids showed 130% collagen invasion. Spheroids treated with neratinib or trametinib as single agents invaded collagen by 202% and 418%, corresponding to 1.55 fold and 3.21 fold more invasion than the vehicle control spheroids. The combination treatment resulted in 9% matrix invasion, i.e., 14.44 fold reduction compared to the vehicle control condition (Fig. 5-8b and d).

Although the combined MEKi and EGFRi treatment synergistically inhibited growth of spheroids, it was ineffective against STAT1 and STAT6 activities in cancer cells. Several studies have shown a role for STAT proteins in promoting invasiveness of colorectal cancer cells. [239], [249], [250] Our analysis showed a cell line dependent effect of upregulated STAT activity on cell invasion. Combination of MEKi and EGFRi suppressed matrix invasion of DLD1 spheroids despite upregulating active STAT6 level. This is in contrast to a study that showed EMT and migration of HT-29 and SW480 colorectal cancer cells due to IL-13 mediated STAT6 upregulation. [250] Combined MEKi and EGFRi also suppressed the growth of HCT116 spheroids, but promoted STAT1

activity and was ineffective against matrix invasion of the cells compared to the use of MEKi only. Overall, our result cannot point to an exact role for activated STAT1 and STAT6 in the colorectal cancer cells due to the lack of immune cells mediated STAT activity. [250], [251] Despite showing the promising effect of the combination of MEKi and EGFRi on blocking growth of tumor spheroids, our study highlights the importance of developing more physiologic tumor models to capture the complexities induced by the signaling of stromal and cancer cells.

5.3 Summary

We demonstrated that colorectal cancer adapts to cyclical treatments of MAPKi by activating AKT, STATs, and EGFRs. Combination of MAPKi and EGFRi reduced drug resistance by reducing growth and invasion of spheroids by blocking both PI3K and MAPK pathways. Our model offers a useful platform to predict onset of adaptive response of cancer cells to molecular inhibitors, identify novel mechanism of drug resistance, and design of rational drug combinations to significantly reduce drug resistance. The use of our model will reduce use of expensive animal models and accelerate the process of drug discovery.

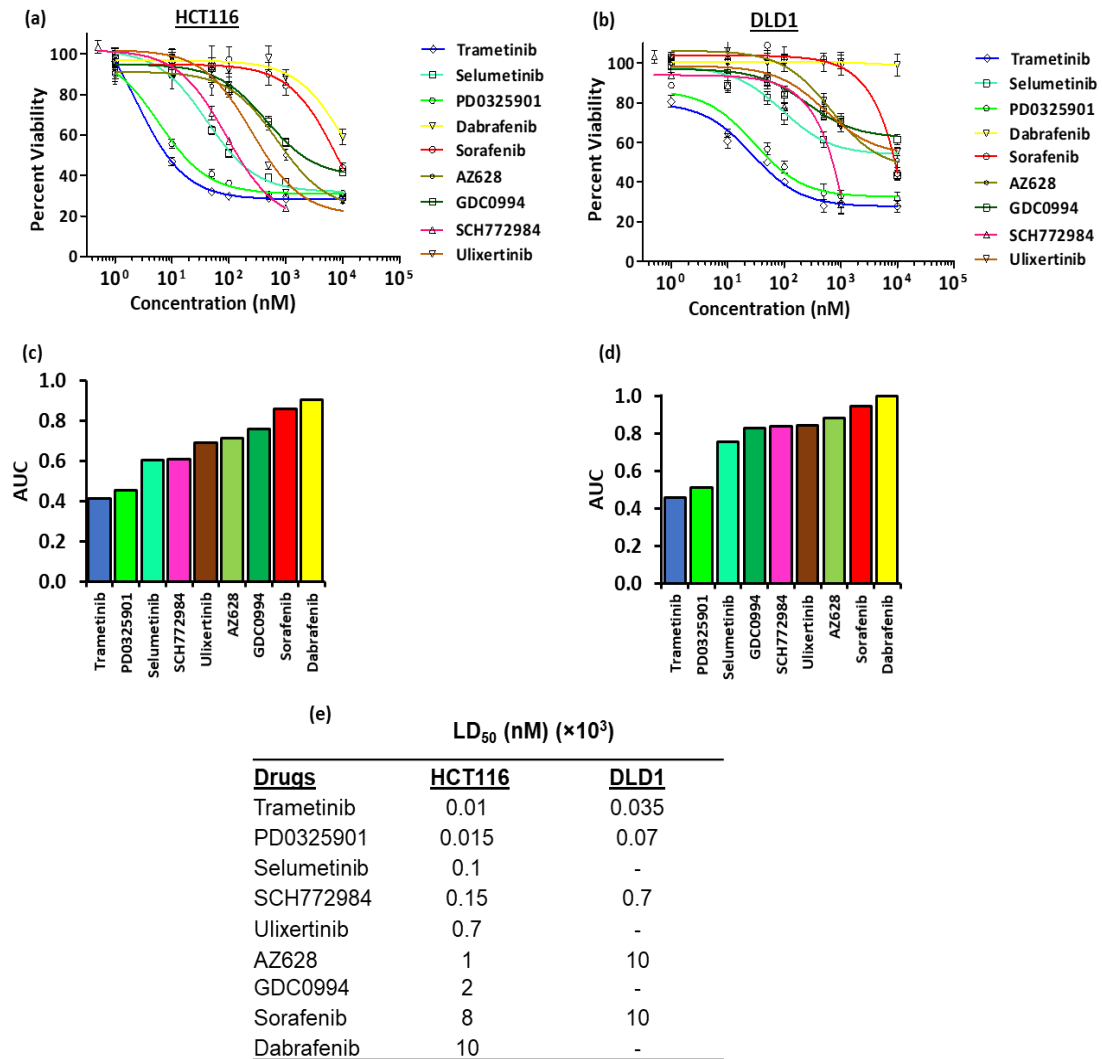


Figure 5-1. Inhibition of MAPK pathway in colorectal tumor spheroids (MAPKi). Dose-response curves of (a) HCT116 and (b) DLD1 spheroids to MAPKi. Ranking of MAPKi according to AUC analysis for spheroids of (c) HCT116 and (d) DLD1 cells. (e) LD₅₀ values of MAPKi against HCT116 and DLD1 spheroids. The symbol ‘-’ indicates lack of an LD₅₀ value.

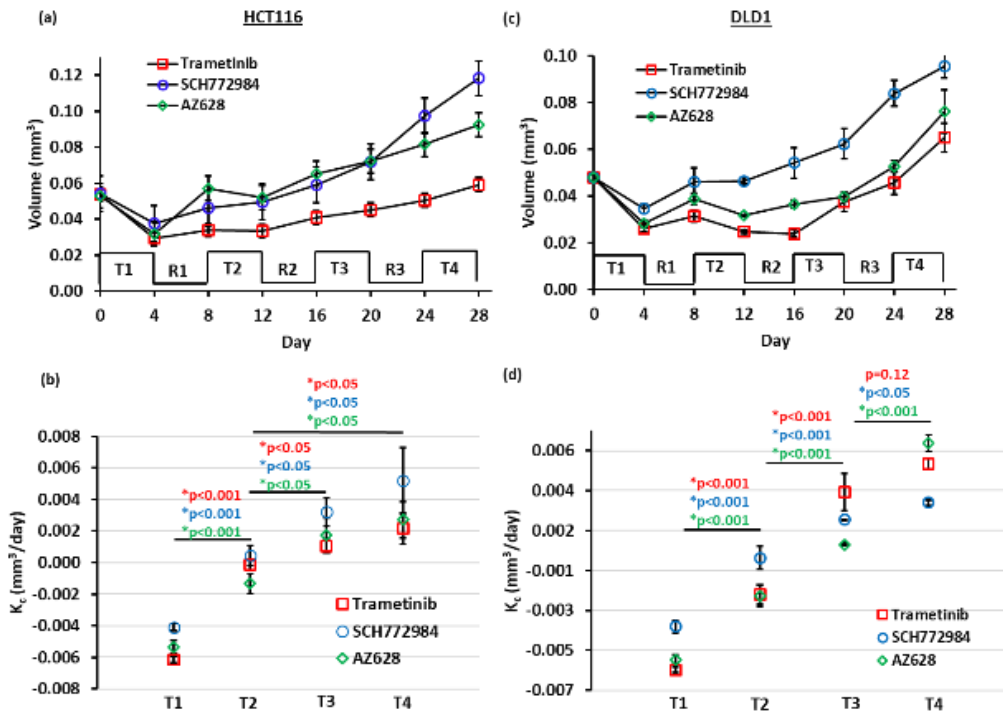


Figure 5-2. Modeling drug resistance with cyclic treatment/recovery of spheroids. Growth kinetics of (a) HCT116 and (c) DLD1 spheroids treated with LD₅₀ concentrations of MAPKi (trametinib, SCH772984, and AZ628) for four treatment cycles T1, T2, T3, and T4 with recovery intervals R1, R2, and R3. Growth rates (k_c) of (b) HCT116 and (d) DLD1 spheroids during four cycles of treatments with MAPKi. * denotes statistically significant differences k_c values. $n=32$. Error bars in are standard error of a mean.

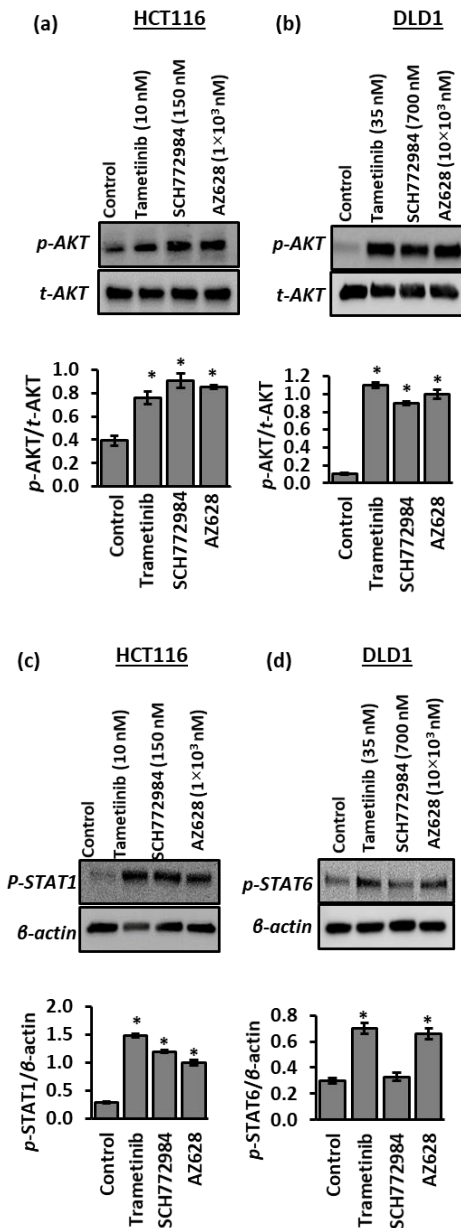


Figure 5-3. Phospho-level of AKT and STAT in MAPKi-treated spheroids. Representative blots for phosphorylated and total levels of AKT and quantified values of p-AKT/t-AKT in (a) HCT116 and (b) DLD1 spheroids at the end of T1 phase. Western blots for phosphorylated level of (c) STAT1 and quantified value of p-STAT1/ β -actin in HCT116 spheroids and (d) STAT6 and quantified value of p-STAT6/ β -actin in DLD1 spheroids at the end of T1 phase. n=2. * denotes statistical significance measured at $p < 0.05$ between control and treatment.

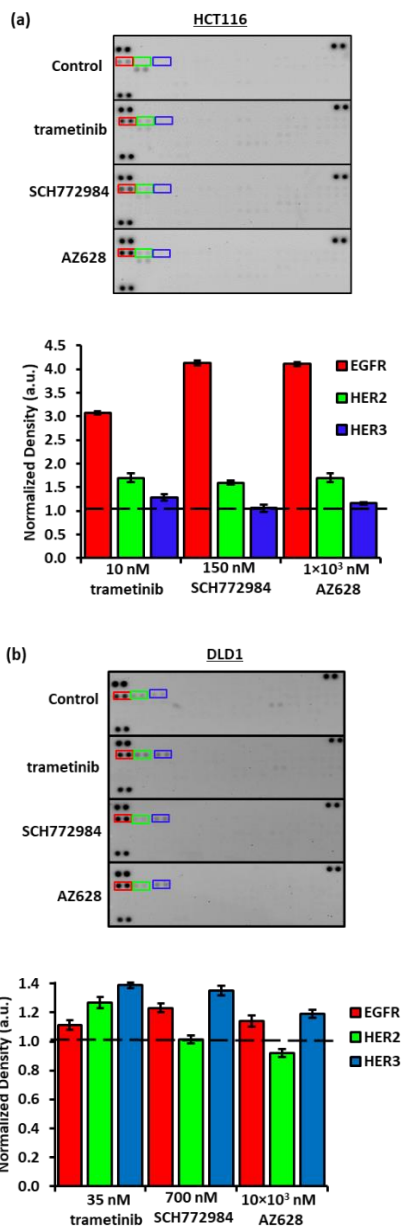


Figure 5-4. Phosphorylated levels of RTKs in MAPKi-treated spheroids. Phospho-RTKs in (a) vehicle control HCT116 spheroids or treated with 10 nM trametinib, 150 nM SCH772984, and 1×10^3 nM AZ628, and (b) vehicle control DLD1 spheroids or treated with 35 nM trametinib, 700 nM SCH772984, and 10×10^3 nM AZ628. Quantified levels of phospho-RTKs upregulated following treatments with MAPKi. The bar graphs show pixel density of each protein from treatments normalized with the respective vehicle control. Error bars are standard errors of mean values ($n=2$).

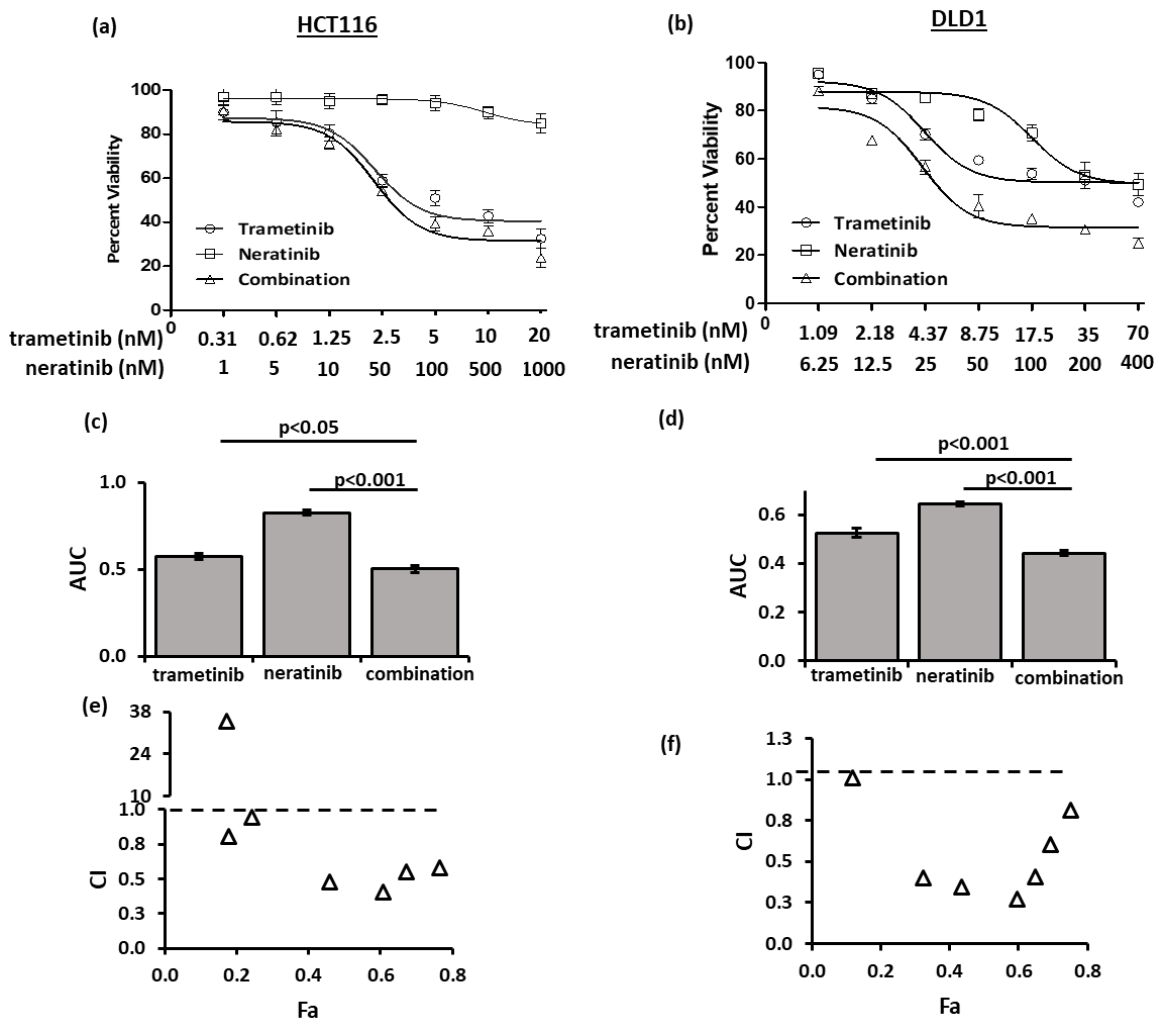


Figure 5-5. Inhibition of MEK1/2 and EGFR in colorectal tumor spheroids. Combination treatment of (a) HCT116 and (b) DLD1 spheroids with trametinib and neratinib and the respective single-agent treatments. AUC values from combination and single-agent treatments of (c) HCT116 and (d) DLD1 spheroids. Synergy plots show the combination index (CI) versus (1-viability) (Fa) by each concentration pair in (e) HCT116 and (f) DLD1 spheroids.

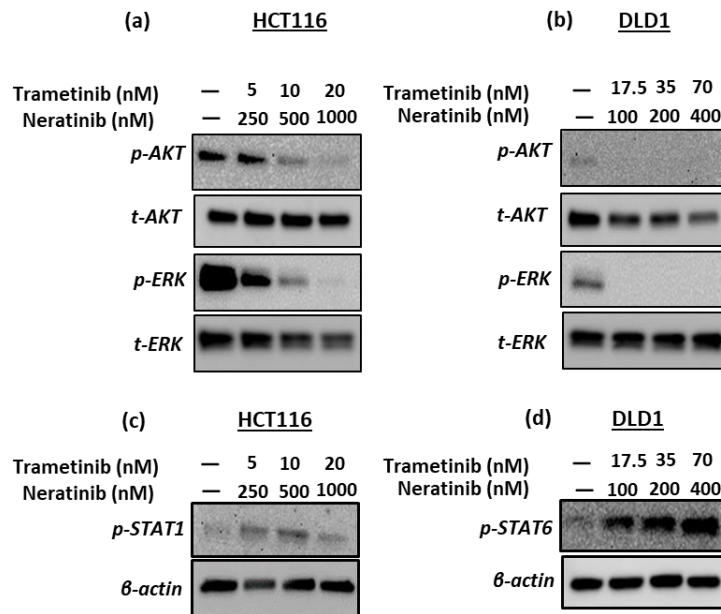


Figure 5-6. Molecular effects of simultaneous inhibition of MEK1/2 and EGFR in colorectal tumor spheroids. Combinations of trametinib and neratinib downregulate p-ERK1/2 and p-AKT in (a) HCT116 and (b) DLD1 spheroids but are ineffective against (c) p-STAT1 in HCT116 cells and (d) p-STAT6 in DLD1 cells.

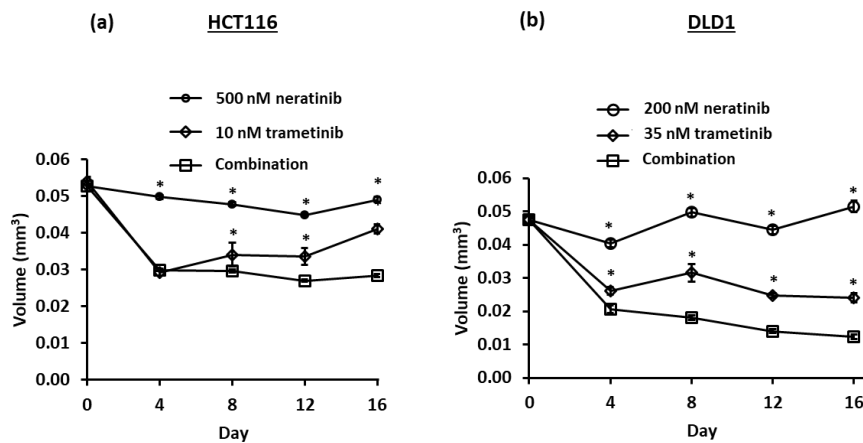


Figure 5-7. Cyclical treatment of single-agent and combination of spheroids. Volumes of (a) HCT116 and (b) DLD1 spheroids under cyclic treatments with trametinib, neratinib, and their combinations. n=32. Error bars are standard errors of the mean values. * on the single-agent treatments represents statistically significant difference with the combination drug treatments (p<0.05).

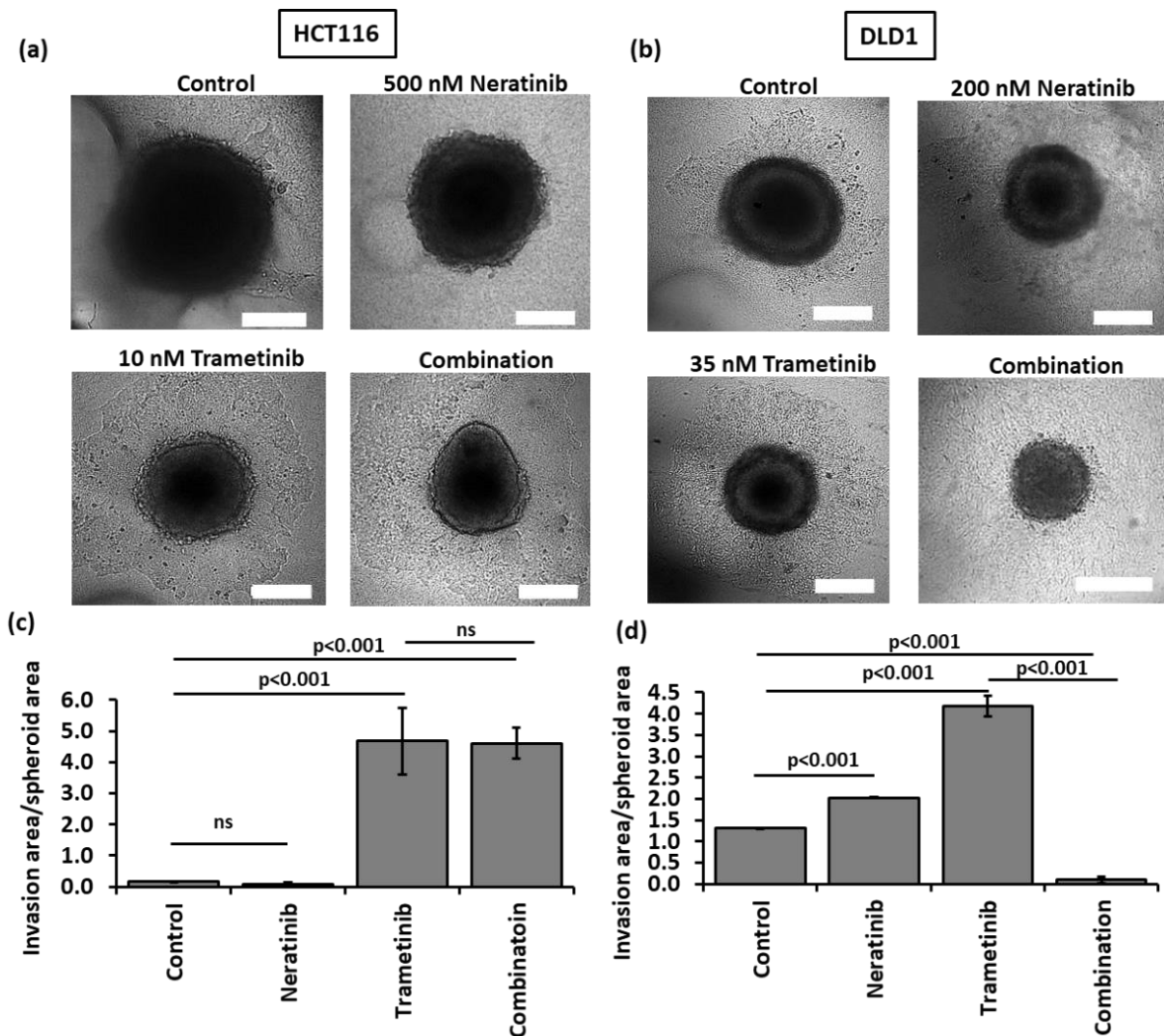
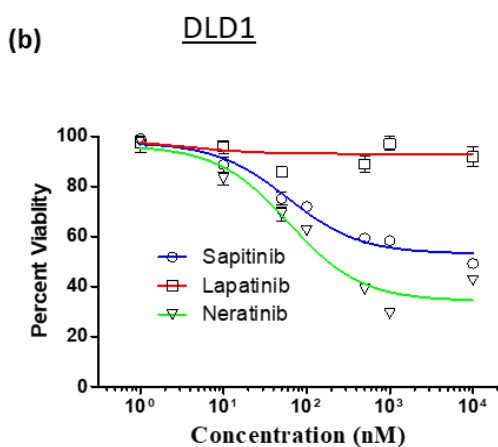
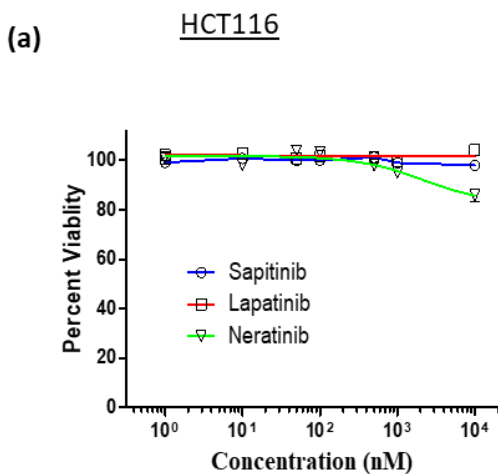


Figure 5-8. Matrix invasion of colorectal tumor spheroids. Spheroids were treated with trametinib alone, neratinib alone, or their combination for 4 days before embedding them in the collagen matrix. Representative images of collagen invasion of vehicle control and pre-treated (a) HCT116 spheroids (b) and DLD1 spheroids after 5 days. Scale bar is 300 μ m. Quantified invasion area/spheroid area for vehicle control and pre-treated spheroids of (c) HCT116 and (d) DLD1 cells. Error bars are standard errors of the mean values. $n=4$. ‘ns’ indicates no significant difference and $p<0.001$ represents statistical difference at a 99.9% confidence interval.



(c)

EGFR inhibitor	Target	HCT116 LD ₅₀ (nM)	DLD1 LD ₅₀ (nM)
Sapitinib	EGFR, ERbB2, ERbB3	-	-
Lapatinib	EGFR, ERbB2	-	-
Neratinib	EGFR, ERbB2	-	200

Figure 5-9. Responses of colorectal tumor spheroids to EGFR inhibitors. (a) Dose-responses of (a) HCT116 spheroids and (b) DLD1 spheroids to molecular inhibitors of EGFR. (c) The EGFR inhibitors, their molecular targets, and LD₅₀ values of these compounds against HCT116 and DLD1 tumor spheroids. The symbol ‘-’ indicates dose dependent treatment did not reach the LD₅₀ value.

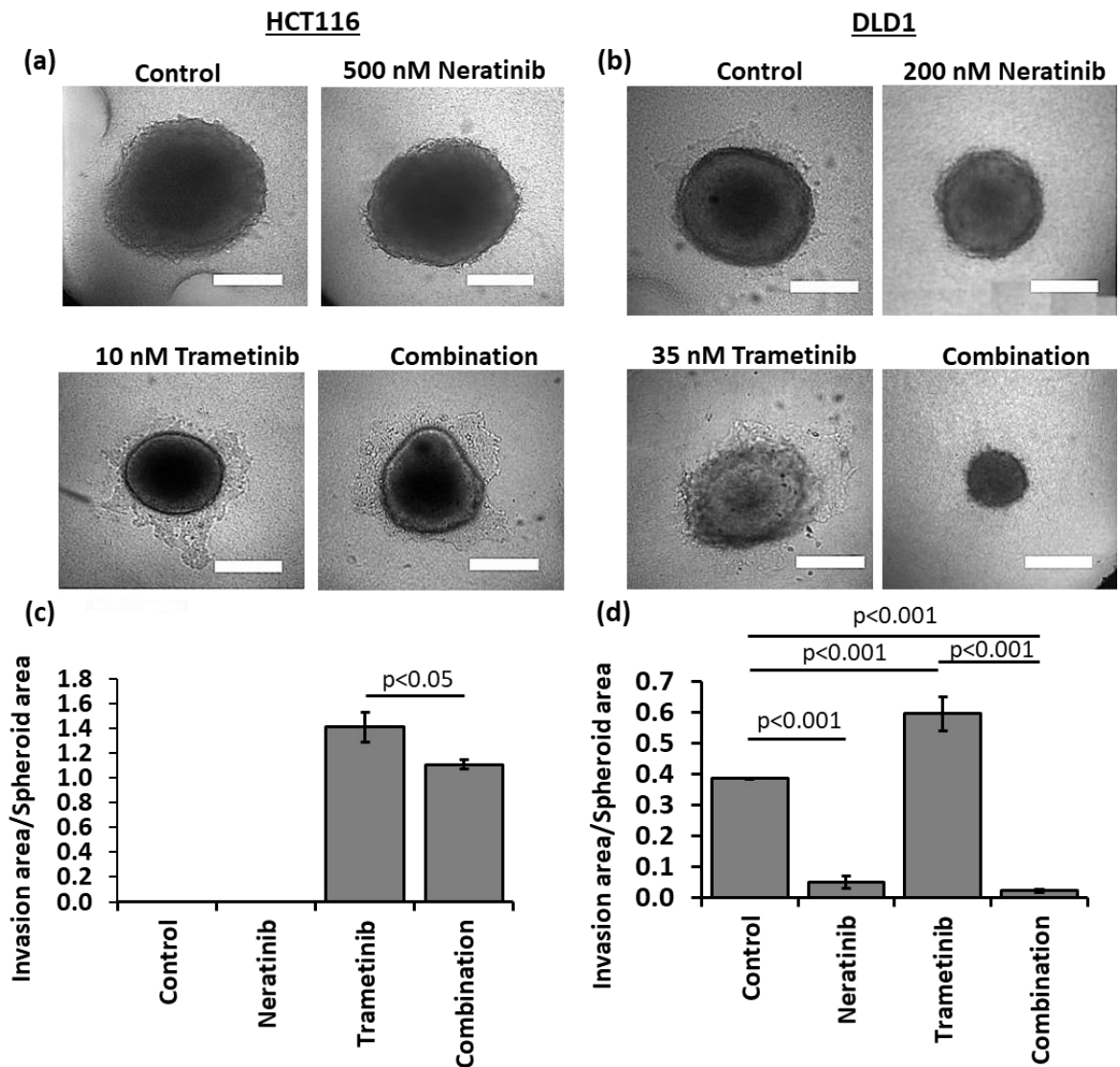


Figure 5-10. Invasion of spheroids into collagen matrix. Spheroids were pre-treated with trametinib only, neratinib only, or their combination for 4 days before embedding them in a collagen matrix. Representative images of collagen invasion of vehicle control and pre-treated (a) HCT116 spheroids and (b) DLD1 spheroids after 3 days. Scale bar is 300 μ m. Quantified invasion area/spheroid area for vehicle control and pre-treated (c) HCT116 and (d) DLD1 spheroids. Error bars are standard error of the mean. n=4. There was no collagen invasion of vehicle control and neratinib-treated HCT116 spheroids after 3 days. ‘ns’ indicates no significant difference. ‘p<0.05’ and ‘p<0.001’ represent statistical difference at 95% and 99.9% confidence intervals.

CHAPTER VI
COMBINATION TREATMENT STRATEGIES TO OVERCOME DRUG
RESISTANCE IN TUMOR SPHEROIDS

Portions of this chapter are reused from P. Shahi Thakuri, G. D. Luker, and H. Tavana, "Synergistic Inhibition of Kinase Pathways Overcomes Drug Resistance of Colorectal Cancer Spheroids To Cyclic Targeted Therapies.," *ACS Pharmacol. Transl. Sci.*, vol. 2, no. 4, pp. 275–284, July. 2019. Copyright @ 2018 by ACS Pharmacology and Translational Science. Reprinted by permission of ACS publications. <https://pubs.acs.org/doi/abs/10.1021/acsptsci.9b00042>

Cytotoxic chemotherapy has been the mainstay treatment for cancer patients. However, standard chemotherapeutics not only generate side effects including toxicity to various tissues, they often fail to produce sustained anti-tumor effects due to development of drug resistance in cancer cells. Increasing understanding of molecular drivers of drug resistance and significant differences in the disease drivers among patients of the same cancer have led to the use of molecularly targeted drugs to treat cancer by targeting oncogenic signaling. Unfortunately, clinical use of molecular therapies has also led to the resistance of cancer cells, caused by a pre-existing resistance population and/or adaptation of cancer cells to the drug due to continuous exposure during the course of treatments. Treating cancer patients with more than one drug is becoming a standard approach to combat drug resistance. [252] Two drugs or more may be combined to suppress both pre-existing and treatment-induced oncogenic signaling pathways. Combination of drugs can be given in parallel or in sequence, and the choice generally depends on the type of disease being treated, the treatments being used, and the biological mechanisms by which the drugs

act. [253]–[256] Administration of two drugs in parallel is a rational strategy to suppress tumor growth. However, administrating two or more drugs in parallel may result in severe toxicities in cancer patients. [100], [204]–[206] For example, it is an exciting approach to block most commonly deregulated MAPK and PI3K pathway kinase signaling in cancer. However, the overlapping toxicities caused by continuous administration of MEK and PI3K inhibitors have limited their use for cancer treatment. [100], [257] Dose interruption and dose reduction is a feasible approach to manage toxicities associated with continuous parallel administration of drugs, particularly with drugs that can generate optimum anti-tumor effects at concentrations lower than a recommended dosage. [258]–[260] Alternatively, sequential administration of anti-cancer drugs over a cycle can reduce toxicities in cancer patients while maintaining the benefit of drug combinations to treat cancer. [261]

Testing toxicity and efficacy of drug combinations using physiologically relevant models is a critical step to evaluate anti-tumor effects of the drugs and their toxicity. Three-dimensional (3D) cell models that reproduce key biological properties of native tissues are useful tools to test safety and efficacy of anti-cancer drug combinations. [56], [165] In this study, we used our aqueous two-phase system (ATPS) tumor spheroid microtechnology to generate 3D cellular models of normal cells and cancer cells and test toxicity and efficacy of drug combinations, respectively. [81], [82] Our previous studies presented in chapters 3 and 4 showed that combinations of MAPK and PI3K effectively reduce growth of colorectal tumors spheroids. [163], [228] Although combination of inhibitors of MAPK and PI3K pathways is rational approach to overcome drug resistance in colorectal cancer due to frequent mutations in these pathway, clinical trials have also shown excessive

toxicities to patients. [257] Therefore, there is a major need to identify combination treatment regimens that are minimally toxic and safe to normal tissues but generate significant anti-tumor effects.

We used cyclic parallel treatment as a dose interruption approach and a sequential combination approach to evaluate the feasibility of testing toxicity to normal cells. As normal cells, we used human umbilical vein endothelial cells (HUVEC). Our preliminary study showed that the combination of MAPK and PI3K pathway inhibitors was minimally toxic to HUVEC spheroids. We then compared efficacy of different drug combination regimens against colorectal cancer spheroids. Both treatment regimens significantly reduced the viability of colorectal cancer spheroids during short-term and long-term studies. Parallel cyclic treatment with trametinib and dactolisib more effectively decreased cell viability and growth of colorectal cancer spheroids and reduced activities of AKT and ERK proteins in the cells than sequential combination of trametinib and dactolisib did. Future studies require extensive validation of these combination regimens to test toxicities in different normal tissues. This will help identify safe and effective dosing regimens to guide preclinical studies in animals and expedite clinical translation of specific effective and safe regimens.

6.1 Materials and Methods

The methods to test toxicity against HUVEC spheroids and efficacy against colorectal tumor spheroids using parallel and sequential combination of MEK and PI3K/mTOR inhibitors are presented.

6.1.1 Cell culture

HCT116, DLD1, and HUVEC cells were purchased from ATCC. Mc Coy's 5A and RPMI-1640 media were used to culture HCT116 and DLD1 cells. Endothelial Cell Growth Medium-2 (EGM-2, Lonza) were used to culture HUVEC cells. Each medium was supplemented with fetal bovine serum (10%) (FBS, Sigma), streptomycin/penicillin (1%) (Life Technologies), and glutamine (1%) (Life Technologies). Cell cultures were done using the methods described in section 2.1.1. Spheroids from each cell line were formed using 1.5×10^4 cells as previously described. [81], [116], [178]

6.1.2 Treatment Regimens

Two different combination regimens were used: intermittent parallel and sequential drug combinations. The intermittent parallel drug treatment involved cyclical treatments with two drugs simultaneously. Trametinib and dactolisib were combined together for four days. After 4 days of treatment, spheroids were recovered by completely removing the drug solutions and adding fresh cell culture medium in the wells containing the spheroids. For the sequential regimen, spheroids were treated with trametinib for 4 days. Then, trametinib was removed and dactolisib was added to the wells for another 4 days. Overall, the concentrations of the drugs and the time of treatments for intermittent parallel and sequential drug combinations were kept the same. We termed this as the round 1 (T1) of combination treatment. To compare the efficacy of drug combinations over long-term, we repeated the drug combinations using the scheme in Figure 1, for second and third rounds, also termed as round 2 (T2) and round 3 (T3). The concentration of drug was kept constant in all treatment rounds.

6.1.3 Testing Treatment Toxicity in HUVEC Spheroids

HUVEC cells were selected to test toxicity of trametinib and dactolisib. For the parallel drug combination, a stock solution of trametinib was serially diluted to obtain the 4 times the desired drug concentrations, i.e., 6.25×10^{-4} μM , 12.5×10^{-4} μM , 25×10^{-4} μM , 50×10^{-4} μM , 100×10^{-4} μM , and 200×10^{-4} μM solutions. Similarly, dactolisib stock solution was serially diluted to obtain 4 times the desired drug concentrations, i.e., 0.2 μM , 0.4 μM , 0.8 μM , 1.6 μM , 3.2 μM , 6.4 μM , and 12.8 μM drug solutions. Of the solutions of trametinib and dactolisib, 20 μl from each was added to the HUVEC spheroids suspended in 40 μl of cell culture medium. After 4 days of treatment, fresh cell culture medium was added after removal of the drug solutions. HUVEC spheroids were recovered for 4 days in the fresh medium.

For sequential drug combination, a stock solution of trametinib was serially diluted to obtain the 2 times the desired drug concentrations, i.e., 3.1×10^{-4} μM , 6.25×10^{-4} μM , 12.5×10^{-4} μM , 25×10^{-4} μM , 50×10^{-4} μM , and 100×10^{-4} μM solutions. Of these drug solutions, 40 μl was added to the HUVEC spheroids suspended 40 μl of cell culture medium. After 4 days of treatment with trametinib, the drug solutions were completely removed. Next, dactolisib was serially diluted to obtain the desired drug concentrations, i.e., 0.05 μM , 0.1 μM , 0.2 μM , 0.4 μM , 0.8 μM , 1.6 μM , and 3.2 μM drug solutions. Of these drug solutions, 80 μl was added to HUVEC spheroids culture that were treated with dactolisib for the next 4 days. Prestoblue assay was used to monitor metabolic activity of cancer cells in the spheroids. Live/dead staining of cells using CalceinAM/propidium iodide was done to confirm the Prestoblue viability data.

6.1.4 Short-term Combination Treatment Regimens

Seven different concentrations of trametinib were prepared at 4 times the desired concentrations for DLD1 cells, i.e., 2.18×10^{-4} μM , 4.37×10^{-4} μM , 8.75×10^{-4} μM , 17.5×10^{-4} μM , 35×10^{-4} μM , 70×10^{-4} μM , and 140×10^{-4} μM . Similarly, seven different drug concentrations of trametinib were prepared separately by serially diluting its stock solution to prepare 4 times the desired concentrations for HCT116 cells, i.e., 0.62×10^{-4} μM , 1.25×10^{-4} μM , 2.5×10^{-4} μM , 5×10^{-4} μM , 10×10^{-4} μM , 20×10^{-4} μM , and 40×10^{-4} μM . For the parallel drug combination, 20 μl of 800 nM dactolisib and 20 μl from seven different drug solutions were added to spheroids suspended in 40 μl of the cell culture medium. Drug solutions were removed after 4 days of treatment and spheroids were recovered for 4 days in the fresh medium. For sequential drug combination, a stock solution of trametinib was serially diluted to obtain solutions of 2 times the desired drug concentrations for DLD1 cells, i.e., 1.09×10^{-4} μM , 2.18×10^{-4} μM , 4.37×10^{-4} μM , 8.75×10^{-4} μM , 17.5×10^{-4} μM , 35×10^{-4} μM , and 70×10^{-4} μM . Similarly, the stock solution of trametinib were serially diluted to obtain the 2 times the desired drug concentrations for HCT116 cells, i.e., 0.31×10^{-4} μM , 0.62×10^{-4} μM , 1.25×10^{-4} μM , 2.5×10^{-4} μM , 5×10^{-4} μM , 10×10^{-4} μM , and 20×10^{-4} μM . Next 40 μl of these drug solutions were added to the spheroids cultures suspended in 40 μl of the culture medium. After 4 days, the drug solutions were completely removed. Next, 80 μl of 200×10^{-4} μM dactolisib was added to the well containing spheroids. Spheroids were treated with dactolisib for the next 4 days. Next viability analysis was performed and dose response curves were generated using protocols described in section 2.1.5.

6.1.5 Long-term Combination Treatment Regimen

Long-term parallel and sequential drug combinations were used the experiment protocol as described in Figure 1. Drug treatments were done using the protocol described above for the short-term combination treatments. Each treatment was repeated for two more cycles, i.e., T2 and T3. Size based growth analysis was used to quantify long-term effectiveness of treatment regimens as described in section 5.1.7.

6.1.6 Western Blotting

DLD1 and HCT116 spheroids were treated with 2.5 nM/200 nM and 1.25 nM/200 nM of trametinib/dactolisib pair. Spheroids were harvested after T1 and T2 phases of parallel and sequential treatments for western blot. Lysing, and Western blot was performed as described in section 2.1.6.

6.2 Results and Discussions

Below results of toxicity test and effectiveness of parallel and sequential combination regimen in HUVEC spheroids and colorectal tumor spheroids are presented and discussed.

6.2.1 Toxicity of Combination Drug Regimens

Combining anti-cancer drugs is essential to tackle drug resistance but it often causes toxicity in patients. Signaling pathways such as MAPK and PI3K are used by normal cells and tissues to regulate physiologic processes and homeostasis. Increased toxicity arises due to the suppression of these signaling pathway in normal cells and tissues. Example of such toxicities include severe skin rash and mucositis with the combination of inhibitors

PI3K/AKT/mTOR and RAS/MAPK pathways; myelosuppression with the combination of VEGF and mTOR inhibitors; hepatotoxicity with the combination of a BRAF inhibitor and anti-CTLA-4 antibody; and ocular toxicity with the combination of BRAF and MEK inhibitors. [204]–[206], [262]

Studies often focus on efficacy of drug combinations using *in vitro* models. However, evaluating the safety of drug combinations is critical to drug development but is not studied extensively *in vitro*. Extrapolating *in vitro* cytotoxicity results to tissues and organs *in vivo* is often difficult. However, recent studies have shown the feasibility of this approach. [263], [264] This underlines the significance of *in vitro* models to identify compounds that will likely cause toxicity in patients. Majority of *in vitro* toxicity tests are performed in 2D cell culture models that lack key structural and biological properties of solid tumors. The use of physiologically relevant 3D *in vitro* model can enhance the reliability of tests to determine toxicity and efficacy of drug combinations. [56], [165]

We evaluated toxicity of combined inhibitors of MAPK and PI3K pathways using intermittent parallel and sequential drug combinations in 3D culture of HUVEC cells. Our previous drug screening showed that trametinib reduces the viability of colorectal tumor spheroids by over 50% starting at low nanomolar concentrations. [86] On the other hand, dactolisib reduced the viability of colorectal tumor spheroids by over 50% starting at micromolar concentrations. We used this information to select a concentration range of trametinib and dactolisib for toxicity tests with HUVEC spheroids. The lowest and highest trametinib/dactolisib concentration pairs were 1.56 nM/50 nM and 100 nM/3200 nM. We dose-dependently treated the spheroids with these inhibitors using intermittent parallel or sequential drug combinations. Result showed that neither approach generated a major

toxicity to HUVEC cells. The viability of cells in spheroids did not reduce significantly and remained above 80% even at the highest concentrations (Figure 6-2a). Our live/dead staining of HUVEC spheroids validated this result and showed that treated spheroids contained primarily live cells (Figure 6-2b). This indicates that combination of trametinib and dactolisib, either used in parallel or sequential, is not toxic to HUVEC spheroids.

Toxicity of combined inhibitors of MAPK and PI3K pathways in clinical trials has been primarily due to the on-target effects of simultaneous targeting of the two pathways. [262] Toxicity is caused due to continuous administration of these inhibitors concurrently. Intermittent dosing of MAPK and PI3K inhibitors are effective in pre-clinical trials, and this model is evaluated in early phase studies. [265] On the other side, sequential drug combinations allow the use of single-drug therapy to reduce potential toxicity risks. Sequential therapy can be potentially beneficial for older who are prone to toxicity of parallel drug combinations. [266] Few clinical trials have shown toxicity of parallel combinations of drugs and reduced toxicity using sequential treatment regimen. [267], [268] Our preliminary test comparing parallel and sequential targeting of MAPK and PI3K pathways in HUVEC spheroids did not show a major difference in toxicity to cells. Here, HUVEC cells are used as a model to test endothelial toxicity. The toxicity test with HUVEC cells can therefore be potentially useful to predict adverse cardiovascular events resulting from endothelial toxicity. This study should be expanded to colon epithelial cells and several normal tissues, particularly primary specimens.

6.2.2 Efficacy of Treatment Regimens

- Short-term Treatment

We compared the effectiveness of one round of combined trametinib and dactolisib using parallel and sequential treatment regimens against growth of colorectal tumor spheroids. Both regimens dose-dependently reduced the viability of DLD1 spheroids (Figure 6-3a). The viability of DLD1 spheroids was significantly higher after sequential treatment compared to that after parallel treatment at all the drug concentrations. The parallel treatment resulted in an AUC value of 0.4, which was significantly lower than the AUC value of 0.59 from the sequential treatment. Similarly, both parallel and sequential approach dose-dependently reduced the viability of HCT116 spheroids (Figure 6-3b). The parallel combination regimen was more effective than the sequential treatment regimen at lowest three combination concentrations. The effects of the two regimens became comparable at higher four combination concentrations. The sequential regimen resulted in an AUC value of 0.66 compared to 0.59 from the parallel regimen with HCT116 spheroids.

- Long-term Treatment

Next, we compared the long-term efficacy of cyclic parallel and sequential combination treatment regimens for three rounds (T1, T2, and T3) using the scheme of Figure 1. To consider potential effects of drug concentrations, we performed the study using three different combination concentrations: 0.5 nM, 4.37 nM, and 35 nM trametinib combined with 200 nM dactolisib against DLD1 spheroids and 0.15 nM, 1.25 nM, and 10 nM trametinib combined with 200 nM dactolisib against HCT116 spheroids. Figure 6-4 shows the volume of spheroids treated with parallel and sequential regimens and measured every 4 days. Both regimens reduced the size of spheroids over the 24 days of treatment. Compared to the sequential regimen, the parallel cyclic treatment significantly reduced the size of DLD1 spheroids at all drug combinations. To quantify cellular responses to drug

combinations, we measured the growth rates of spheroids after 24 days of treatments. k_c values of DLD1 spheroids after cyclic parallel treatment were $-0.0023 \text{ mm}^3/\text{day}$, $-0.0028 \text{ mm}^3/\text{day}$, and $-0.0035 \text{ mm}^3/\text{day}$. After sequential treatment, k_c values were $-0.0013 \text{ mm}^3/\text{day}$, $-0.0021 \text{ mm}^3/\text{day}$, and $-0.0032 \text{ mm}^3/\text{day}$. Similarly, for HCT116 spheroids, k_c values after cyclic parallel treatment were $0.0032 \text{ mm}^3/\text{day}$, $-0.0049 \text{ mm}^3/\text{day}$, and $-0.0058 \text{ mm}^3/\text{day}$, and after sequential treatment were $-0.0030 \text{ mm}^3/\text{day}$, $-0.0042 \text{ mm}^3/\text{day}$, and $-0.0058 \text{ mm}^3/\text{day}$. Our result shows that the sequential regimen was as effective as the parallel regimen against HCT116 spheroids, except at the lowest combination concentrations.

- Molecular Analysis of Drug Combinations

Next, we compared active phospho-levels of AKT and ERK1/2 after two cycles (T1 and T2) of parallel and sequential combination treatments. The rationale for selecting these signaling proteins is overcome extensive cross-talk between them in colorectal cancer cells following inhibition of MAPK pathway. In DLD1 spheroids, the parallel regimen significantly reduced p-AKT and p-ERK by 1.3 and 7.5 folds after T1, and by 1.25 and 5.77 folds after T2 compared to the sequential treatment (Figure 6-5 a-c). The suppression of p-ERK and p-AKT is consistent with the significant growth inhibition of DLD1 spheroids after parallel cyclic treatment (Figure 6-4). In HCT116 spheroids, the respective levels of p-AKT and p-ERK after T1 of cyclic parallel and sequential treatments were comparable. After T2, the sequential treatment downregulated p-AKT and p-ERK significantly and by 1.44 and 1.30 folds more than the parallel treatment (Figure 6-5d-f).

Our study demonstrated that the sequential combination of MAPK and PI3K signaling pathway effectively reduces the viability/growth of colorectal tumor spheroids

and the growth inhibitory effect of sequential treatment was comparable with the intermittent parallel inhibition. A clinical trial of patients with non-respectable colorectal cancer demonstrated effectiveness of sequential regimen over parallel combination of chemotherapies. [267] Furthermore the sequential regimen was tolerable to patients but parallel combination of chemotherapies resulted in toxicity. The sequential therapy is promising approach to effectively reduce tumor with minimal toxicity to normal tissues. Future studies are needed to test efficacy and toxicity of both parallel and sequential treatment regimen.

6.3 Summary

We established that sequential combination of MEKi and PI3Ki effectively suppress the growth of spheroids and the effect was comparable to parallel drug combination. Sequential inhibition may potentially reduce toxicity associated with on-target effects of simultaneously inhibiting active kinase pathways in the normal tissues. Future studies incorporating 3D culture of normal tissues including primary cells and cancer cells are crucial to identify the safety and efficacy of drug combination regimens.

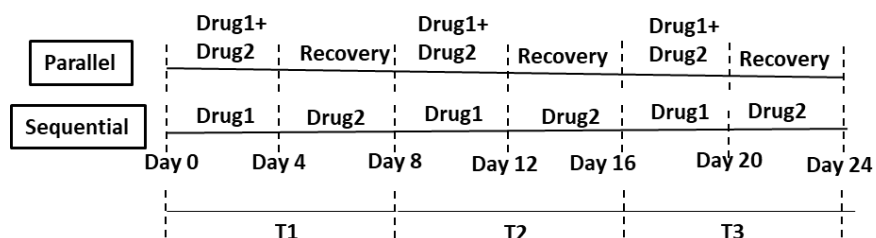


Figure 6-1. The schematic of parallel (top) and sequential (bottom) treatment regimens.

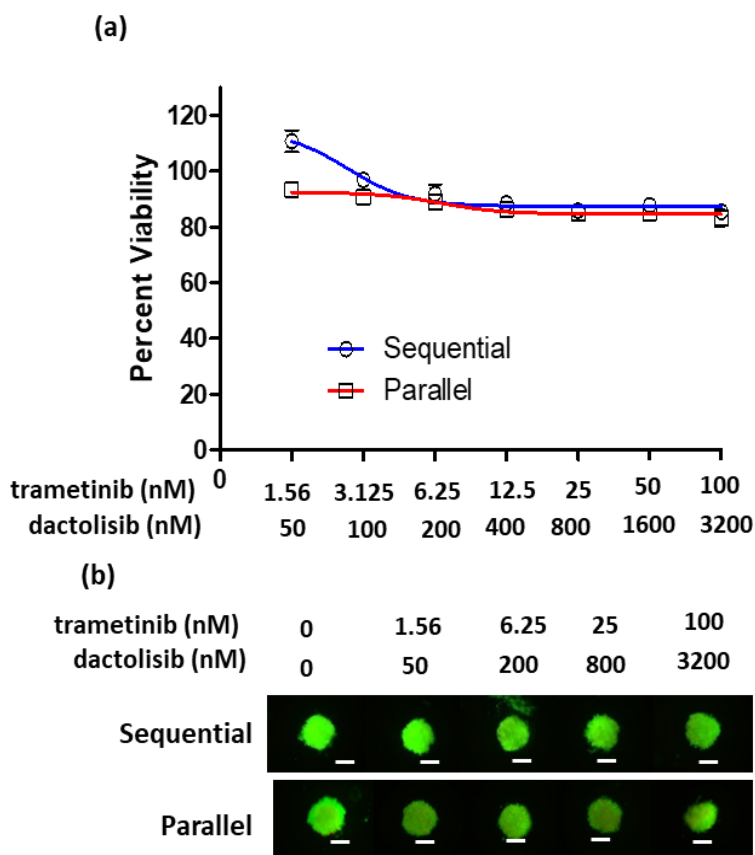


Figure 6-2. Cytotoxicity test with parallel and sequential combinations of MEK and PI3K inhibitors against HUVEC spheroids. (a) Viability of spheroids after T1 of parallel and sequential treatments. Inset images below shows live/dead staining of HUVEC spheroids following sequential (b, top) and parallel (b, below) treatment regimens. Scale bar is 250 μ m.

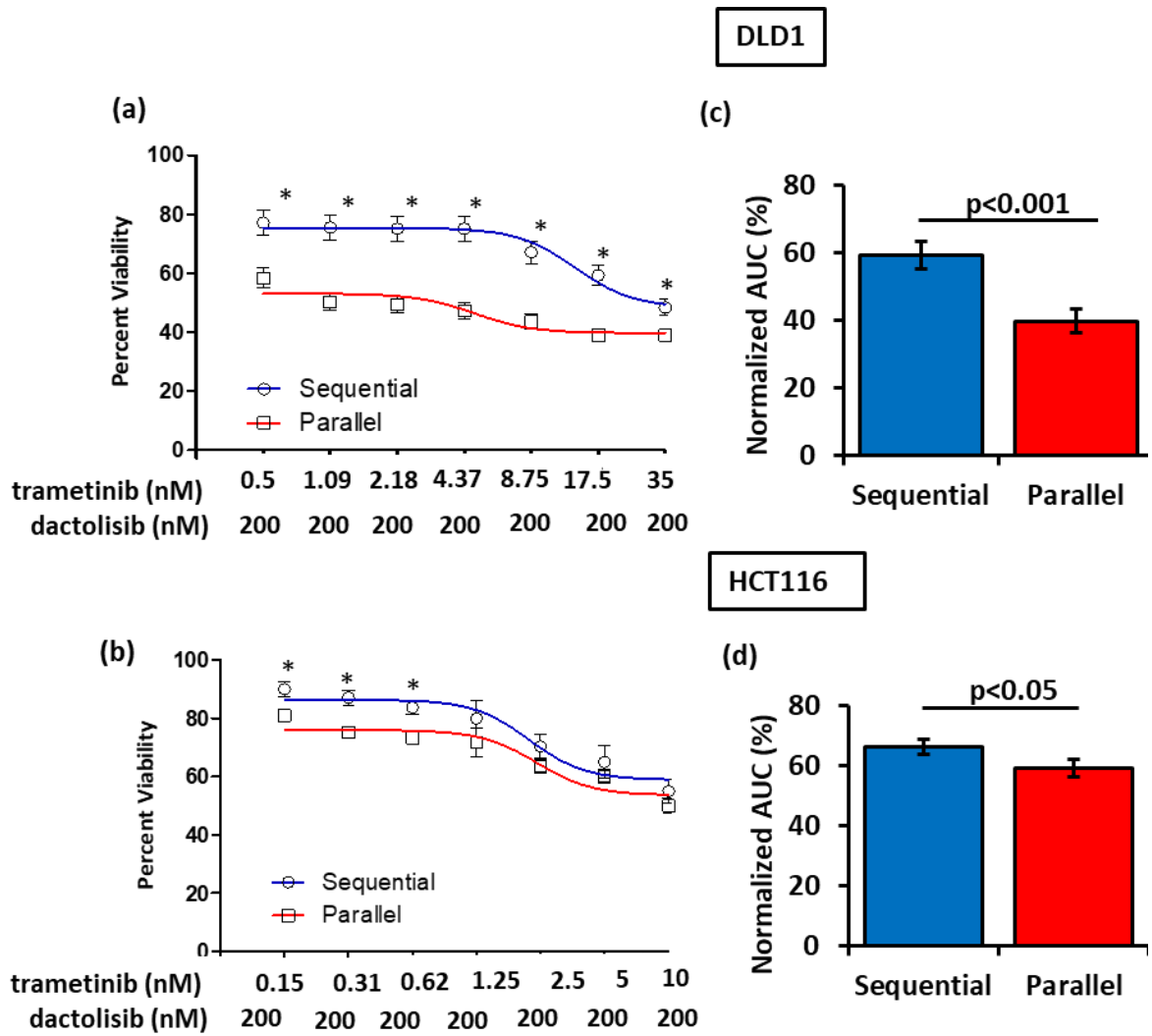


Figure 6-3. Parallel and sequential combinations in colorectal tumor spheroids. Viability of spheroids after T1 of parallel and sequential treatments in (a) DLD1 and (b) HCT116 tumor spheroids. Area under the curve (AUC) compares the two regimens.

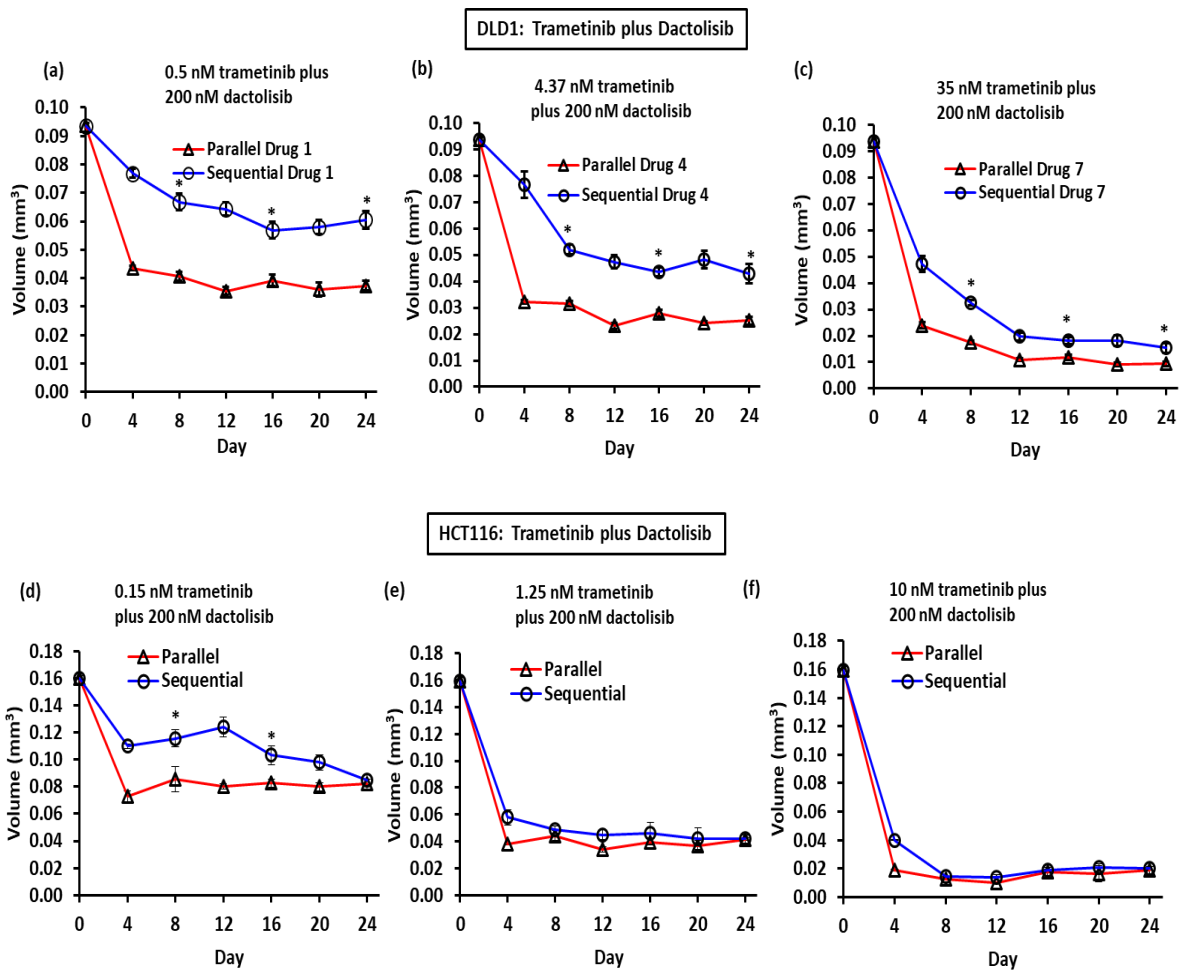


Figure 6-4. Long-term parallel and sequential combinations of MEK and PI3K inhibitors against colorectal tumor spheroids of MEK and PI3K inhibitors. (a-f) Volume of spheroids is shown during parallel and sequential combination treatments of DLD1 and HCT116 spheroids. n=14 and * represent statistical significance at p<0.001.

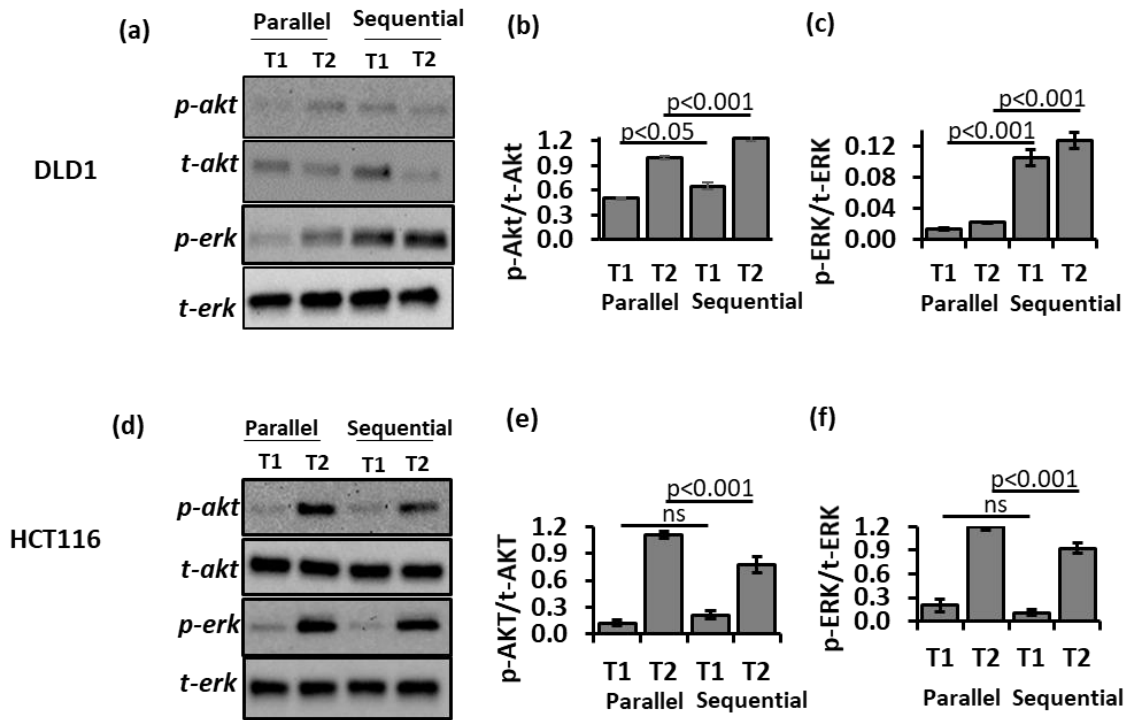


Figure 6-5. Parallel and sequential combinations of trametinib and dactolisib against colorectal tumor spheroids. 4.37 nM/200 nM and 1.25 nM/200 nM drug pairs were used against DLD1 and HCT116 spheroids. Representative western blot of p-ERK1/2, t-ERK1/2, p-AKT, and t-AKT from spheroids of (a) DLD1 and (d) HCT116 cells after T1 and T2 of parallel and sequential treatments. Quantified p-AKT/t-AKT in (b) DLD1 and (e) HCT116 spheroids. Quantified p-ERK1/2/t-ERK1/2 in (c) DLD1 and (f) HCT116 spheroids. n=2. Error bars are standard errors of means.

CHAPTER VII

CONCLUSIONS

We established a novel model of adaptive resistance to kinase inhibitors using tumor spheroids under cyclic treatments, identified mechanisms of resistance, and used data-driven drug combination approaches to block drug resistance of cancer cells. We validated our 3D tumor model for high throughput phenotypic drug screening and molecular analysis of targeted drugs. We modeled adaptive resistance to targeted therapies using a clinically-relevant cyclic treatment regimen. We demonstrated that colorectal cancer cells adapt to this treatment regimen by activation of multiple signaling pathways and RTKs. Combination treatments targeting initially active pathway and treatment-induced signaling synergistically reduced the growth of tumor spheroids. Overall, major conclusions of this study are as follows:

(1) Our ATPS technology allowed formation of consistently-sized spheroids to ensure that changes in the size and metabolic activity of spheroids were due to inhibitory effects of drugs. Our histological examination of spheroids showed actively proliferating cells that deposit extracellular matrix proteins during culture. We generated spheroids of multiple cells lines of different origin (brain, colon, and breast) and used them to perform high throughput screening of drug compounds. Using a quantitative multi-parametric approach based on IC_{50} , E_{max} , and AUC, and a statistical tool (SSMD), we identified effective compounds and distinguished them from moderately effective and ineffective compounds. In addition, we showed that morphological analysis of spheroids may be used to classify the drug compounds as cytostatic or cytotoxic.

(2) We modeled adaptive resistance of cancer cells to drug compounds using cyclical treatment approach to mimic clinical chemotherapy regimen. We used colorectal cancer as the disease model and MEK inhibitors to target the oncogenic MAPK signaling pathway. Although single-agent treatments with MEKi initially suppressed growth of spheroids, cells adapted to the inhibitors and showed increasing in growth during subsequent treatments. Our molecular analysis showed significant activation of PI3K/AKT pathway in MEKi-treated cancer cells. Simultaneous inhibition of MAPK and a PI3K pathways synergistically inhibited growth of spheroids both during short-term and cyclic long-term treatments.

(3) Our comprehensive molecular analysis showed that despite inhibiting MAPK signaling pathway at various levels such as RAF, MEK, ERK in KRAS mutant colorectal cancer cells, cells adapted to the inhibitors by activating PI3K/AKT and STAT pathways and upstream RTKs. We demonstrated therapeutic effects of combining an inhibitor of MAPK pathway with an inhibitor of PI3K/AKT pathway or with an RTK inhibitor to suppress compensatory signaling at relatively low-dose combinations. Considering the significant difficulty of treating KRAS mutant cancers due to the activities of multiple signaling pathways downstream of KRAS, our promising results with parallel targeting of pathways downstream of KRAS or simultaneously inhibiting a downstream pathway and an RTK provides evidence that these approaches may be effective against KRAS mutant cancers, where multiple cancer signaling pathways are active.

(4) We demonstrated the utility of spheroids for safety and efficacy testing of different treatment regimens and drug combinations. We demonstrated that a sequential treatment regimen effectively reduced growth of tumor spheroids and that the effect was comparable

to the parallel drug combination. It is expected that sequential drug combination will reduce toxicity compared to simultaneous administration of two drug compounds. Although our preliminary experiments with parallel and sequential combinations of MEKi and PI3Ki showed low toxicity to in HUVEC cells in spheroid cultures, extensive studies with different types of normal cells and tissues are needed to compare these regimens.

Altogether, the work presented here established the use of 3D cancer spheroids to model adaptive drug resistance, identify various mechanisms of resistance to specific molecular inhibitors, and perform safety/efficacy testing of different treatment regimens with multiple drug combinations. Future use of patient-derived cells will allow understanding of patient-specific mechanisms of drug resistance, which will be a significant step towards designing safe and effective drug combinations to block drug resistance in patients and minimize toxic effects in normal tissues.

CHAPTER VIII

FUTURE WORK

The study presented here lays the foundation to investigate intrinsic and acquired resistance to therapeutic compounds using a physiologically relevant 3D tumor model. We demonstrated that 3D tumor spheroids can be cultured for about one month to study adaptive resistance of cancer cells, mechanistically study drug resistance, and design effective combination therapies to inhibit it. Sequencing of resistant populations potentially allow tracking of evolution of drug resistance to drug compounds. While the spheroid culture is a simple 3D tumor model, the APTS technology is very versatile to incorporate multiple components of the tumor microenvironment like extracellular matrix (ECM) and stromal cells, as well as primary patient-derived cells, to test safety/efficacy of drug combinations. This work can be extended in several directions as briefly described below.

1. Physiologic tumor microenvironment: Throughout our studies, we used mono-culture cancer cell spheroids to model adaptive resistance to targeted therapies. However, tumors reside in complex microenvironments that also contain extracellular matrix (ECM) proteins, fibroblast cells, immune cells, blood vessels, etc. [56] Interactions among cancer cells and the components of the tumor microenvironment are critical for tumor growth and drug resistance. For example, integrin-mediated binding of cancer cells to ECM and biochemical signaling between cancer cells and fibroblasts promote drug resistance. [84], [269] Cancer cell spheroids can be embedded in matrix resembling the ECM composition of a native tumor to model drug resistance and other events such as cancer cell invasion of the matrix during using cyclic treatment and recovery of spheroids. A more complex

organotypic tumor model incorporating ECM, stromal cells, and a cancer cell mass representing a more physiological system can be conveniently developed with our technology. A potential difficulty will be to analyze effects of drug compounds with increase in the complexity of the tumor model. Our modular approach to identify the effect of each individual component may help address this difficulty.

2. Patient-derived tumor models: Cancer is a highly heterogenous disease and differs among individual patients of the same cancer. [158], [270] The best strategy to predict drug resistance in cancer patients is by using a patient's own tumor cells. This will enable testing and identifying single drug compounds to which cells may develop adaptive resistance, and subsequently designing rationale combinations of drugs to overcome resistance to single-agent therapies. Although the use of patient-derived cells is an important step toward personalized medicine for cancer, there are also challenges associated with it. For example, this approach requires a large number of tumor cells not usually available from biopsies. One approach to address difficulties with culturing of primary cells is by conditionally reprogramming of cells that allows culturing normal and tumor epithelial cells from many tissues indefinitely *in vitro* while retaining the properties of native tumors. [271] The ATPS technology may be used to form 3D cultures and tumor models with these primary normal and tumor epithelial cells. The normal primary cells can be used as a control to test toxic effects of drug combinations, whereas the primary tumor cancer cells can be used to study resistance to specific targeted therapies and elucidate the underlying molecular mechanisms. For example, growing KRAS mutant primary colon tumor cells would allow to identify mechanisms of resistance to targeted therapies such as MAPK pathway inhibition.

3. Role of hypoxia in drug resistance: Hypoxia inhibits proliferation of cancer cells and promote cell cycle arrest. The absence of actively proliferating cells in solid tumors results in resistance to chemotherapeutic drugs as they target actively proliferating cells. When tumors grow sufficiently large, they develop hypoxic zones due to the reduced diffusion of oxygen. Hypoxia alters cellular metabolism, causes genetic instability of tumor cells, and reduces drug responsiveness of cancer cells. [272] Targeting hypoxia is a strategy to promote therapeutic efficacy of anti-cancer drugs. In this work, we did not take into account hypoxia and its potential contribution to resistance to targeted therapies. Future studies that evaluate generation of hypoxia during cyclic treatment and recovery of 3D tumor models will help elucidate its effects on drug resistance and test drug combinations to block it. Such drug combinations should use hypoxia pro-drugs that only become activate in low-oxygen environments.

4. Cancer stem cells: Tumors often contain sub-population of undifferentiated cancer cells that manifest properties of stem cell. These sub-populations of cancer cells are termed as cancer stem cells (CSCs). CSCs have the ability to switch between dormant and active states. Chemotherapeutic drugs are effective against actively dividing cells and fail to target the dormant CSCs. These dormant CSCs become activated after treatment resulting in their proliferation and differentiation, causing regrowth of tumor. [273], [274] Furthermore, CSCs are enriched after treatments with anti-cancer drugs. [275] Stem cell-like populations in tumors cause failure of drug treatments. Our cyclical treatment of spheroids is an ideal approach to identify drug compounds that induce and enrich for CSCs. Various methods including quantitative polymerase chain reaction (q-PCR), clonogenicity assay, and 3D invasion assay may be employed for quantitative studies of CSCs in our model. Using our

high throughput screening ATPS platform, we can then screen for compounds with therapeutic effects against CSCs.

5. Toxicity models: Toxicity of drug combinations is a major impediment in cancer treatments. Alternative strategies to continuous parallel drug combinations, such as sequential treatments, should be developed and tested to minimize toxicity to normal tissues, e.g., cardiotoxicity, nephrotoxicity, pulmonary toxicity, and gastrointestinal toxicity. Primary human tissues are excellent sources but limited availability of tissues and difficulty with passaging of primary cells limit their use for long-term chronic toxicity studies. Using conditional reprogramming of cells, primary cells can be cultured for long periods of time and expanded for toxicity tests. [271] Human induced pluripotent stem cells (iPSC) are extensively used to generate organoids/mini-organs of interest for biological studies. [276] Organoids can also be used to test chronic toxicities of different drug combination regimens. [277] Use of these physiologically relevant organ models will allow identifying safe drug combinations to treat cancer.

BIBLIOGRAPHY

- [1] R. L. Siegel, K. D. Miller, and A. Jemal, “Cancer statistics, 2019,” *CA. Cancer J. Clin.*, vol. 69, no. 1, pp. 7–34, Jan. 2019.
- [2] K. D. Miller *et al.*, “Cancer treatment and survivorship statistics, 2019,” *CA. Cancer J. Clin.*, p. caac.21565, Jun. 2019.
- [3] R. M. Lowenthal and K. Eaton, “Toxicity of chemotherapy,” *Hematol. Oncol. Clin. North Am.*, vol. 10, no. 4, pp. 967–90, Aug. 1996.
- [4] J. D. Wulfschlegel, L. A. Liotta, and E. F. Petricoin, “Proteomic applications for the early detection of cancer,” *Nat. Rev. Cancer*, vol. 3, no. 4, pp. 267–275, Apr. 2003.
- [5] I. Belczacka *et al.*, “Proteomics biomarkers for solid tumors: Current status and future prospects,” *Mass Spectrom. Rev.*, vol. 38, no. 1, pp. 49–78, Jan. 2019.
- [6] D. A. Kessler, R. H. Austin, and H. Levine, “Resistance to Chemotherapy: Patient Variability and Cellular Heterogeneity,” *Cancer Res.*, vol. 74, no. 17, pp. 4663–4670, Sep. 2014.
- [7] T. A. Yap and P. Workman, “Exploiting the Cancer Genome: Strategies for the Discovery and Clinical Development of Targeted Molecular Therapeutics,” *Annu. Rev. Pharmacol. Toxicol.*, vol. 52, no. 1, pp. 549–573, Feb. 2012.
- [8] H. K. Weir, T. D. Thompson, A. Soman, B. Møller, and S. Leadbetter, “The past, present, and future of cancer incidence in the United States: 1975 through 2020,” *Cancer*, vol. 121, no. 11, pp. 1827–1837, Jun. 2015.
- [9] H. Maeda and M. Khatami, “Analyses of repeated failures in cancer therapy for solid tumors: poor tumor-selective drug delivery, low therapeutic efficacy and unsustainable costs,” *Clin. Transl. Med.*, vol. 7, no. 1, p. 11, Mar. 2018.
- [10] F. H. Groenendijk and R. Bernards, “Drug resistance to targeted therapies: Déjà vu all over again,” *Mol. Oncol.*, vol. 8, no. 6, pp. 1067–1083, Sep. 2014.
- [11] D. R. Minor, I. Puzanov, M. K. Callahan, B. A. Hug, and A. Hoos, “Severe gastrointestinal toxicity with administration of trametinib in combination with dabrafenib and ipilimumab,” *Pigment Cell Melanoma Res.*, vol. 28, no. 5, pp. 611–612, Sep. 2015.
- [12] P. L. Bedard, A. R. Hansen, M. J. Ratain, and L. L. Siu, “Tumour heterogeneity in the clinic,” *Nature*, vol. 501, no. 7467, pp. 355–64, Sep. 2013.

- [13] B. Marte, “Tumour heterogeneity,” *Nature*, vol. 501, no. 7467, pp. 327–327, Sep. 2013.
- [14] M. Gerlinger *et al.*, “Intratumor Heterogeneity and Branched Evolution Revealed by Multiregion Sequencing,” *N. Engl. J. Med.*, vol. 366, no. 10, pp. 883–892, Mar. 2012.
- [15] N. Navin *et al.*, “Tumour evolution inferred by single-cell sequencing,” *Nature*, vol. 472, no. 7341, pp. 90–4, Apr. 2011.
- [16] P.-L. Chen *et al.*, “Analysis of Immune Signatures in Longitudinal Tumor Samples Yields Insight into Biomarkers of Response and Mechanisms of Resistance to Immune Checkpoint Blockade,” *Cancer Discov.*, vol. 6, no. 8, pp. 827–37, 2016.
- [17] N. McGranahan, F. Favero, E. C. de Bruin, N. J. Birkbak, Z. Szallasi, and C. Swanton, “Clonal status of actionable driver events and the timing of mutational processes in cancer evolution,” *Sci. Transl. Med.*, vol. 7, no. 283, p. 283ra54, Apr. 2015.
- [18] I. Dagogo-Jack and A. T. Shaw, “Tumour heterogeneity and resistance to cancer therapies,” *Nat. Rev. Clin. Oncol.*, vol. 15, no. 2, pp. 81–94, Nov. 2017.
- [19] L. A. Garraway and P. A. Jänne, “Circumventing cancer drug resistance in the era of personalized medicine,” *Cancer Discov.*, vol. 2, no. 3, pp. 214–26, Mar. 2012.
- [20] D. J. Konieczkowski, C. M. Johannessen, and L. A. Garraway, “A Convergence-Based Framework for Cancer Drug Resistance,” *Cancer Cell*, vol. 33, no. 5, pp. 801–815, May 2018.
- [21] T. Lippert, H.-J. Ruoff, and M. Volm, “Intrinsic and Acquired Drug Resistance in Malignant Tumors,” *Arzneimittelforschung*, vol. 58, no. 06, pp. 261–264, Dec. 2011.
- [22] F. Morgillo, M. A. Bareschino, R. Bianco, G. Tortora, and F. Ciardiello, “Primary and acquired resistance to anti-EGFR targeted drugs in cancer therapy,” *Differentiation*, vol. 75, no. 9, pp. 788–799, Nov. 2007.
- [23] D. W. Sherbenou and B. J. Druker, “Applying the discovery of the Philadelphia chromosome,” *J. Clin. Invest.*, vol. 117, no. 8, pp. 2067–2074, Aug. 2007.
- [24] F. Michor *et al.*, “Dynamics of chronic myeloid leukaemia,” *Nature*, vol. 435, no. 7046, pp. 1267–1270, Jun. 2005.
- [25] N. P. Shah *et al.*, “Multiple BCR-ABL kinase domain mutations confer polyclonal resistance to the tyrosine kinase inhibitor imatinib (STI571) in chronic phase and blast crisis chronic myeloid leukemia,” *Cancer Cell*, vol. 2, no. 2, pp. 117–25, Aug. 2002.

- [26] S. Kobayashi *et al.*, “EGFR Mutation and Resistance of Non–Small-Cell Lung Cancer to Gefitinib,” *N. Engl. J. Med.*, vol. 352, no. 8, pp. 786–792, Feb. 2005.
- [27] L. V. Sequist *et al.*, “Genotypic and Histological Evolution of Lung Cancers Acquiring Resistance to EGFR Inhibitors,” *Sci. Transl. Med.*, vol. 3, no. 75, pp. 75ra26–75ra26, Mar. 2011.
- [28] Y. Gao *et al.*, “V211D Mutation in MEK1 Causes Resistance to MEK Inhibitors in Colon Cancer,” *Cancer Discov.*, Jun. 2019.
- [29] H. Shi *et al.*, “Acquired Resistance and Clonal Evolution in Melanoma during BRAF Inhibitor Therapy,” *Cancer Discov.*, vol. 4, no. 1, pp. 80–93, Jan. 2014.
- [30] A. B. Turke *et al.*, “Preexistence and Clonal Selection of MET Amplification in EGFR Mutant NSCLC,” *Cancer Cell*, vol. 17, no. 1, pp. 77–88, Jan. 2010.
- [31] A. Bardelli *et al.*, “Amplification of the MET Receptor Drives Resistance to Anti-EGFR Therapies in Colorectal Cancer,” *Cancer Discov.*, vol. 3, no. 6, pp. 658–673, Jun. 2013.
- [32] S. Huang *et al.*, “MED12 Controls the Response to Multiple Cancer Drugs through Regulation of TGF- β Receptor Signaling,” *Cell*, vol. 151, no. 5, pp. 937–950, Nov. 2012.
- [33] D. Lake, S. A. L. Corrêa, and J. Müller, “Negative feedback regulation of the ERK1/2 MAPK pathway,” *Cell. Mol. Life Sci.*, vol. 73, no. 23, pp. 4397–4413, 2016.
- [34] S. Chandarlapaty *et al.*, “AKT Inhibition Relieves Feedback Suppression of Receptor Tyrosine Kinase Expression and Activity,” *Cancer Cell*, vol. 19, no. 1, pp. 58–71, Jan. 2011.
- [35] T. Muranen *et al.*, “Inhibition of PI3K/mTOR Leads to Adaptive Resistance in Matrix-Attached Cancer Cells,” *Cancer Cell*, vol. 21, no. 2, pp. 227–239, Feb. 2012.
- [36] A. B. Turke *et al.*, “MEK Inhibition Leads to PI3K/AKT Activation by Relieving a Negative Feedback on ERBB Receptors,” *Cancer Res.*, vol. 72, no. 13, pp. 3228–3237, Jul. 2012.
- [37] H. Ebi *et al.*, “Receptor tyrosine kinases exert dominant control over PI3K signaling in human KRAS mutant colorectal cancers,” *J. Clin. Invest.*, vol. 121, no. 11, pp. 4311–21, Nov. 2011.
- [38] E. Martinelli, F. Morgillo, T. Troiani, and F. Ciardiello, “Cancer resistance to therapies against the EGFR-RAS-RAF pathway: The role of MEK,” *Cancer Treat. Rev.*, vol. 53, pp. 61–69, Feb. 2017.

- [39] R. B. Corcoran *et al.*, “EGFR-Mediated Reactivation of MAPK Signaling Contributes to Insensitivity of *BRAF* -Mutant Colorectal Cancers to RAF Inhibition with Vemurafenib,” *Cancer Discov.*, vol. 2, no. 3, pp. 227–235, Mar. 2012.
- [40] A. Prahallad *et al.*, “Unresponsiveness of colon cancer to BRAF(V600E) inhibition through feedback activation of EGFR,” *Nature*, vol. 483, no. 7387, pp. 100–103, Mar. 2012.
- [41] R. G. Amado *et al.*, “Wild-Type *KRAS* Is Required for Panitumumab Efficacy in Patients With Metastatic Colorectal Cancer,” *J. Clin. Oncol.*, vol. 26, no. 10, pp. 1626–1634, Apr. 2008.
- [42] C. S. Karapetis *et al.*, “*K-ras* Mutations and Benefit from Cetuximab in Advanced Colorectal Cancer,” *N. Engl. J. Med.*, vol. 359, no. 17, pp. 1757–1765, Oct. 2008.
- [43] L. A. Diaz *et al.*, “The molecular evolution of acquired resistance to targeted EGFR blockade in colorectal cancers,” *Nature*, vol. 486, no. 7404, pp. 537–40, Jun. 2012.
- [44] S. Misale *et al.*, “Emergence of *KRAS* mutations and acquired resistance to anti-EGFR therapy in colorectal cancer,” *Nature*, vol. 486, no. 7404, pp. 532–536, Jun. 2012.
- [45] E. Valtorta *et al.*, “*KRAS* gene amplification in colorectal cancer and impact on response to EGFR-targeted therapy,” *Int. J. Cancer*, vol. 133, no. 5, pp. 1259–1265, Sep. 2013.
- [46] M. Wang *et al.*, “Role of tumor microenvironment in tumorigenesis,” *J. Cancer*, vol. 8, no. 5, pp. 761–773, 2017.
- [47] B. Son, S. Lee, H. Youn, E. Kim, W. Kim, and B. Youn, “The role of tumor microenvironment in therapeutic resistance,” *Oncotarget*, vol. 8, no. 3, pp. 3933–3945, Jan. 2017.
- [48] B. I. Rini and M. B. Atkins, “Resistance to targeted therapy in renal-cell carcinoma,” *Lancet Oncol.*, vol. 10, no. 10, pp. 992–1000, Oct. 2009.
- [49] R. Straussman *et al.*, “Tumour micro-environment elicits innate resistance to RAF inhibitors through HGF secretion,” *Nature*, vol. 487, no. 7408, pp. 500–504, Jul. 2012.
- [50] F. A. Venning, L. Wullkopf, and J. T. Erler, “Targeting ECM Disrupts Cancer Progression,” *Front. Oncol.*, vol. 5, p. 224, Jan. 2015.
- [51] R. Rosa, F. Monteleone, N. Zambrano, and R. Bianco, “In vitro and in vivo models for analysis of resistance to anticancer molecular therapies,” *Curr. Med. Chem.*,

vol. 21, no. 14, pp. 1595–606, 2014.

- [52] S. E. Burdall, A. M. Hanby, M. R. J. Lansdown, and V. Speirs, “Breast cancer cell lines: friend or foe?,” *Breast Cancer Res.*, vol. 5, no. 2, pp. 89–95, 2003.
- [53] T. Vargo-Gogola and J. M. Rosen, “Modelling breast cancer: one size does not fit all,” *Nat. Rev. Cancer*, vol. 7, no. 9, pp. 659–672, Sep. 2007.
- [54] A. F. Gazdar, L. Girard, W. W. Lockwood, W. L. Lam, and J. D. Minna, “Lung cancer cell lines as tools for biomedical discovery and research.,” *J. Natl. Cancer Inst.*, vol. 102, no. 17, pp. 1310–21, Sep. 2010.
- [55] W. C. G. van Staveren, D. Y. W. Solís, A. Hébrant, V. Detours, J. E. Dumont, and C. Maenhaut, “Human cancer cell lines: Experimental models for cancer cells in situ? For cancer stem cells?,” *Biochim. Biophys. Acta - Rev. Cancer*, vol. 1795, no. 2, pp. 92–103, Apr. 2009.
- [56] S. L. Ham, R. Joshi, P. S. Thakuri, and H. Tavana, “Liquid-based three-dimensional tumor models for cancer research and drug discovery.,” *Exp. Biol. Med.*, vol. 241, no. 9, pp. 939–54, Apr. 2016.
- [57] K. Kersten, K. E. Visser, M. H. Miltenburg, and J. Jonkers, “Genetically engineered mouse models in oncology research and cancer medicine,” *EMBO Mol. Med.*, vol. 9, no. 2, pp. 137–153, Feb. 2017.
- [58] K. Jin, L. Teng, Y. Shen, K. He, Z. Xu, and G. Li, “Patient-derived human tumour tissue xenografts in immunodeficient mice: a systematic review,” *Clin. Transl. Oncol.*, vol. 12, no. 7, pp. 473–480, Jul. 2010.
- [59] F. Shojaei and N. Ferrara, “Refractoriness to Antivascular Endothelial Growth Factor Treatment: Role of Myeloid Cells,” *Cancer Res.*, vol. 68, no. 14, pp. 5501–5504, Jul. 2008.
- [60] J. Jung, H. S. Seol, and S. Chang, “The Generation and Application of Patient-Derived Xenograft Model for Cancer Research.,” *Cancer Res. Treat.*, vol. 50, no. 1, pp. 1–10, Jan. 2018.
- [61] E. Marangoni *et al.*, “A New Model of Patient Tumor-Derived Breast Cancer Xenografts for Preclinical Assays,” *Clin. Cancer Res.*, vol. 13, no. 13, pp. 3989–3998, Jul. 2007.
- [62] G. Jiménez-Valerio *et al.*, “Resistance to Antiangiogenic Therapies by Metabolic Symbiosis in Renal Cell Carcinoma PDX Models and Patients,” *Cell Rep.*, vol. 15, no. 6, pp. 1134–1143, May 2016.
- [63] B. Weigelt, C. M. Ghajar, and M. J. Bissell, “The need for complex 3D culture models to unravel novel pathways and identify accurate biomarkers in breast

- cancer,” *Adv. Drug Deliv. Rev.*, vol. 69–70, pp. 42–51, Apr. 2014.
- [64] T.-Y. Tu *et al.*, “Rapid Prototyping of Concave Microwells for the Formation of 3D Multicellular Cancer Aggregates for Drug Screening,” *Adv. Healthc. Mater.*, vol. 3, no. 4, pp. 609–616, Apr. 2014.
- [65] W. L. Haisler, D. M. Timm, J. A. Gage, H. Tseng, T. C. Killian, and G. R. Souza, “Three-dimensional cell culturing by magnetic levitation,” *Nat. Protoc.*, vol. 8, no. 10, pp. 1940–1949, Sep. 2013.
- [66] A. Pavesi *et al.*, “Engineering a 3D microfluidic culture platform for tumor-treating field application,” *Sci. Rep.*, vol. 6, no. 1, p. 26584, Jul. 2016.
- [67] L.-B. Weiswald, D. Bellet, and V. Dangles-Marie, “Spherical Cancer Models in Tumor Biology,” *Neoplasia*, vol. 17, no. 1, pp. 1–15, Jan. 2015.
- [68] A. Y. Hsiao *et al.*, “Microfluidic system for formation of PC-3 prostate cancer co-culture spheroids,” *Biomaterials*, vol. 30, no. 16, pp. 3020–3027, Jun. 2009.
- [69] B. Patra, Y.-H. Chen, C.-C. Peng, S.-C. Lin, C.-H. Lee, and Y.-C. Tung, “A microfluidic device for uniform-sized cell spheroids formation, culture, harvesting and flow cytometry analysis.,” *Biomicrofluidics*, vol. 7, no. 5, p. 54114, 2013.
- [70] K. A. T. Naipal *et al.*, “Tumor slice culture system to assess drug response of primary breast cancer.,” *BMC Cancer*, vol. 16, p. 78, Feb. 2016.
- [71] K. A. Paschos, D. Canovas, and N. C. Bird, “The role of cell adhesion molecules in the progression of colorectal cancer and the development of liver metastasis,” *Cell. Signal.*, vol. 21, no. 5, pp. 665–674, 2009.
- [72] P. Friedl and K. Wolf, “Tumour-cell invasion and migration: diversity and escape mechanisms.,” *Nat. Rev. Cancer*, vol. 3, no. 5, pp. 362–74, May 2003.
- [73] R. Fa, K. R. Legate, S. A. Wickstro, S. A. Wickstrom, and R. Fassler, “Genetic and cell biological analysis of integrin outside-in signaling,” *Genes Dev.*, vol. 23, no. 4, pp. 397–418, Feb. 2009.
- [74] I. Vivanco and C. L. Sawyers, “The phosphatidylinositol 3-Kinase AKT pathway in human cancer.,” *Nat. Rev. Cancer*, vol. 2, no. 7, pp. 489–501, Jul. 2002.
- [75] M. Van Dijk, S. A. Göransson, and S. Strömblad, “Cell to extracellular matrix interactions and their reciprocal nature in cancer,” *Exp. Cell Res.*, vol. 319, no. 11, pp. 1663–1670, 2013.
- [76] A. Borah, S. Raveendran, A. Rochani, T. Maekawa, and D. S. Kumar, “Targeting self-renewal pathways in cancer stem cells : clinical implications for cancer therapy,” *Oncogenesis*, vol. 4, no. 11, pp. e177-11, Nov. 2015.

- [77] T. Shibue and R. A. Weinberg, “EMT, CSCs, and drug resistance: the mechanistic link and clinical implications,” *Nat. Rev. Clin. Oncol.*, Apr. 2017.
- [78] P. Swietach, A. Hulikova, S. Patiar, R. D. Vaughan-Jones, and A. L. Harris, “Importance of intracellular pH in determining the uptake and efficacy of the weakly basic chemotherapeutic drug, doxorubicin,” *PLoS One*, vol. 7, no. 4, pp. 1–9, 2012.
- [79] P. Albertsson, “macromolecules: separation and purification of biomolecules, cell organelles, membranes, and cells in aqueous polymer two-phase systems and their use,” Wiley, 1986.
- [80] H. Tavana *et al.*, “Nanolitre liquid patterning in aqueous environments for spatially defined reagent delivery to mammalian cells,” *Nat. Mater.*, vol. 8, no. 9, pp. 736–41, Sep. 2009.
- [81] S. Lemmo, E. Atefi, G. D. Luker, and H. Tavana, “Optimization of aqueous biphasic tumor spheroid microtechnology for anti-cancer drug testing in 3D culture,” *Cell. Mol. Bioeng.*, vol. 7, no. 3, pp. 344–354, Sep. 2014.
- [82] E. Atefi, S. Lemmo, D. Fyffe, G. D. Luker, and H. Tavana, “High throughput, polymeric aqueous two-phase printing of tumor spheroids,” *Adv. Funct. Mater.*, vol. 24, no. 41, pp. 6509–6515, Nov. 2014.
- [83] E. Atefi, R. Joshi, J. A. Mann, and H. Tavana, “Interfacial tension effect on cell partition in aqueous two-phase systems,” *ACS Appl. Mater. Interfaces*, vol. 7, no. 38, pp. 21305–14, Sep. 2015.
- [84] S. L. Ham *et al.*, “Three-dimensional tumor model mimics stromal breast cancer cells signaling,” *Oncotarget*, vol. 9, no. 1, pp. 249–267, Jan. 2018.
- [85] Sunil Singh; Lucille Ray; Pradip Shahi Thakuri; Sydnie Tran; Michael Konopka; Gary Luker; Hossein Tavana, “Organotypic Breast Tumor Model Elucidates Dynamic Remodeling of Tumor Microenvironment,” *Submitted*.
- [86] P. Shahi Thakuri, S. L. Ham, G. D. Luker, and H. Tavana, “Multiparametric analysis of oncology drug screening with aqueous two-phase tumor spheroids,” *Mol. Pharm.*, vol. 13, no. 11, pp. 3724–3735, Nov. 2016.
- [87] R. Siegel, C. DeSantis, and A. Jemal, “Colorectal cancer statistics, 2014,” *CA. Cancer J. Clin.*, vol. 64, no. 2, pp. 104–117, Mar. 2014.
- [88] Cancer Genome Atlas Network, “Comprehensive molecular characterization of human colon and rectal cancer,” *Nature*, vol. 487, no. 7407, pp. 330–7, Jul. 2012.
- [89] J. Guinney *et al.*, “The consensus molecular subtypes of colorectal cancer,” *Nat. Med.*, vol. 21, no. 11, pp. 1350–6, Nov. 2015.

- [90] B. Margolis and E. Y. Skolnik, "Activation of Ras by receptor tyrosine kinases.," *J. Am. Soc. Nephrol.*, vol. 5, no. 6, pp. 1288–99, Dec. 1994.
- [91] J. S. Sebolt-Leopold *et al.*, "Blockade of the MAP kinase pathway suppresses growth of colon tumors in vivo," *Nat. Med.*, vol. 5, no. 7, pp. 810–816, Jul. 1999.
- [92] H. Yang *et al.*, "Antitumor activity of BRAF inhibitor vemurafenib in preclinical models of BRAF-mutant colorectal cancer.," *Cancer Res.*, vol. 72, no. 3, pp. 779–89, Feb. 2012.
- [93] R. Carson *et al.*, "HDAC Inhibition Overcomes Acute Resistance to MEK Inhibition in BRAF-Mutant Colorectal Cancer by Downregulation of c-FLIPL.," *Clin. Cancer Res.*, vol. 21, no. 14, pp. 3230–3240, Jul. 2015.
- [94] R. B. Corcoran *et al.*, "EGFR-mediated re-activation of MAPK signaling contributes to insensitivity of BRAF mutant colorectal cancers to RAF inhibition with vemurafenib.," *Cancer Discov.*, vol. 2, no. 3, pp. 227–35, Mar. 2012.
- [95] G. Bon *et al.*, "Dual targeting of HER3 and MEK may overcome HER3-dependent drug-resistance of colon cancers," *Oncotarget*, vol. 8, no. 65, pp. 108463–108479, Dec. 2017.
- [96] C. Sun *et al.*, "Intrinsic Resistance to MEK Inhibition in KRAS Mutant Lung and Colon Cancer through Transcriptional Induction of ERBB3," *Cell Rep.*, vol. 7, no. 1, pp. 86–93, Apr. 2014.
- [97] H. Wang *et al.*, "Identification of the MEK1(F129L) activating mutation as a potential mechanism of acquired resistance to MEK inhibition in human cancers carrying the B-RafV600E mutation.," *Cancer Res.*, vol. 71, no. 16, pp. 5535–45, Aug. 2011.
- [98] L. G. Ahronian *et al.*, "Clinical Acquired Resistance to RAF Inhibitor Combinations in BRAF-Mutant Colorectal Cancer through MAPK Pathway Alterations.," *Cancer Discov.*, vol. 5, no. 4, pp. 358–67, Apr. 2015.
- [99] R. B. Corcoran, D. Dias-Santagata, K. Bergethon, A. J. Iafrate, J. Settleman, and J. A. Engelman, "BRAF Gene Amplification Can Promote Acquired Resistance to MEK Inhibitors in Cancer Cells Harboring the BRAF V600E Mutation," *Sci. Signal.*, vol. 3, no. 149, pp. ra84–ra84, Nov. 2010.
- [100] T. Shimizu *et al.*, "The clinical effect of the dual-targeting strategy involving PI3K/AKT/mTOR and RAS/MEK/ERK pathways in patients with advanced cancer," *Clin. Cancer Res.*, vol. 18, no. 8, pp. 2316–2325, Apr. 2012.
- [101] H. Eagle and G. E. Foley, "Cytotoxicity in Human Cell Cultures as a Primary Screen for the Detection of Anti-Tumor Agents," *Cancer Res.*, vol. 18, no. 9, pp. 1017–1025, Oct. 1958.

- [102] K. S. M. Smalley, M. Lioni, and M. Herlyn, "Life isn't flat: taking cancer biology to the next dimension.," *In Vitro Cell. Dev. Biol. Anim.*, vol. 42, no. 8–9, pp. 242–7, Jan. .
- [103] M. J. Waring *et al.*, "An analysis of the attrition of drug candidates from four major pharmaceutical companies.," *Nat. Rev. Drug Discov.*, vol. 14, no. 7, pp. 475–86, Jun. 2015.
- [104] B. P. Zambrowicz and A. T. Sands, "Knockouts model the 100 best-selling drugs--will they model the next 100?," *Nat. Rev. Drug Discov.*, vol. 2, no. 1, pp. 38–51, Jan. 2003.
- [105] L. Hutchinson and R. Kirk, "High drug attrition rates--where are we going wrong?," *Nat. Rev. Clin. Oncol.*, vol. 8, no. 4, pp. 189–90, Apr. 2011.
- [106] W. N. Hait, "Anticancer drug development: the grand challenges.," *Nat. Rev. Drug Discov.*, vol. 9, no. 4, pp. 253–4, Apr. 2010.
- [107] F. Pampaloni, E. G. Reynaud, and E. H. K. Stelzer, "The third dimension bridges the gap between cell culture and live tissue.," *Nat. Rev. Mol. Cell Biol.*, vol. 8, no. 10, pp. 839–45, Oct. 2007.
- [108] M. H. Park, B. Song, S. Hong, S. H. Kim, and K. Lee, "Biomimetic 3D Clusters Using Human Adipose Derived Mesenchymal Stem Cells and Breast Cancer Cells: A Study on Migration and Invasion of Breast Cancer Cells.," *Mol. Pharm.*, May 2016.
- [109] J. K. Tunggal, D. S. Cowan, H. Shaikh, and I. F. Tannock, "Penetration of anticancer drugs through solid tissue: a factor that limits the effectiveness of chemotherapy for solid tumors.," *Clin. Cancer Res.*, vol. 5, no. 6, pp. 1583–6, Jun. 1999.
- [110] X. Xu, M. C. Farach-Carson, and X. Jia, "Three-dimensional in vitro tumor models for cancer research and drug evaluation," *Biotechnology Advances*, vol. 32, no. 7. pp. 1256–1268, 2014.
- [111] S.-H. Lee *et al.*, "Colorectal cancer-derived tumor spheroids retain the characteristics of original tumors.," *Cancer Lett.*, vol. 367, no. 1, pp. 34–42, Oct. 2015.
- [112] S. Eetezadi, R. De Souza, M. Vythilingam, R. Lessa Cataldi, and C. Allen, "Effects of Doxorubicin Delivery Systems and Mild Hyperthermia on Tissue Penetration in 3D Cell Culture Models of Ovarian Cancer Residual Disease.," *Mol. Pharm.*, vol. 12, no. 11, pp. 3973–85, Nov. 2015.
- [113] E. H. Flach, V. W. Rebecca, M. Herlyn, K. S. M. Smalley, and A. R. A. Anderson, "Fibroblasts contribute to melanoma tumor growth and drug resistance.," *Mol.*

Pharm., vol. 8, no. 6, pp. 2039–49, Dec. 2011.

- [114] P. A. Kenny *et al.*, “The morphologies of breast cancer cell lines in three-dimensional assays correlate with their profiles of gene expression,” *Mol. Oncol.*, vol. 1, no. 1, pp. 84–96, Jun. 2007.
- [115] E. L. S. Fong *et al.*, “Hydrogel-based 3D model of patient-derived prostate xenograft tumors suitable for drug screening,” *Mol. Pharm.*, vol. 11, no. 7, pp. 2040–2050, 2014.
- [116] H. Tavana *et al.*, “Nanolitre liquid patterning in aqueous environments for spatially defined reagent delivery to mammalian cells,” *Nat. Mater.*, vol. 8, no. 9, pp. 736–41, Sep. 2009.
- [117] S. L. Ham, E. Atefi, D. Fyffe, and H. Tavana, “Robotic production of cancer cell spheroids with an aqueous two-phase system for drug testing,” *J. Vis. Exp.*, no. 98, p. e52754, Apr. 2015.
- [118] E. Atefi, J. A. Mann, and H. Tavana, “Ultralow interfacial tensions of aqueous two-phase systems measured using drop shape,” *Langmuir*, vol. 30, no. 32, pp. 9691–9, Aug. 2014.
- [119] G. Da Violante *et al.*, “Evaluation of the cytotoxicity effect of dimethyl sulfoxide (DMSO) on Caco2/TC7 colon tumor cell cultures,” *Biol. Pharm. Bull.*, vol. 25, no. 12, pp. 1600–1603, 2002.
- [120] X. D. Zhang, “Illustration of SSMD, z score, SSMD*, z* score, and t statistic for hit selection in RNAi high-throughput screens,” *J. Biomol. Screen.*, vol. 16, no. 7, pp. 775–85, Aug. 2011.
- [121] T.-C. Chou, “Drug combination studies and their synergy quantification using the Chou-Talalay method,” *Cancer Res.*, vol. 70, no. 2, pp. 440–6, Jan. 2010.
- [122] S. Walenta, J. Doetsch, W. Mueller-Klieser, and L. A. Kunz-Schughart, “Metabolic Imaging in Multicellular Spheroids of Oncogene-transfected Fibroblasts,” *J. Histochem. Cytochem.*, vol. 48, no. 4, pp. 509–522, Apr. 2000.
- [123] M. Ingram *et al.*, “Three-dimensional growth patterns of various human tumor cell lines in simulated microgravity of a NASA bioreactor,” *In Vitro Cell. Dev. Biol. Anim.*, vol. 33, no. 6, pp. 459–66, Jun. 1997.
- [124] J. M. Kelm, N. E. Timmins, C. J. Brown, M. Fussenegger, and L. K. Nielsen, “Method for generation of homogeneous multicellular tumor spheroids applicable to a wide variety of cell types,” *Biotechnol. Bioeng.*, vol. 83, no. 2, pp. 173–80, Jul. 2003.
- [125] A. Y. Hsiao *et al.*, “Micro-ring structures stabilize microdroplets to enable long

term spheroid culture in 384 hanging drop array plates.,” *Biomed. Microdevices*, vol. 14, no. 2, pp. 313–23, Apr. 2012.

- [126] K. Lee *et al.*, “Extracellular matrix protein 1 regulates cell proliferation and trastuzumab resistance through activation of epidermal growth factor signaling.,” *Breast Cancer Res.*, vol. 16, no. 6, p. 479, Jan. 2014.
- [127] C. Gérard and A. Goldbeter, “The balance between cell cycle arrest and cell proliferation: control by the extracellular matrix and by contact inhibition.,” *Interface Focus*, vol. 4, no. 3, p. 20130075, Jun. 2014.
- [128] T. A. Ulrich, E. M. de Juan Pardo, and S. Kumar, “The mechanical rigidity of the extracellular matrix regulates the structure, motility, and proliferation of glioma cells.,” *Cancer Res.*, vol. 69, no. 10, pp. 4167–74, May 2009.
- [129] J. Y. Fang and B. C. Richardson, “The MAPK signalling pathways and colorectal cancer,” *Lancet Oncol.*, vol. 6, no. 5, pp. 322–327, May 2005.
- [130] J. J. Yeh *et al.*, “KRAS/BRAF mutation status and ERK1/2 activation as biomarkers for MEK1/2 inhibitor therapy in colorectal cancer.,” *Mol. Cancer Ther.*, vol. 8, no. 4, pp. 834–43, Apr. 2009.
- [131] C. B. Knobbe, A. Merlo, and G. Reifenberger, “Pten signaling in gliomas,” *Neuro. Oncol.*, vol. 4, no. 3, pp. 196–211, Jul. 2002.
- [132] M. Klingler-Hoffmann, P. Bukczynska, and T. Tiganis, “Inhibition of phosphatidylinositol 3-kinase signaling negates the growth advantage imparted by a mutant epidermal growth factor receptor on human glioblastoma cells.,” *Int. J. cancer*, vol. 105, no. 3, pp. 331–9, Jun. 2003.
- [133] M. J. Clark *et al.*, “U87MG decoded: the genomic sequence of a cytogenetically aberrant human cancer cell line.,” *PLoS Genet.*, vol. 6, no. 1, p. e1000832, Jan. 2010.
- [134] R. T. Lawrence *et al.*, “The Proteomic Landscape of Triple-Negative Breast Cancer.,” *Cell Rep.*, vol. 11, no. 4, pp. 630–44, Apr. 2015.
- [135] D. Walerych, M. Napoli, L. Collavin, and G. Del Sal, “The rebel angel: mutant p53 as the driving oncogene in breast cancer.,” *Carcinogenesis*, vol. 33, no. 11, pp. 2007–17, Nov. 2012.
- [136] H. Yuen *et al.*, “Impact of oncogenic driver mutations on feedback between the PI3K and MEK pathways in cancer cells,” *Biosci. Rep.*, vol. 32, no. 4, pp. 413–422, 2012.
- [137] M. K. VanKlombenberg, C. O. Bedalov, K. F. Soto, and J. R. Prosperi, “APC selectively mediates response to chemotherapeutic agents in breast cancer.,” *BMC*

Cancer, vol. 15, p. 457, Jan. 2015.

- [138] P. L. Olive and R. E. Durand, “Drug and radiation resistance in spheroids: Cell contact and kinetics,” *Cancer Metastasis Rev.*, vol. 13, no. 2, pp. 121–138, 1994.
- [139] R. S. Kerbel, B. St Croix, V. A. Florenes, and J. Rak, “Induction and reversal of cell adhesion-dependent multicellular drug resistance in solid breast tumors.,” *Hum. Cell*, vol. 9, no. 4, pp. 257–64, Dec. 1996.
- [140] M. Fallahi-Sichani, S. Honarnejad, L. M. Heiser, J. W. Gray, and P. K. Sorger, “Metrics other than potency reveal systematic variation in responses to cancer drugs.,” *Nat. Chem. Biol.*, vol. 9, no. 11, pp. 708–14, Nov. 2013.
- [141] D. Ahmed *et al.*, “Epigenetic and genetic features of 24 colon cancer cell lines.,” *Oncogenesis*, vol. 2, p. e71, Jan. 2013.
- [142] A. K. M. Chow *et al.*, “Preclinical analysis of the anti-tumor and anti-metastatic effects of Raf265 on colon cancer cells and CD26(+) cancer stem cells in colorectal carcinoma.,” *Mol. Cancer*, vol. 14, p. 80, Jan. 2015.
- [143] E. Oikonomou, E. Makrodouli, M. Evagelidou, T. Joyce, L. Probert, and A. Pintzas, “BRAF(V600E) efficient transformation and induction of microsatellite instability versus KRAS(G12V) induction of senescence markers in human colon cancer cells.,” *Neoplasia*, vol. 11, no. 11, pp. 1116–31, Nov. 2009.
- [144] L. McDermott and C. Qin, “Allosteric MEK1/2 Inhibitors for the Treatment of Cancer: an Overview | Drug Research and Development Journal | Sci Forschen,” *J. drug Res. Dev.*, vol. 1, no. 1, pp. 1–9, 2015.
- [145] T. Yamaguchi, R. Kakefuda, N. Tajima, Y. Sowa, and T. Sakai, “Antitumor activities of JTP-74057 (GSK1120212), a novel MEK1/2 inhibitor, on colorectal cancer cell lines in vitro and in vivo,” *Int. J. Oncol.*, vol. 39, no. 1, pp. 23–31, Jul. 2011.
- [146] L. Qiao *et al.*, “Staurosporine inhibits the proliferation, alters the cell cycle distribution and induces apoptosis in HT-29 human colon adenocarcinoma cells.,” *Cancer Lett.*, vol. 107, no. 1, pp. 83–9, Oct. 1996.
- [147] A. Mueller *et al.*, “Selective PI3K inhibition by BKM120 and BEZ235 alone or in combination with chemotherapy in wild-type and mutated human gastrointestinal cancer cell lines.,” *Cancer Chemother. Pharmacol.*, vol. 69, no. 6, pp. 1601–15, Jun. 2012.
- [148] M. N. Harmalkar and N. V. Shirsat, “Staurosporine-induced growth inhibition of glioma cells is accompanied by altered expression of cyclins, CDKs and CDK inhibitors.,” *Neurochem. Res.*, vol. 31, no. 5, pp. 685–92, May 2006.

- [149] K. V Lu *et al.*, “Fyn and SRC are effectors of oncogenic epidermal growth factor receptor signaling in glioblastoma patients.,” *Cancer Res.*, vol. 69, no. 17, pp. 6889–98, Sep. 2009.
- [150] J. H. Cha, Y. J. Choi, S. H. Cha, C. H. Choi, and W. H. Cho, “Allicin inhibits cell growth and induces apoptosis in U87MG human glioblastoma cells through an ERK-dependent pathway.,” *Oncol. Rep.*, vol. 28, no. 1, pp. 41–8, Jul. 2012.
- [151] F. Végran, R. Boidot, C. Oudin, C. Defrain, M. Rebucci, and S. Lizard-Nacol, “Association of p53 gene alterations with the expression of antiapoptotic survivin splice variants in breast cancer.,” *Oncogene*, vol. 26, no. 2, pp. 290–7, Jan. 2007.
- [152] S. L. Ham *et al.*, “Phytochemicals potently inhibit migration of metastatic breast cancer cells.,” *Integr. Biol. (Camb)*., vol. 7, no. 7, pp. 792–800, Jul. 2015.
- [153] Y. Arima *et al.*, “Loss of p16 expression is associated with the stem cell characteristics of surface markers and therapeutic resistance in estrogen receptor-negative breast cancer.,” *Int. J. cancer*, vol. 130, no. 11, pp. 2568–79, Jun. 2012.
- [154] S. Akashi-Tanaka and C. Watanabe, “BRCAness predicts resistance to taxane-containing regimens in triple negative breast cancer during neoadjuvant chemotherapy,” *Clin. breast ...*, 2015.
- [155] A. A. Sprouse and B.-S. Herbert, “Resveratrol augments paclitaxel treatment in MDA-MB-231 and paclitaxel-resistant MDA-MB-231 breast cancer cells.,” *Anticancer Res.*, vol. 34, no. 10, pp. 5363–74, Oct. 2014.
- [156] M. S. Song, L. Salmena, and P. P. Pandolfi, “The functions and regulation of the PTEN tumour suppressor.,” *Nat. Rev. Mol. Cell Biol.*, vol. 13, no. 5, pp. 283–96, May 2012.
- [157] R. B. Corcoran *et al.*, “Combined BRAF and MEK Inhibition With Dabrafenib and Trametinib in BRAF V600-Mutant Colorectal Cancer.,” *J. Clin. Oncol.*, vol. 33, no. 34, pp. 4023–31, Dec. 2015.
- [158] T. C. G. A. Network, “Comprehensive molecular characterization of human colon and rectal cancer.,” *Nature*, vol. 487, no. 7407, pp. 330–337, Jul. 2012.
- [159] T. Chou, “Theoretical Basis , Experimental Design , and Computerized Simulation of Synergism and Antagonism in Drug Combination Studies,” vol. 58, no. 3, pp. 621–681, 2006.
- [160] L. Trusolino and A. Bertotti, “Compensatory pathways in oncogenic kinase signaling and resistance to targeted therapies: six degrees of separation.,” *Cancer Discov.*, vol. 2, no. 10, pp. 876–80, Oct. 2012.
- [161] J. S. Logue and D. K. Morrison, “Complexity in the signaling network: insights

from the use of targeted inhibitors in cancer therapy.," *Genes Dev.*, vol. 26, no. 7, pp. 641–50, Apr. 2012.

- [162] E. J. Haagenzen, S. Kyle, G. S. Beale, R. J. Maxwell, and D. R. Newell, "The synergistic interaction of MEK and PI3K inhibitors is modulated by mTOR inhibition.," *Br. J. Cancer*, vol. 106, no. 8, pp. 1386–94, Apr. 2012.
- [163] P. Shahi Thakuri, G. D. Luker, and H. Tavana, "Cyclical treatment of colorectal tumor spheroids induces resistance to MEK inhibitors.," *Transl. Oncol.*, vol. 12, no. 3, pp. 404–416, Dec. 2019.
- [164] S. L. Ham, R. Joshi, G. D. Luker, and H. Tavana, "Engineered breast cancer cell spheroids reproduce biologic properties of solid tumors," *Adv. Healthc. Mater.*, vol. 5, no. 21, pp. 2788–2798, Nov. 2016.
- [165] P. Shahi Thakuri, C. Liu, G. D. Luker, and H. Tavana, "Biomaterials-based approaches to tumor spheroid and organoid modeling," *Adv. Healthc. Mater.*, vol. 7, no. 6, p. e1700980, 2017.
- [166] C. R. Thoma, M. Zimmermann, I. Agarkova, J. M. Kelm, and W. Krek, "3D cell culture systems modeling tumor growth determinants in cancer target discovery," *Adv. Drug Deliv. Rev.*, vol. 69–70, pp. 29–41, Apr. 2014.
- [167] X. Liu, M. Jakubowski, and J. L. Hunt, "KRAS Gene Mutation in Colorectal Cancer Is Correlated With Increased Proliferation and Spontaneous Apoptosis," *Am. J. Clin. Pathol.*, vol. 135, no. 2, pp. 245–252, Feb. 2011.
- [168] H. Davies *et al.*, "Mutations of the BRAF gene in human cancer," *Nature*, vol. 417, no. 6892, pp. 949–954, Jun. 2002.
- [169] Z. B. Mei, C. Y. Duan, C. B. Li, L. Cui, and S. Ogino, "Prognostic role of tumor PIK3CA mutation in colorectal cancer: a systematic review and meta-analysis," *Ann. Oncol.*, vol. 27, no. 10, pp. 1836–1848, Oct. 2016.
- [170] H. Wang *et al.*, "Identification of the MEK1(F129L) activating mutation as a potential mechanism of acquired resistance to MEK inhibition in human cancers carrying the B-RafV600E mutation.," *Cancer Res.*, vol. 71, no. 16, pp. 5535–45, Aug. 2011.
- [171] L. G. Ahronian *et al.*, "Clinical Acquired Resistance to RAF Inhibitor Combinations in BRAF-Mutant Colorectal Cancer through MAPK Pathway Alterations.," *Cancer Discov.*, vol. 5, no. 4, pp. 358–67, Apr. 2015.
- [172] E. P. Spugnini, E. Dragonetti, B. Vincenzi, N. Onori, G. Citro, and A. Baldi, "Pulse-mediated chemotherapy enhances local control and survival in a spontaneous canine model of primary mucosal melanoma," *Melanoma Res.*, vol. 16, no. 1, pp. 23–27, Feb. 2006.

- [173] D. B. Solit *et al.*, “Pulsatile Administration of the Epidermal Growth Factor Receptor Inhibitor Gefitinib Is Significantly More Effective than Continuous Dosing for Sensitizing Tumors to Paclitaxel,” *Clin. Cancer Res.*, vol. 11, no. 5, pp. 1983–1989, Mar. 2005.
- [174] M. F. Rimawi *et al.*, “Reduced Dose and Intermittent Treatment with Lapatinib and Trastuzumab for Potent Blockade of the HER Pathway in HER2/neu-Overexpressing Breast Tumor Xenografts,” *Clin. Cancer Res.*, vol. 17, no. 6, pp. 1351–1361, Mar. 2011.
- [175] M. Das Thakur *et al.*, “Modelling vemurafenib resistance in melanoma reveals a strategy to forestall drug resistance,” *Nature*, vol. 494, no. 7436, pp. 251–255, Jan. 2013.
- [176] J. Bennouna *et al.*, “Continuation of bevacizumab after first progression in metastatic colorectal cancer (ML18147): a randomised phase 3 trial,” *Lancet Oncol.*, vol. 14, no. 1, pp. 29–37, Jan. 2013.
- [177] P. Shahi Thakuri and H. Tavana, “Single and combination drug screening with aqueous biphasic tumor spheroids,” *SLAS Discov.*, vol. 22, no. 5, pp. 507–515, Jun. 2017.
- [178] E. Atefi, S. Lemmo, D. Fyffe, G. D. Luker, and H. Tavana, “High throughput, polymeric aqueous two-phase printing of tumor spheroids,” *Adv. Funct. Mater.*, vol. 24, no. 41, pp. 6509–6515, 2014.
- [179] E. Atefi, D. Fyffe, K. B. Kaylan, and H. Tavana, “Characterization of Aqueous Two-Phase Systems from Volume and Density Measurements,” *J. Chem. Eng. Data*, vol. 61, no. 4, pp. 1531–1539, Apr. 2016.
- [180] J. A. Engelman, “Targeting PI3K signalling in cancer: opportunities, challenges and limitations,” *Nat. Rev. Cancer*, vol. 9, no. 8, pp. 550–562, Aug. 2009.
- [181] W. De Roock, V. De Vriendt, N. Normanno, F. Ciardiello, and S. Tejpar, “KRAS, BRAF, PIK3CA, and PTEN mutations: implications for targeted therapies in metastatic colorectal cancer,” *Lancet Oncol.*, vol. 12, no. 6, pp. 594–603, Jun. 2011.
- [182] A. S. Dhillon, S. Hagan, O. Rath, and W. Kolch, “MAP kinase signalling pathways in cancer,” *Oncogene*, vol. 26, no. 22, pp. 3279–3290, May 2007.
- [183] C. J. Caunt, M. J. Sale, P. D. Smith, and S. J. Cook, “MEK1 and MEK2 inhibitors and cancer therapy: the long and winding road,” *Nat. Rev. Cancer*, vol. 15, no. 10, pp. 577–592, Sep. 2015.
- [184] X. Sun, J. Bao, and Y. Shao, “Mathematical Modeling of Therapy-induced Cancer Drug Resistance: Connecting Cancer Mechanisms to Population Survival Rates,”

Sci. Rep., vol. 6, no. 1, p. 22498, Apr. 2016.

- [185] J. Foo and F. Michor, “Evolution of Resistance to Targeted Anti-Cancer Therapies during Continuous and Pulsed Administration Strategies,” *PLoS Comput. Biol.*, vol. 5, no. 11, p. e1000557, Nov. 2009.
- [186] D. P. Ivanov *et al.*, “Multiplexing spheroid volume, resazurin and acid phosphatase viability assays for high-throughput screening of tumour spheroids and stem cell neurospheres,” *PLoS One*, vol. 9, no. 8, p. e103817, Aug. 2014.
- [187] M. Vinci *et al.*, “Advances in establishment and analysis of three-dimensional tumor spheroid-based functional assays for target validation and drug evaluation,” *BMC Biol.*, vol. 10, no. 1, p. 29, 2012.
- [188] K. P. Hoeflich *et al.*, “Intermittent administration of MEK inhibitor GDC-0973 plus PI3K inhibitor GDC-0941 triggers robust apoptosis and tumor growth inhibition,” *Cancer Res.*, vol. 72, no. 1, pp. 210–9, Jan. 2012.
- [189] M. L. Sos *et al.*, “Identifying genotype-dependent efficacy of single and combined PI3K- and MAPK-pathway inhibition in cancer,” *Proc. Natl. Acad. Sci.*, vol. 106, no. 43, pp. 18351–18356, Oct. 2009.
- [190] K. Balmanno, S. D. Chell, A. S. Gillings, S. Hayat, and S. J. Cook, “Intrinsic resistance to the MEK1/2 inhibitor AZD6244 (ARRY-142886) is associated with weak ERK1/2 signalling and/or strong PI3K signalling in colorectal cancer cell lines,” *Int. J. Cancer*, vol. 125, no. 10, pp. 2332–2341, Nov. 2009.
- [191] A. B. Turke *et al.*, “MEK Inhibition Leads to PI3K/AKT Activation by Relieving a Negative Feedback on ERBB Receptors,” *Cancer Res.*, vol. 72, no. 13, pp. 3228–3237, Jul. 2012.
- [192] O. K. Mirzoeva *et al.*, “Subtype-Specific MEK-PI3 Kinase Feedback as a Therapeutic Target in Pancreatic Adenocarcinoma,” *Mol. Cancer Ther.*, vol. 12, no. 10, pp. 2213–2225, Oct. 2013.
- [193] E. Manchado *et al.*, “A combinatorial strategy for treating KRAS-mutant lung cancer,” *Nature*, vol. 534, no. 7609, pp. 647–651, Jun. 2016.
- [194] M. Raja, M. Zverev, K. Seipel, G. T. Williams, A. R. Clarke, and P. H. S. Shaw, “Assessment of the in vivo activity of PI3K and MEK inhibitors in genetically defined models of colorectal cancer,” *Mol. Cancer Ther.*, vol. 14, no. 10, pp. 2175–2186, Oct. 2015.
- [195] A. S. Little *et al.*, “Amplification of the driving oncogene, KRAS or BRAF, underpins acquired resistance to MEK1/2 inhibitors in colorectal cancer cells,” *Sci. Signal.*, vol. 4, no. 166, p. ra17, Mar. 2011.

- [196] T.-C. Chou, “Drug Combination Studies and Their Synergy Quantification Using the Chou-Talalay Method,” *Cancer Res.*, vol. 70, no. 2, pp. 440–446, 2010.
- [197] K. M. Kinross *et al.*, “In vivo activity of combined PI3K/mTOR and MEK inhibition in a KrasG12D;pten deletion mouse model of ovarian cancer,” *Mol. Cancer Ther.*, vol. 10, no. 8, pp. 1440–1449, Aug. 2011.
- [198] T. M. Pitts *et al.*, “Dual Pharmacological Targeting of the MAP Kinase and PI3K/mTOR Pathway in Preclinical Models of Colorectal Cancer,” *PLoS One*, vol. 9, no. 11, p. e113037, Nov. 2014.
- [199] M. L. Sos *et al.*, “Identifying genotype-dependent efficacy of single and combined PI3K- and MAPK-pathway inhibition in cancer,” *Proc. Natl. Acad. Sci.*, vol. 106, no. 43, pp. 18351–18356, Oct. 2009.
- [200] E. J. Haagenesen *et al.*, “The enhanced in vivo activity of the combination of a MEK and a PI3K inhibitor correlates with [18F]-FLT PET in human colorectal cancer xenograft tumour-bearing mice,” *PLoS One*, vol. 8, no. 12, p. e81763, Jan. 2013.
- [201] C. Sun *et al.*, “Intrinsic Resistance to MEK Inhibition in KRAS Mutant Lung and Colon Cancer through Transcriptional Induction of ERBB3,” *Cell Rep.*, vol. 7, no. 1, pp. 86–93, Apr. 2014.
- [202] T. C. G. A. Network, “Comprehensive molecular characterization of human colon and rectal cancer,” *Nature*, vol. 487, no. 7407, pp. 330–337, Jul. 2012.
- [203] T. Shimizu *et al.*, “The Clinical Effect of the Dual-Targeting Strategy Involving PI3K/AKT/mTOR and RAS/MEK/ERK Pathways in Patients with Advanced Cancer,” *Clin. Cancer Res.*, vol. 18, no. 8, pp. 2316–2325, Apr. 2012.
- [204] K. T. Flaherty *et al.*, “Combined BRAF and MEK Inhibition in Melanoma with BRAF V600 Mutations,” *N. Engl. J. Med.*, vol. 367, no. 18, pp. 1694–1703, Nov. 2012.
- [205] A. M. Molina *et al.*, “Phase 1 trial of everolimus plus sunitinib in patients with metastatic renal cell carcinoma,” *Cancer*, vol. 118, no. 7, pp. 1868–1876, Apr. 2012.
- [206] A. Ribas, F. S. Hodi, M. Callahan, C. Konto, and J. Wolchok, “Hepatotoxicity with Combination of Vemurafenib and Ipilimumab,” *N. Engl. J. Med.*, vol. 368, no. 14, pp. 1365–1366, Apr. 2013.
- [207] R. Joshi, P. S. Thakuri, J. C. Buchanan, J. Li, and H. Tavana, “Microprinted Stem Cell Niches Reveal Compounding Effect of Colony Size on Stromal Cells-Mediated Neural Differentiation,” *Adv. Healthc. Mater.*, vol. 7, no. 5, p. 1700832, Mar. 2018.

- [208] R. Joshi, J. C. Buchanan, and H. Tavana, "Self-regulatory factors of embryonic stem cells in co-culture with stromal cells enhance neural differentiation.," *Integr. Biol. (Camb).*, vol. 9, no. 5, pp. 418–426, 2017.
- [209] P. S. Thakuri, M. Gupta, M. Plaster, and H. Tavana, "Quantitative Size-Based Analysis of Tumor Spheroids and Responses to Therapeutics," *Assay Drug Dev. Technol.*, vol. 17, no. 3, pp. 140–149, Apr. 2019.
- [210] S. L. Ham, E. Atefi, D. Fyffe, and H. Tavana, "Robotic production of cancer cell spheroids with an aqueous two-phase system for drug testing.," *J. Vis. Exp.*, no. 98, p. e52754, Jan. 2015.
- [211] O. K. Mirzoeva *et al.*, "Basal subtype and MAPK/ERK kinase (MEK)-phosphoinositide 3-kinase feedback signaling determine susceptibility of breast cancer cells to MEK inhibition," *Cancer Res.*, vol. 69, no. 2, pp. 565–572, Jan. 2009.
- [212] B. P. Zhou, Y. Liao, W. Xia, B. Spohn, M.-H. Lee, and M.-C. Hung, "Cytoplasmic localization of p21^{Cip1}/WAF1 by Akt-induced phosphorylation in HER-2/neu-overexpressing cells," *Nat. Cell Biol.*, vol. 3, no. 3, pp. 245–252, Mar. 2001.
- [213] L. Rössig, C. Badorff, Y. Holzmann, A. M. Zeiher, and S. Dimmeler, "Glycogen Synthase Kinase-3 Couples AKT-dependent Signaling to the Regulation of p21^{Cip1} Degradation," *J. Biol. Chem.*, vol. 277, no. 12, pp. 9684–9689, Mar. 2002.
- [214] L. Rössig, A. S. Jadidi, C. Urbich, C. Badorff, A. M. Zeiher, and S. Dimmeler, "Akt-Dependent Phosphorylation of p21^{Cip1} Regulates PCNA Binding and Proliferation of Endothelial Cells," *Mol. Cell. Biol.*, vol. 21, no. 16, pp. 5644–5657, Aug. 2001.
- [215] S.-M. Maira, F. Stauffer, C. Schnell, and C. García-Echeverría, "PI3K inhibitors for cancer treatment: where do we stand?," *Biochem. Soc. Trans.*, vol. 37, no. 1, pp. 265–272, Feb. 2009.
- [216] D. Kong, S. Yaguchi, and T. Yamori, "Effect of ZSTK474, a novel phosphatidylinositol 3-kinase inhibitor, on DNA-dependent protein kinase.," *Biol. Pharm. Bull.*, vol. 32, no. 2, pp. 297–300, Feb. 2009.
- [217] J. A. Engelman *et al.*, "Effective use of PI3K and MEK inhibitors to treat mutant Kras G12D and PIK3CA H1047R murine lung cancers," *Nat. Med.*, vol. 14, no. 12, pp. 1351–1356, Dec. 2008.
- [218] S. Gong, D. Xu, J. Zhu, F. Zou, and R. Peng, "Efficacy of the MEK Inhibitor Cobimetinib and its Potential Application to Colorectal Cancer Cells," *Cell. Physiol. Biochem.*, vol. 47, no. 2, pp. 680–693, 2018.
- [219] F. Chang *et al.*, "Involvement of PI3K/Akt pathway in cell cycle progression,

apoptosis, and neoplastic transformation: a target for cancer chemotherapy,” *Leukemia*, vol. 17, no. 3, pp. 590–603, Mar. 2003.

- [220] J. R. Infante *et al.*, “Safety, pharmacokinetic, pharmacodynamic, and efficacy data for the oral MEK inhibitor trametinib: A phase 1 dose-escalation trial,” *Lancet Oncol.*, vol. 13, no. 8, pp. 773–781, Aug. 2012.
- [221] Y. Deng *et al.*, “KRAS as a predictor of poor prognosis and benefit from postoperative FOLFOX chemotherapy in patients with stage II and III colorectal cancer,” *Mol. Oncol.*, vol. 9, no. 7, pp. 1341–1347, Aug. 2015.
- [222] C. Tan and X. Du, “KRAS mutation testing in metastatic colorectal cancer.,” *World J. Gastroenterol.*, vol. 18, no. 37, pp. 5171–80, Oct. 2012.
- [223] P. P. Vitiello *et al.*, “Receptor tyrosine kinase-dependent PI3K activation is an escape mechanism to vertical suppression of the EGFR/RAS/MAPK pathway in KRAS-mutated human colorectal cancer cell lines,” *J. Exp. Clin. Cancer Res.*, vol. 38, no. 1, p. 41, Dec. 2019.
- [224] S. Van Schaeybroeck *et al.*, “ADAM17-Dependent c-MET-STAT3 Signaling Mediates Resistance to MEK Inhibitors in KRAS Mutant Colorectal Cancer,” *Cell Rep.*, vol. 7, no. 6, pp. 1940–1955, Jun. 2014.
- [225] S. A. Flanigan *et al.*, “Overcoming IGF1R/IR resistance through inhibition of MEK signaling in colorectal cancer models.,” *Clin. Cancer Res.*, vol. 19, no. 22, pp. 6219–29, Nov. 2013.
- [226] C. R. Thoma, M. Zimmermann, I. Agarkova, J. M. Kelm, and W. Krek, “3D cell culture systems modeling tumor growth determinants in cancer target discovery,” *Adv. Drug Deliv. Rev.*, vol. 69–70, pp. 29–41, 2014.
- [227] A. S. Nunes, A. S. Barros, E. C. Costa, A. F. Moreira, and I. J. Correia, “3D tumor spheroids as in vitro models to mimic in vivo human solid tumors resistance to therapeutic drugs,” *Biotechnol. Bioeng.*, vol. 116, no. 1, pp. 206–226, Jan. 2019.
- [228] P. S. Thakuri, M. Gupta, R. Joshi, S. Singh, and H. Tavana, “Synergistic Inhibition of Kinase Pathways Overcomes Resistance of Colorectal Cancer Spheroids to Cyclic Targeted Therapies,” *ACS Pharmacol. Transl. Sci.*, vol. 2, no. 4, pp. 275–284, Aug. 2019.
- [229] K.-M. Choi *et al.*, “Prolonged MEK inhibition leads to acquired resistance and increased invasiveness in KRAS mutant gastric cancer,” *Biochem. Biophys. Res. Commun.*, vol. 507, no. 1–4, pp. 311–318, Dec. 2018.
- [230] W. J. van Houdt *et al.*, “Oncogenic KRAS desensitizes colorectal tumor cells to epidermal growth factor receptor inhibition and activation.,” *Neoplasia*, vol. 12, no. 6, pp. 443–52, Jun. 2010.

- [231] R. Pal *et al.*, “Molecular subtypes of colorectal cancer in pre-clinical models show differential response to targeted therapies: Treatment implications beyond KRAS mutations,” *PLoS One*, vol. 13, no. 8, p. e0200836, Aug. 2018.
- [232] R. Herr, S. Halbach, M. Heizmann, H. Busch, M. Boerries, and T. Brummer, “BRAF inhibition upregulates a variety of receptor tyrosine kinases and their downstream effector Gab2 in colorectal cancer cell lines,” *Oncogene*, vol. 37, no. 12, pp. 1576–1593, Mar. 2018.
- [233] C. Zhao *et al.*, “Rational combination of MEK inhibitor and the STAT3 pathway modulator for the therapy in K-Ras mutated pancreatic and colon cancer cells,” *Oncotarget*, vol. 6, no. 16, pp. 14472–87, Jun. 2015.
- [234] N. Itoh, S. Semba, M. Ito, H. Takeda, S. Kawata, and M. Yamakawa, “Phosphorylation of Akt/PKB is required for suppression of cancer cell apoptosis and tumor progression in human colorectal carcinoma,” *Cancer*, vol. 94, no. 12, pp. 3127–3134, Jun. 2002.
- [235] K. Khaleghpour, Y. Li, D. Banville, Z. Yu, and S.-H. Shen, “Involvement of the PI 3-kinase signaling pathway in progression of colon adenocarcinoma,” *Carcinogenesis*, vol. 25, no. 2, pp. 241–248, Oct. 2003.
- [236] F. Yang, J.-Y. Gao, H. Chen, Z.-H. Du, X.-Q. Zhang, and W. Gao, “Targeted inhibition of the phosphoinositide 3-kinase impairs cell proliferation, survival, and invasion in colon cancer,” *Onco. Targets. Ther.*, vol. 10, p. 4413, 2017.
- [237] H. Wang *et al.*, “Activation of the PI3K/Akt/mTOR/p70S6K Pathway is Involved in S100A4-induced Viability and Migration in Colorectal Cancer Cells,” *Int. J. Med. Sci.*, vol. 11, no. 8, pp. 841–849, 2014.
- [238] Q. Lin *et al.*, “Constitutive Activation of JAK3/STAT3 in Colon Carcinoma Tumors and Cell Lines: Inhibition of JAK3/STAT3 Signaling Induces Apoptosis and Cell Cycle Arrest of Colon Carcinoma Cells,” *Am. J. Pathol.*, vol. 167, no. 4, pp. 969–980, Oct. 2005.
- [239] H. Xiong *et al.*, “Inhibition of JAK1, 2/STAT3 Signaling Induces Apoptosis, Cell Cycle Arrest, and Reduces Tumor Cell Invasion in Colorectal Cancer Cells,” *Neoplasia*, vol. 10, no. 3, pp. 287–297, Mar. 2008.
- [240] J. Roper *et al.*, “Combination PI3K/MEK inhibition promotes tumor apoptosis and regression in PIK3CA wild-type, KRAS mutant colorectal cancer,” *Cancer Lett.*, vol. 347, no. 2, pp. 204–211, Jun. 2014.
- [241] J. Jin, Q. Guo, J. Xie, D. Jin, and Y. Zhu, “Combination of MEK Inhibitor and the JAK2-STAT3 Pathway Inhibition for the Therapy of Colon Cancer,” *Pathol. Oncol. Res.*, vol. 25, no. 2, pp. 769–775, Apr. 2019.




- [242] R. B. Mokhtari *et al.*, “Combination therapy in combating cancer,” *Oncotarget*, vol. 8, no. 23, pp. 38022–38043, Jun. 2017.
- [243] P. Wee and Z. Wang, “Epidermal Growth Factor Receptor Cell Proliferation Signaling Pathways.,” *Cancers (Basel)*, vol. 9, no. 5, p. pii: E52, May 2017.
- [244] K. M. Quesnelle, A. L. Boehm, and J. R. Grandis, “STAT-mediated EGFR signaling in cancer,” *J. Cell. Biochem.*, vol. 102, no. 2, pp. 311–319, Oct. 2007.
- [245] J. Bromberg, “Stat proteins and oncogenesis.,” *J. Clin. Invest.*, vol. 109, no. 9, pp. 1139–42, May 2002.
- [246] J. R. Testa and A. Bellacosa, “AKT plays a central role in tumorigenesis,” *Proc. Natl. Acad. Sci.*, vol. 98, no. 20, pp. 10983–10985, Sep. 2001.
- [247] A. Bardelli *et al.*, “Concomitant blockade of EGFR and MEK overcomes acquired resistance to anti-EGFR therapy in colorectal cancer cells and patients’ avatars.,” *J. Clin. Oncol.*, vol. 32, no. 15_suppl, pp. 2626–2626, May 2014.
- [248] T. Troiani *et al.*, “Primary and Acquired Resistance of Colorectal Cancer Cells to Anti-EGFR Antibodies Converge on MEK/ERK Pathway Activation and Can Be Overcome by Combined MEK/EGFR Inhibition,” *Clin. Cancer Res.*, vol. 20, no. 14, 2014.
- [249] L. Jiang *et al.*, “MTMR2 promotes invasion and metastasis of gastric cancer via inactivating IFN γ /STAT1 signaling,” *J. Exp. Clin. Cancer Res.*, vol. 38, no. 1, p. 206, Dec. 2019.
- [250] H. Cao *et al.*, “IL-13/STAT6 signaling plays a critical role in the epithelial-mesenchymal transition of colorectal cancer cells,” *Oncotarget*, vol. 7, no. 38, p. 61183, Sep. 2016.
- [251] X. Zhang *et al.*, “Human colorectal cancer-derived mesenchymal stem cells promote colorectal cancer progression through IL-6/JAK2/STAT3 signaling,” *Cell Death Dis.*, vol. 9, no. 2, p. 25, Feb. 2018.
- [252] R. B. Mokhtari *et al.*, “Combination therapy in combating cancer,” *Oncotarget*, vol. 8, no. 23, pp. 38022–38043, Jun. 2017.
- [253] M. L. Citron *et al.*, “Randomized Trial of Dose-Dense Versus Conventionally Scheduled and Sequential Versus Concurrent Combination Chemotherapy as Postoperative Adjuvant Treatment of Node-Positive Primary Breast Cancer: First Report of Intergroup Trial C9741/Cancer and Leukemia Group B Trial 9741,” *J. Clin. Oncol.*, vol. 21, no. 8, pp. 1431–1439, Apr. 2003.
- [254] C. Pico *et al.*, “Epirubicin-cyclophosphamide adjuvant chemotherapy plus tamoxifen administered concurrently versus sequentially: randomized phase III


- trial in postmenopausal node-positive breast cancer patients. A GEICAM 9401 study,” *Ann. Oncol.*, vol. 15, no. 1, pp. 79–87, Jan. 2004.
- [255] D. Bedognetti *et al.*, “Concurrent vs Sequential Adjuvant Chemotherapy and Hormone Therapy in Breast Cancer: A Multicenter Randomized Phase III Trial,” *JNCI J. Natl. Cancer Inst.*, vol. 103, no. 20, pp. 1529–1539, Oct. 2011.
- [256] E. A. Perez *et al.*, “Sequential Versus Concurrent Trastuzumab in Adjuvant Chemotherapy for Breast Cancer,” *J. Clin. Oncol.*, vol. 29, no. 34, pp. 4491–4497, Dec. 2011.
- [257] C. D. Britten, “PI3K and MEK inhibitor combinations: examining the evidence in selected tumor types,” *Cancer Chemother. Pharmacol.*, vol. 71, no. 6, pp. 1395–1409, Jun. 2013.
- [258] J. S. W. Lind, P. E. Postmus, D. A. M. Heideman, E. B. Thunnissen, O. Bekers, and E. F. Smit, “Dramatic Response to Low-Dose Erlotinib of Epidermal Growth Factor Receptor Mutation-Positive Recurrent Non-small Cell Lung Cancer After Severe Cutaneous Toxicity,” *J. Thorac. Oncol.*, vol. 4, no. 12, pp. 1585–1586, Dec. 2009.
- [259] H. Satoh *et al.*, “Low-Dose Gefitinib Treatment for Patients with Advanced Non-small Cell Lung Cancer Harboring Sensitive Epidermal Growth Factor Receptor Mutations,” *J. Thorac. Oncol.*, vol. 6, no. 8, pp. 1413–1417, Aug. 2011.
- [260] J. J. Caumanns *et al.*, “Low-dose triple drug combination targeting the PI3K/AKT/mTOR pathway and the MAPK pathway is an effective approach in ovarian clear cell carcinoma,” *Cancer Lett.*, vol. 461, pp. 102–111, Oct. 2019.
- [261] M. J. Lee *et al.*, “Sequential Application of Anticancer Drugs Enhances Cell Death by Rewiring Apoptotic Signaling Networks,” *Cell*, vol. 149, no. 4, pp. 780–794, May 2012.
- [262] T. Shimizu *et al.*, “The Clinical Effect of the Dual-Targeting Strategy Involving PI3K/AKT/mTOR and RAS/MEK/ERK Pathways in Patients with Advanced Cancer,” *Clin. Cancer Res.*, vol. 18, no. 8, pp. 2316–2325, Apr. 2012.
- [263] J. W. Benbow, J. Aubrecht, M. J. Banker, D. Nettleton, and M. D. Aleo, “Predicting safety toleration of pharmaceutical chemical leads: Cytotoxicity correlations to exploratory toxicity studies,” *Toxicol. Lett.*, vol. 197, no. 3, pp. 175–182, Sep. 2010.
- [264] N. Greene, M. D. Aleo, S. Louise-May, D. A. Price, and Y. Will, “Using an in vitro cytotoxicity assay to aid in compound selection for in vivo safety studies,” *Bioorg. Med. Chem. Lett.*, vol. 20, no. 17, pp. 5308–5312, Sep. 2010.
- [265] G. Shapiro *et al.*, “Clinical combination of the MEK inhibitor GDC-0973 and the

PI3K inhibitor GDC-0941: A first-in-human phase Ib study testing daily and intermittent dosing schedules in patients with advanced solid tumors.,” *J. Clin. Oncol.*, vol. 29, no. 15_suppl, pp. 3005–3005, May 2011.

- [266] D. Miles, G. von Minckwitz, and A. D. Seidman, “Combination versus sequential single-agent therapy in metastatic breast cancer.,” *Oncologist*, vol. 7 Suppl 6, no. Supplement 6, pp. 13–9, Dec. 2002.
- [267] M. Ducreux *et al.*, “Sequential versus combination chemotherapy for the treatment of advanced colorectal cancer (FFCD 2000–05): an open-label, randomised, phase 3 trial,” *Lancet Oncol.*, vol. 12, no. 11, pp. 1032–1044, Oct. 2011.
- [268] H. I. Hurwitz *et al.*, “Phase II Randomized Trial of Sequential or Concurrent FOLFOXIRI-Bevacizumab Versus FOLFOX-Bevacizumab for Metastatic Colorectal Cancer (STEAM),” *Oncologist*, p. theoncologist.2018-0344, Dec. 2018.
- [269] P. S. Hodgkinson and T. Sethi, “Extracellular Matrix-Mediated Drug Resistance,” in *Drug Resistance in Cancer Cells*, New York, NY: Springer US, 2009, pp. 115–135.
- [270] R. Fisher, L. Pusztai, and C. Swanton, “Cancer heterogeneity: implications for targeted therapeutics.,” *Br. J. Cancer*, vol. 108, no. 3, pp. 479–85, Feb. 2013.
- [271] X. Liu *et al.*, “ROCK Inhibitor and Feeder Cells Induce the Conditional Reprogramming of Epithelial Cells,” *Am. J. Pathol.*, vol. 180, no. 2, pp. 599–607, Feb. 2012.
- [272] B. A. Teicher, “Hypoxia and drug resistance,” *Cancer Metastasis Rev.*, vol. 13, no. 2, pp. 139–168, 1994.
- [273] T. Reya, S. J. Morrison, M. F. Clarke, and I. L. Weissman, “Stem cells, cancer, and cancer stem cells,” *Nature*, vol. 414, no. 6859, pp. 105–111, Nov. 2001.
- [274] L. Milas and W. N. Hittelman, “Cancer Stem Cells and Tumor Response to Therapy: Current Problems and Future Prospects,” *Semin. Radiat. Oncol.*, vol. 19, no. 2, pp. 96–105, Apr. 2009.
- [275] X. Hu *et al.*, “Induction of cancer cell stemness by chemotherapy,” *Cell Cycle*, vol. 11, no. 14, pp. 2691–2698, Jan. 2012.
- [276] H. A. McCauley and J. M. Wells, “Pluripotent stem cell-derived organoids: using principles of developmental biology to grow human tissues in a dish.,” *Development*, vol. 144, no. 6, pp. 958–962, Mar. 2017.
- [277] A. Astashkina and D. W. Grainger, “Critical analysis of 3-D organoid in vitro cell culture models for high-throughput drug candidate toxicity assessments,” *Adv. Drug Deliv. Rev.*, vol. 69–70, pp. 1–18, 2014.

APPENDIX

 **Copyright Clearance Center**  [Home](#) [Create Account](#) [Help](#) 

 **ACS Publications** Most Trusted. Most Cited. Most Read. **Title:** Multiparametric Analysis of Oncology Drug Screening with Aqueous Two-Phase Tumor Spheroids

Author: Pradip Shahi Thakuri, Stephanie L. Ham, Gary D. Luker, et al

Publication: Molecular Pharmaceutics

Publisher: American Chemical Society

Date: Nov 1, 2016

Copyright © 2016, American Chemical Society


LOGIN

If you're a [copyright.com](#) user, you can login to RightsLink using your [copyright.com](#) credentials. Already a RightsLink user or want to [learn more?](#)

PERMISSION/LICENSE IS GRANTED FOR YOUR ORDER AT NO CHARGE

This type of permission/license, instead of the standard Terms & Conditions, is sent to you because no fee is being charged for your order. Please note the following:

- Permission is granted for your request in both print and electronic formats, and translations.
- If figures and/or tables were requested, they may be adapted or used in part.
- Please print this page for your records and send a copy of it to your publisher/graduate school.
- Appropriate credit for the requested material should be given as follows: "Reprinted (adapted) with permission from (COMPLETE REFERENCE CITATION). Copyright (YEAR) American Chemical Society." Insert appropriate information in place of the capitalized words.
- One-time permission is granted only for the use specified in your request. No additional uses are granted (such as derivative works or other editions). For any other uses, please submit a new request.

 **Copyright Clearance Center**  [Home](#) [Create Account](#) [Help](#) 

 **Title:** Quantitative Size-Based Analysis of Tumor Spheroids and Responses to Therapeutics

Author: Pradip Shahi Thakuri, Megha Gupta, Madison Plaster, et al

Publication: ASSAY and Drug Development Technologies

Publisher: Mary Ann Liebert, Inc.

Date: Apr 1, 2019

Copyright © 2019, Mary Ann Liebert, Inc.

LOGIN

If you're a [copyright.com](#) user, you can login to RightsLink using your [copyright.com](#) credentials. Already a RightsLink user or want to [learn more?](#)

Permissions Request

Mary Ann Liebert, Inc. publishers does not require authors of the content being used to obtain a license for their personal reuse of full article, charts/graphs/tables or text excerpt.



Title: Single and Combination Drug Screening with Aqueous Biphasic Tumor Spheroids
Author: Pradip Shahi Thakuri, Hossein Tavana
Publication: SLAS Discovery
Publisher: SAGE Publications
Date: 06/01/2017
Copyright © 2017, © SAGE Publications

LOGIN
If you're a [copyright.com](#) user, you can login to RightsLink using your [copyright.com](#) credentials.
Already a RightsLink user or want to [learn more?](#)

If you are a SAGE journal author requesting permission to reuse material from your journal article, please note you may be able to reuse your content without requiring permission from SAGE. Please review SAGE's author re-use and archiving policies at <https://us.sagepub.com/en-us/nam/journal-author-archiving-policies-and-re-use> for more information.

If your request does not fall within SAGE's reuse guidelines, please proceed with submitting your request by selecting one of the other reuse categories that describes your use. Please note, a fee may be charged for reuse of content requiring permission. Please contact permissions@sagepub.com if you have questions.



Title: Synergistic Inhibition of Kinase Pathways Overcomes Resistance of Colorectal Cancer Spheroids to Cyclic Targeted Therapies
Author: Pradip Shahi Thakuri, Megha Gupta, Ramila Joshi, et al
Publication: ACS Pharmacology & Translational Science
Publisher: American Chemical Society
Date: Aug 1, 2019
Copyright © 2019, American Chemical Society

LOGIN
If you're a [copyright.com](#) user, you can login to RightsLink using your [copyright.com](#) credentials.
Already a RightsLink user or want to [learn more?](#)

PERMISSION/LICENSE IS GRANTED FOR YOUR ORDER AT NO CHARGE

This type of permission/license, instead of the standard Terms & Conditions, is sent to you because no fee is being charged for your order. Please note the following:

- Permission is granted for your request in both print and electronic formats, and translations.
- If figures and/or tables were requested, they may be adapted or used in part.
- Please print this page for your records and send a copy of it to your publisher/graduate school.
- Appropriate credit for the requested material should be given as follows: "Reprinted (adapted) with permission from (COMPLETE REFERENCE CITATION). Copyright (YEAR) American Chemical Society." Insert appropriate information in place of the capitalized words.
- One-time permission is granted only for the use specified in your request. No additional uses are granted (such as derivative works or other editions). For any other uses, please submit a new request.